

**Human disease variants in the ryanodine receptor have
effects *in vivo* for *Caenorhabditis elegans*
neuromuscular function**

Brittany Laura Graham

Submitted in accordance with the requirements for the degree
of Doctor of Philosophy

The University of Leeds

School of Biology

February 2020

The candidate confirms that the work submitted is her own and that appropriate credit has been given where reference has been made to the work of others.

This copy has been supplied on the understanding that it is copyright material and that no quotation from the thesis may be published without proper acknowledgement.

The right of Brittany Laura Graham to be identified as Author of this work has been asserted by Brittany Laura Graham in accordance with the Copyright, Designs and Patents Act 1988.

Acknowledgements

I would like to express my appreciation to my supervisor Ian Hope; for providing the opportunity, for all the scientific advice, for his feedback during my write-up and for his overall support through this process. Thank you for training me to think like a scientist.

I would also like to thank my co-supervisor Marie-Anne Shaw. Her encouragement, comments and different point of view have helped widen my research and made me a better scientist.

I must also acknowledge the White Rose DTP, the BBSRC and the FBS graduate office at the University of Leeds without whom this project would not have been possible.

My special thanks are extended to NemaMetrix for hosting me on my internship and their help in generating the variant strains used in this thesis.

Additional thanks go to David Pertab and Alex Jubb, for generating two further variant strains used in this research. I also appreciate the advice and many discussions had with Elpi Kalogeropoulou, Célia Ferreira and Ros Clifford in the Hope lab.

I would like to recognise the help provided by the Cohen group at the University of Leeds, particularly Omer Yuval and Rob Holbrook. The multi-worm tracker and guidance on coding and software were vital to the crawling analysis in this research.

My friends in the postgrad office: Zatul, Ellie, Francis, Dayah, Rosie, Nok, Victoria, Jens, Jake and Brad, provided an enjoyable environment to work for which I will always be thankful. To all my friends, wherever in the world you are, thank you for being there for me. A special mention made to Elpi and Rosie whose friendships have meant the world to me.

Tanner, I am forever grateful for your endless reassurance, positivity and belief in me.

Finally, to my family, I would not be where I am without your unconditional love and encouragement. I am thankful to have your support in anything I decide to do.

I could not end without thanking my mum for the cups of tea that kept me going, and for everything else. Having a strong and proud woman as a role model made me believe I could do and be anything.

I would like to dedicate this thesis to women in science.

“I was taught that the way of progress was neither swift nor easy.” – Marie Curie

The women before me have made my way easier, and I hope to do the same for the
future women in science.

Abstract

The ryanodine receptor is a key intracellular calcium ion channel in nerve and muscle cells. A number of links have been made between the ryanodine receptor and age-related muscular and neurodegeneration. Variants of the *RYR1* gene are associated with malignant hyperthermia, which is a hypermetabolic reaction to inhalational anaesthetics. I used eight genome-edited *Caenorhabditis elegans* strains expressing ryanodine receptors with modifications equivalent to known *RYR1* disease variants to characterise the consequences of these variants on neuromuscular function *in vivo*. Animals expressing variant ryanodine receptors exhibited increased sensitivity to halothane when both homozygous and heterozygous for the variants. This mirrors the situation in humans where malignant hyperthermia is inherited in an autosomal dominant pattern. Novel, subtle, locomotion defects were found in animals expressing variant ryanodine receptors even in the absence of halothane. In-depth analysis of crawling suggested that these variant channels release excessive calcium, resulting in increased muscle contraction. Exaggerated age-related degeneration of locomotion was observed in variant strains, which may be a result of excessive calcium release via variant ryanodine receptors throughout the lifespan resulting in cellular damage. Cholinergic pharmacological agents were used to characterise if the consequences of the variants were pre and/ or post-synaptic. A range of complex phenotypes were found, reflecting the complexity of regulatory inputs to the ryanodine receptor. The altered properties of variant ryanodine receptors and effects of long-term calcium mishandling found here are anticipated to have consequences for human carriers, which may be in the nerve cells. Assessment of these phenotypes in a whole organism was important to fully appreciate the significant effects of variant ryanodine receptors.

Table of Contents

Acknowledgements	iii
Abstract.....	v
Table of Contents	vi
List of Tables.....	x
List of Figures.....	xi
List of Abbreviations	xiii
Chapter 1 General introduction	1
1.1. The ryanodine receptor	1
1.1.1. Ryanodine receptor isoforms and evolution	2
1.1.2. Structure of the ryanodine receptor.....	5
1.1.3. Control of ryanodine receptor activation	9
1.1.4. Ryanodine receptor related diseases	12
1.1.5. Malignant hyperthermia and its triggering agents	15
1.2. Caenorhabditis elegans as a model	18
1.2.1. <i>C. elegans</i> as a model for malignant hyperthermia.....	23
1.3. Focus of this research	26
1.3.1. Modelling RyR1-related disease in <i>C. elegans</i>	26
1.3.2. Pre- and postsynaptic effects of <i>RYR1</i> gene variants	26
1.4. Thesis outline	27
Chapter 2 General Methods	28
2.1. <i>C. elegans</i> maintenance and strains	28
2.1.1. <i>C. elegans</i> maintenance.....	28
2.1.2. <i>C. elegans</i> strains	28
2.2. Generating strains through CRISPR-Cas9 genome editing.....	29
2.2.1. Genotyping ryanodine receptor variant strains	33
2.3. Synchronisation and ageing	34
2.3.1. Generating an age-synchronised population of <i>C. elegans</i>	34
2.3.2. Ageing <i>C. elegans</i>	35
2.3.3. Statistical and graphical analysis	35
Chapter 3 Confirming a malignant hyperthermia related phenotype in genome- edited <i>RYR1</i> variant <i>C. elegans</i>: modelling malignant hyperthermia in the worm	38
3.1. Introduction	38
3.1.1. Aim of this chapter.....	38
3.1.2. A malignant hyperthermia related phenotype in <i>C. elegans</i>	38

3.2. Methods	39
3.2.1. Halothane and thrashing assays	39
3.2.2. L1 thrashing assay	39
3.3. Results	40
3.3.1. Identification of pathogenic <i>RYR1</i> gene variants in residues conserved in <i>C. elegans</i>	40
3.3.2. Confirmation of hypersensitivity to halothane for variant strains and discovery of novel locomotion defects in the absence of halothane	41
3.3.3. Ageing effects of ryanodine receptor variants on halothane sensitivity	52
3.3.4. Ryanodine receptor variants reduce thrashing rate in larval stage <i>C. elegans</i>	60
3.4. Discussion	63
3.4.1. <i>RYR1</i> gene variants expressed at the endogenous level in <i>C. elegans</i> show hypersensitivity to halothane	63
3.4.2. Endogenous expression of ryanodine receptor variants reveal subtle locomotion defects	65
3.4.3. Ryanodine receptor variants have age-related consequences for locomotion in <i>C. elegans</i>	66
3.4.4. Sensitivity to halothane is not affected by age in most ryanodine receptor variant strains	68
Chapter 4 Investigating the subtle locomotion phenotype found in the absence of a malignant hyperthermia trigger in <i>C. elegans</i> ryanodine receptor variant strains: Quantifying crawling	69
4.1. Introduction	69
4.1.1. Aim of this chapter	69
4.1.2. <i>C. elegans</i> locomotion.....	69
4.2. Methods	74
4.2.1. Locomotion analysis via multi-worm tracking	74
4.2.2. Video analysis.....	74
4.2.3. Worm Length, crawling speed and waveform parameters	76
4.2.4. Degree of curvature	77
4.2.5. Kymograms	78
4.3. Results	78
4.3.1. Ryanodine receptor variants affect young adult worm length	78
4.3.2. The sinusoidal wave of crawling in young adult <i>C. elegans</i> is affected by the presence of ryanodine receptor variants	82
4.3.3. Crawling speed is increased in young adult ryanodine receptor variant strains	88
4.3.4. Ryanodine receptor variant strains have altered adult growth rates	89
4.3.5. Ryanodine receptor variants exacerbate age-related changes to crawling in <i>C. elegans</i>	91
4.4. Discussion	98
4.4.1. Growth rate is reduced in ryanodine receptor variant strains.....	99
4.4.2. Ryanodine receptor variants have subtle consequences for crawling in the young adults	102

4.4.3. Ryanodine receptor variants exacerbate age-related changes in crawling parameters.....	106
-----------------------------------------------------------------------------------------------	-----

Chapter 5 Exploring effects of ryanodine receptor variants on cholinergic pharmacology: Pre- and postsynaptic ryanodine receptor effects 109

5.1. Introduction	109
5.1.1. Aim of this chapter.....	109
5.1.2. The role of ryanodine receptors in neurons.....	109
5.1.3. Acetylcholine signal transduction pathway.....	111
5.1.4. Cholinergic pharmacological agents.....	112
5.2. Methods.....	115
5.2.1. Aldicarb assays.....	115
5.2.2. Levamisole assays.....	116
5.3. Results	116
5.3.1. Sensitivity to aldicarb is differential among the ryanodine receptor variants strains	116
5.3.2. Ryanodine receptor variant strains show novel responses to levamisole	119
5.4. Discussion	123
5.4.1. Ryanodine receptor variants may have presynaptic effects as indicated by an altered response to aldicarb.....	124
5.4.2. The responses to levamisole suggest postsynaptic effects of ryanodine receptor variants.....	126
5.4.3. Effects of ryanodine receptor variants in neural and muscle cells.....	128

Chapter 6 Confirming a malignant hyperthermia related phenotype in heterozygous ryanodine receptor variant *C. elegans*: genetic dominance in ryanodine receptor related pathologies..... 131

6.1. Introduction	131
6.1.1. Aim of this chapter.....	131
6.1.2. Genetic dominance in malignant hyperthermia.....	131
6.2. Methods.....	133
6.2.1. Generating heterozygous ryanodine receptor variant individuals in <i>C. elegans</i>	133
6.2.2. Halothane and thrashing assays for the heterozygote variant animals	134
6.3. Results	135
6.3.1. Halothane hypersensitivity and locomotion defects are present in all ryanodine receptor variant heterozygote animals	135
6.3.2. Ryanodine receptor variants in the heterozygote animals disrupt locomotion more than in the homozygotes	139
6.4. Discussion	142
6.4.1. Thrashing defects are intensified in ryanodine receptor variant heterozygote animals	142

Chapter 7 General Discussion..... 145

7.1. Ryanodine receptor variants increase <i>C. elegans</i> sensitivity to halothane independently of age and zygosity.....	145
7.2. Ryanodine receptor variants have inherent consequences for locomotion in <i>C. elegans</i>	147
7.2.1. Worm length may affect thrashing rate in young adults	149
7.2.2. Muscle contraction is increased in young adult ryanodine receptor variant strains	150
7.2.3. Ryanodine receptor variants increase crawling speed of young adult <i>C. elegans</i>	152
7.3. Ryanodine receptor variants exacerbate the effects of ageing in <i>C. elegans</i>	154
7.3.1. Thrashing rate in liquid decreased more in ryanodine receptor variant strains, with age ...	154
7.3.2. Crawling parameters show exaggerated changes with age in ryanodine receptor variant strains.....	155
7.4. Patterns throughout this thesis	156
7.5. Future work.....	162
Appendix A UNC-68 alignment to human RYR1, RYR2 and RYR3	166
Appendix B Design information for the CRISPR-Cas9 genome-edited strains	167
Appendix C Example sequencing alignment.....	168
Appendix D Comparison of Leeds and NemaMetrix N2 background strains	169
Appendix E Statistical comparison of thrashing rate of the ryanodine receptor variant strains, the wild type and CB540 null mutant when exposed to 4% DMSO	170
Appendix F Crawling parameters for individual wild type animals.....	171
Appendix G Young and old adult crawling parameters.....	173
Appendix H Aldicarb concentration comparison	178
Appendix I Images showing kinking upon exposure to 1 mM levamisole	179
References.....	180

List of Tables

Table 2.1. <i>C. elegans</i> strains used in this research.....	29
Table 2.2. Aligned <i>unc-68</i> nucleic acid sequence and encoded amino acid sequence for wild type and the variant strains after genome editing.	30
Table 3.1: Amino acid alignments of human RYR1 and <i>C. elegans</i> UNC-68 in the regions of the studied variants, and the <i>C. elegans</i> strains that were generated expressing the variant UNC-68.....	41
Table 3.2: Percentage change of mean thrashing rates from the absence of halothane to 1 mM, 2.5 mM and 5 mM concentrations of halothane for wild type, the CB540 (<i>unc-68(e540)</i>) null mutant and RyR variant <i>C. elegans</i> strains.....	47
Table 3.3: Percentage change of mean thrashing rates in S medium from young to old adult stages for wild type, the CB540 (<i>unc-68(e540)</i>) null mutant and RyR variant <i>C. elegans</i> strains.....	58
Table 4.1: Mean and standard deviation (SD) of crawling parameters amplitude, wavelength and frequency for the RyR variant strains, wild type and the CB540 (<i>unc-68(e540)</i>) null mutant.	82
Table 4.2: Mean percentage change from the wild type to RyR variant strains or the CB540 (<i>unc-68(e540)</i>) null mutant in wavelength, amplitude, frequency and degree of curvature (curve).	87
Table 4.3: Mean and standard deviation (SD) of midbody crawling speed for RyR variant strains, wild type, and the CB540 (<i>unc-68(e540)</i>) null mutant.	89
Table 4.4: Mean percentage change from young adult to old adult in length, wavelength, amplitude, frequency, crawling speed and degree of curvature (curve).	92
Table 5.1: Response of RyR variant strains, wild type and the CB540 (<i>unc-68(e540)</i>) null mutant, to levamisole in M9 buffer over 2 hours.	122
Table 6.1: Percentage change of mean thrashing rates from the absence of, to presence of 5 mM halothane for RyR variant heterozygote animals, and wild type and CB540 (<i>unc-68(e540)</i>) null mutant controls.....	138
Table B.1. Sequences used to guide cutting and repair of the genome in the CRISPR-Cas9 genome-edited strain generated at NemaMetrix.....	167
Table G.1: Mean and standard deviation (SD) of old adult midbody crawling speed for wild type, RyR variant strains and the CB540 (<i>unc-68(e540)</i>) null mutant. ...	175

List of Figures

Figure 1.1: The ryanodine receptor.....	1
Figure 1.2: Evolution of the ryanodine receptor.....	5
Figure 1.3: Structure of the ryanodine receptor.	6
Figure 1.4: Open and closed ryanodine receptor conformation.	8
Figure 1.5: Neural and muscular RyRs are activated in different ways.	12
Figure 1.6: Pathologies and tissues affected by RyR dysfunction.	13
Figure 1.7: <i>C. elegans</i> anatomy.....	18
Figure 1.8: CRISPR-Cas9 genome editing.....	22
Figure 2.1: Generating a single amino acid change, corresponding to the R2163H <i>RYR1</i> human disease variant, in <i>unc-68</i>	32
Figure 2.2: Location of RyR1 variants in the ryanodine receptor.....	36
Figure 3.1: Halothane assay set up and counting of body bends.....	42
Figure 3.2: RyR variants confer an MH-related phenotype of hypersensitivity to halothane.....	46
Figure 3.3: High concentration of DMSO has some effect on <i>C. elegans</i> locomotion, but halothane further decreases thrashing rate.	51
Figure 3.4: Aged RyR variant individuals are less sensitive to halothane.....	56
Figure 3.5: Thrashing rate in S medium is reduced in all RyR variant strains at the L1 stage.	62
Figure 4.1: Arrangement of adult hermaphrodite body wall muscle.	70
Figure 4.2: Quantifying <i>C. elegans</i> locomotion using parameters that describe a wave.	73
Figure 4.3: Multi-worm tracker system set up.....	75
Figure 4.4: Measuring the degree of curvature for RyR variant strains.	77
Figure 4.5: Kymograms show curvature down the body axis.	78
Figure 4.6: The presence of RyR variants affect the length of young adults.....	81
Figure 4.7: The RyR variant strains have decreased amplitude and wavelength of the crawling waveform compared to wild type, but increased frequency.	86
Figure 4.8: RyR variants affect growth rates of adult <i>C. elegans</i>	90
Figure 4.9: Effect of RyR variants on crawling changes with age.	95
Figure 4.10: RyR variants intensify age-related reduction in crawling coordination..	97

Figure 4.11: Increased muscle contraction due to increased calcium release via variant RyRs.	105
Figure 5.1: Aldicarb and levamisole disrupt cholinergic signal transmission.....	114
Figure 5.2: RyR variants alter time to paralysis in 1 mM aldicarb.....	118
Figure 6.1: Quaternary structure of the RyR in wild type / variant <i>unc-68</i> animals.	132
Figure 6.2: Heterozygous wild type / variant <i>unc-68</i> animals were generated by mating.	134
Figure 6.3: Locomotion effects and halothane hypersensitivity in heterozygous RyR variant individuals.	136
Figure 6.4: Comparison of heterozygous and homozygous RyR variants on locomotion and halothane sensitivity.	141
Figure A.1: BLASTP results for <i>C. elegans</i> UNC-68 when searched for in humans. ..	166
Figure C.1: Example sequencing alignments for RyR variant strains to confirm correct genomic sequence.	168
Figure D.1: Leeds N2 and NemaMetrix N2 strains show no differences in response to halothane.....	169
Figure E.1: RyR variant strains are not more sensitive to DMSO than wild type.	170
Figure F.1: Crawling parameters for individual wild type animals.	172
Figure G.1: Amplitude, wavelength and frequency of young adults.	173
Figure G.2: Length, amplitude, wavelength, frequency and degree curvature of old adults.....	174
Figure G.3: Representative kymogram for one young and one old adult individual of each strain.	177
Figure H.1: Aldicarb concentration comparison for wild type and the hR2163H variant strain.	178
Figure I.1: Kinking response in 1 mM levamisole after 1 hour exposure.....	179

List of Abbreviations

ACh = Acetylcholine	ER = Endoplasmic reticulum
AChE = Acetylcholine esterase	FKBP12 = Peptidyl-prolyl cis-trans isomerase
AChR (nAChR and mAChR) = Acetylcholine receptor (nicotinic, and muscarinic)	FUdR = 5-fluoro-2'-deoxyuridine
AD = Alzheimer's disease	GABA = Gamma-aminobutyric acid
ApoCaM = Apocalmodulin, calcium-free calmodulin	gnomAD = The Genome Aggregation Database
BWM = Body wall muscle	HD = Helical domain
Ca²⁺-CaM = Calcium-bound calmodulin	HDR = Homology direct repair
CASQ = Calsequestrin	IIS = Insulin/ IGF-I-like signalling
CCD = Central core disease	IP₃ = Inositol triphosphate
CICR = Calcium-induced calcium release	IP₃R = Inositol triphosphate receptor
CNS = Central nervous system	IVCT = In vitro contracture test
CPVT = Catecholaminergic polymorphic ventricular tachycardia	L/R = Left/Right
crRNA = CRISPR RNAs	L1 = Larval stage 1
CTD = C-terminal domain	LOAM = Late onset axial myopathy
D/V = Dorsal/Ventral	MH = Malignant hyperthermia
DHPR = Dihydropyridine receptor	MHN = Malignant hyperthermia non-susceptible
DMSO = dimethyl sulfoxide	MHS (MHSc / MHS_h) = Malignant hyperthermia susceptible (caffeine/ halothane)
DNC = Dorsal nerve cord	MmD = Multi-minicore disease
E-C = Excitation-contraction	mPSCs = Miniature postsynaptic currents
EHI = Exertional heat illness	NGM = Nematode growth medium
EMHG = European malignant hyperthermia group	

NHEJ = Non-homologous end joining

nt = Nucleotide

NTD = N-terminal domain

P1 = Pore helix 1

P2 = Pore helix 1

PAM = Proto-spacer adjacent motif

PNS = Peripheral nervous system

RNAi = RNA interference

PDB = Protein Data Bank

RyR = Ryanodine receptor

SERCA = Sarcoplasmic reticulum
Ca²⁺ATPase

sgRNA = Short guide rna

NMJ = Neuromuscular junction

SOICR = Store-overload-induced
calcium release

SPRY = SplA/ RyR

SR = Sarcoplasmic reticulum

ssDNA = Single stranded DNA

TMD = Transmembrane domain

unc = uncoordinated

VAR = Variant

VGCCs = Voltage-gated calcium
channels

VNC = Ventral nerve cord

WT = Wild type

Chapter 1

General introduction

1.1. The ryanodine receptor

Despite its name, the ryanodine receptor (RyR) is not a receptor but a large intracellular calcium release channel in both excitable and non-excitable cells. They are so named due to their ryanodine binding ability; ryanodine is a plant alkaloid, which these channels bind with high affinity (Callaway *et al.*, 1994). RyRs are found in the sarco- and endoplasmic reticulum (SR/ ER) membrane and play a vital role in the calcium signalling required for many cellular processes (Lanner *et al.*, 2010). Together with the dihydropyridine receptor (DHPR), RyRs are most well-known for their role in excitation-contraction (E-C) coupling, which facilitates muscle contraction through calcium release from the SR upon electrical excitation of the plasma membrane (Marks *et al.*, 1989; Mickelson and Louis, 1996; Avila *et al.*, 2001; Mouton *et al.*, 2001; Cheng *et al.*, 2005). RyRs are mushroom shaped homotetramers, with a transmembrane domain forming the stalk-like pore of the protein, which allows calcium release from the SR/ ER upon RyR activation (Van Petegem, 2012) (Figure 1.1).

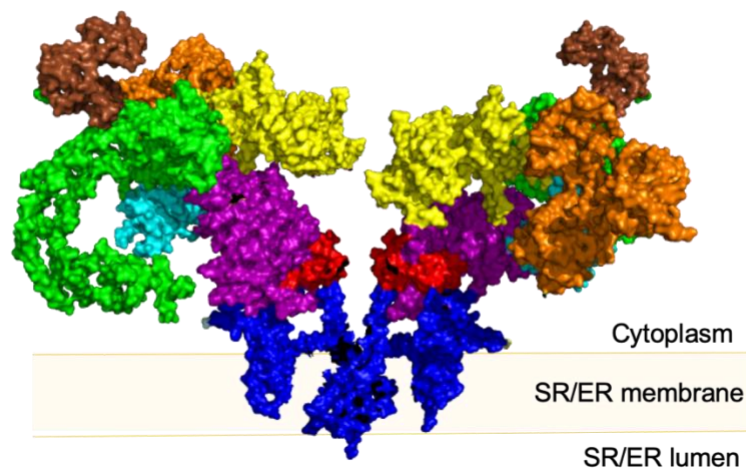


Figure 1.1: The ryanodine receptor.

Two opposing RyR protomers, viewed from within the plane of the SR/ ER membrane. The bulk of the RyR protein sits in the cell cytoplasm. Colours relate to different domains. Generated using PyMOL, based on the closed conformation of rabbit RYR1, as predicted from Yan *et al.* (2015) (Protein Data Bank (PDB) code 3J8H).

1.1.1. Ryanodine receptor isoforms and evolution

There are three RyR isoforms in mammals, encoded by three different genes, *RYR1*, *RYR2* and *RYR3*. RyR1 is widely expressed in mammalian skeletal muscle and was the first RyR isoform to be cloned, from rabbit skeletal muscle sarcoplasmic reticulum (Takeshima *et al.*, 1989). RyR2 is predominantly in smooth muscle and the heart while RyR3 is generally known as the brain isoform (Lanner *et al.*, 2010).

Despite each isoform being associated with these discrete locations, their expression is much broader. For example, RyR1 is also expressed at low levels in cardiac and smooth muscle, as well as in organs such as the stomach, kidney, adrenal glands, ovaries and testis, and in the brain, in the hippocampus, cerebellum and Purkinje cells (Furuichi *et al.*, 1994; Giannini *et al.*, 1995; Neylon *et al.*, 1995; Hertle and Yeckel, 2007; Abu-Omar *et al.*, 2018). Both RyR2 and RyR3 have broad expression too. RyR2 is also expressed in the cerebellum and cerebral cortex of the brain at high levels (Nakai *et al.*, 1990; Furuichi *et al.*, 1994). Lower levels of RyR2 expression have been found in the stomach, kidney, adrenal glands, ovaries, thymus, lungs and smooth muscle (Giannini *et al.*, 1995; Neylon *et al.*, 1995; Hertle and Yeckel, 2007). The highest levels of RyR3 expression in the brain are in the cerebellum, hippocampus, caudate nucleus and amygdala (Hakamata *et al.*, 1992; Giannini *et al.*, 1995), but RyR3 also has expression in skeletal muscle, with high expression levels in the diaphragm (Rossi *et al.*, 2007). Furthermore, RyR3 expression has been found in a number of organs in mice and rabbits, including lungs, kidneys, stomach and aorta (Giannini *et al.*, 1995; Ottini *et al.*, 1996).

RyRs show high levels of conservation of key domains with the transmembrane inositol triphosphate receptor (IP₃R) (Figure 1.2A). IP₃Rs, like RyRs, are channels that mediate calcium release from intracellular stores (Taylor and Tovey, 2010). The highest sequence homology for these two calcium ion channels is within the N-terminal and transmembrane regions, with approximately 30% identity across these regions and higher homology, up to 60% identity, within specific domains. The inositol 1,4,5-triphosphate/ ryanodine receptor domain (Figure 1.2A, orange 'Ins145_P3_rec' domain) corresponds to the inositol triphosphate (IP₃) ligand binding region on IP₃Rs and the N-terminal domain of RyRs, although RyRs lack the ability to bind IP₃ (Bosanac

et al., 2005). The N-terminal domains of both IP₃R and RyR also possess a quartet of protein mannosyltransferase IP₃R and RyR domains (Figure 1.2A, dark blue 'MIR' domain); the MIR domains may have a ligand transferase function (Ponting, 2000). There are two RyR and IP₃R Homology (RIH) domains (Figure 1.2A, yellow 'RYDR_ITPR' domains) and an RyR and IP₃R homology associated domain (Figure 1.2A, green 'RIH_assoc' domain) in RyRs and IP₃Rs, which are significantly similar. The ion transport transmembrane domains of RyRs and IP₃Rs share the greatest sequence similarity, likely due to their conduction of calcium ions (Bosanac *et al.*, 2005; Taylor and Tovey, 2010). The IP₃R gene superfamily divided into two subfamilies in the Opisthokonta, IP₃R-A and IP₃R-B/ RyR, and the latter subfamily further divided into two distinct families, IP₃R-B and RyR in the Filozoa (Figure 1.2B). Later two rounds of whole genome duplication resulted in three isoforms of IP₃R-A (*ITPR1*, *ITPR2* and *ITPR3*) in vertebrates; IP₃R-B was lost in vertebrates (Alzayady *et al.*, 2015). IP₃Rs underwent many independent losses and expansions in the eukaryotic lineage. In *Caenorhabditis elegans* there is one IP₃R and one RyR gene; the IP₃R gene groups within the vertebrate IP₃R-A clade, suggesting loss of IP₃R-B in *C. elegans*. This is independent to the loss of IP₃R-B in vertebrates as there is wide-spread occurrence of IP₃R-B amongst other metazoans, such as the acorn worm (Alzayady *et al.*, 2015).

The three different RyR genes in mammals (*RYR1*, *RYR2* and *RYR3*) are thought to have arisen from sub-functionalisation following the two rounds of genome duplication, which occurred in early vertebrate expansion, with subsequent loss of one copy (Sorrentino *et al.*, 2000). The first genome duplication event gave rise to the RyR2 and RyR3 ancestral forms, and the subsequent event gave rise to RyR1 from the RyR3 ancestral form (Figure 1.2C). In non-mammalian vertebrates, such as the frog, there are only two isoforms of RyR, which have been shown to be homologous to mammalian RyR1 and RyR3 through sequencing of bullfrog and chicken skeletal muscles (Oyamada *et al.*, 1994; Ottini *et al.*, 1996; Ogawa *et al.*, 2002); this suggests secondary loss of RyR2. In teleost fish there are two distinct isoforms of RyR1; RyR1a in slow twitch muscle and RyR1b in fast twitch muscle, presumed to be the result of sub-functionalisation following a further gene duplication event in this lineage (Morrissette *et al.*, 2000) (Figure 1.2C). In many invertebrates there is only one RyR gene. In *Drosophila melanogaster* this single RyR gene is expressed in muscles and neuronal

tissues (Hasan and Rosbash, 1992). In *C. elegans* there is also a single RyR gene (Figure 1.2C), with expression in the body wall, vulval, anal and pharyngeal muscles, as well as in neurons (Maryon *et al.*, 1998). Conservation of the RyR from *C. elegans* through to mammals demonstrates the vital role that this protein plays in calcium signalling in muscle and neural tissues, as well as other organs in higher organisms.

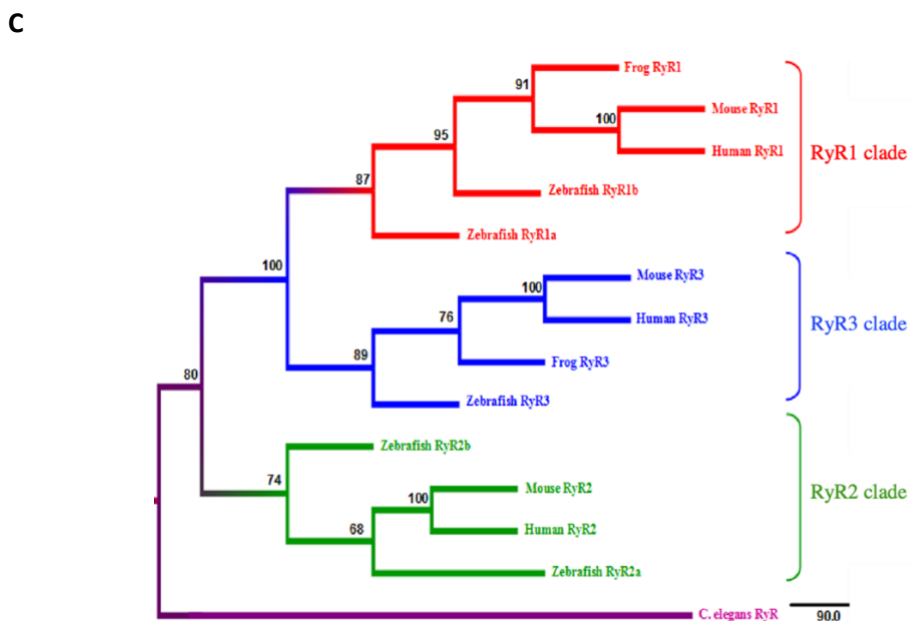
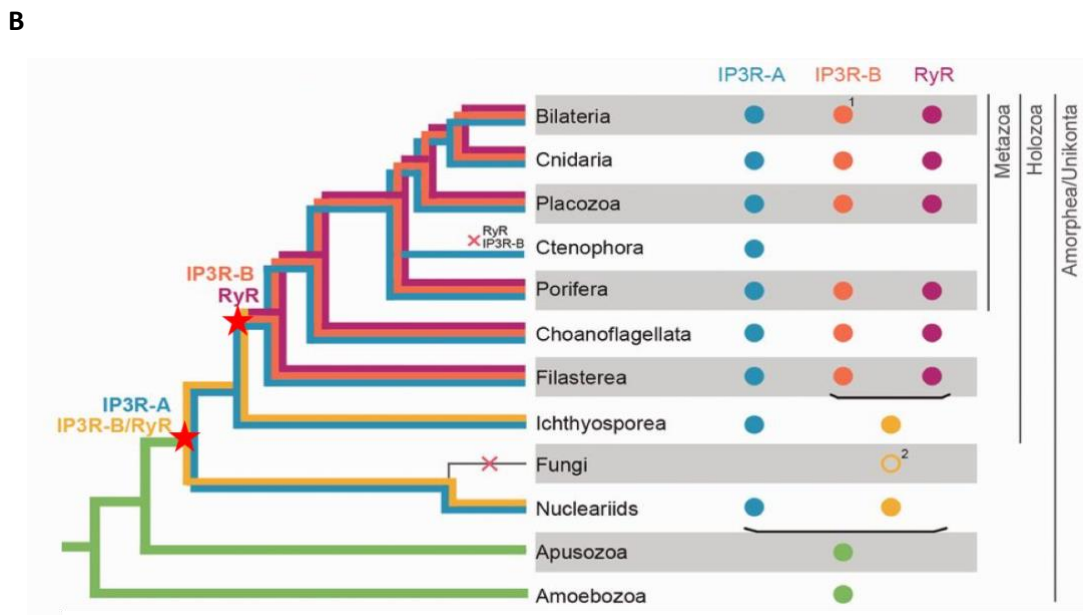
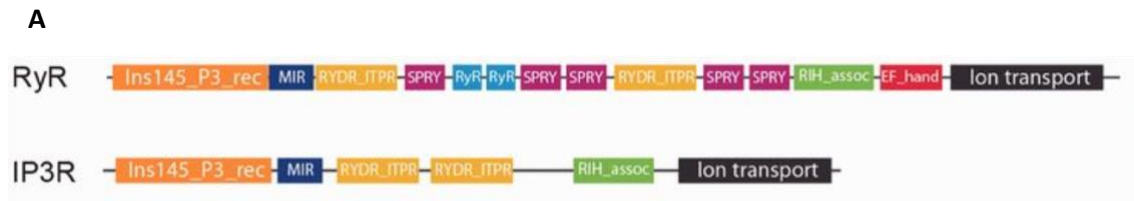


Figure 1.2: Evolution of the ryanodine receptor.

Evolution of IP₃R and RyR in Eukaryotes. (A) The consensus domains of IP₃Rs and RyRs showing conservation of domains, represented by their Pfam ID (El-Gebali *et al.*, 2018); the Ins145_P3_rec domain in orange (PF08709), MIR domain in dark blue (PF02815), two RYDR_ITPR domains in yellow (PF01365), the RIH_assoc domain in green (PF08454) and ion transport domain in black (PF00520). (B) Eukaryotic tree showing IP₃R and RyR diversification. Colours represent the origin and presence of particular genes and their diversification into paralogue families. Red crosses indicate secondary losses. Red stars indicate the division of the IP₃R superfamily into IP₃R-A and IP₃R-B/ RyR in the Opisthokonta and the division of IP₃R-B and RyR into distinct families in the Filozoa. ¹Lost in vertebrates. ²Lost in most fungi, except two species. Adapted from Alzayady *et al.* (2015), within the eukaryotic tree consensus from (Derelle and Lang, 2011; He *et al.*, 2014). (C) Phylogenetic tree showing evolution of the RyR in vertebrates. Generated from Multiple alignment of full-length published RyR amino acid sequences for human, mouse, frog and zebrafish. The *C. elegans* RyR sequence was used a designated outgroup. Phylogenetic tree adapted from Darbandi (2010).

1.1.2. Structure of the ryanodine receptor

The large cap-like region of the mushroom-shaped RyR protein is located in the cell cytoplasm while the 'stalk' crosses the membrane into the lumen of the SR or ER (Van Petegem, 2012) (Figure 1.3). RyRs are homotetrameric proteins made up of four identical subunits each approximately 5000 amino acids long. The structure of RyR1 has now been resolved in detail (Efremov *et al.*, 2015; Yan *et al.*, 2015; Zalk *et al.*, 2015).

Of the cytoplasmic portion of RyR, each protomer is made up of nine domains; the N-terminal domain (NTD), three SPRY (SpIA/ RyR) domains, P1 and P2 (pore helix 1 and 2) domains, the handle, helical domain and central domain (Efremov *et al.*, 2015; Yan *et al.*, 2015) (Figure 1.3). The central domain and NTD form a central tower, which is the core of the RyR, and the helical and handle domains form a corona around this central tower (Yan *et al.*, 2015). The central tower interacts with both the pore-forming transmembrane portion of the channel and other channel modulators to control RyR

activation (Yan *et al.*, 2015; Samsó, 2017). The transmembrane portion of the protein is made up by the C-terminal domain (CTD) and transmembrane domain (TMD) (Yan *et al.*, 2015).

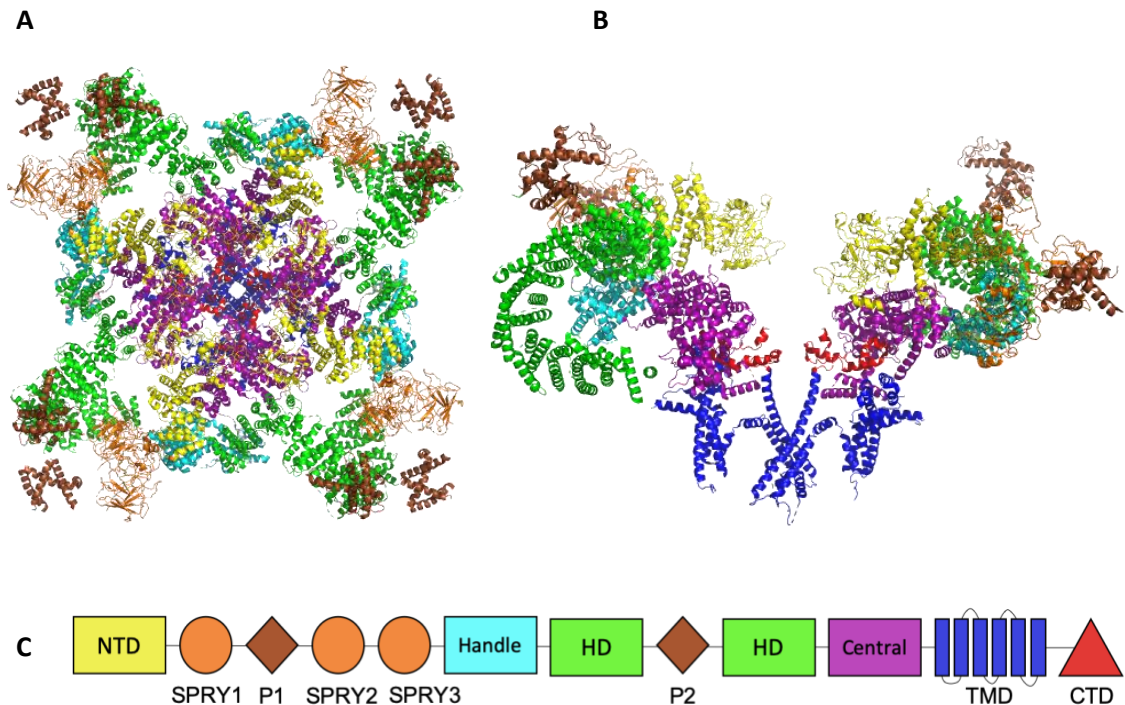


Figure 1.3: Structure of the ryanodine receptor.

(A) The tetrameric RyR protein, viewed from the cytosol. (B) Two opposing protomers, viewed from within the plane of the membrane. (C) The linear sequence of RyR1 domains. N-terminal domain (NTD) in yellow, SPRY1, 2 and 3 in orange, P1 and P2 in brown, handle in cyan, helical domain (HD) in green, central domain in purple, transmembrane domain (TMD) in blue and C-terminal domain (CTD) in red. Generated using PyMOL, based on the closed conformation of rabbit RYR1, as predicted from Yan *et al.* (2015) (PDB code 3J8H).

Structural changes to the handle domain result in corresponding changes in the NTD, due to the intradomain interaction RyR (Yan *et al.*, 2015; Wei *et al.*, 2016; Samsó, 2017). Upon RyR activation the NTD moves both upwards and outwards, affecting interactions between three NTD subdomains as well as interactions between NTDs of the neighbouring subunits (Wei *et al.*, 2016). Both of these interactions are thought to be important for calcium-induced channel gating.

The SPRY domains (SPRY1-3) are protein-protein interaction modules; RyR forms a macromolecular complex with a number of other proteins that control activation and calcium release. SPRY1 protrudes on the edge of the cytoplasmic portion of RyR and is predicted to be part of the binding site for a peptidyl-prolyl cis-trans isomerase (FKBP12) (Samsó, 2017). The interaction site of one subunit of the dihydropyridine receptor (DHPR) lies within the SPRY2 domain in RyR1 (Leong and MacLennan, 1998). This domain of RyR2 was not found to bind the DHPR, suggesting a role of this domain specifically in skeletal muscle. The interaction of the RyR's SPRY3 domain with other proteins has not been extensively studied. However, the location of SPRY3 on the surface of RyR1, facing the muscle cell's transverse-tubule, suggests a potential role in the RyR1-DHPR interaction, similar to that seen for SPRY2 (Samsó, 2017).

The handle domain, forming part of the corona around the channel's central tower, contains a number of protein binding sites. The FKBP12 binding site, which the SPRY1 domain forms part of, is also partly formed by the handle domain (Yan *et al.*, 2015). As well as FKBP12, apocalmodulin (calcium-free calmodulin, ApoCaM) and Calcium-bound calmodulin (Ca²⁺-CaM) both bind to the handle domain of RyR (Samsó, 2017; Brohus *et al.*, 2019).

The helical domain is the other corona-forming domain (Yan *et al.*, 2015). When RyR is activated, the helical domain moves outwards; one subpart moves upwards with the NTD, while the other subpart moves downwards (Wei *et al.*, 2016) (Figure 1.4). The two parts of the helical domain are separated by the P2 domain (Yan *et al.*, 2015). This outward and upward or downward movement of the helical domain subparts increases the height and width of the cytoplasmic region substantially, and this change in conformation from closed to open state has been compared to a breathing motion (Wei *et al.*, 2016).

The central domain, forming the other portion of RyR's central tower, interacts with the transmembrane domain (Yan *et al.*, 2015; Samsó, 2017). EF hands are involved in intracellular calcium binding. There are two EF hands in the RyR, formed by the central domain (Xiong *et al.*, 1998). EF hands are a motif found in a large family of calcium-binding proteins and EF hand 1 is likely to be responsible for calcium activation of RyR1

(Wei *et al.*, 2016). Upon activation of the RyR, the EF hands move outward, taking the central domain upwards and outwards. A U-motif of the central domain clamps the C-terminal Domain (CTD), which forms part of the transmembrane stalk of RyR, and the structural change to the central domain is propagated to the CTD, which moves outward (Wei *et al.*, 2016; Samsó, 2017) (Figure 1.4).

The four CTDs of neighbouring RyR subunits touch each other in the closed state of RyR (Samsó, 2017). The CTD is tightly connected to the transmembrane domain (TMD) (Yan *et al.*, 2015). The movement of the CTD, mediated by the movement of the central domain, is propagated to the TMD and results in the channel opening (Wei *et al.*, 2016).

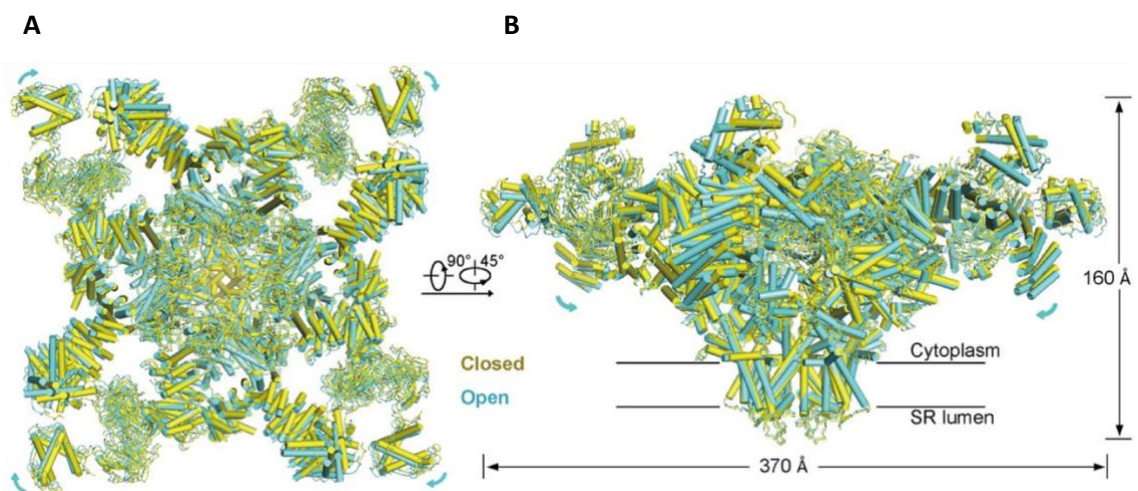


Figure 1.4: Open and closed ryanodine receptor conformation.

Conformation changes between open and closed states for the tetrameric RyR protein, viewed from the cytosol (A) and from within the plane of the membrane (B). The closed state is shown in yellow, and the open state in cyan. The cyan arrows indicated the overall shifts of the cytoplasmic domains from the closed to open state. Adapted from Peng *et al.* (2016) (PDB code 3J8H).

The TMD is made up of six segments (S1-6) (Yan *et al.*, 2015; Zalk *et al.*, 2015). The TMD forms the actual pore of the channel, specifically the S6 segments, which have a hydrophobic constriction site at residue Ile4937, in rabbit RyR1 (Yan *et al.*, 2015). This gate-residue creates a bottleneck when the protein is in the closed state with a pore radius $<1 \text{ \AA}$, which is too small for calcium ions to pass through; the radius of a

hydrated Ca^{2+} ion is 4.1 Å (Volkov *et al.*, 1997). Upon activation of the RyR the movement of the CTD is propagated to the TMD and moves the S6 segment outwards, opening the channel wide enough for calcium ions to move from the SR or ER lumen to the cytosol (Efremov *et al.*, 2015; Yan *et al.*, 2015; Wei *et al.*, 2016).

1.1.3. Control of ryanodine receptor activation

The RyR interacts with a number of proteins to form a macromolecular complex, to regulate calcium release from the SR/ ER. Most of the modulators of the RyR interact with the large cytoplasmic region of the protein (Lanner *et al.*, 2010; Yan *et al.*, 2015). The macromolecular complex that tightly controls calcium release via the RyR reflects the importance of calcium homeostasis in a number of different cell types.

Calmodulin is a calcium binding protein, which regulates all three RyR isoforms by directly binding to the RyR (Chen and MacLennan, 1994; Guerrini *et al.*, 1995).

Calmodulin has been shown to bind to the RyR when bound to calcium (Ca^{2+} -CaM) and when calcium free (apoCaM) (Lanner *et al.*, 2010). At micromolar to millimolar calcium concentrations calmodulin inhibits RyR1, while it activates skeletal muscle calcium release at sub-micromolar calcium concentrations (Tripathy *et al.*, 1995). RyR2, however, does not show activation by apoCaM (Fruen *et al.*, 2000), but does show inhibition by Ca^{2+} -CaM (Meissner and Henderson, 1987).

The DHPR is a voltage dependant calcium channel, which is a key regulator of RyR1 and RyR2 activation in skeletal and cardiac muscle; the DHPR is a key player in E-C coupling. In skeletal muscle the DHPR physically interacts with RyR1 to communicate membrane depolarisation and activate RyR channel opening directly, through allosteric interactions (Ríos *et al.*, 1991; Lee, 2010) (Figure 1.5). In cardiac muscle the DHPR activates RyR2 by calcium induced calcium release (CICR), where calcium influx via the DHPR activates the RyR channel opening (Laver, 2018) (Fabiato, 1983). Calcium ions bind directly to the RyR to activate opening; coupled gating between RyRs can activate neighbouring RyRs (Bers, 2002).

Triadin and junctin are two SR transmembrane proteins that tether calsequestrin (CASQ), a calcium-binding SR luminal protein, close to the release pore of RyR1 and

RyR2 (Györke *et al.*, 2004; Beard *et al.*, 2005). The interaction between CASQ and triadin and junctin regulates RyR1 and RyR2 opening in a calcium dependant manner. The SR luminal calcium concentration is sensed by CASQ, which inhibits the RyR when the calcium concentration is low; triadin/ junctin may be required to mediate this interaction (Györke *et al.*, 2004).

Binding of the protein FKBP12 to RyR decreases the open probability of RyR (Brini, 2004). Four molecules of FKBP12 in skeletal muscle and of FKBP12.6 in cardiac muscle bind to RyR, one per RyR protomer.

Cytosolic calcium can directly activate RyR2, as in CICR described above. Furthermore, cytosolic calcium has been shown to directly activate RyR1 in low, micromolar, calcium ion concentrations by binding to a high-affinity calcium site (Meissner *et al.*, 1986; des Georges *et al.*, 2016). High, millimolar, cytosolic calcium ion concentrations inhibit RyR1 by binding to low-affinity calcium sites. Luminal calcium can also bind to, and regulate, the RyR in a process known as store-overload-induced calcium release (SOICR) (Jones *et al.*, 2017). Calcium ions activate RyR2 by binding to a luminal facing calcium site (Sitsapesan and Williams, 1997), and the negative charge at, or near, residue E4872 in mouse RyR2 was shown to be essential for luminal calcium activation (Chen *et al.*, 2014). The malignant hyperthermia disease-associated RyR1 R615C variant, in pigs, has been shown to increase luminal calcium activation of RyR1, with reduced luminal calcium load required to trigger SOICR (Nelson *et al.*, 1991; Jiang *et al.*, 2008).

Furthermore, RyR channels interact with each other in inter-RyR interactions (Samsó, 2017). In skeletal muscle RyRs self-associate in checkerboard arrays, where each of the four corners of an RyR1 channel interacts with a corner of another RyR1 channel (Yin *et al.*, 2008). The function of this checkerboard pattern is uncertain; every other RyR1 is associated with a DHPR channel, but it does not appear that CICR from these DHPR-associated RyR1s activates non DHPR-associated RyR1s (Ríos *et al.*, 2019). Presumably, the non-DHPR-associated RyR1 channels do not open upon skeletal muscle activation, or they open through an allosteric interaction with the DHPR-associated RyR1s. In cardiac muscle RyR2 homotetramers are organised into clusters, where the number of

channels and distance between adjacent channels effects SR calcium release rate as well as termination of CICR (Cannell *et al.*, 2013).

RyR activity has a central role in skeletal muscle E-C coupling, the canonical process by which an electrical impulse triggers muscle contraction (Figure 1.5A) (Ríos *et al.*, 1991; Calderón *et al.*, 2014). Upon electrical impulse, the sarcolemma is depolarised. Depolarisation is propagated along the sarcolemma and down t-tubules (Calderón *et al.*, 2014). Voltage-sensing DHPRs in the sarcolemma of t-tubules sense the depolarisation, and undergo a conformational change (Ríos *et al.*, 1991). The conformational change to the DHPR results in opening of RyR1 and calcium ion release from the SR. The increase in cytoplasmic calcium ion concentration allows calcium ion binding to troponin C, inducing a conformational change in the troponin-tropomyosin complex and removing tropomyosin from the myosin-binding site on actin, resulting in the myofilaments sliding past each other, achieving muscle contraction (Szent-Györgyi, 1975). Cytoplasmic calcium ions are pumped back into the SR by sarcoplasmic reticulum Ca^{2+} ATPase (SERCA), which allows muscle relaxation. Cardiac muscle contraction is achieved in a similar way, except that RyR2 is activated by CICR upon DHPR activation leading to calcium release from the SR (Periasamy and Kalyanasundaram, 2007).

RyRs also control calcium release from intracellular stores in neural cells, which modulates many important neural processes (McPherson *et al.*, 1991). Neural RyRs are located on the ER close to the presynaptic membrane and the active zone (Bouchard *et al.*, 2003). Upon excitation of the nerve cell, the intracellular calcium concentration rises due to calcium influx through voltage-gated calcium channels (VGCCs). Calcium-induced calcium release (CICR) from the ER via RyR further raises intracellular calcium levels, increasing the signal and increasing the release of neurotransmitters (Narita *et al.*, 2000; Südhof, 2012) (Figure 1.5B).

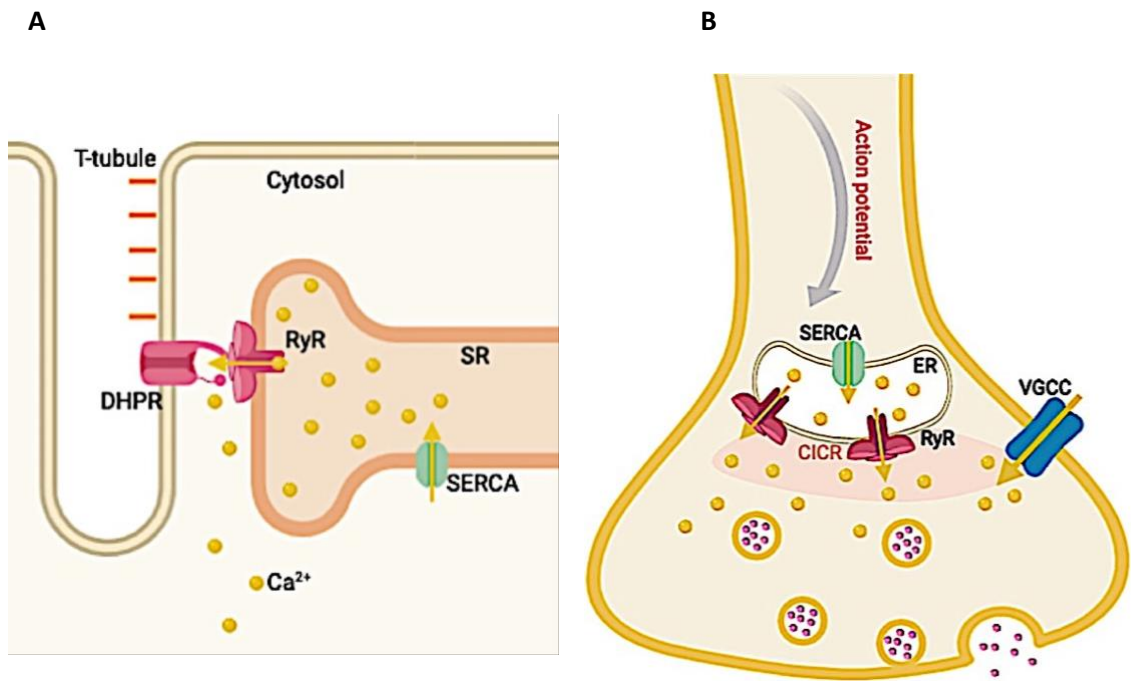


Figure 1.5: Neural and muscular RyRs are activated in different ways.

(A) In skeletal muscle cells RyRs are activated by physical interaction with the dihydropyridine receptor (DHPR), which communicates across the cytosol upon depolarisation of the t-tubule. Calcium ions (yellow spheres) are released from the sarcoplasmic reticulum (SR) and facilitate muscle contraction. (B) Neural RyRs are stimulated to open through calcium induced calcium release (CICR) more like as in cardiac muscle cells. Calcium ion influx via voltage gated calcium channels (VGCCs), upon an action potential reaching the nerve terminal, increases calcium ion concentration of the axoplasm, which activates RyRs to open and release calcium ions from the endoplasmic reticulum (ER). Increased calcium ion concentration of the axoplasm stimulates the release of neurotransmitters (pink spheres). Calcium ions are pumped back into the ER and SR by SERCA (Sarco-/ endoplasmic reticulum Ca^{2+} ATPase pump). Yellow arrows show movement of calcium ions through protein channels. Images were created with BioRender (<https://biorender.com/>) based on information from Bouchard *et al.* (2003) and Lanner *et al.* (2010).

1.1.4. Ryanodine receptor related diseases

The vital role that RyR plays in intracellular calcium homeostasis is highlighted by the number and range of disorders that RyR dysfunction is associated with. The range of

human disorders that RyR plays a role in were described and discussed in a review by Kushnir *et al.* (2018) (Figure 1.6).

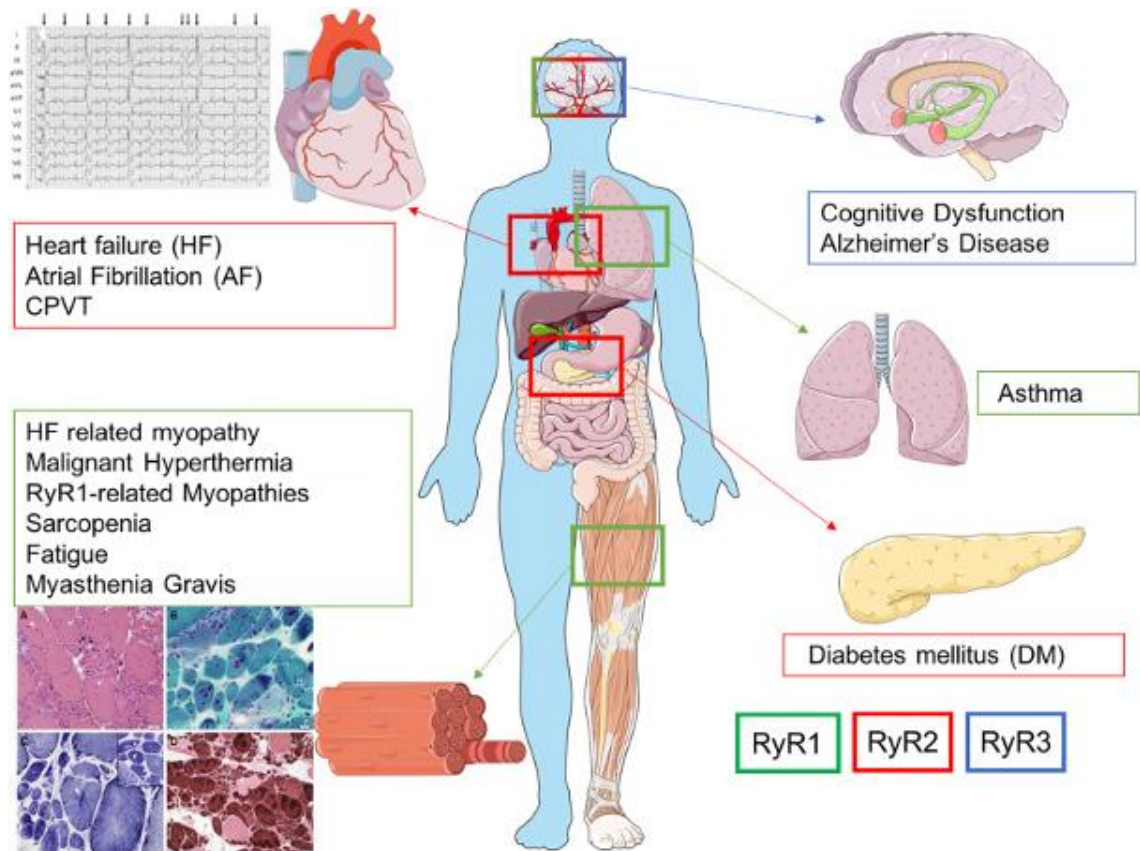


Figure 1.6: Pathologies and tissues affected by RyR dysfunction.

Organ systems with pathologies that are associated with dysfunction of RyRs. Coloured boxes indicate the RyR isoform associated with the pathology and tissue. Note that RyR3 is also found in skeletal muscle at lower levels than RyR1. The ECG (top left) is from a patient with catecholaminergic polymorphic ventricular tachycardia (CPVT). Histology images (bottom left) are from patients with RYR1-related central core disease (CCD) and multi-minicore disease (MmD). Adapted from Kushnir *et al.* (2018).

Mutations in *RYR1* cause a number of myopathies, including malignant hyperthermia (MH) and the congenital myopathies central core disease (CCD) and multi-minicore disease (MmD) (MacLennan, 2000; Robinson *et al.*, 2006; MacLennan and Zvaritch, 2011; Rosenberg *et al.*, 2015; Miller *et al.*, 2018). *RYR1*-related disorders are the most frequent of the congenital myopathies, which present as muscle weakness at birth or during the neonatal period (Todd *et al.*, 2018). The prevalence of congenital

myopathies due to a mutation in *RYR1* is estimated at 1:90,000 in the United States (Amburgey *et al.*, 2011). Patients diagnosed with the *RYR1*-related congenital myopathies CCD or MmD may also be 'MH-susceptible'. MH manifests as a hypermetabolic crisis upon exposure to inhalational anaesthetics (Rosenberg *et al.*, 2015; Litman *et al.*, 2018). The prevalence of MH is estimated to range from 1:2-3,000 (Monnier *et al.*, 2002) to 1:100,000 (Brady *et al.*, 2009). MH is more prevalent in males than females (Strazis and Fox, 1993; Islander *et al.*, 2007), and most common in young adults, the mean age of an MH episode is 18.3 years old (Strazis and Fox, 1993; Rosenberg *et al.*, 2007). It was thought that the majority of MH and CCD causing *RYR1* mutations were clustered into three 'hot spot' regions of *RYR1*, the NTD, central domain and CTD (Sei *et al.*, 2004), however many disease causing *RYR1* mutations exist outside of these 'hot spots' (Laforgia *et al.*, 2018). Whole exome sequencing now allows fast and cost-efficient sequencing of all protein coding regions and identification of novel mutations outside of the 'hot spot' regions (Riazi *et al.*, 2014). MH is inherited in an autosomal dominant pattern, RyR1 variants associated with MH susceptibility are most often heterozygous missense changes (Halsall and Hopkins, 2003; Loy *et al.*, 2011; Miller *et al.*, 2018); however, homozygous RyR1 amino acid substitutions have been reported in cases of MH, as well congenital myopathies (Carpenter *et al.*, 2009a; Riazi *et al.*, 2018). MH has been associated with over two hundred heterozygous single amino acid missense mutations in *RYR1* with 50 being functionally characterised and a list of 48 being considered diagnostic by the European Malignant Hyperthermia Group (The European Malignant Hyperthermia Group, n.d.). While MH is often referred to as asymptomatic without a triggering agent, *RYR1*-related myopathies, such as CCD and MmD, are associated with cores in muscle biopsies and muscle weakness (MacLennan, 2000; Robinson *et al.*, 2006; Illingworth *et al.*, 2014; Laforgia *et al.*, 2018). RyR1 mutations have also been associated with age-related muscle weakness and blocking leaky RyR1 channels increased muscle strength in mouse models (Andersson *et al.*, 2011; Løseth *et al.*, 2013). Age-related muscle degeneration is known as sarcopenia.

The predominant cardiac and smooth muscle RyR isoform, RyR2, has been associated with heart failure and arrhythmias (Dobrev and Wehrens, 2014). Catecholaminergic polymorphic ventricular tachycardia (CPVT) is characterised by an abnormal heart

rhythm, an estimated 60% of CPVT cases have been attributed to single amino acid missense mutations in *RYR2* (Priori *et al.*, 2001; Ackerman *et al.*, 2011). Changes in the structure and function of the RyR2 channel in the heart are thought to result in an increase in calcium ion leakage from the sarcoplasmic reticulum via RyR2, which has been linked to atrial fibrillation (Shan *et al.*, 2012). Arrhythmogenic right ventricular cardiomyopathy is another cardiac pathology reportedly caused by mutations in *RYR2*, as well as a number of other genes (Ohno, 2016). Arrhythmogenic right ventricular cardiomyopathy is a cause of sudden cardiac death in young people. Furthermore, altered calcium signalling in the heart of type 1 diabetic animals has been associated with *RYR2* (Yaras *et al.*, 2005). Patients with diabetes have a two-fold increased risk of sudden cardiac death, with over 50% of patients suffering from cardiovascular complications (Hamilton and Terentyev, 2018). In diabetic rat models SR calcium content was reduced, as were the number of ryanodine binding sites, suggesting that the capacity of the SR to store and release calcium was reduced (Yu *et al.*, 1994).

All three isoforms of RyR have been found in the brain (Furuichi *et al.*, 1994; Giannini *et al.*, 1995; Hertle and Yeckel, 2007; Galeotti *et al.*, 2008; Liu *et al.*, 2012; Abu-Omar *et al.*, 2018). Intracellular calcium leak has been associated with cognitive dysfunction after brain trauma (Deshpande *et al.*, 2008). RyR2 in mouse models of post-traumatic stress disorder had elevated ER calcium leak, suggesting a role of RyR2 in cognitive dysfunction (Liu *et al.*, 2012). Further evidence of RyR dysfunction effecting cognitive function is the link made between RyRs and Alzheimer's disease (AD). AD is characterised by extracellular beta-amyloid plaques in the brain, which has been associated with calcium dysregulation (LaFerla, 2002; Itkin *et al.*, 2011). Links have been suggested between the accumulation of beta-amyloid plaques and RyR activity (Stutzmann *et al.*, 2006; Demuro *et al.*, 2010). Blocking RyRs has been shown to reduce beta-amyloid plaques as well as slowing down memory and learning deficits in AD mouse models (Oulès *et al.*, 2012).

1.1.5. Malignant hyperthermia and its triggering agents

Malignant hyperthermia (MH) is a potentially fatal disorder, whereby pharmacological agents interfere with calcium ion regulation. When a genetically susceptible patient

undergoing surgery receives an inhalational anaesthetic, a hypermetabolic crisis is triggered (Robinson *et al.*, 2006; Hopkins, 2011; Litman *et al.*, 2018).

Single amino acid missense mutations in *RYR1* do account for the majority of MH cases; screening MH susceptible (MHS) families for genetic variants found that 76% of a European Caucasian MHS population carried a variant in *RYR1* (Miller *et al.*, 2018). However, pathogenic MH variants have also been identified in *CACNA1S*, which encodes the alpha 1 subunit of the DHPR; there are two *CACNA1S* mutations accepted as diagnostic MH variants by the EMHG (Weiss *et al.*, 2004; Eltit *et al.*, 2012). A homozygous mutation in *STAC3* has also been linked to MH susceptibility in one Native American family (Horstick *et al.*, 2013) and has also been found in a patient from the Middle East (Miller *et al.*, 2018). *STAC3* encodes a protein that is involved in trafficking of the DHPR to the correct position in the t-tubules (Polster *et al.*, 2015). The RyR, DHPR and *STAC3* proteins all have a role in skeletal muscle E-C coupling (Bannister, 2016). Not all cases of MH are explained by genetic variants in these three genes, and an estimate of 14%-23% of MHS families do not have a mutation in *RYR1*, *CACNA1S* or *STAC3* (Miller *et al.*, 2018).

During an MH crisis, triggering agents induce prolonged opening of RyRs, allowing the myoplasmic calcium ion concentrations to increase outside normal bounds in all skeletal muscle cells, resulting in sustained muscle contraction. There is an increased demand for ATP production, to keep up with energy requirements of sustained muscle contraction (Hopkins, 2000); mitochondria are the main site for ATP synthesis. Higher mitochondrial content, but impaired mitochondrial function, has been found in skeletal muscle of MHS patients, and exposure to halothane increased mitochondrial respiratory states in MHS skeletal muscle samples (Chang *et al.*, 2019). Beyond sustained muscle contraction, oxygen consumption is enhanced while excessive heat and carbon dioxide are produced, correlating with increased mitochondrial activity. Eventually, ATP production fails to keep up with the energy demands of the sustained muscle contraction (Hopkins, 2000; Chang *et al.*, 2019). The final stage of an MH crisis is muscle rigidity, hypoxemia, acidosis and rhabdomyolysis (Monnier *et al.*, 1997; Hopkins, 2000). Without rapid treatment, an MH episode can result in death of the patient. However, treatment is available. Dantrolene blocks the ryanodine receptor,

countering the effects of halothane and allowing the muscle to relax (Paul-Pletzer *et al.*, 2002 ; Riazi *et al.*, 2014).

Volatile anaesthetics, including halothane, isoflurane, sevoflurane and desflurane, are known MH triggering agents (Hopkins, 2011). Also implicated as a triggering agent is succinylcholine, a muscle relaxant, although this remains controversial (Kunst *et al.*, 1999; Hopkins, 2011). Exertional heat illness (EHI) has been linked to MH, where exposure to heat or vigorous exercise stress triggers a response similar to that seen by inhalational anaesthetics in MH (Hopkins *et al.*, 2016; Gardner *et al.*, 2020), indeed a high proportion of EHI patients tested positive in the diagnostic *In Vitro* Contracture Test (IVCT) used to detect MH susceptibility (Hopkins *et al.*, 2015; Gardner *et al.*, 2020).

In cases where patients are known or suspected to be MHS, non-volatile inhalational anaesthetics or intravenous anaesthetics are used for patients requiring surgery (Halsall and Hopkins, 2003). Diagnosing MH is important to ensure that patients receive appropriate care. Where there is a known MH-diagnostic variant present in the family, genetic diagnosis is possible. Where a variant is not known, but a relative is designated MHS, an IVCT can provide diagnosis of MH (Ellis *et al.*, 1984; Riazi *et al.*, 2014; Hopkins *et al.*, 2015).

The IVCT discriminates MHS and non-susceptible (MHN) patients based on the sensitivity of a muscle biopsy to incrementally increasing concentrations of caffeine and halothane and measurement of the muscle contraction in response to the applied triggering agents (Carpenter *et al.*, 2009b). A patient may be designated MHSc (caffeine) or MHS_h (halothane), if they show hypersensitivity to only one of the stimulants (Gupta and Hopkins, 2017). Discordance between *RYR1* genotype and IVCT phenotype has been reported; individuals may carry an *RYR1* familial mutation but have an MHN IVCT phenotype or individuals may have an MHS IVCT phenotype but not carry the familial *RYR1* mutation (Deufel *et al.*, 1995; Adekun *et al.*, 1997; Robinson *et al.*, 2003; Miller *et al.*, 2018). This suggests there are additional loci, which modify the response to the IVCT.

Halothane is listed on the WHO Essential Medicines List for inhalational anaesthetics (World Health Organization, 2019). Halothane, as with most general anaesthetics, acts by potentiating the inhibitory GABA_A receptor (Scholfield, 1980), as well as desensitising the nicotinic acetylcholine receptor (nAChR) (Firestone *et al.*, 1994), possibly through a conformational change to the nAChR upon application of clinical concentrations (Lin *et al.*, 1995). Although not the only anaesthetic MH trigger as mentioned previously, halothane is the volatile anaesthetic most associated with MH.

1.2. *Caenorhabditis elegans* as a model

Caenorhabditis elegans is a model laboratory system in which MH could be studied. This species is a free-living nematode worm (Figure 1.7). First used as a model organism for genetic study of the neural system by Sydney Brenner in the early 1960s (Brenner, 1973; Brenner, 1974), *C. elegans* has proven to be a useful model for neural development, as well as many other research areas.

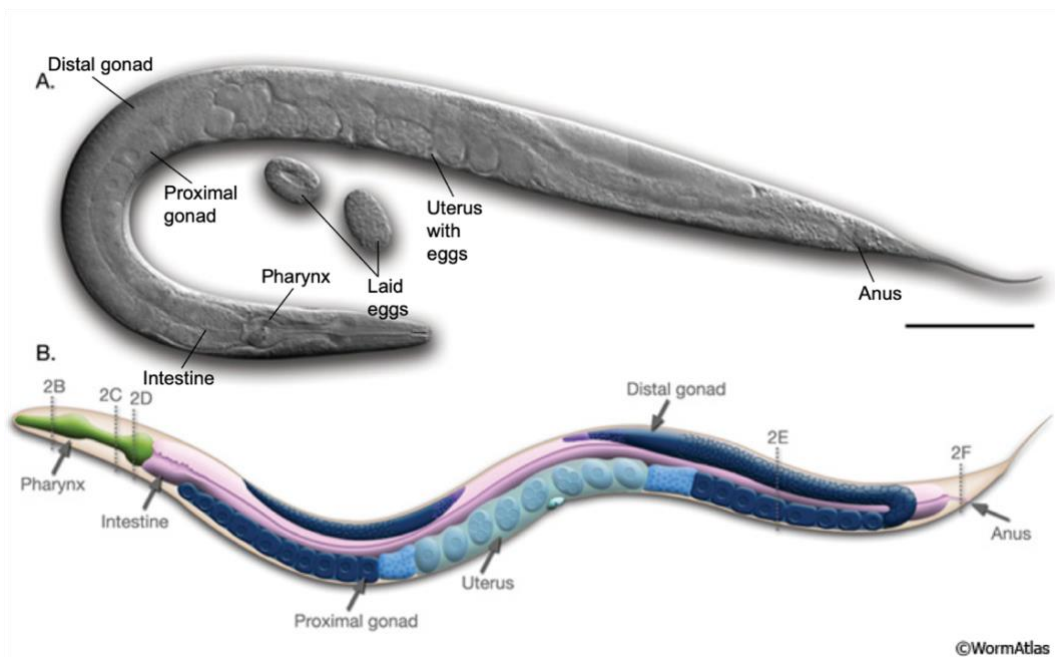


Figure 1.7: *C. elegans* anatomy.

(A) Differential interference contrast (DIC) image of an adult hermaphrodite *C. elegans*. Scale bar is 0.1 mm. (B) Schematic of anatomical structures. Figure adapted from Altun and Hall (2009a).

The main benefits of 'the worm' for use as a model organism are its small size of approximately 1 mm as an adult, transparent body and short life span. Its small size

allows culture of large numbers of animals easily within a laboratory environment (Stiernagle, 2006). The transparency of the worm has allowed its cell lineage to be mapped from zygote to adult (Sulston and Horvitz, 1977; Sulston *et al.*, 1983), and the discovery of genes that control apoptosis in *C. elegans*, which led to the award of the 2002 Nobel Prize in Medicine (Brenner, 2003; Horvitz, 2003; Sulston, 2003). The short lifespan of the worm also makes it a convenient animal for studying development and ageing.

A further benefit of *C. elegans* is its hermaphroditic lifestyle. Individuals are able to self-fertilise. This is especially beneficial in genetic studies; a single homozygote hermaphrodite can generate an entire population of genetically identical offspring. Males are generated at a low frequency, allowing for crosses between different strains. The worm was the first multicellular organism to have its whole genome sequenced (The *C. elegans* Sequencing Consortium, 1998). It also has its neuronal wiring diagram fully mapped (White *et al.*, 1986). Although the worm has a much more compact genome than humans, it contains a similar number of genes, furthermore 83% of the *C. elegans* proteome has human homologous genes (Lai *et al.*, 2000). Genetic studies in the worm have been extremely useful for modelling human diseases with approximately 42% of human disease genes having an orthologue in *C. elegans* (Markaki and Tavernarakis, 2010).

By studying genetic mutant phenotypes in *C. elegans* the functions of genes can be discerned (Fire *et al.*, 1998). Many methods of genetic manipulation have been applied to *C. elegans*, including both forward and reverse mutagenesis. Initially, Sydney Brenner used a chemical mutagen to induce mutations in the germline and studied the behaviour of *C. elegans* resulting from these mutations (Brenner, 1974). Brenner named mutants and genes based on the phenotype produced. For example, uncoordinated, or *unc* mutants, were any mutants with detectable defects in the smooth sinusoidal wave movement exhibited by wild type *C. elegans*. *unc* genes are usually associated with muscle or neural function. Such screens have been vital in understanding many biological processes in *C. elegans* which are also relevant in humans. The million mutation project is a collaborative effort studying 2007 *C. elegans* strains mutagenized by chemical mutagens (Thompson *et al.*, 2013). By sequencing

these strains, with multiple mutations in each strain, it was possible to identify multiple mutations in almost every gene. Projects such as this demonstrate the ease of genetic manipulation in *C. elegans*.

Specifically targeting mutagenesis at a single gene, and observing the resulting phenotype, identifies the specific contributions of that gene to biological processes and disorders. Gene function can be studied by knockdown of target genes through RNA interference (RNAi); feeding, injecting or soaking *C. elegans* with double stranded RNA results in targeted degradation of its cognate mRNA (Fire *et al.*, 1998; Tabara *et al.*, 1998; Timmons and Fire, 1998). Generating transgenic *C. elegans* that express foreign DNA allows expression of altered genes, as well as gene fusions to reporters, such as fluorescent protein genes (Rieckher *et al.*, 2009). Microinjection of foreign DNA into the worm's gonad or microparticle bombardment whereby gold microparticles are coated with DNA and then fired at high speeds at worms are two methods for introducing foreign DNA into the worm (Praitis *et al.*, 2001; Rieckher *et al.*, 2009). DNA that reaches the germline can be replicated and inherited through subsequent generations. Transgenic animals generated in these ways usually carry the transgenes in heritable extrachromosomal DNA arrays. However, these large extrachromosomal arrays have some drawbacks including incomplete inheritance, gene overexpression and gene silencing (Nance and Frøkjær-Jensen, 2019). Microparticle bombardment provides a higher rate of integration of the transgene into the chromosomes, but with risks of simultaneous chromosomal rearrangements. More recently, precise, heritable genome editing of endogenous gene loci has been developed (Jinek *et al.*, 2012). CRISPR-Cas9 genome editing can be used to precisely edit the *C. elegans* genome with relative ease.

CRISPR (Clustered Regularly Interspersed Short Palindromic Repeats) DNA repeats and associated Cas proteins have been identified in bacteria and archaea, providing the organisms with an adaptive antiviral defence system (Barrangou, 2015). In 2005 it was found that spacer sequences, non-repetitive elements, within the CRISPR loci of bacteria were often identical to sequences from bacteriophages (Bolotin *et al.*, 2005; Pourcel *et al.*, 2005; Mojica *et al.*, 2005). It is now appreciated that the integration of bacteriophage DNA into the CRISPR loci of bacteria provides adaptive immunity,

similar to the RNA interference mechanism utilised by eukaryotes (Sorek *et al.*, 2013). The CRISPR-Cas system provides adaptive immunity through a three-step process; adaptation, expression and interference. The repeat spacer is transcribed and processed as interfering CRISPR RNAs (crRNAs). The crRNAs guide the Cas proteins to the complementary sequence for sequence-specific targeting, cleavage and degradation of the foreign DNA (Barrangou, 2015).

In 2012 it was proposed by Jennifer Doudna and Emmanuelle Charpentier that the CRISPR-Cas9 system could be used to precisely edit genomes (Jinek *et al.*, 2012). This is arguably one of the most significant and exciting discoveries in modern biology. In *C. elegans* a number of strategies have been proposed allowing researchers to make, essentially, any desired change to the genome (Dickinson and Goldstein, 2016). Briefly, a single guide RNA (sgRNA) with a specific sequence upstream allows the Cas9 protein to cleave DNA, while a 20-bp downstream guide sequence directs the Cas9 to the sequence of choice within the genome (Figure 1.8). In human cells, double stranded breaks are repaired by non-homologous end joining (NHEJ), however this repair mechanism is error-prone and induces insertions and deletions (indels), which disrupt gene function. Homology directed repair (HDR) allows incorporation of precise modifications where, along with the sgRNA and Cas9, an exogenous DNA molecule is introduced to serve as a repair template (Zhang *et al.*, 2014). The donor DNA has arms homologous to the endogenous DNA, with the desired edit in between. Introduction of these components into the germline allows precise modification of the genome in a heritable fashion. In *C. elegans* CRISPR-Cas9 can be employed to generate specific mutations.

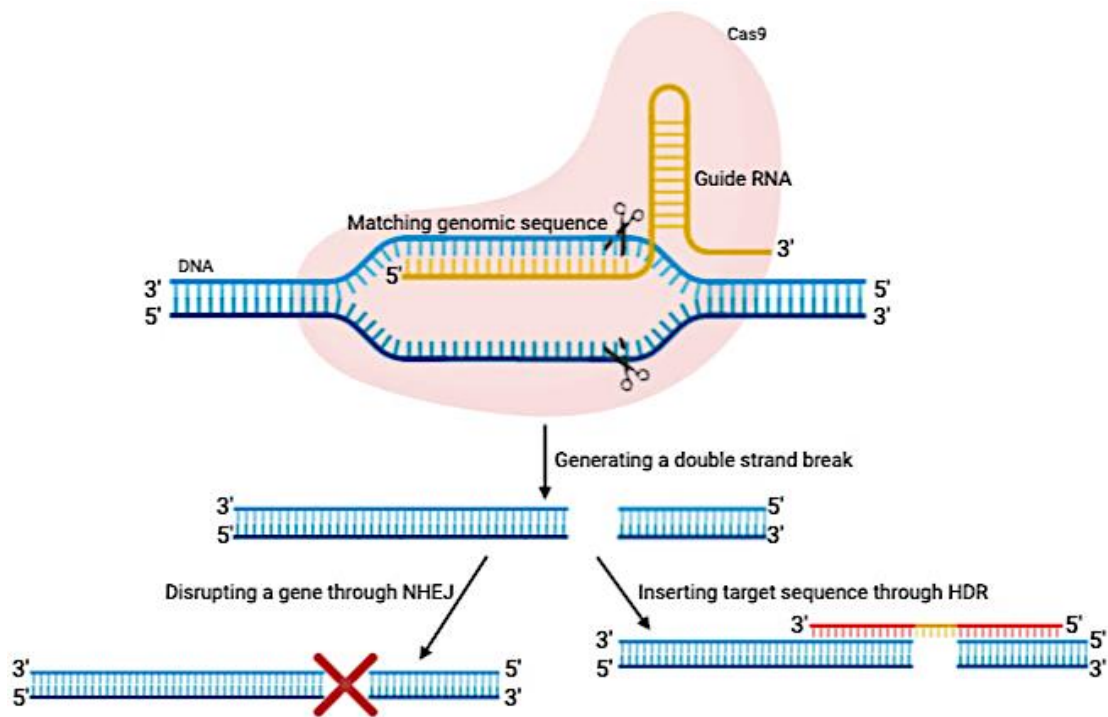


Figure 1.8: CRISPR-Cas9 genome editing.

A guide RNA with a specific upstream sequence forms a complex with the Cas9 protein. A 20-bp sequence that is complementary to the target genomic sequence guides the Cas9 protein to create a double stranded break in the desired region of the genome. Double stranded breaks repaired by non-homologous end joining (NHEJ) produce small insertions and deletions, which can disrupt the gene. Providing a template for homology-directed DNA repair (HDR) allows insertion of a specific desired sequence. The image was created with BioRender (<https://biorender.com/>), and based on information from Dickinson and Goldstein (2016)

Over the past years efforts have been made to innovate the CRISPR-Cas9 system with advancements in ease, accuracy and efficiency. While HDR allows for precise DNA changes, after inducing double stranded breaks, it may result in indels from end-joining repair of the double stranded breaks and is not very efficient. A system called 'base editing' results in C to T or G to A substitution without needing to generate a double-strand break (Komor *et al.*, 2016). Fusions of a catalytically impaired Cas9 nickase and a base modification enzyme were engineered to be programmed by a guide RNA and operate on single stranded DNA. A DNA nickase can generate a single-stranded cut, 'nicking' rather than cutting the DNA (Gasiunas *et al.*, 2012). Base pairing between the guide RNA and target DNA displaces a small segment of single stranded

DNA, which allows modification of DNA bases within this segment by the base modification deaminase enzyme (Rees and Liu, 2018). The catalytically disabled Cas9 generates a nick in the non-edited DNA strand to induce repair of the non-edited strand, using the edited strand as a template. However, base editing cannot perform all twelve transversion mutations but the development of prime editing allows this (Anzalone *et al.*, 2019). Prime editing allows for targeted insertions, deletions and all base-to-base transversions without requiring double stranded breaks or donor homology templates. Instead prime editing uses a reverse transcriptase fused to a nickase, and a prime editing guide RNA to copy genetic information directly from an extension on the prime editing guide RNA into the genomic locus (Anzalone *et al.*, 2019).

1.2.1. *C. elegans* as a model for malignant hyperthermia

C. elegans can be a useful model for studying human diseases, ranging from neurodegenerative diseases (Alexander *et al.*, 2014), to cancers (Kirienko *et al.*, 2010), as well as metabolic diseases (Hashmi *et al.*, 2013). Studying human diseases in *C. elegans* may allow better understanding of the cause of particular pathologies as well as the identification of potential therapies (Markaki and Tavernarakis, 2010).

C. elegans has been used previously to study specific RyR disease variants (Fischer *et al.*, 2017; Nicoll Baines *et al.*, 2017). The worm has only one RyR gene, *unc-68*, that produces at least four isoforms confirmed by cDNA, but up to 15 potential isoforms (Wormbase.org, 2016). The longest confirmed UNC-68 isoform is 5201 amino acids in length and shares approximately 40% identity and 60% similarity with all three human RyR isoforms (see Appendix A for BLAST results). The UNC-68 protein is found in body wall muscle, which is striated and could be considered the functional equivalent of human skeletal muscle (Gieseler *et al.*, 2005), the pharynx, which has been compared to the mammalian heart (Mango, 2007), and in neurons (Chen *et al.*, 2017a).

Specific mutations associated with CPVT and RyR2, and MH and RyR1 have been introduced into *C. elegans* as extrachromosomal arrays and the consequences studied (Fischer *et al.*, 2017; Nicoll Baines *et al.*, 2017). At the time of publication, fosmid recombineering was a powerful genetic tool, allowing for introduction of precise point

mutations in large genomic DNA clones (Hirani *et al.*, 2013). For CPVT and RyR2, two RyR2 human disease mutations, R2474S and R4497C, were inserted into UNC-68 through fosmid recombineering; the fosmid used contains a slightly truncated promoter, but expression of this promoter fragment was confirmed in pharyngeal muscles. Transgenic animals were generated by microinjection with the engineered fosmid, and a co-injection mCherry marker, in the deletion mutant TR2171 (*unc-68(r1162)*), which is considered a molecular null (Fischer *et al.*, 2017). Expression of the mutant UNC-68 proteins resulted in complete rescue of the reduced pumping rate observed in the TR2171 (*unc-68(r1162)*) mutant strain. To mirror a rhythmically beating heart, the pharynx was optically paced by expressing channelrhodopsin-2 in the pharyngeal muscle cells (Schüler *et al.*, 2015). One of the extrachromosomal array variant strains, that for the human R4497C RyR2 variant, demonstrated a 'worm arrhythmic' phenotype of decreased ability to follow high rates of paced pumping (Fischer *et al.*, 2017). However, the extra chromosomal array strain for the R2474S human RyR2 variant had no effect on paced pumping ability but did show altered swimming locomotion. The effect on locomotion is likely due to the role of UNC-68 in body wall muscle.

To study specific RyR1 mutations thought to cause MH, fifteen *C. elegans* strains carrying modifications in the *unc-68* gene equivalent to eight RyR1 associated human variants were generated after fosmid recombineering (Nicoll Baines *et al.*, 2017). The eight human RyR1 variants chosen were R163C, G341R, R2163H, R2454H, R2458H, K3452Q, A4940T and R4861H, all of which have conservation of the non-variant residue with *unc-68* in *C. elegans*. One clone of the *C. elegans* Vancouver fosmid library (Perkins *et al.*, 2005), WRM069cA02, contained the entirety of the *unc-68* gene, making it the ideal subject for such recombineering. Successful generation of eight different variant fosmids led to microinjection of these engineered fosmids, with and without the wild type fosmid, into the *unc-68* null strain, CB540 (*unc-68(e540)*) (Nicoll Baines *et al.*, 2017). The CB540 (*unc-68(e540)*) strain carries a point mutation toward the centre of the gene and behaves genetically as a null (Maryon *et al.*, 1996). Rescue of the uncoordinated null phenotype was used to indicate successful introduction of the fosmid as an extrachromosomal array, which was subsequently confirmed by DNA sequencing (Nicoll Baines *et al.*, 2017). All fifteen of these extrachromosomal array

strains demonstrated an MH-related phenotype of hypersensitivity to halothane, an MH trigger and agent used in the IVCT. Sensitivity of these strains to caffeine, another IVCT agent, was found for several strains and demonstrated to depend on neural function. The strains also conferred a subtly but significantly reduced lifespan, as well as an accelerated decline in muscle integrity with age.

The 'worm arrhythmic' and MH-related phenotypes conferred by *C. elegans* when modelling CPVT and MH disease variants in *unc-68* demonstrate that this is a good system for studying RyR-related diseases. However, the use of extrachromosomal array strains has its drawbacks. Firstly, not being at the native locus may affect expression patterns and expression levels (Evans, 2006; Nance and Frøkjær-Jensen, 2019). Previous work found 80 to 300 copies of the transgenic DNA per haploid genome, and this was considered to be an underestimate (Stinchcomb et al., 1985). While a wild type fosmid was injected to generate a control strain in each study (Fischer et al., 2017; Nicoll Baines et al., 2017), each array strain will have different transgene copy numbers. Additionally, strains modelling heterozygosity were generated by injection with a mix of wild type and variant fosmids (Nicoll Baines et al., 2017), but the copy number of the variant and wild type transgene will not be precisely equal. An additional disadvantage of extrachromosomal array strains is the incomplete heredity; not all the progeny of a transgenic animal will inherit the array. This may result in *unc-68* null animals, lacking the transgene, being included in phenotyping assays.

The recent developments in genome editing have led to the opportunity for precise manipulation of *unc-68* at the endogenous locus, via CRISPR-Cas9. Employing this technique allowed for introduction of modifications equivalent to eight human *RYR1* variants associated with MH into the *C. elegans* genome. Seven of the eight RyR1 variants are the same as those introduced into *C. elegans* as extrachromosomal arrays (Nicoll Baines et al., 2017). The variants chosen are all located in RyR residues where the wild type sequence is conserved from humans to *C. elegans*. Such genome-edited strains would express the modified RyR at wild type levels and locations, allowing better assessment of their consequence *in vivo*.

1.3. Focus of this research

1.3.1. Modelling RyR1-related disease in *C. elegans*

RyR1-related myopathies, and predominantly MH, are the most studied of the RyR-related diseases. The Genome Aggregation Database (gnomAD) lists over 2500 missense RyR1 variants (Karczewski *et al.*, 2019), while the European Malignant Hyperthermia Group (EMHG) recognise 48 RyR1 variants as diagnostic of MH (The European Malignant Hyperthermia Group, n.d.). Although this means under 2% of the listed variants on gnomAD have been demonstrated to be causative of MH (Urwyler *et al.*, 2001), other RyR1 variants not on the EMHG diagnostic list have been found in MHS families (Tammaro *et al.*, 2011; Miller *et al.*, 2018) although these have not been functionally characterised. Furthermore, additional RyR1 missense variants have been associated with other RyR1-related myopathies such as CCD (Lynch *et al.*, 1999; MacLennan, 2000; Chen *et al.*, 2014). Understanding the consequences of RyR1 variants is important due to the number of RyR1 variants found within the human population and because calcium mishandling has many consequences.

While MH is typically considered asymptomatic in the absence of a triggering agent, some of the other RyR1-related myopathies do have overt phenotypes, such as muscle weakness (MacLennan, 2000; Robinson *et al.*, 2006; Illingworth *et al.*, 2014; Laforgia *et al.*, 2018). Consequences of RyR1 variants in the absence of an MH-triggering agent requires further research and understanding.

This research aims to understand subtle consequences of RyR1 variants introduced into *C. elegans unc-68*, at the endogenous locus. The use of CRISPR-Cas9 genome editing to express RyR1 variants differs from previous work with extrachromosomal arrays where overexpression may have exacerbated or masked consequences (Nicoll Baines *et al.*, 2017).

1.3.2. Pre- and postsynaptic effects of *RYR1* gene variants

Studying RyR variants in *C. elegans* has uncovered a role of these variants presynaptically (Nicoll Baines *et al.*, 2017; Ferreira and Kalogeropoulou, 2019). The hypersensitivity to caffeine observed for several RyR variant extrachromosomal array

strains was eliminated or reduced in the presence of RNAi targeting genes for chemosensory nerve function (Nicoll Baines *et al.*, 2017). UNC-68 has been found in neurons (Chen *et al.*, 2017a), and as the only RyR in *C. elegans* is required to fulfil all RyR function. However, the presence of RyR1 in mammalian brain increases the significance of the effects of these *unc-68* mutations equivalent to known *RYR1* gene variants in *C. elegans* nerve cells. Therefore, this research also aims to further understand and discern the pre- and postsynaptic consequences of such RyR variants.

1.4. Thesis outline

To investigate the subtle consequences of RyR1 variants as well as discern their pre- and postsynaptic effects in *C. elegans*, I conducted a number of phenotypic assays on strains genetically engineered to express RyRs equivalent to known human myopathic RyR1 variants, at the endogenous level. To validate the use of these strains as a model for MH, I assayed responses to the MH triggering agent halothane. As some RyR1 variants cause age-related disorders, I examined the response of both young adult and old adult *C. elegans* to the triggering agent. Subtle locomotion defects were detected in liquid in the absence of the triggering agent and had not been seen before for *C. elegans* strains carrying RyR variants equivalent to RyR1 disease variants. To further explore these defects, the locomotion of these strains was further investigated in a thorough analysis of *C. elegans* crawling. The effects of RyR variants on locomotion in aged animals are also described. To assess the pre- versus postsynaptic contributions of these RyR1 variants to altered phenotype in *C. elegans*, two cholinergic pharmacology assays, aldicarb and levamisole, were pursued. The phenotypic effects of these variants when present in the heterozygous state was also characterised. Finally, the potential implications of my findings with *C. elegans* for human biology and disease are considered.

Chapter 2

General Methods

2.1. *C. elegans* maintenance and strains

2.1.1. *C. elegans* maintenance

Animals were maintained at 20°C, on 50 mm plates of nematode growth medium (NGM) (3 g NaCl, 17 g Agar, 2.5 g Peptone in 975 ml water, autoclaved and cooled to 55°C before addition of 1 ml 1 M CaCl₂, 1 ml 1 M MgSO₄, 1 ml cholesterol (5 mg/ml in ethanol) and 25 ml 1 M KPO₄ (pH 6), and pouring) (Stiernagle, 2006). Plates were seeded with 150 µl of an OP50 *Escherichia coli* overnight culture, grown in LB broth. When ageing *C. elegans*, animals were maintained on 90 mm plates of NGM plates containing 50 µM FUdR, seeded with 450 µl of OP50 (see section 2.3.2).

2.1.2. *C. elegans* strains

The RyR null strain CB540 (*unc-68(e540)*) was obtained from the MRC-LMB, Cambridge (Table 2.1). The RyR variant strains were generated at the University of Leeds and by NemaMetrix by microinjection of the N2 Bristol strain, described below. Heterozygous *unc-68* variant / wild type and control individuals were generated by mating. N2 wild type males, from stocks maintained at Leeds, were mated with hermaphrodites of the *unc-119* fluorescent reporter strain OH441 (*otIs45[unc-119::gfp]*), provided by the Caenorhabditis Genetics Center, in a 3:2 male to hermaphrodite ratio on 50 mm plates seeded with 150 µl of OP50 to generate large numbers of *otIs45[unc-119::gfp]* / wild type heterozygous cross progeny. Males from this cross were then mated with *unc-68* variant homozygous hermaphrodites or CB540 (*unc-68(e540)*) or N2 wild type hermaphrodites in a 4:2 male to hermaphrodite ratio on 50 mm plates seeded with 150 µl of OP50. Hermaphrodites carrying the GFP marker as a result of this second cross were assayed.

The different N2 wild type backgrounds used to generate the RyR variant strains were assessed for differences prior to comparison of the RyR variant strains (Chapter 3).

Table 2.1. *C. elegans* strains used in this research.

Strain (Allele)	<i>unc-68</i> Variant	Obtained from/ Generated by
CB540 (<i>unc-68(e540)</i>)	Null	MRC-LMB (Cambridge)
OH441 (<i>otIs45[unc-119::gfp]</i>)	WT	Caenorhabditis Genetics Center
UL4239 (<i>le4239</i>)	hR163C	Generated at the University of Leeds
UL4285 (<i>le4285</i>)	hN2342S	Generated at the University of Leeds
COP1879 (<i>knu765</i>)	hG341R	Generated by NemaMetrix
COP1883 (<i>knu769</i>)	hR2163H	Generated by NemaMetrix
COP1947 (<i>knu825</i>)	hR2454H	Generated by NemaMetrix
COP1944 (<i>knu822</i>)	hR2458H	Generated by NemaMetrix
COP1932 (<i>knu810</i>)	hK3452Q	Generated by NemaMetrix
COP1950 (<i>knu828</i>)	hR4861H	Generated by NemaMetrix
N2 "NemaMetrix"	WT	Obtained from NemaMetrix
N2 "Leeds"	WT	MRC-LMB (Cambridge)

2.2. Generating strains through CRISPR-Cas9 genome editing

Specific modifications were made to the *C. elegans* genome, corresponding to known *RYR1* human disease variants, by CRISPR-Cas9 genome editing (Table 2.2). UL4239 (hR163C) (*le4239*) and UL4285 (hN2342S) (*le4285*) were generated at the University of Leeds by David Pertab and Alex Jubb from an N2 Bristol strain obtained from the MRC-LMB, Cambridge. Strains COP1879 (hG341R) (*knu765*), COP1883 (hR2163H) (*knu769*), COP1947 (hR2454H) (*knu825*), COP1944 (hR24548H) (*knu822*), COP1932 (hK3452Q) (*knu810*), and COP1950 (hR4861H) (*knu828*) were designed by me and generated by NemaMetrix, through injection of an N2 Bristol strain maintained by NemaMetrix.

Table 2.2. Aligned *unc-68* nucleic acid sequence and encoded amino acid sequence for wild type and the variant strains after genome editing.

Strain		Alignment
UL4239 (hR163C)	WT	GCATCCAAACAAAGATCAGAAGGAGAAAAGGTGCGCGTCCGGTGATGACGTCATTTTGGTCTCA
	VAR	GCATCCAAACAAAGATCAGAAGGAGAAAAAGTCTGTGTCGGTGATGACGTCATTTTGGTCTCA
	WT	A S K Q R S E G E K V <u>R</u> V G D D V I L V S
	VAR	A S K Q R S E G E K V <u>C</u> V G D D V I L V S
COP1879 (hG341R)	WT	AAATGCTACAATCAGATATGGAGAGACAAATGCTTTTATTCAACACGTGAAAACCTCAGCTCTGG
	VAR	CAACGCCACCATTAGATATAAGAGAGACAAATGCTTTTATTCAACACGTGAAAACCTCAGCTCTGG
	WT	N A T I R Y <u>G</u> E T N A F I Q H V K T Q L W
	VAR	N A T I R Y <u>R</u> E T N A F I Q H V K T Q L W
COP1883 (hR2163H)	WT	TTCCTGGTGACCTCATACAAATCCGCGAGCTTCTTACCGTACAATTTGAGCATACTGAAGAG
	VAR	TTCCTGGTGACCTCATCCAGATTCACGAGCTTCTTACCGTACAATTTGAGCATACTGAAGAG
	WT	F L V Y L I Q I <u>R</u> E L L T V Q F E H T E E
	VAR	F L V Y L I Q I <u>H</u> E L L T V Q F E H T E E
UL4285 (hN2342S)	WT	GATTTCTGAGATTCTGTGTCTGGATCAATGGGGAAAACGTGGAAGAAAATGCAAATCTTGTC
	VAR	GATTTCTGAGATTCTGTGTCTGGATATCTGGGGAAAACGTGGAAGAAAATGCAAATCTTGTC
	WT	D F L R F C V W I <u>N</u> G E N V E E N A N L V
	VAR	D F L R F C V W I <u>S</u> G E N V E E N A N L V
COP1947 (hR2454H)	WT	CCAATGGCTATACAG <i>INTRON</i> GCCGGAAAAGGAGATTCTCTTCGCGCTCGTGCTATTCTCAGATCTCTTATTTCACTCGACGATCTTGGTCAGATCTTGGCTCTAAGATTTACAATCCCC
	VAR	CCATATGGCCATCCAA_____GCTGGTAAGGGTGACTCCCTCCGTGCCACGCCATCCTCCGTTCCCTCATCTCCCTIGATGACCTCGGACAAATCCTCGCCCTCCGTTTCACCATITCCA
	WT	P M A I Q A G K G D S L R A <u>R</u> A I L R S L I S L D D L G Q I L A L R F T I P
	VAR	P M A I Q A G K G D S L R A <u>H</u> A I L R S L I S L D D L G Q I L A L R F T I P
COP1944 (hR2458H)	WT	CCAATGGCTATACAG <i>INTRON</i> GCCGGAAAAGGAGATTCTCTTCGCGCTCGTGCTATTCTCAGATCTCTTATTTCACTCGACGATCTTGGTCAGATCTTGGCTCTAAGATTTACAATCCCC
	VAR	CCATATGGCCATCCAA_____GCTGGTAAGGGTGACTCCCTCCGTGCCACGCCATCCTCCGTTCCCTCATCTCCCTIGATGACCTCGGACAAATCCTCGCCCTCCGTTTCACCATITCCA
	WT	P M A I Q A G K G D S L R A R A I L <u>R</u> S L I S L D D L G Q I L A L R F T I P
	VAR	P M A I Q A G K G D S L R A R A I L <u>H</u> S L I S L D D L G Q I L A L R F T I P
COP1932 (hK3452Q)	WT	ACGGACGGAGTATATGAAAATGTAGTGTTCATCTTCCGTATTTGGAGTCAAAGTCAACATTTCAACGTTGAAGAGCTGAACTATGTGGCTCAATTTGAA
	VAR	ACCGACGGCGCTCTACGAGAACGTCGCCGTCATTTTCAAGATCTGGTCCCAATCCCAACACTTCCCAACGCGAGGAGCTCAACTACGTCGCCCAATTCGAA
	WT	T D G V Y E N V A V I F R I W S Q S Q H F <u>K</u> R E E L N Y V A Q F E
	VAR	T D G V Y E N V A V I F R I W S Q S Q H F <u>Q</u> R E E L N Y V A Q F E
COP1950 (hR4861H)	WT	ACACTTGTAGTCGTGTATCTCTACACTGTCATCGCGTTCAATTTCTTCCGTAATTTCTATGTTCAAGAGGGTGAAGAGGGCGAAGAG
	VAR	ACCCTCGTCTAGTCTACCTCTATACCGTCATTCGCTTCAACTTTTCCACAAGTTCTACGTCGAAGAGGGAAGAGGGCGAAGAG
	WT	T L V V V Y L Y T V I A F N F F <u>R</u> K F Y V Q E G E E G E E
	VAR	T L V V V Y L Y T V I A F N F F <u>H</u> K F Y V Q E G E E G E E

Bold underlined bases and amino acids correspond to the point mutations that change the amino acid sequence. Red underlined residues correspond to all mutations in the variant genomic sequence, including silent mutations introduced to prevent re-editing of the genome during strain generation. The intron (grey) in the wild type has been deleted in the COP1947 (hR2454H) and COP1944 (hR2458H) mutant strains.

Different approaches were used to introduce single amino acid changes to UNC-68 by the University of Leeds and NemaMetrix. The six RyR variant strains generated at NemaMetrix were injected with two single guide RNAs (sgRNAs), Cas9 protein and a single stranded DNA (ssDNA) donor homology oligonucleotide into the distal gonads of N2 Bristol strain animals. The two 20 nucleotide (nt) sgRNAs guide cutting of the genome, in the location of intended modification, by the Cas9 protein (Figure 2.1). The 3' end of the binding site for each sgRNA target sequence must have a proto-spacer adjacent motif (PAM) sequence (NGG); the 20 nt sgRNA sequence is complementary to the 20 nts upstream of the PAM sequence in the genome. The Cas9 protein cleaves the DNA approximately three nucleotides upstream of the PAM sequence, generating two double-stranded breaks in the DNA, either side of the desired edit.

The ssDNA oligonucleotide guides repair of the cut genome to include specific missense mutations corresponding to known RyR1 disease variants, as well as silent mutations to prevent re-cutting of the genome by Cas9. The ssDNA oligonucleotide also has 35 nts of unmodified sequence either side, known as the left and right homology arms, which guide homology direct repair (HDR). Silent mutations, or 'recoding' are changes made to the nucleotide sequence that do not alter the amino acid sequence. Up to every 6th nucleotide between the left and right homology arms was changed to induce a silent mutation in the protein sequence. The homology arms complement the sequence either side of the Cas9 cut sites, starting 3 nucleotides upstream of the PAM sequence.

The COP1947 (hR2454H) and COP1944 (hR2458H) mutant strains were designed using the same sgRNAs, due to the proximity of the mutations to each other within the same exon (exon 19 of *unc-68* isoform a). The PAM sequence for the first sgRNA was located in the exon upstream of the two mutations (exon 18 of *unc-68* isoform a). Limitations on the size of the ssDNA oligonucleotide used for short-range HDR require the ssDNA template to be no longer than 200 nt in length (Dickinson and Goldstein, 2016). To limit the size of the ssDNA oligonucleotide required to bridge between the two cut sites, the intron in the wild type was deleted in these two mutant strains (COP1947 (hR2454H) and COP1944 (hR2458H)) (Table 2.2). The deletion of this intron is not thought to affect isoform diversity.

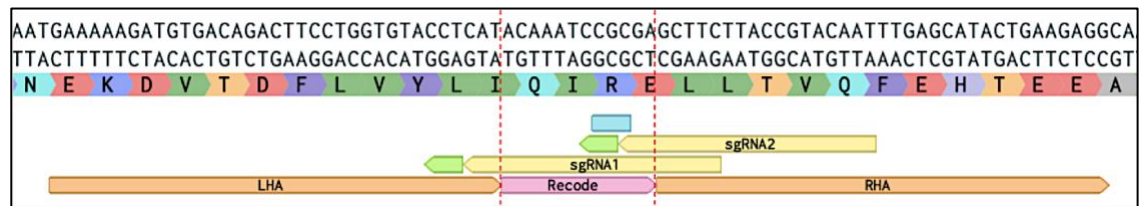


Figure 2.1: Generating a single amino acid change, corresponding to the R2163H *RYR1* human disease variant, in *unc-68*.

The two sgRNAs (shown in yellow) guide the Cas9 protein to cut 3 nts upstream of the PAM sequences (shown in green), cut sites are shown by dashed red lines. The desired edit, hR2163H, is shown in blue. Changing the codon from CGC to CAC in the ssDNA oligonucleotide alters the amino acid sequence. Silent mutations were introduced within the pink 'Recode' sequence of the ssDNA oligonucleotide, to prevent re-cutting. The 35 nt left homology arm (LHA) and right homology arm (RHA) are shown in orange and are unmodified in the ssDNA oligonucleotide. Image taken from the design file in Benchling [Biology Software] (2020), retrieved from <https://benchling.com>.

The design of the two RyR variant strains generated at the University of Leeds employed the co-CRISPR approach (Arribere *et al.*, 2014; Kim *et al.*, 2014). Co-CRISPR uses a visible phenotype at one locus to help identify edits at a second locus (Dickinson and Goldstein, 2016). The gain of function *dpy-10 (cn64)* mutation was used as a co-CRISPR marker, this mutation confers a different phenotype when homozygous (*dpy-10 (cn65) / dpy-10 (cn65)* (dumpy)), heteroallelic (*dpy-10 (cn65) / dpy-10(o)* (dumpy roller)) and heterozygous (*dpy-10 (cn65) / +* (roller)) (Arribere *et al.*, 2014).

N2 Bristol strain animals were injected with the pDD162 plasmid (*Peft-3::Cas9* + Empty sgRNA) to express Cas9 in the germline (Dickinson *et al.*, 2013), the pJA58 plasmid to guide cleavage by Cas9 at the *dpy-10 (cn64)* locus (Arribere *et al.*, 2014), an sgRNA specific to the hR163C or hN2342S modification in *unc-68* to guide cleavage by Cas9 and two ssDNA donor homology oligonucleotides to guide repair of the double stranded breaks in *dpy-10* and *unc-68* with the inclusion of the desired edits at each locus. As before, the 3' end of the binding site for the sgRNA target sequence had a PAM sequence and the 20 nt sgRNA sequence was complementary to the 20 nts

upstream of the PAM sequence in the genome. The pJA58 plasmid contains a 19 nt guide RNA (gRNA) sequence, which is complimentary to the wild type genomic sequence in the region of the desired *dpy-10* edit with a PAM sequence at the 3' end. The ssDNA donor homology oligonucleotides contained silent mutations to prevent re-cutting of the genome by Cas9, however these two strains had only one or two nucleotides changed to induce a silent mutation.

Injected animals were picked to fresh plates each day after injection to allow for observation of F1s. F1s heterozygous for the *dpy-10* (*cn64*) mutation, showing the dominant roller phenotype, revealed animals that were derived from oocytes that received active Cas9 and were therefore most likely to carry the desired modification in *unc-68*. These animals were picked out and allowed to propagate before screening by PCR for the desired *unc-68* edit. Of the animals found to carry the desired edit, the non-roller and non-dumpy F2 progeny, indicating they were wild type at the *dpy-10* (*cn65*) locus, were allowed to propagate before PCR screening to identify animals homozygous for desired *unc-68* edit.

2.2.1. Genotyping ryanodine receptor variant strains

All modifications to *unc-68* were confirmed by PCR and sequencing. DNA for PCR was prepared from individual animals.

Single adult animals were picked directly into 10 μ l of worm lysis buffer in a PCR tube (5 μ l 1 mg/ml proteinase K, 20 μ l 5x Phusion buffer (BioLabs B0518S) and 75 μ l nuclease free water). Animals were picked using a platinum wire from outside the OP50 lawn to avoid inclusion of bacteria. Tubes containing worms in buffer were frozen at -80°C for at least 1 hour; the freeze/ thaw is thought to help lysis. Worms were lysed using a thermocycler by heating to 60°C for one hour, then 95°C for 15 minutes to inactivate the proteinase K, and then held at 4°C . After lysis, the digested heat inactivated prep was used as a template for PCR. 50 μ l PCR reactions were prepared and run in a thermocycler following the standard MyTaq (BioLine BIO-21105) protocol. DNA was prepared for sequencing by gel electrophoresis and gel extraction of the appropriate size band. A 1% agarose gel was prepared and loaded with 25 μ l of

the PCR products into every other well of the gel to allow for easier extraction. The gel was run and DNA bands of the appropriate size were excised using a 302 nm wavelength transilluminator and razor blade. DNA fragments were extracted from the gel using a DNA gel extraction kit (Monarch® NEB #T1020) following the standard protocol. 5 µl of the purified DNA was sent to GeneWiz (<https://www.genewiz.com/>), with 5 µl of 5 µM primer for sequencing. Returned sequences were viewed with Benchling [Biology Software] (2020), retrieved from <https://benchling.com>. Example alignments of returned sequencing results to the desired variant sequence are included in Appendix C.

2.3. Synchronisation and ageing

Three different ages of hermaphrodite *C. elegans* were used to assess the varying effects of RyR variants *in vivo*; young adult, day 10 adult and larval stage one. Larval stage *C. elegans* were only used in thrashing assays (Chapter 3). Young and old adult *C. elegans* were used for assessing the effects of RyR variants on thrashing rate, halothane sensitivity and crawling (Chapters 3 and 4). Young adults were also used in cholinergic pharmaceutical assays and halothane assays on heterozygous RyR variant strains (Chapters 5 and 6).

2.3.1. Generating an age-synchronised population of *C. elegans*

A synchronised population of young adult animals was obtained by bleaching mixed stage populations containing gravid adults. Mixed stage plates were washed twice with 750 µl of M9 buffer to a 1.5 ml microcentrifuge tube, and the worms, in M9 buffer, were mixed with 0.3 volumes of a dilute hypochlorite solution, as in household bleach, and 0.2 volumes of 4 M NaOH, until only eggs remained, approximately 5 minutes. Bleaching kills all post-embryonic stages, while embryos are protected by the egg-shell. After 5 minutes in the bleaching solution, tubes were spun in a table-top centrifuge at 12,000 g for 30 seconds to pellet the eggs. The supernatant was removed by gentle pipetting and the pellet of eggs resuspended in 1 ml of M9 buffer, this was repeated twice to remove bleach residue. Prepared eggs, resuspended in 50 µl of M9 buffer, were transferred to seeded plates and allowed to develop. All animals hatch within 14 hours of each other. 3.5 days after bleaching, with the presence of a few eggs on the

plate, animals were considered young adults. The *unc-68* null mutant, CB540 (*unc-68(e540)*), and the hR4861H RyR variant strain both took an extra day to reach the young adult stage, as indicated by the onset of egg laying.

2.3.2. Ageing *C. elegans*

Age synchronised populations of 10-day old adults were obtained by first bleaching in the same way as for young adults. Two days after synchronisation, at the L4 stage, animals were washed from 50 mm NGM plates with M9 buffer to 90 mm NGM plates containing 50 μ M FUdR (5-fluoro-2'-deoxyuridine) (Sigma-Aldrich) and seeded with 450 μ l OP50 *E. coli* overnight culture. Fertilised eggs are prevented from developing and hatching in the presence of FUdR as it inhibits DNA synthesis, while still allowing adults to lay eggs. Adult *C. elegans* have no somatic cell division and should not be affected by FUdR in the same way as larval *C. elegans*. Assay animals were only transferred to plates containing FUdR just before maturation to avoid developmental abnormalities associated with FUdR treatment. The *unc-68* null mutant and hR4861H RyR variant strain were transferred to FUdR plates one day later than wild type and other RyR variant strains to match the developmental delay in these two strains. Lifespan extension and stress resistance have been associated with FUdR treatment (Anderson *et al.*, 2016). Neither lifespan or stress resistance are assessed in this research, and so it was deemed appropriate to use FUdR to limit progeny hatching.

2.3.3. Statistical and graphical analysis

Statistical parameters are reported in figures and corresponding figure legends. None of the data were removed from statistical analysis as outliers. All statistical analysis was performed in GraphPad Prism (version 8.0), GraphPad Software, La Jolla California USA, www.graphpad.com.

Colour coding for the RyR variant strains, CB540 (*unc-68(e540)*) null mutant and wild type is applied consistently and, for the RyR variants, corresponds to variant residue location in the protein. Yellow/ orange variants, hR163C and hG341R, are located within the N-terminal domain (NTD), green coloured variants are within the helical domain (HD), hR2163H, hN2342S, hR2454H, hR2458H and hK3452Q, and the blue

variant, hR4861H, is located in the transmembrane domain (TMD) (Figure 2.2). Grey represents wild type and lilac the *unc-68* null mutant.

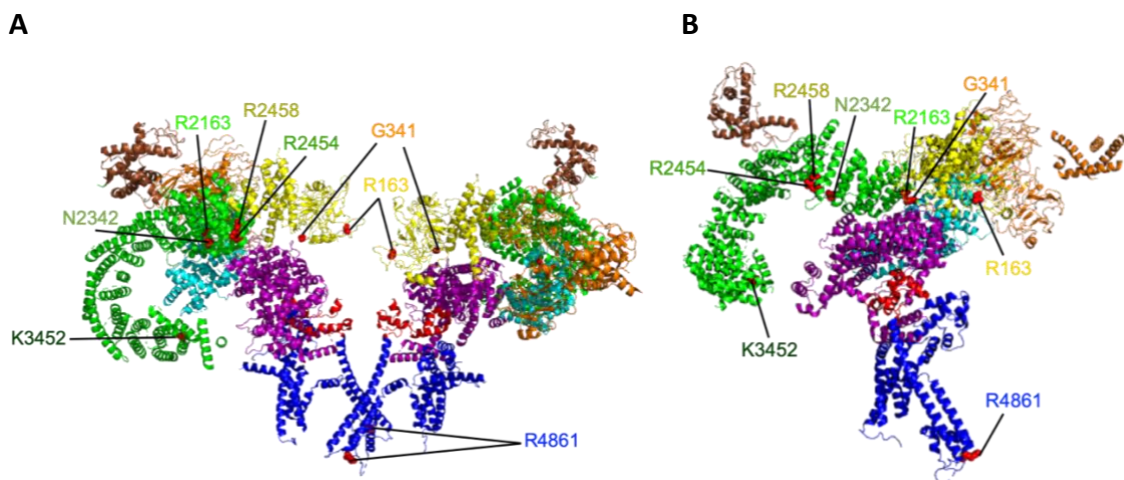


Figure 2.2: Location of RyR1 variants in the ryanodine receptor.

(A) Two opposing RyR protomers, viewed from within the plane of the membrane.
 (B) One RyR protomer viewed from within the pore. N-terminal domain (NTD) in yellow, SPRY1, 2 and 3 in orange, P1 and P2 in brown, handle in cyan, helical domain (HD) in green, central domain in purple, transmembrane domain (TMD) in blue and C-terminal domain (CTD) in red. RyR variants are shown as spheres in red with labels coloured corresponding to the colour coding applied in this research. Generated using PyMOL, based on the closed conformation of rabbit RYR1, as predicted from Yan *et al.* (2015) (PDB code 3J8H).

Comparisons of thrashing rate and halothane sensitivity between genotypes in each condition assayed are expressed as 10-90 percentile box and whisker plots. Differences between genotypes and differences between conditions for each genotype were identified as ns, not significant, or significant to $*P < 0.05$ or $**P < 0.005$ using one-way ANOVA with Tukey's or Sidak's test for multiple comparisons respectively.

Crawling amplitude, wavelength and frequency are represented as scatterplots, for two of the three crawling parameters, with both vertical and horizontal error bars (standard error) for young adult and old adult. Error bars that are smaller than the height of the data point are not shown. Worm lengths and degree of curvature are expressed as 10-90 percentile box and whisker plots. Comparisons of degree of

curvature between genotypes were identified as ns, not significant, or significant to $*P<0.05$ or $**P<0.005$ using one-way ANOVA with Tukey's multiple comparisons. Worm length and crawling amplitude, wavelength, frequency and speed were extracted from 1 minute long videos, recorded at 25 frames per second (fps), using Tierpsy Tracker 1.4.0 (Javer *et al.*, 2018) and MATLAB. Video recordings were made using a multi-worm tracker system set up by, and used with permission of, the Cohen lab at the University of Leeds. 20-30 animals were transferred to 90 mm NGM plates, without food, and recorded crawling freely for 1 minute. Worm length was hand measured using ImageJ (Schneider *et al.*, 2012) in 5 individual frames for 5 individuals of each strain and compared to extracted worm length data. Degree of curvature was measured in individual frames using GeoGebra version 6.0562.0, www.geogebra.org (Hohenwarter, 2002). Kymograms for single individuals were generated using the Tierpsy Tracker 1.4.0 software and MATLAB. Methods of extracting crawling parameters are described in section 4.2.

Survival fractions in aldicarb are expressed as a Kaplan-Meier survival curve produced in GraphPad Prism. The survival curve for each individual strain was compared to wild type (or the *unc-68* null mutant for the hR4861H variant strain) using a Gehan-Breslow-Wilcoxon test.

Comparisons between heterozygous and homozygous strains for the RyR variants, *unc-68* null mutant or wild type are expressed as 10-90 percentile box and whisker plots. Differences between the variant heterozygotes and homozygotes were identified as ns, not significant, or significant to $*P<0.05$ or $**P<0.005$ using one-way ANOVA with Sidak's multiple comparison test.

Chapter 3

Confirming a malignant hyperthermia related phenotype in genome-edited *RYR1* variant *C. elegans*: modelling malignant hyperthermia in the worm

3.1. Introduction

3.1.1. Aim of this chapter

The aim of the research described in this chapter was to determine whether CRISPR-Cas9 genome-edited strains, designed to express ryanodine receptors (RyRs) equivalent to human RyR1 malignant hyperthermia (MH) disease variants, exhibit an MH-related phenotype. Further phenotypic assessment and the consequences of the presence of these variants in *C. elegans*, pursued subsequently, are only of relevance to human disease if it is known that these variant strains are sensitive to MH triggering agents like susceptible humans and other animal models of MH.

3.1.2. A malignant hyperthermia related phenotype in *C. elegans*

Previous work, using extrachromosomal array strains carrying modifications equivalent to RyR1 associated human variants in *unc-68*, demonstrated the viability of *C. elegans* as a model for RyR1-related myopathies, predominantly MH (Nicoll Baines *et al.*, 2017). Halothane and caffeine are two test agents used in an *In Vitro* Contracture Test (IVCT) for MH (Ellis *et al.*, 1984; Hopkins *et al.*, 2015). The response of the extrachromosomal array strains to these test agents demonstrated measurable differences between wild type controls and RyR variant carrying strains (Nicoll Baines *et al.*, 2017). The extrachromosomal array strains all showed hypersensitivity to halothane with complete paralysis in 2.5 mM halothane while wild type retained motility.

Hypersensitivity to the MH triggering agent halothane is considered an MH-related phenotype in strains carrying modifications in *unc-68* that are equivalent to RyR1 associated human disease variants. The response of the extrachromosomal array strains to halothane was seen as a demonstration of the conservation of function of RyR from *C. elegans* to humans (Nicoll Baines *et al.*, 2017). In order to verify that

CRISPR-Cas9 genome-edited RyR variant strains are valid models for MH, and demonstrate a similar MH-related phenotype, strains were subjected to a similar halothane test.

3.2. Methods

3.2.1. Halothane and thrashing assays

Halothane assays were conducted on individuals of particular ages. Well-fed individuals were selected from NGM plates and transferred to 1 ml of S medium, or S medium containing 1 mM, 2.5 mM or 5 mM halothane. S medium contains 1 litre S Basal (5.85 g NaCl, 1 g K₂HPO₄, 6 g KH₂PO₄, 1 ml cholesterol (5 mg/ml in ethanol), H₂O to 1 litre and autoclaved), 10 ml 1 M potassium citrate pH 6, 10 ml trace metals solution (1 Litre stock: 1.86 g Na₂ EDTA, 0.69 g FeSO₄•7H₂O, 0.2 g MnCl₂•4H₂O, 0.29 g ZnSO₄•7H₂O, 0.025 g CuSO₄•5H₂O, H₂O to 1 litre, autoclaved and stored in the dark), 3 ml 1 M CaCl₂, 3 ml 1 M MgSO₄ (Stiernagle, 2006). Body bends were counted after 1 minute of exposure. 25 worms were assayed for each strain at each concentration, across several days to confirm reproducibility.

Halothane was prepared as a 125 mM stock in dimethyl sulfoxide (DMSO). Just prior to assaying, 500 µL of S medium was added to a well of a 24-well plate, followed by 500 µL of S medium with or without halothane. An individual was immediately transferred into the S medium using a sterile worm pick. This method was used to avoid the halothane/ DMSO mixture damaging the plastic of the plate when at higher concentrations. Assays were carried out immediately due to the volatility of halothane.

3.2.2. L1 thrashing assay

L1 animals were prepared by washing a mixed stage population of *C. elegans* to a microcentrifuge tube with 1 ml of S medium. Worms were allowed to settle for 1 minute allowing larger, older animals settle and form a loose pellet at the bottom of the tube while younger animals remain in the supernatant. 10 µl of the S medium/worm supernatant was pipetted into each well of an 8-well microscope slide.

C. elegans transferred to the slide were allowed 1 minute to acclimate. One L1 animal

was identified per well of the 8-well slide and body bends were counted for that individual. 32 animals were assayed per strain, across two different days.

3.3. Results

3.3.1. Identification of pathogenic *RYR1* gene variants in residues conserved in *C. elegans*

In addition to the 48 MH diagnostic variants, a number of other *RYR1* variants are linked with MH and other myopathic conditions. To broaden the scope of this research, beyond MH, several of these other variants were studied. It should be acknowledged, however, that the relationship between *RYR1* variants and different disease conditions is complex, with lots of cross over (Guis *et al.*, 2004; Litman *et al.*, 2018).

Six of eight variants used here are currently on the MH diagnostic list; R163C, G341R, R2163H, R2454H, R2458H and R4861H (Table 3.1). Of these MH diagnostic variants, several are also associated with other myopathies. R2163H has been associated with both MH and Central Core Disease (CCD), as has R163C (Yan *et al.*, 2015). The R163C variant, however, has also been reported in a case of Exertional Heat Illness (EHI) (Tobin *et al.*, 2001). The two additional variants used, which are not on the MH diagnostic list but are suspected *RYR1* myopathic variants are N2342S and K3452Q. The N2342S variant has also been associated with MH after a patient had an MH response to anaesthetic and a subsequent positive IVCT (Marchant *et al.*, 2004), but this variant is not considered diagnostic and has not been functionally characterised. The K3452Q variant has been linked with Late-Onset Axial Myopathy (LOAM) (Løseth *et al.*, 2013). LOAM typically presents between the third and eighth decade of life, hence 'late-onset', while most other *RYR1* variant myopathies, such as CCD, present in infancy or childhood (Jungbluth *et al.*, 2009; Løseth *et al.*, 2013). Patients with LOAM have pronounced lumbar hyperlordosis, muscle pain and weakness.

In order to model the human condition, *RYR1* variants were chosen based on conservation with *unc-68* in *C. elegans*, where the non-variant residue in human *RYR1* was the same as the wild type residue in *unc-68*. The mammalian *RYR1* gene is

approximately 160 kb, with 106 exons of which 2 are alternatively spliced. Despite the much more compact genome of *C. elegans* the only ryanodine receptor gene, *unc-68*, is still large at approximately 30 kb with 49 exons. Both genes encode proteins comprising just over 5000 amino acids. As described the human and *C. elegans* RyR proteins share 40% identity and 60% similarity, along their entire length.

Table 3.1: Amino acid alignments of human RYR1 and *C. elegans* UNC-68 in the regions of the studied variants, and the *C. elegans* strains that were generated expressing the variant UNC-68.

Human RyR variant (<i>C. elegans</i> variant)	Alignment		<i>C. elegans</i> strain	MH diagnostic	Associated disease
R163C (R169C)	RYR1	ASKQRSEGEKVRVGDDIILVS	UL4239	Y	MH / CCD/ EHI
	UNC-68	ASKQRSEGEKVRVGDDVILVS			
G341R (G350R)	RYR1	PPEIKYGESLCFVQHVASGLW	COP1879	Y	MH
	UNC-68	NATIRYGETNAFIQHVKTQLW			
R2163H (R2246H)	RYR1	LLECLGQIRSLIVQMGPQEE	COP1883	Y	MH / CCD
	UNC-68	FLVYLIQIRELLTVQFEHTEE			
N2342S (N2441S)	RYR1	DFLRFVAVFVNGESVEENANVV	UL4285	N	MH
	UNC-68	DFLRFVWINGENVEENANLV			
R2454H (R2560H)	RYR1	AGKGEALRIRAILRSLVPLED	COP1947	Y	MH
	UNC-68	AGKGDSLRRARAILRSLISLDD			
R2458H (R2564H)	RYR1	AGKGEALRIRAILRSLVPLED	COP1944	Y	MH
	UNC-68	AGKGDSLRRARAILRSLISLDD			
K3452Q (K3675Q)	RYR1	IYWSKSHNFKREEQNFVVQNE	COP1932	N	LOAM
	UNC-68	RIWSQSQHFKREELNYVAQFE			
R4861H (R5021H)	RYR1	VVVYLYTVVAFNFFRKFY-NK	COP1950	Y	MH
	UNC-68	VVVYLYTVIAFNFFRKFYVQE			

Box shading is consistent with the colour coding used throughout this thesis. The residue changed in the variants is underlined. RyR variant strains are listed according to the human variant they correspond to. Variants that are on the EMHG diagnostic list (The European Malignant Hyperthermia Group, n.d.) are shown as Y (Yes) and those not included are shown as N (No). Diseases associated with each variant are shown malignant hyperthermia (MH), central core disease (CCD), exertional heat illness (EHI) and late-onset axial myopathy (LOAM).

3.3.2. Confirmation of hypersensitivity to halothane for variant strains and discovery of novel locomotion defects in the absence of halothane

To confirm the previous findings of increased sensitivity to halothane due to the missense changes in *unc-68*, as assayed in the extrachromosomal array variant strains

(Nicoll Baines *et al.*, 2017), the CRISPR-Cas9 generated RyR variant strains were subjected to a halothane test.

Young adults, 3.5 days after synchronisation were assayed. For each halothane assay fresh stocks of S medium buffer, with and without halothane, were prepared. Fresh solutions were prepared to avoid problems arising due to the volatility of halothane, to increase reproducibility. The volatility of halothane made accurate delivery of a small volume difficult. DMSO was used to dissolve halothane to provide a reliable stock solution that was diluted into the assay medium.

Individual animals were picked from a well-fed plate, at the young adult stage into one of four concentrations of halothane, ranging from 0 to 5 mM, dissolved in S medium. Each individual was allowed one-minute acclimation time after which body bends were counted. A body bend was recorded as the movement from the midline either dorsally or ventrally and back to the midline (Figure 3.1).

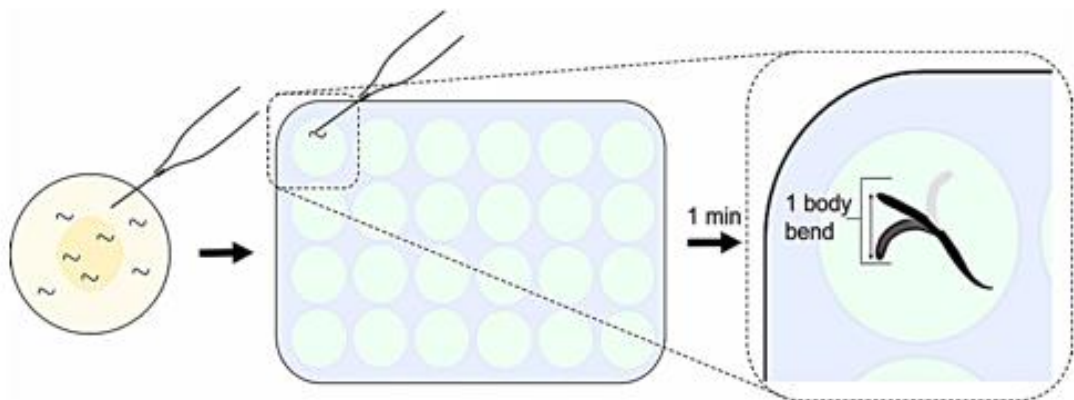


Figure 3.1: Halothane assay set up and counting of body bends.

Young adult worms were picked from well fed plates, placed into a solution of halothane, given 1 minute to acclimate and then body bends were counted. One body bend corresponds to the head thrashing from the centre line and back.

Due to different sources of background strain used to generate the RyR variant strains, the Leeds N2 strain and NemaMetrix N2 strain were assessed for differences in thrashing rate and halothane sensitivity. No differences were found between the two N2 strains (see Appendix D). All references to wild type in this research refer to the N2

wild type strain provided by NemaMetrix due to six of eight RyR variant strains originating from this background.

In the absence of halothane, consequences of the RyR residue changes for these animals for locomotion in liquid were noted (Figure 3.2A). Previously, no differences between RyR variants and wild type extrachromosomal array strains were observed in the absence of halothane (Nicoll Baines *et al.*, 2017). This was consistent with MH being considered asymptomatic without exposure to a triggering agent (Robinson *et al.*, 2006). Contrastingly, it was found here that four of the eight genome-edited RyR variant strains showed reduced thrashing rate when swimming in S medium.

The wild type completed 199 (± 14) body bends per minute (Figure 3.2A). Strains for variants hR163C, hG341R, hR2458H and hR4861H all demonstrated a reduced thrashing compared to this.

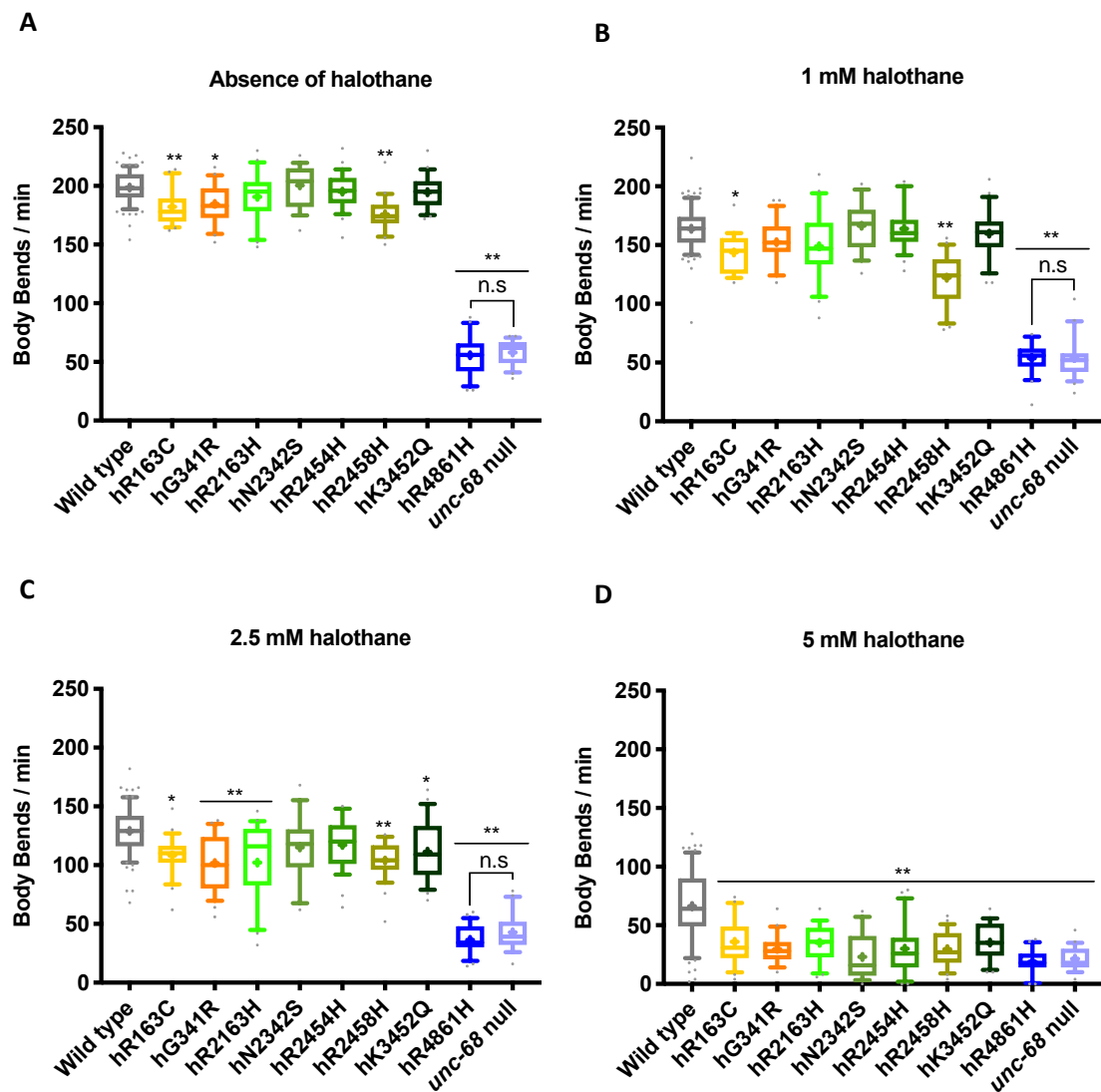
Strains for variants hR163C, hG341R and hR2458H demonstrated subtle, but statistically significant, locomotion defects when compared to wild type with body bends per minute of 182 (± 16) for hR163C ($P < 0.005$), 185 (± 18) for hG341R ($P < 0.05$) and 176 (± 15) for hR2458H ($P < 0.005$, One-way ANOVA with Tukey's multiple comparisons test).

The hR4861H variant strain had a more exaggerated locomotion defect and only completed 56 (± 19) body bends in 1 minute. Interestingly, the CB540 (*unc-68(e540)*) strain, which carries a point mutation and behaves genetically like a null (Maryon *et al.*, 1996), completed only 58 (± 11) body bends per minute. The thrashing rates for the two strains, the hR4861H RyR variant strain and the *unc-68* null strain, were indistinguishable from each other ($P > 0.99$, One-way ANOVA with Tukey's multiple comparisons test). The reduced thrashing rate seen for the null mutant is consistent with the uncoordinated phenotype associated with its naming. The similarity between the hR4861H variant strain and the *unc-68* null mutant suggests that the presence of this change in the UNC-68 protein eliminated the function of the ryanodine receptor, however it will later be shown that the hR4861H variant strain is non-null.

The strains for variants hR2163H, hN2342S, hN2454H and hK3452Q all completed a similar number of body bends per minute to wild type, 191 (± 21), 201 (± 18), 195 (± 16) and 195 (± 14) respectively (Figure 3.2A). These strains were considered to have a fully functional ryanodine receptor, in the absence of a triggering agent, in agreement with previous work.

The discrepancy between the extrachromosomal array RyR variant strains and the genome-edited RyR variant strains for thrashing rate in the absence of halothane was thought to be caused by high transgene copy numbers in extrachromosomal array strains. The additional transgene copy numbers may result in additional variant channels. Additional channels functioning sub-optimally may result in a wild type-like thrashing rate.

Previously, the halothane response of the extrachromosomal array variant strains was assessed across 0.5 mM increments with several strains showing increased sensitivity to halothane at 1 mM and all showing almost complete paralysis at 2.5 mM halothane (Nicoll Baines *et al.*, 2017). Therefore, initially, 1 mM and 2.5 mM halothane were chosen to assess the sensitivity of the genome-edited RyR variant strains. It was expected that at 2.5 mM halothane the genome-edited variant strains would also show almost complete paralysis.



E

Mean and standard deviation of thrashing rates in the absence of halothane and 1 mM, 2.5 mM and 5 mM concentrations of halothane for wild type, the CB540 (*unc-68(e540)*) null mutant and RyR variant *C. elegans* strains.

	Absence of halothane		1 mM halothane		2.5 mM halothane		5 mM halothane	
	Mean	SD	Mean	SD	Mean	SD.	Mean	SD
Wild type	199	14	164	19	129	22	66	30
hR163C	182	16	144	16	108	17	36	20
hG341R	185	18	152	19	102	25	30	13
hR2163H	191	21	149	30	102	34	35	16
hN2342S	201	18	166	21	115	27	23	20
hR2454H	195	16	164	19	117	22	30	24
hR2458H	176	15	122	22	104	17	30	15
hK3452Q	195	14	160	22	111	25	35	16
hR4861H	56	19	54	14	36	12	19	11
<i>unc-68</i> null	58	11	54	18	43	16	22	10

Box shading is consistent with the colour coding used throughout this thesis. RyR variant strains are listed according to the human variant they correspond to.

Figure 3.2: RyR variants confer an MH-related phenotype of hypersensitivity to halothane.

Thrashing rate in S medium, in body bends per minute, for RyR variant strains, labelled by the human variant they correspond to, in the absence of (A) and presence of 1 mM (B), 2.5 mM (C) and 5 mM (D) halothane, and the mean and standard deviation (SD) of thrashing rates, in body bends per minute, in each condition (E). 25 individuals were examined per strain. Boxes indicate the median and interquartile range, with whiskers to the 10-90 percentile, outliers as dots, and + to indicate the mean. Significance is between variant strains and the wild type, apart from where indicated to the CB540 (*unc-68(e540)*) null mutant. * $P < 0.05$, ** $P < 0.005$, n.s = not significant (one-way ANOVA, with Tukey's multiple comparison test) (A-D). Colouring corresponds to variant location in the protein as explained in section 2.4 (Figure 2.2). Yellow/ orange variants are located within the N-terminal domain (NTD), green in the helical domain (HD) and blue in the transmembrane domain (TMD). Grey represents wild type and lilac the null mutant.

At 1 mM halothane all strains, including wild type, showed reduced thrashing and this was not determined as hypersensitivity to halothane in the majority of the RyR variant strains (Figure 3.2B). Some reduction in locomotion is expected due to the anaesthetic properties of halothane. The strains for variants hR163C and hR2458H did appear to show a significantly reduced thrashing rate in 1 mM halothane compared to wild type ($P < 0.05$ and $P < 0.005$ respectively, One-way ANOVA with Tukey's test for multiple comparisons). However, both of these variants also exhibited statistically significantly reduced thrashing in the absence of halothane. With different starting thrashing rates in the absence of halothane it is difficult to determine whether the significance in thrashing rate of the hR2458H and hR163C variant strains compared to wild type was due to increased sensitivity to 1 mM halothane or the locomotion defect. To address this issue, the mean percentage locomotion decrease in thrashing rate upon exposure to difference concentrations of halothane was determined for all strains, using the absence of halothane as the baseline (Table 3.2).

From the percentage decrease between mean thrashing rates in no halothane and the 1 mM halothane, the smallest decrease was seen for the *unc-68* null strain and the hR4861H RyR variant strain that behaved like the null, with only a 7% and 4% decrease for each. The small reduction seen for these two strains may suggest that the mode of action of the anaesthetic requires functional RyRs for full effect. However, the uncoordinated locomotion could minimise the extent to which the effect can be observed.

Table 3.2: Percentage change of mean thrashing rates from the absence of halothane to 1 mM, 2.5 mM and 5 mM concentrations of halothane for wild type, the CB540 (*unc-68(e540)*) null mutant and RyR variant *C. elegans* strains.

Strain (variant)	Absence to 1 mM	Absence to 2.5 mM	Absence to 5 mM
Wild type	-18%	-35%	-66%
hR163C	-21%	-41%	-80%
hG341R	-18%	-45%	-81%
hR2163H	-22%	-48%	-82%
hN2342S	-17%	-43%	-89%
hR2454H	-17%	-40%	-78%
hR2458H	-31%	-41%	-83%
hK3452Q	-18%	-43%	-82%
hR4861H	-4%	-35%	-66%
<i>unc-68</i> null	-7%	-26%	-63%

Box shading is consistent with the colour coding used throughout this thesis. RyR variant strains are listed according to the human variant they correspond to. Percent change is calculated as $((C1-C2)/C1)*100$ where C1 is the absence of halothane and C2 is the different concentrations of halothane. All strains showed a decrease from C1 to C2, indicated by a minus sign (-).

Most strains, including the wild type, exhibited a 17-22% decrease in body bends per minute when exposed to 1 mM halothane compared to the absence of halothane (Table 3.2). The hR163C variant strain sits within this group with a 21% decrease in thrashing, suggesting the statistically significant difference between this variant and wild type is not due to increased sensitivity to 1 mM halothane, but rather due to the subtle locomotion defect seen even in the absence of halothane.

The strain for variant hR2458H, however, showed a 31% difference between the mean thrashing rate in the absence of halothane and 1 mM halothane, which is much higher than all other variant strains and wild type (Table 3.2). This strain is considered to show increased sensitivity to halothane at this concentration. Interestingly, while the

presence of this variant as an extrachromosomal array strain resulted in hypersensitivity to 1 mM halothane, five other variant array strains also showed such sensitivity (Nicoll Baines *et al.*, 2017). Again, the discrepancy between the previous study and this work is attributed to the high transgene copy number in the extrachromosomal array strains. If low concentrations of halothane result in an increased open probability of RyR channels, additional variant channels could result in increased sensitivity to the trigger. It could be argued that the hR2458H variant is the only variant in the previous study to confer real hypersensitivity to 1 mM halothane under natural conditions.

It was expected that 2.5 mM halothane would reveal hypersensitivity for all of the RyR variant strains generated through CRISPR-Cas9 genome editing, as it did for all variant array strains generated as extrachromosomal arrays (Nicoll Baines *et al.*, 2017). This was not the case (Figure 3.2C). While six of eight of the variant strains demonstrated a statistically reduced thrashing rate compared to wild type, the reduction was not to the same extent as seen previously. Thrashing rates were still over 100 body bends per minute in 2.5 mM halothane for all strains, apart from the *unc-68* null and the hR4861H variant strain. This reduced sensitivity in the genome-edited variant strains compared to the extrachromosomal array variant strains is accredited to the endogenous expression level of UNC-68 in the former compared to over expression in the latter.

All of the RyR variant strains, except that for hR4861H, exhibited a 40-48% decline in thrashing from the baseline, in S medium in the absence of halothane, to 2.5 mM halothane (Table 3.2). Wild type only showed a 35% decrease, completing 129 (± 22) body bends per minute (Figure 3.2C). There appears to be some increased sensitivity in the RyR variant strains when exposed to 2.5 mM halothane, however it is limited. The two variant strains that were determined as not significantly different to wild type, hN2342S ($P=0.42$) and hR2454H ($P=0.33$), also showed a 43% and 40% decrease in thrashing rate completing 115 (± 27) and 117 (± 22) body bends per minute each. However, other variant strains, which were determined as significantly different to wild type, showed reductions of a similar magnitude, making interpretation of these results difficult.

It could be argued that all genome-edited RyR variant strains show slightly increased sensitivity to 2.5 mM halothane, and for the variants hN2342S and hR2454H further repeats would be required to see this reflected in the statistical analysis.

As 2.5 mM halothane was not sufficient to induce a clear MH-related phenotype of halothane hypersensitivity in the RyR variant strains, a higher concentration of 5 mM halothane was applied (Figure 3.2D). At this higher dose of halothane, hypersensitivity was seen for all RyR variant strains as shown by the larger percentage decrease in thrashing rate in 5 mM halothane observed for these strains compared to wild type (Table 3.2). A one-way ANOVA identified all RyR variant strains to have significantly reduced thrashing compared to wild type at 5 mM halothane ($P < 0.005$, Tukey's multiple comparisons). While the wild type was able to complete an average of 66 (± 33) body bends per minute in 5 mM halothane, none of the RyR variant strains completed more than 36 (± 20) as seen for the hR163C variant strain (Figure 3.2D). The *unc-68* null and the hR4861H variant both achieved even fewer; 22 (± 10) and 19 (± 10) body bends per minute.

The use of DMSO to dissolve halothane for the stock solution meant that the apparent differences in sensitivity to 5 mM halothane could actually reflect differences in response to DMSO. DMSO is a popular solvent for compounds that will not dissolve in water, and thus has been used in many *C. elegans* drug discovery assays, including lifespan experiments (Frankowski *et al.*, 2013; Xiong *et al.*, 2017). DMSO can extend lifespan and high concentrations are toxic to *C. elegans* (Wang *et al.*, 2010). While DMSO was considered an innocuous organic solvent and was diluted 25-fold in the assay, the effect of DMSO at this concentration on locomotion needed to be evaluated. Individuals were exposed to the 4% DMSO in S medium, as in the 5 mM halothane treatment, allowed to acclimate for 1 minute and body bends counted (Figure 3.3).

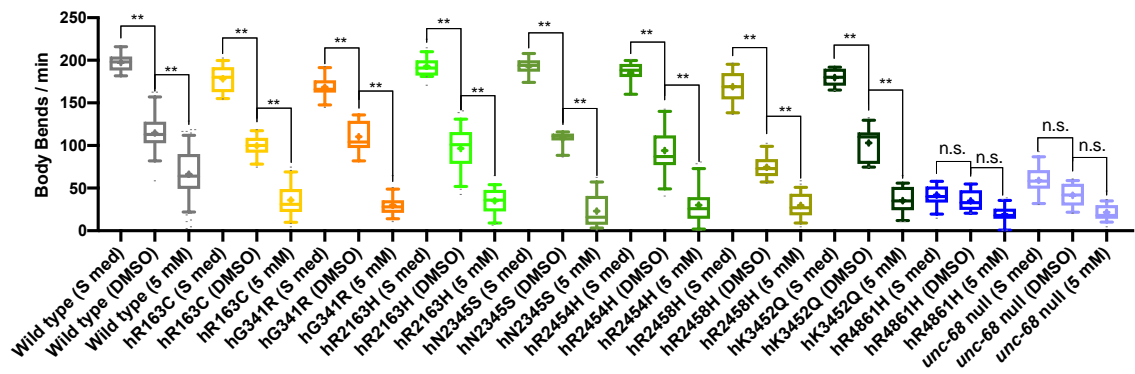
Wild type and all of the RyR variant strains, except for the hR4861H variant, did have a significant reduction in thrashing rate in the presence of DMSO, compared to S medium alone (Figure 3.3). Thrashing rate for the null mutant and the hR4861H

variant, however, did not appear to be affected by the DMSO. This is likely due to the effect being small and therefore not detectable when the baseline rate was already very low. It could also suggest some involvement of a functional ryanodine receptor in the effect of DMSO.

Despite the effect of DMSO on *C. elegans* thrashing rate, comparison between thrashing rate in S medium with DMSO and in S medium with DMSO and halothane, reveals that the RyR variants enhance the decrease in thrashing rate due to halothane compared to wild type (Figure 3.3, Appendix E). This effect is seen for all of the RyR variant strains in comparison to the wild type, once again, with the exception of hR4861H. Both the hR4861H variant strain and the *unc-68* null mutant showed no difference between S medium and DMSO and S medium with DMSO and halothane. Again, the explanation for this most likely lies within the relatively few body bends completed per minute, in these strains. A significant reduction is seen between S medium and S medium with DMSO and 5 mM halothane for these two strains.

Aside from the *unc-68* null mutant and the similarly behaving hR4861H variant strain that showed no significant effect of DMSO on thrashing rate, the RyR variant strains appeared to be affected to the same degree by DMSO in the S medium as wild type (Appendix E). No statistically significant differences in thrashing rates were seen between these two treatments, apart from for the hR2458H variant strain. The hR2458H variant strain completed significantly fewer body bends per minute than wild type when exposed to 4% DMSO in S medium, 75 (± 14) compared to 115 (± 25) ($P < 0.005$ One-way ANOVA with Tukey's test) (Figure 3.2, Appendix E). However, this can be attributed to the reduced locomotion seen in S medium for this strain, even in the absence of DMSO, rather than an effect of DMSO. The subtle locomotion defects noted for the hR163C and hG341R variant strains in S medium alone were no longer detectable in the presence of DMSO and these strains had similar thrashing rates to wild type ($P = 0.59$ and $P > 0.99$ respectively, One-way ANOVA with Tukey's test).

A



B

Mean and standard deviation of thrashing rates in S medium alone, with the addition of DMSO, and with DMSO and 5 mM halothane for wild type, the CB540 (*unc-68(e540)*) null mutant and RyR variant *C. elegans* strains.

	S medium		S medium + DMSO		S medium + DMSO + 5 mM halothane	
	Mean	SD	Mean	SD	Mean	SD
Wild type	197	11	115	25	66	30
hR163C	178	16	100	12	36	20
hG341R	169	13	110	18	30	13
hR2163H	193	12	97	27	35	16
hN2342S	193	11	108	9	23	20
hR2454H	185	13	94	29	30	24
hR2458H	169	19	75	14	30	15
hK3452Q	180	10	103	20	35	16
hR4861H	42	13	35	13	19	11
<i>unc-68</i> null	59	17	42	13	22	10

Box shading is consistent with the colour coding used throughout this thesis. RyR variant strains are listed according to the human variant they correspond to.

Figure 3.3: High concentration of DMSO has some effect on *C. elegans* locomotion, but halothane further decreases thrashing rate.

Thrashing rate in S medium (S med), S medium + DMSO (DMSO) and S medium + DMSO + 5 mM halothane (5 mM) for RyR variants, labelled by the human variant they correspond to, along with the wild type and the CB540 (*unc-68(e540)*) null mutant. 25 individuals were examined per strain. (A) Boxes indicate the median and interquartile range, with whiskers to the 10-90 percentile, outliers as dots, and + to indicate the mean. Significance is between S medium and S medium + DMSO or S medium + DMSO and S medium + DMSO + 5 mM halothane, for each strain. ** $P < 0.005$, n.s = not significant (one-way ANOVA, with Sidak's multiple comparison test). (B) Mean and standard deviation (SD) of thrashing rate, in body bends per minute, in each condition.

In S medium containing DMSO *and* halothane the single amino acid changes clearly decrease locomotion of all of the variant strains in comparison to wild type, the same is not seen in S medium with just DMSO. If anything, the presence of DMSO reduces the subtle locomotion differences between RyR variant strains and wild type. In the context of the MH background of the selected variants, and this project, it appears that the reduction in thrashing rate in the presence of DMSO and halothane is attributable to the RyR variants response to halothane.

3.3.3. Ageing effects of ryanodine receptor variants on halothane sensitivity

Many links have been made between ageing and the function of the ryanodine receptor. Specifically for RyR1 variants, in the previous work with *C. elegans* modelling RyR1 variants in *unc-68* expressed as extrachromosomal arrays, the hK3452Q variant, associated with late-onset axial myopathy (LOAM), had an age-related caffeine response phenotype. Furthermore, the median lifespan of all the extrachromosomal array strains was found to be slightly reduced compared to the wild type controls (Nicoll Baines *et al.*, 2017). Additionally, the presence of the *unc-68* variant fosmid in *C. elegans* induced faster muscle ageing, as measured by myofilament disorganisation. A key theory in age-related muscle weakness is a possible reduction in the calcium ion supply available for triggering muscle contraction (Boncompagni *et al.*, 2006). It is specifically thought to be the effect of uncoupling between the dihydropyridine receptor (DHPR) and the RyR, which reduces the amount of calcium available and consequently impairs the function of aged muscle (Delbono *et al.*, 1995; Renganathan *et al.*, 1997). A brief reminder that it is the DHPR, sitting in the t-tubule sarcolemma, which physically interacts with the RyR to signal depolarisation of the vertebrate muscle cell membrane, from neural input at neuromuscular junctions (NMJs). Upon this interaction, the RyR opens, allowing calcium ions to flow into the myoplasm where they activate the contractile machinery. RyRs from aged rat skeletal muscle are shown to have reduced responsiveness that is thought to contribute to depressed calcium ion release in aged skeletal muscle and may result in reduced strength of muscle contraction (Gaboardi *et al.*, 2018). Links have also been made between the RyR and ageing in cardiac muscle and neuronal ageing (Clodfelter *et al.*, 2002; Zhu *et al.*, 2005).

With the incidence of age-related diseases increasing with the increasing average human lifespan, it is important to determine 1) if the ryanodine receptor does play a role and, 2) what that role is. As already outlined, the number of RyR1 variants present in the human population is larger than just those associated with MH. Subtle effects of any of these variants across the entire lifespan may result in much larger effects for the carriers, with age. For this reason, the aspect of age was considered for the both thrashing rate and halothane sensitivity of *C. elegans* carrying *unc-68* mutations equivalent to known human RyR1 variants.

The average lifespan of a wild type *C. elegans* is approximately 15 days, although this varies greatly, due to stochastic environmental and genetic variation (Gems and Riddle, 2000). The average lifespan of the extrachromosomal array RyR variant strains was previously measured as 14-17 days, which was strikingly shorter than the 22-24 days for the direct control wild type extrachromosomal array strains (Nicoll Baines *et al.*, 2017). As the number of live animals rapidly reduces, the remaining animals in an ageing population become more difficult to work with as they are extremely fragile and do not move well. These factors made assays challenging past day ten of adulthood. Therefore, day ten of adulthood was decided as being sufficiently late in life for ageing effects to have accumulated, but not so old that statistically significant assays would be unrealistic and effects would still reflect a large proportion of the population. Any effects found in the few exceptionally long-lived individuals may not be relevant to the majority of the population.

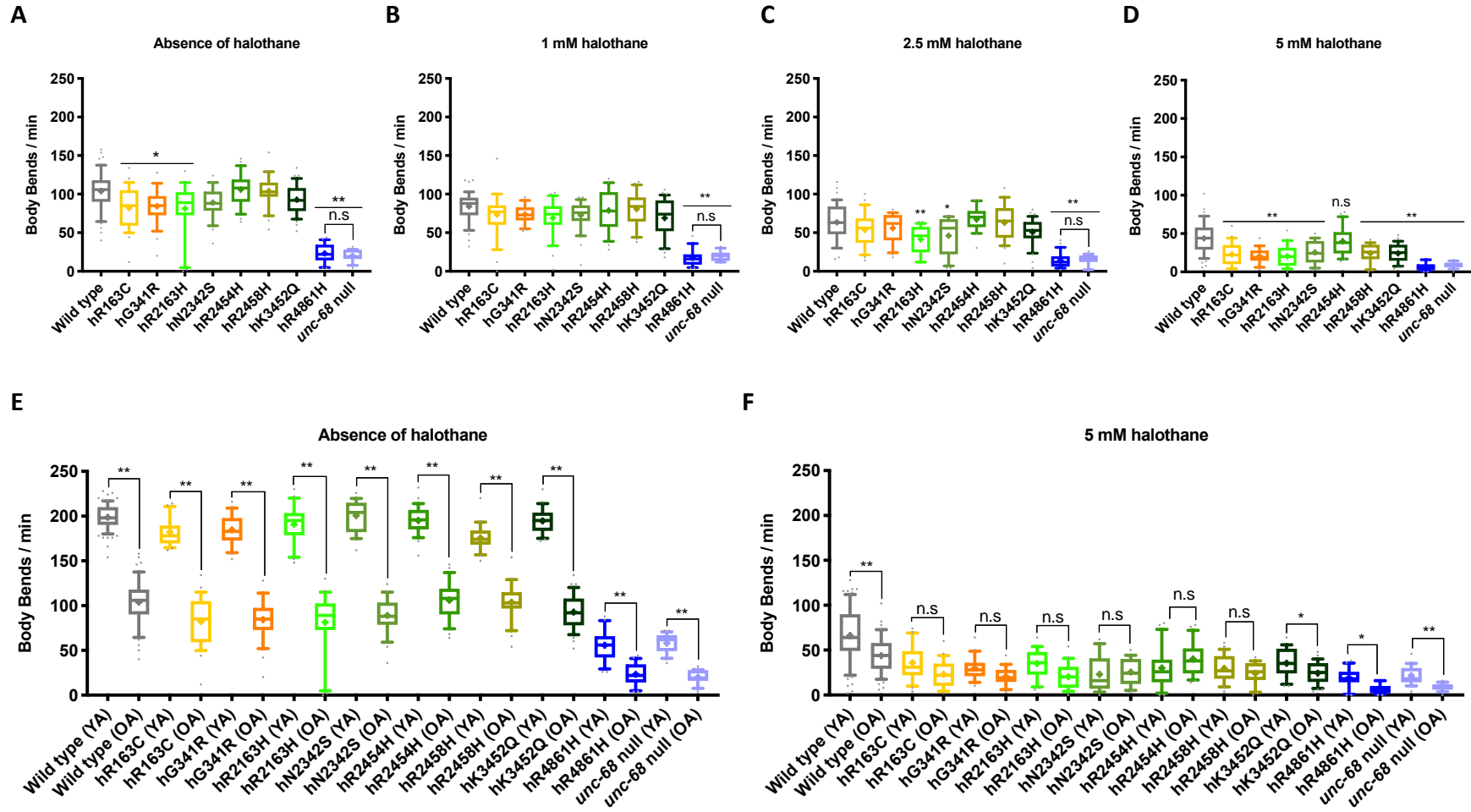
Age-synchronised *C. elegans* were grown until young adulthood and then aged as described in section 2.3.2. On day ten of adulthood the procedure used to test halothane sensitivity in young adults was followed.

In S medium alone, it was evident that ageing reduces the locomotion rate of all strains (Figure 3.4A and E). The thrashing rate for the wild type old adult, with a mean of 104 (± 26) body bends per minute, was approximately half that of the wild type young adult. The old adults of strains for RyR variants hN2342S, hR2454H, hR2458H and hK3452Q were statistically indistinguishable from the wildtype with 89 (± 20), 106 (± 21), 104 (± 21) and 93 (± 19) body bends per minute (Figure 3.4A). Interestingly the

variant hR2458H was the most different to wild type at young adult, excluding the *unc-68* null and the hR4861H variant.

The thrashing rate of old adults of four of the RyR variant strains were statistically less than for the wild type (Figure 3.4A). The hR4861H variant strain was, again, the least active and statistically significantly different from wild type while being indistinguishable from the *unc-68* null mutant ($P < 0.005$ and $P > 0.99$ respectively, One-way ANOVA with Tukey's test).

The three other RyR variant strains that exhibited statistically slower thrashing rates compared to wild type showed more subtle reductions than the hR4861H variant strain, comparable to the locomotion defects seen for young adults earlier. The strains for variants hR163C and hG341R both exhibited subtly reduced thrashing rates at both ages, while the hR2163H variant strain exhibited reduced locomotion only as an old adult. The mean thrashing rates for these strains at day 10 were found to be 82 (± 27), 84 (± 24) and 81 (± 34) body bends a minute (figure 3.4A). The hN2342S variant strain also had a very low thrashing rate at 89 (± 20) body bends per minute, but the variance in the data eliminated any statistically significant difference compared to wild type. For most strains the variance in the data was larger in old adults compared to young adults (Figure 3.4E). The larger variance coupled with the reduced thrashing rate explains why subtle differences are not as readily detectable in old adults. The sampling rate used for young adults was powerful enough to find these subtle effects, but the same sampling rate for old adults was, potentially, not powerful enough.



G

Mean and standard deviation of thrashing rates of old adults in the absence of halothane and 1 mM, 2.5 mM and 5 mM concentrations of halothane for wild type, the CB540 (*unc-68(e540)*) null mutant and RyR variant *C. elegans* strains.

	S medium		1 mM halothane		2.5 mM halothane		5 mM halothane	
	Mean	SD	Mean	SD	Mean	SD	Mean	SD
Wild type	104	26	84	19	63	24	44	21
hR163C	82	27	73	29	54	22	23	15
hG341R	84	24	74	12	56	20	21	10
hR2163H	81	34	69	23	41	18	20	15
hN2342S	89	20	73	19	46	24	25	15
hR2454H	106	21	79	26	67	15	40	19
hR2458H	104	21	81	22	63	24	24	12
hK3452Q	93	19	69	24	51	18	24	12
hR4861H	23	12	17	11	14	10	7	5
<i>unc-68</i> null	20	7	20	6	15	7	9	4

Box shading is consistent with the colour coding used throughout this thesis. RyR variant strains are listed according to the human variant they correspond to.

Figure 3.4: Aged RyR variant individuals are less sensitive to halothane.

Thrashing rate in S medium, in body bends per minute, for RyR variant strains, labelled by the human variant they correspond to, for ten day old adults in the absence of (A) and presence of 1 mM (B), 2.5 mM (C) and 5 mM (D) halothane and comparison between young and old adult in the absence of halothane (E) and in 5 mM halothane (F). 25 individuals were examined per strain. Boxes indicate the median and interquartile range, with whiskers to the 10-90 percentile, outliers as dots, and + to indicate the mean. Significance is between variant strains and the wild type, apart from where indicated to the CB540 (*unc-68(e540)*) null mutant (A-D) and between ages of each variant strain (E and F). * $P < 0.05$, ** $P < 0.005$, n.s = not significant (one-way ANOVA, with Tukey's multiple comparison test (A-D) and Sidak's multiple comparison test for preselected pairs (E and F)). (G) Mean and standard deviation (SD) of thrashing rate, measure in body bends per minute, of old adults in the absence of and increasing concentrations of halothane.

The application of 1 mM halothane removed the statistical differences between the thrashing rates for the wild type and the three RyR variant strains with subtle locomotion defects in the absence of halothane (Figure 3.4B). The three strains for variants hR163C, hG341R and hR2163H do appear to have slightly reduced locomotion in 1 mM halothane, 73 (± 29), 74 (± 12) and 69 (± 23) compared to 84 (± 19) for the

wild type, although not statistically significant. Again, the large inter-individual variance of strains at old age and the reduced thrashing rate may make subtle difference between variant strains and wild type harder to detect. The hN2342S, which was identified as possibly having a similar subtle locomotion defect in S medium, and the hK3452Q variant may also have similarly reduced thrashing rates at this halothane concentration compared to wild type with 73 (± 19) and 68 (± 24) body bends per minute each. This low concentration of halothane may affect thrashing rate of aged *C. elegans*, but further replicates would be needed to confirm that these differences are statistically significant.

In 2.5 mM halothane, it is these same five RyR variant strains that have the lowest thrashing rates, excluding the hR4861H variant strain, adding further support for this distinction being real (Figure 3.4C). At this halothane concentration, the hR2163H and hN2342S variant strains were statistically different to wild type ($P < 0.005$ and $P < 0.05$ respectively, One-way ANOVA with Tukey's test) with 41 (± 18) and 46 (± 24) body bends per minute, versus to 63 (± 24) for wild type. While not significant, the hR163C, hG341R and hK3452Q variant strains thrashing rate was, again, lower than wild type at 54 (± 22), 56 (± 20) and 51 (± 18) body bends per minute. Thrashing rates of hR2454H and hR2458H variant strains, at 63 (± 24) and 67 (± 15) body bends per minute, were close to that for the wild type.

Once again, it was the 5 mM concentration of halothane that revealed the most significant differences in sensitivity to halothane between wild type and RyR variant strains (Figure 3.4D). All the RyR variant strains except that for hR2454H showed statistically significant hypersensitivity compared to the wild type at 5 mM halothane. The hR2454H variant strain performed an average of 40 (± 19) body bends per minute, compared to 44 (± 21) for wild type ($P > 0.99$, One-way ANOVA with Tukey's test). This result led to the question of whether this variant strain became less sensitive to halothane with age.

To decipher the relative loss in sensitivity of the hR2454H RyR variant strain to halothane when compared to wild type, the thrashing rate of all RyR variant strains, wild type and the *unc-68* null were compared as both young and old adults in S

medium and 5 mM halothane (Figure 3.4E and F). All strains showed a significant reduction between young and old adult thrashing rate in the absence of halothane ($P < 0.005$, One-way ANOVA with Sidak's comparison test for predefined pairs) (Figure 3.4E). A significant reduction in thrashing rate was even seen for the hR4861H variant strain and the *unc-68* null mutant, despite the already low thrashing rate as young adults.

To compare the extent of the effect of age on thrashing rate the thrashing rate in old adults can be determined as a percentage of the thrashing rate in young adults, in the absence of halothane (Table 3.3).

Table 3.3: Percentage change of mean thrashing rates in S medium from young to old adult stages for wild type, the CB540 (*unc-68(e540)*) null mutant and RyR variant *C. elegans* strains.

Strain (variant)	YA to OA absence of halothane
Wild type	48%
hR163C	55%
hG341R	54%
hR2163H	55%
hN2342S	56%
hR2454H	46%
hR2458H	41%
hK3452Q	52%
hR4861H	58%
<i>unc-68</i> null	65%

Box shading is consistent with the colour coding used throughout this thesis. RyR variant strains are listed according to the human variant they correspond to. RyR variants are listed in Percent change is calculated as $((C1-C2)/C1)*100$ where C1 is young adult and C2 is old adult.

The wild type and the RyR variant strains thrashing rates decreased by 41-58% between young adult and old adult stages (Table 3.3). The thrashing rate decreased by 48% in wild type from the young to old adult stage. While wild type did group within the RyR variant strains, six of the eight showed a bigger decrease in thrashing rate between the two ages than wild type. The strains for variants hR2454H and hR2458H had smaller decreases in thrashing rate between young and old adult stages, 46% and 41% respectively. The other RyR variant strains had decreases of over 52% between the two ages. The thrashing rate of old adults of the hR4861H variant strain and the

unc-68 null mutant showed larger decreases, 58% and 65% respectively. This may suggest that for the RyR variant strains, except those for hR2454H and hR2458H, age-related decrease in locomotion is slightly exaggerated compared to wild type.

Thrashing rates in 5 mM halothane in the old adults must be considered with respect to the decrease in thrashing rate with age in the absence of halothane. It appears the majority of the RyR variant strains are not as affected by the age-related reduction in thrashing rate seen in the absence of halothane when in 5 mM halothane (Figure 3.4E and F). The only strains that showed a significant reduction in thrashing rate in 5 mM halothane between young and old adult were wild type, the *unc-68* null mutant and the strains for variants hR4861H and hK3452Q. The further reduction in thrashing rate in 5 mM halothane, with age, seen for wild type and not for the hR2458H variant strain explains the apparent loss in statistical significance between these two strains thrashing rates (Figure 3.4D).

Wild type thrashing rate reduced from 66 (± 30) to 44 (± 20) body bends per minute from young to old adult in 5 mM halothane ($P < 0.005$, One-way ANOVA with Sidak's test for predefined pairs) (Figure 3.4F). The *unc-68* null mutant thrashing rate in 5 mM halothane reduced from 22 (± 10) to 9 (± 4) body bends per minute between the two ages ($P < 0.005$, One-way ANOVA with Sidak's test for predefined pairs). A similar response was seen for the hR4861H variant strain, thrashing rate reduced from 19 (± 11) to 9 (± 4) body bends per minute ($P < 0.05$, One-way ANOVA with Sidak's test for predefined pairs), as expected due to its apparent null phenotype.

The hK3452Q variant strain also showed significantly reduced thrashing in 5 mM halothane at old adult compared to young adult (Figure 3.4F). The hK3452Q variant performed 35 (± 16) body bends per minute at young adult in 5 mM halothane and only 24 (± 12) as an old adult ($P < 0.05$, One-way ANOVA with Sidak's test). This was the one variant that was also found to have an age-related increased sensitivity to caffeine previously (Nicoll Baines *et al.*, 2017). The implication of this variant in the age-related RyR1 disease, LOAM, is noteworthy. As mentioned previously, it is usually between the third and eighth decade of life that LOAM is diagnosed. Coupled with the previous caffeine response data with the extrachromosomal array strains, this halothane

response data with the genome-edited strain supports that in *C. elegans* the hK3452Q variant has consequences in later life not conferred by the other RyR1 variants assessed.

As described, there was no further decrease in thrashing rate in the old adults for most RyR variant strains in 5 mM halothane, compared to young adults in 5 mM halothane (Figure 3.4F), however, most RyR variant strains still showed hypersensitivity to 5 mM halothane compared to wild type (Figure 3.4D). This may suggest that the thrashing rate of these strains at young adult is as affected as it can be by 5 mM halothane and, therefore, no further effect of age can be seen. RyRs in these strains are fully compromised by 5 mM halothane.

The wild type, *unc-68* null mutant and the hR4861H and hK3452Q variant strains, showed an age-related decrease in thrashing in 5 mM halothane; this suggests that the RyRs in these strains are not completely compromised by 5 mM halothane in the young adults. Therefore, ageing effects on thrashing rate can be seen. The loss of statistical significance between wild type and the hR2458H variant strain in 5 mM halothane in the old adults is due to a further decrease in thrashing rate in wild type at this concentration, which is not seen for the hR2458H variant strain, not a decrease in halothane sensitivity of this RyR variant strain.

3.3.4. Ryanodine receptor variants reduce thrashing rate in larval stage *C. elegans*

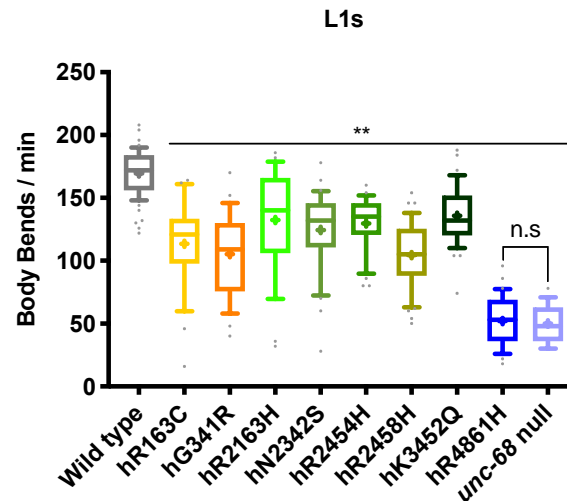
Given the change in effects of halothane on aged adults compared to young adults, the effects of RyR variants on larval *C. elegans* were assessed. During post-embryonic development in the worm, the muscular and nervous system is further developed. Larval stage 1 (L1) is the first of four larval stages, hatching from the egg and are freely moving. The effects of the RyR variants on the earliest freely moving life stage of the worm may reveal an important part of ryanodine receptor function in the worm and, indeed, humans.

At the L1 stage all of the RyR variant strains had much lower thrashing rate compared to wild type, in the absence of halothane ($P < 0.005$, One-way ANOVA with Tukey's test) (Figure 3.5). The L1 wild type did perform fewer body bends per minute than the

young adults. Both the *unc-68* null mutant and the hR4861H variant strain are the only two strains to not show a difference in locomotion between L1 and young adult. Perhaps the effect that the total loss of *unc-68* function, as in the CB540 (*unc-68* (*e540*)) mutant strain, has at L1 is not improved with further neuromuscular development. More subtle RyR modifications, such as the missense single amino acid changes, may allow for improvement in thrashing rate with neuromuscular development.

If the variants are affecting calcium homeostasis in the neuro-muscular system, the less developed animals may well be more sensitive to the RyR variants than the wild type. Alternatively, animals with a defective ryanodine receptor may be able to gradually compensate for the channel's dysfunction with age. There is a tight control system in place around the calcium channel, which may respond by adjusting amounts or activities of other neuromuscular components involved in controlling calcium ion levels in different compartments.

A



B

Mean and standard deviation of L1 thrashing rate in S medium for wild type, the CB540 (*unc-68(e540)*) null mutant and RyR variant *C. elegans* strains.

	L1s	
	Mean	SD
Wild type	197	11
hR163C	178	16
hG341R	169	13
hR2163H	193	12
hN2342S	193	11
hR2454H	185	13
hR2458H	169	19
hK3452Q	180	10
hR4861H	42	13
<i>unc-68</i> null	59	17

Box shading is consistent with the colour coding used throughout this thesis. RyR variant strains are listed according to the human variant they correspond to.

Figure 3.5: Thrashing rate in S medium is reduced in all RyR variant strains at the L1 stage.

Thrashing rate in S medium, in body bends per minute, for RyR variant strains, labelled by the human variant they correspond to, along with the wild type and the CB540 (*unc-68(e540)*) null mutant. Comparisons are between strains as L1s in the absence of halothane. 25 individuals were examined per strain. (A) Boxes indicate the median and interquartile range, with whiskers to the 10-90 percentile, outliers as dots, and + to indicate the mean. ** $P < 0.005$, n.s = not significant (one-way ANOVA, with Tukey's multiple comparison test). (B) Mean and standard deviation (SD) of thrashing rates, measured in body bends per minute, of L1 *C. elegans* in S medium.

3.4. Discussion

The aim of this research was to confirm hypersensitivity of the RyR variant strains when the variant is expressed at the native genomic locus. A higher halothane concentration than expected was required to see clear hypersensitivity, 5 mM instead of 2.5 mM halothane, based on prior observation with expression of the variants from an extrachromosomal array. Aged RyR variant strains were found to be similarly sensitive to halothane as their young adult counterparts, still showing hypersensitivity compared to wildtype. The hypersensitivity of these RyR variant strains to halothane supports the use of these worms as a model for the effects these RyR1 variants may have on the human population. Following on from this, the presence of a subtle locomotion at a range of ages, from L1 to old adults, is a novel result and may be of significance to human carriers of RyR1 variants and requires further, in depth, assessment.

3.4.1. *RYR1* gene variants expressed at the endogenous level in *C. elegans* show hypersensitivity to halothane

Previously, consequences were found for mutations equivalent to known RyR1 disease variants in *unc-68* expressed in *C. elegans* as extrachromosomal arrays (Nicoll Baines *et al.*, 2017). These consequences have now been observed again but with the mutations being expressed from the natural genomic location, rather than from extrachromosomal arrays.

Previously, generation of an extrachromosomal array strain carrying the hR4861H modification did not rescue the *unc-68* null mutant phenotype (Nicoll Baines *et al.*, 2017). Here, this same modification in the genome-edited strains resulted in an apparently null phenotype, suggesting that the presence of this change in the UNC-68 protein eliminated the function of the ryanodine receptor. Indeed, not one example of an hR4861H *RYR1* allele was identified amongst the 125,748 exome sequences or the 71,702 genome sequences on gnomAD (Karczewski *et al.*, 2019), let alone an example of a homozygote. Therefore, the human R4861H RyR1 may also be non-functional, even though the heterozygous state is viable (see section 6.3.1). Similarly, in

C. elegans, the *unc-68* null phenotype was rescued in the extrachromosomal array model of the heterozygous hR4861H state (Nicoll Baines *et al.*, 2017).

Transgene overexpression has been found to result in a more severe phenotype than when the same mutation is introduced via targeted knock-in (Prior *et al.*, 2017). It is likely that the RyR variants present in high copy number as an extrachromosomal array resulted in additional variant channels existing in the animal. This may explain why, upon exposure to 2.5 mM halothane a greater sensitivity was seen in the extrachromosomal array strains than the genome-edited strains. With additional defective channels present in the transgenic strains, the consequences were more severe, and a higher dose of halothane would be required to see a similar effect in animals where the variant channels are only expressed at the endogenous level.

While hypersensitivity was observed in all of the RyR variant strains in the highest concentration of halothane, varying levels of sensitivity were seen by different strains in lower concentrations. In humans, different MH associated *RYR1* genotypes respond differently to halothane, caffeine and ryanodine (Carpenter *et al.*, 2009b). Carpenter *et al.* (2009b) assessed muscle samples from patients with known *RYR1* variants for their responses to known triggers of the calcium channel and compared them to the response for the most common RyR1 variant, G2434R. Of the 22 RyR1 variants assessed, five also feature in this work. When muscle biopsies were exposed to static caffeine the samples from carriers of these five variants showed severe contraction reactions, compared to the most common variant. The same comparison was made for response to static halothane, and only two of these five, R163C and R2454H, were more sensitive and experienced more tension than the G2434R control variant. Upon application of dynamic halothane, the R2454H variant no longer showed increased sensitivity, while the R2163H variant still did. Many other variants were also assessed, with different responses in some conditions and not others, suggesting that the variants respond differently to each trigger (Carpenter *et al.*, 2009b). Here, only one type of analysis was conducted, sensitivity to one concentration of halothane at a time. Both the human biopsy study and the work conducted here show that different RyR variants result in varying severities of responses when exposed to triggering agents.

3.4.2. Endogenous expression of ryanodine receptor variants reveal subtle locomotion defects

No locomotion defect was found for the RyR variant extrachromosomal array strains (Nicoll Baines *et al.*, 2017) and it is often said that MH is asymptomatic, apart from the response to anaesthetics (Robinson *et al.*, 2006). However, in this work a novel phenotype in the absence of halothane was found in several RyR variant strains. The extremely subtle phenotype was not initially detected until cumulation of the data and comparison to the wild type was done. The apparent locomotion defect was then questioned for accuracy. The S medium buffer and its components were remade and the assay of the wild type was repeated directly alongside strains that showed an apparently subtle locomotion phenotype. The result was always reproducible.

It is possible that while the presence of additional defective RyR channels in the extrachromosomal array strains made them more sensitive to a lower dose of halothane, their presence also masked the subtle locomotion phenotype in the absence of halothane. If the variant RyR channels operate only sub-optimally, additional channels may enable the muscle cell to regulate calcium more effectively, thus disguising the slightly reduced thrashing rate.

Although MH patients are referred to as asymptomatic in the absence of a trigger, other RyR1-related diseases do show inherent consequences for neuromuscular function (MacLennan, 2000; Robinson *et al.*, 2006; Illingworth *et al.*, 2014; Laforgia *et al.*, 2018). Individuals with Central Core Disease (CCD) associated *RYR1* variants range from asymptomatic to having severe disability as a result of muscle weakness (MacLennan, 2000; Robinson *et al.*, 2006). The variants R163C and R2163H are both associated with CCD (Robinson *et al.*, 2006). The hR163C variant strain exhibited reduced thrashing speed in S medium alone as both young and old adults, as well as demonstrating the reduced thrashing seen by all strains as L1s. The hR2163H variant strain showed the subtle locomotion defect as old adults, suggesting some age-related effect for this phenotype. *RYR1*-related congenital myopathies are the most common congenital myopathies; >90% of CCD patients have been identified as carrying an *RYR1* variant (Todd *et al.*, 2018). The presence of measurable muscle weakness resulting in

disability in CCD gives support to the subtle locomotion defects found here, in the absence of an MH triggering agent. While CCD is only associated with two variants assessed in this work, subtle locomotion defects are seen in additional variant strains, not just those associated with CCD. Such subtle defects, as seen here, for RyR1 variants in humans would likely go undetected due to the large amount of variation inherent in the human population. These locomotion defects are explored further in chapter 4.

3.4.3. Ryanodine receptor variants have age-related consequences for locomotion in *C. elegans*

The very subtle locomotion defect seen for the hR2163H variant in the absence of halothane in the old adults, described above, was also detected in other variant strains. Although statistical significance for this locomotion defect was only seen between wild type and four variant strains, the hN2342S variant may also exhibit an age-related locomotion defect. Further to this, reduced thrashing was seen for old adults in the intermediate concentrations of halothane by five of the variant strains.

The lack of statistical significance for the reduced thrashing rate of old adults was attributed to the increased variance in the data seen with age. The increase in variance of genetically identical individuals within a strain, with age, is of interest. It has been suggested previously that at least one factor controlling age-related decline in locomotion is stochastic (Herndon *et al.*, 2002). A same-age, isogenic *C. elegans* population was assessed for deteriorating locomotion phenotypes across their lifespan, and it was found that individuals' time to onset and rate of locomotion decline varied greatly, and better predicted lifespan than chronological age. This may suggest that the strains for variants with more reduced locomotion in the old adults would have a shorter lifespan than those with less affected thrashing rates. It may also suggest that, in strains with more variance at old age, the RyR variant is having a greater effect on the stochastic factor(s) that affect age-related decline in locomotion. While lifespan was not assessed here, it has been assessed previously for RyR variants expressed as extrachromosomal arrays in *C. elegans* and found to be reduced in the variant strains (Nicoll Baines *et al.*, 2017).

While there was limited statistical power due to the numbers of individuals examined, further investigation could reveal that more RyR variant strains demonstrate differences to the wild type, with age. Assessing this number of strains at old age is relatively intensive work, even for *C. elegans*, but these preliminary results offer an important starting point for further investigation. This result suggests that *RYR1* variants may have subtle age-related effects on carriers. Indeed many links have been made between ageing and the ryanodine receptor (Delbono *et al.*, 1995; Renganathan *et al.*, 1997; Clodfelter *et al.*, 2002; Zhu *et al.*, 2005; Jungbluth *et al.*, 2009; Løseth *et al.*, 2013; Gaboardi *et al.*, 2018). If indeed the RyR is contributing to age-related decline in muscle function, a variant with a subtle effect on channel function could well have further consequences. The effects of old age on locomotion are explored further in chapter 4.

Interestingly, old age was not the only life stage to show an age-specific effect on locomotion. RyR variant strains in their first larval stage exhibited a strongly reduced rate of thrashing in liquid when compared to the wild type. In comparison only some of these *unc-68* mutations showed a significant reduction at the young and old adult stages. In *C. elegans* the nervous and muscular system undergo postembryonic development from the L1 to the young adult stage (Sulston and Horvitz, 1977). Five of the eight motor neuron classes are generated at the end of L1, as well as 14 of the 95 body wall muscles present in the adult are generated at the end of L1. Furthermore, during the L1 stage one class of ventral cord motor neuron undergoes complete synaptic reorganisation for synaptic connections to the dorsal and ventral body wall muscle. With so much development of the neuromuscular system during and after the L1 stage, it is possible that mutations affecting the calcium levels in the neuromuscular system have larger effects on these cells at this age. It is also possible that the simpler neuromuscular system of this life stage makes L1 stage *C. elegans* more sensitive to perturbation in RyR function.

It is speculated that the physiology of the worm could adapt gradually across the lifespan specifically to subtle defects in RyR function and calcium ion regulation, due to the presence of RyR variants. Such adaptation would allow locomotion to progressively improve with age. The ryanodine receptor is tightly controlled through interactions

with a number of other proteins, forming a macromolecular complex. It is possible that this large regulatory complex could allow for such an adaptation to occur. Other proteins are also involved in calcium ion distribution across the sarco- and endoplasmic reticulum membrane and could contribute to such compensation. A compensatory mechanism has been suggested previously in mouse models of RyR1 variants, which is discussed in detail in section 4.4.2 (Andronache *et al.*, 2009). Further analysis on thrashing rate in S medium could be conducted at all larval stages and at several intermediate adult stages to find evidence of such adaptation.

3.4.4. Sensitivity to halothane is not affected by age in most ryanodine receptor variant strains

The effect of age on halothane sensitivity for human carriers of RyR1 variants is not readily available. Here, aged *C. elegans* were exposed to the same halothane concentrations as the young adult animals. The lack of increased reaction to halothane in aged animals, compared to their young adult counterparts, suggests that variant RyRs are fully compromised by 5 mM halothane as young adults. With such dramatic reductions in thrashing in S medium at old age compared to young adult, it would be expected that a similar reduction would be seen in 5 mM halothane. Part of this reduction in thrashing speed would be due to halothane sensitivity and part to ageing effects. However, locomotion of young and old adult RyR variant strains in 5 mM halothane were not distinguished, except in two cases, suggesting that the halothane effect in young adults is to such an extent that no age-related effects can be seen in old adults.

The exception to the lack of age-related decrease in thrashing rate in halothane in RyR variant strains with age, are the strains for variants hK3452Q and hR4861H. Both show an age-related decrease in thrashing rate in 5 mM halothane. The hK3452Q variant is linked to an age-specific RyR1-related myopathy and so this result is not surprising (Jungbluth *et al.*, 2009; Løseth *et al.*, 2013). Previously this variant was found to have an age-related caffeine response (Nicoll Baines *et al.*, 2017). The increase in halothane response for hR4861H mirrors what was seen for the *unc-68* null mutant, once again suggesting this variant disrupts RyR function entirely.

Chapter 4

Investigating the subtle locomotion phenotype found in the absence of a malignant hyperthermia trigger in *C. elegans* ryanodine receptor variant strains: Quantifying crawling

4.1. Introduction

4.1.1. Aim of this chapter

The aim of the research described in this chapter was to quantify the locomotion defects described in chapter 3. Subtle differences in thrashing rate between several RyR variant strains and wild type were observed. However, the cause of these differences could only be speculated upon. By exploring how locomotion differs between wild type and these RyR variant strains, the mechanism underlying the change can begin to be unravelled. Since a locomotion defect was observed in both young and old adult RyR variant strains in liquid both of these life stages were investigated.

4.1.2. *C. elegans* locomotion

For the first time, locomotion defects were observed in strains carrying mutations in *unc-68* equivalent to known human RyR1 variants in the absence of an MH triggering agent. These defects were identified in liquid thrashing assays and *C. elegans* is routinely maintained on an agar surface, where it crawls. Crawling is restricted to the flat surface of the agar plate with the animal lying on its left or right side; animals propel themselves forward in the form of a wave by alternatively contracting dorsal and ventral muscles (Seddon, 2016; Shaw *et al.*, 2018) (Figure 4.1). Crawling on an agar surface and thrashing in liquid are two forms of locomotion in *C. elegans*, however, it is debated whether these are two distinct gaits or two ends of a continuum (Pierce-Shimomura *et al.*, 2008; Vidal-Gadea *et al.*, 2011; Boyle *et al.*, 2012). The worm's crawling locomotion is well understood (Berri *et al.*, 2009; Zhen and Samuel, 2015). Therefore, this was considered the best focus for quantification of the subtle locomotion differences that were observed for several of the RyR variant strains, compared to wild type, at young and old adult stages in liquid (chapter 3).

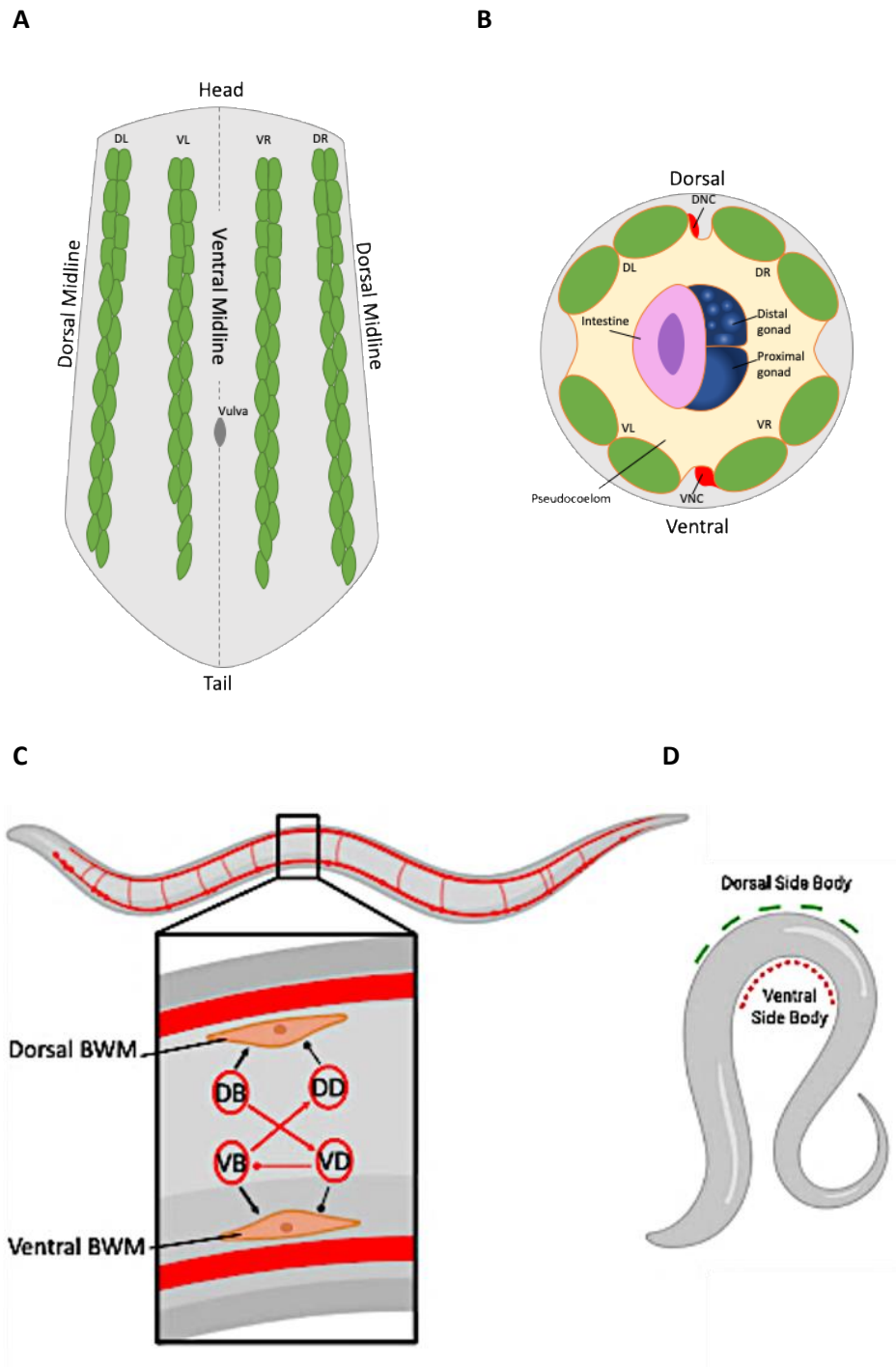


Figure 4.1: Arrangement of adult hermaphrodite body wall muscle.

Body wall muscles are arranged in four sets of longitudinal bundles, each containing 24 interleaved muscle cells, except for the ventral left quadrant (VL) that has 23 as shown in a filleted adult hermaphrodite (A). (B) A cross-section through an adult hermaphrodite shows arrangement of muscle quadrants. Dorsal Left (DL), Ventral Left (VL), Ventral Right (VR) and Dorsal Right (DR) body wall muscle quadrants are indicated; ventral nerve cord (VNC) and dorsal nerve cord (DNC) are shown. The body

wall is separated from the digestive and reproductive systems by the pseudocoelom. Excitation of the VB motor neurons activates the ventral muscle cells (Ventral BWM) and excitation of the DD motor neurons inhibits contraction of dorsal muscle cells (Dorsal BWM) (C). This pattern of excitation results in the body bending away from the dorsal side (D). Created with BioRender (<https://biorender.com/>) based on information from Sulston and Horvitz (1977) (A), Altun and Hall (2009b) (B) and White *et al.* (1986) (C).

Crawling is a slower motion than the thrashing motion discussed previously and measuring parameters of crawling is easier than for thrashing. The slower and more restricted locomotion on an agar plate, compared to in liquid, may put greater or lesser demands upon an RyR variant challenged neuromuscular system due to the increased resistance and/ or slower speed of locomotion. In 'the wild' the worm would move in a three-dimensional environment, which has been observed and measured in a laboratory setting but is much harder to parameterise (Holbrook, 2016; Shaw *et al.*, 2018). Therefore, only the restricted, two-dimensional, crawling locomotion will be described here.

The wave generated by the alternative contraction of ventral and dorsal body wall muscles travels posteriorly along the body length (Seddon, 2016). The body wall muscles of the worm are organised into four longitudinal bundles, dorsal left (DL), dorsal right (DR), ventral left (VL) and ventral right (VR) (Figure 4.1A and B). Each longitudinal bundle is made up of 23 or 24 paired muscle cells in an interwoven pattern (Sulston and Horvitz, 1977).

For sinusoidal forward locomotion, the body wall muscles are innervated by four classes of ventral nerve cord (VNC) motor neurons, VB, VD, DB and DD (White *et al.*, 1986) distributed along the length of the worm (Figure 4.1C). The B-type motor neurons, VB and DB, are stimulatory cholinergic neurons (Duerr *et al.*, 2008), while the D-type, VD and DD, are GABAergic and inhibitory (McIntire *et al.*, 1993). The D-type inhibitory motor neurons are post synaptic to the A and B-type excitatory motor neurons, which allows the B-type motor neurons to excite the muscle cell, as well as the D-type motor neurons on the opposite side of the body inhibiting the opposite

muscle cell (Pereira *et al.*, 2015; Zhen and Samuel, 2015). For a body bend away from the dorsal side, the ventral body wall muscles would be excited to contract, via the VB motor neurons, while contraction of the dorsal body wall muscles would be inhibited by activation of the inhibitory DD motor neurons (Riddle *et al.*, 1997). This would lead to the ventral side body contracting while the dorsal side body relaxed, resulting in a bend away from the dorsal side of the animal (Figure 4.1D). While the neural network controlling excitations of the VB, VD, DB and DD motor neurons and sinusoidal locomotion is more complex than this, this basic explanation of sinusoidal wave propagation is sufficient for purposes here.

Propagation of the sinusoidal wave down the body requires coordination of the neuromuscular system (Riddle *et al.*, 1997). Motor neurons are connected to muscle cells via neuromuscular junctions (NMJs). In most organisms, neurons send processes to their target muscle cells to make synapses; in *C. elegans* it is the muscle cells that have processes, muscle arms, which extend toward the motor neurons (Dixon and Roy, 2005). Nevertheless, the principles of synaptic transmission at NMJs remain the same. As described previously, calcium plays an important role in neurotransmission, increasing calcium ion concentration in presynaptic terminals upon receipt of an action potential triggers neurotransmitter release (Südhof, 2012). Upon excitatory neurotransmission at NMJs, the sarcolemma of *C. elegans* muscle cell is depolarised. Calcium signalling also plays an important role in E-C coupling required for muscle contraction (Ríos *et al.*, 1991). Calcium mishandling in the neural and/ or muscular system may have large consequences for the sinusoidal wave of *C. elegans* crawling.

RyR1, the human protein in which the variants studied here are found, is often considered the skeletal muscle isoform of this calcium ion channel (Marks *et al.*, 1989; Takeshima *et al.*, 1989). However, RyR1 is also present in other excitable cells, such as nerve cells in the brain, as described previously (Zissimopoulos *et al.*, 2006; Abu-Omar *et al.*, 2018). The only *C. elegans* ryanodine receptor, UNC-68, is found in both muscle and neural tissues (Maryon *et al.*, 1996). Quantifying parameters of the crawling sinusoidal waveform and how they change in the RyR variant strains compared to wild type may be used to infer how RyR function is perturbed by the presence of each variant. The RyR variants could have different consequences for calcium release in

different cell types in the worm, meaning how they alter calcium release in neural cells may not be the same in muscle cells.

The body shape generated by alternatively contracting body wall muscles in *C. elegans* during forward crawling locomotion results in a movement that resembles a transverse wave. Therefore, the locomotion of *C. elegans* can be quantified by studying wave parameters such as amplitude, wavelength and frequency (Figure 4.2A).

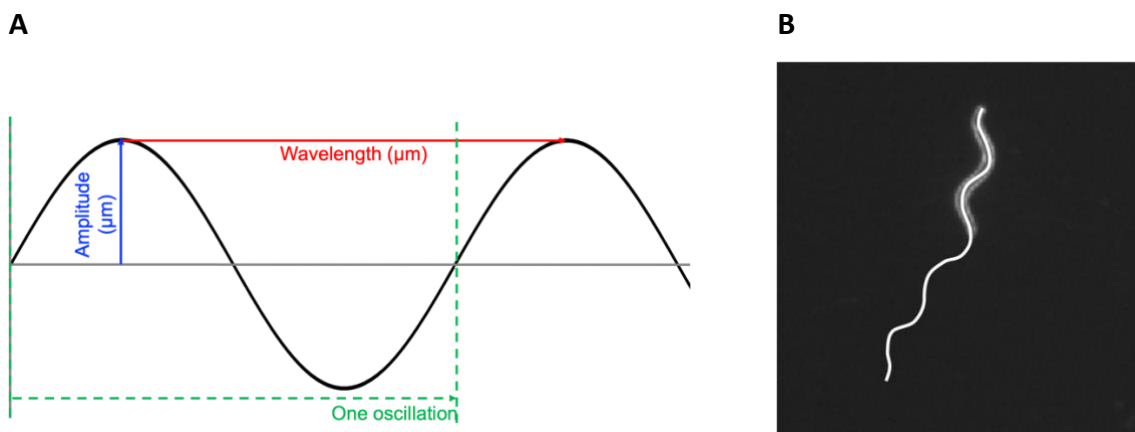


Figure 4.2: Quantifying *C. elegans* locomotion using parameters that describe a wave.

(A) Amplitude, wavelength and frequency are parameters used to describe a wave. Amplitude is the distance from equilibrium to the peak (or trough), shown in blue. The wavelength is the distance between two successive amplitudes, shown in red. The frequency is the number of oscillations (one oscillation is shown in green) per second, measured in Hertz (Hz). (B) A single *C. elegans* is shown crawling across an agar plate, the path of the worm is traced in white; although the worm is moving in time the wave path it is tracing out is not. Image captured in ImageJ (Schneider *et al.*, 2012), and the path traced by hand and overlaid. The parameters in A can be used to describe the wave form of the worm crawling in B.

The amplitude of the wave is defined as the distance that the wave moves on either side of the equilibrium position (Figure 4.2A in blue). The distance between two successive amplitudes of the wave, and therefore the distance the wave travels for one oscillation, is defined as the wavelength (Figure 4.2A in red). The frequency is the number of oscillations per second (Hz). While the body of the worm forms the shape of a wave, the wave shape never moves in time, but the animal's body forms a new,

static, wave shape (Figure 4.2B). Due to the crawling locomotion only resembling a transverse wave, the speed of crawling was assessed and refers to the speed at which the worm moves, not the speed of the wave. The degree of curvature of body bends was also analysed to understand how the RyR variants affect muscle contraction during crawling. Together, these parameters were used here to investigate the consequences that RyR variants in *C. elegans* have on crawling locomotion.

4.2. Methods

4.2.1. Locomotion analysis via multi-worm tracking

Animals were grown to the appropriate age as described (see section 2.3) factoring in the developmental delay seen for the *unc-68* null mutant and hR4861H variant strain (see section 2.3.1). One unseeded 90 mm 25 ml NGM plate at 20°C was prepared per strain at each life stage. Prior to recording, a 1 mm scale was placed face down on the NGM surface and a picture captured, the scale was then carefully removed. 20-30 individuals per strain at each life stage were transferred to the plate, avoiding transfer of food. The animals were recorded crawling freely for 1 minute.

Videos were recorded using a multi-worm tracker system set up by, and used with permission of, the Cohen group at the University of Leeds (Figure 4.3). The system uses a Navitar telemetric lens and a Ximea xiQ USB camera to capture video of worms crawling on an NGM plate, with dark field illumination by a PolyTech LED red light ring. Videos were recorded at 25 fps using StreamPix 7 (version 7.2.1). Scales were calculated for each video using ImageJ software (Schneider *et al.*, 2012).

4.2.2. Video analysis

Videos were analysed, post-recording, using TierpsyTracker 1.4.0 software (Javer *et al.*, 2018). Prior to analysis parameters were set for each video. Each video had its own precise scale set, as measured previously in ImageJ (Schneider *et al.*, 2012). Frame rate was always 25 fps and the automatic 'Light Background' option was unchecked. Due to the red-light ring animals appeared white on a dark background. The minimum area that could be determined as a worm was set between 50 and 100 pixels to reduce

noise from debris on the plate being mistakenly tracked. Recordings of the *unc-68* null mutant and the hR4861H variant strain had smaller minimum areas than wild type and the other RyR variant strains, due to their reduced size.

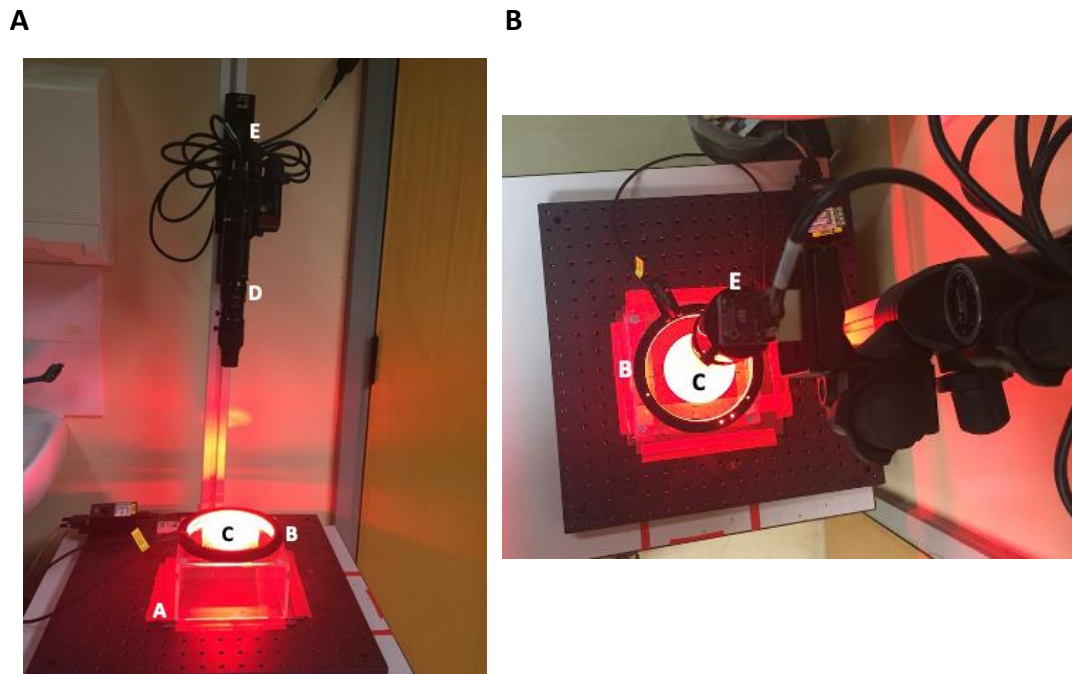


Figure 4.3: Multi-worm tracker system set up.

The multi-worm tracker system was used with permission of the Cohen group. A 90 mm agar plate (C) was placed on a transparent block (A) and lit by a red-light ring (B). The use of a red-light ring is to illuminate the animals and increase the contrast between the transparent animals and the background, allowing easier detection in post-video analysis. A telemetric lens (D) was attached to a Ximea USB camera (E).

Analysis examples, available online (https://github.com/aexbrown/tierpsy_tools) were used to work with the timeseries data directly by reading the ‘features’ files from TierpsyTracker 1.4.0 in MATLAB. Some code was adapted by Omer Yuval from the Cohen group at the University of Leeds and used with permission. Raw length, maximum amplitude, primary wavelength, midbody crawling frequency and midbody crawling speed values were extracted for each strain. To extract data, features files from TierpsyTracker 1.4.0 were converted and opened in MATLAB. Data was available per frame, per individual, for each parameter, for each strain.

Worm lengths were manually measured for comparison to extracted worm length data to ensure accuracy of the software (Figure 4.6). The length of 5 individuals per strain were measured in 5 random frames using ImageJ (Schneider *et al.*, 2012), for a total of 25 measurements per strain.

4.2.3. Worm Length, crawling speed and waveform parameters

Worm length, crawling speed, maximum amplitude, primary wavelength and midbody frequency of each worm in each frame of each video was measured by TierpsyTracker 1.4.0 (Javer *et al.*, 2018).

Worm length was measured as the length of the skeleton, in micrometres (μm). The skeleton is calculated as the midline of the animal from head to tail. This value was calculated for each of 20-30 individuals in each frame of the 1 minute video for each strain.

The maximum amplitude is measured as the maximum distance between the midline and peak or trough of the worm's sinusoidal wave, in micrometres (μm) (Figure 4.2A). This value was calculated for each of 20-30 individuals in each frame of the 1 minute video for each strain. These values were then divided by the length of the strain to account for differences in worm length. The amplitude:length ratios were then compared between strains.

The same approach was used for primary wavelength. The primary wavelength is a measure of the largest wave in each frame for each individual, in micrometres (μm) (Figure 4.2A). Again, the values for wavelength were calculated as a fraction of the length.

The frequencies presented here were calculated for the midbody. Frequency is a measure of the number of oscillations completed per second, in Hertz (Hz). Worm crawling speed was also determined for the midbody and is a measure of micrometres moved per second ($\mu\text{m/s}$). Frequency and speed values were converted to positive as directional distinctions were not considered significant for this research.

The data points recorded for each of the 20-30 animals per strain were merged into one data set for each strain. To confirm the compiled data set extracted for each strain was an accurate reflection of individual variation, the crawling parameters of individual animals for wild type were also extracted and compared (Appendix F).

4.2.4. Degree of curvature

In order to quantify the effects of RyR variants on degree of muscle contraction the degree of curvature was measured (Kalogeropoulou, 2018) (Figure 4.4). The sharpness or flatness of a curve is defined by the degree of curvature; a flatter curve has a smaller degree of curvature and vice versa. Degree of curvature was measured for 26 individuals in random frames from the recorded videos, for each strain, using GeoGebra version 6.0562.0, www.geogebra.org (Hohenwarter, 2002).

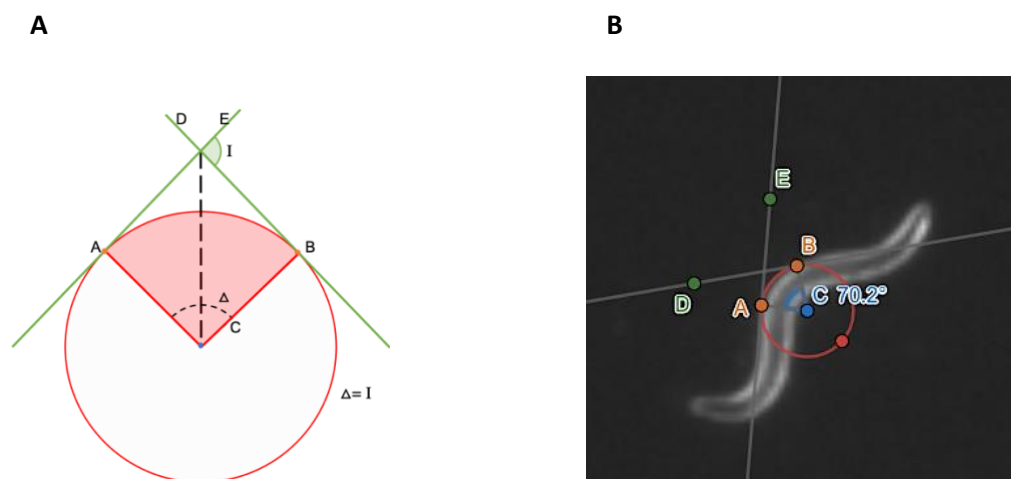


Figure 4.4: Measuring the degree of curvature for RyR variant strains.

Elements of a curve (A), adapted from <http://www.tpub.com/inteng/11a.htm> (Integrated publishing Inc.), used to measure degree of curvature of an individual (B). A circle was drawn fitting to the curve of the outside body wall of the worm. Backward and forward tangents, D and E, were drawn passing through the start and end of the curve, points A and B. Δ is the degree of curvature measure at C. Degree of curvature was only measured on animals showing regular undulatory forward crawling.

4.2.5. Kymograms

Kymograms provide a visual representation of worm crawling. The spatial position of points along the body across time and the frequency with which the wave is propagated down the body axis can be seen; kymograms are used to show curvature along the body (Denham *et al.*, 2018). Colours represent bend angles, with dark blue and dark red representing deep dorsal or ventral bends (Figure 4.5). Inclination and overlap between stripes reflect the frequency and wavelength of the crawling wave form.

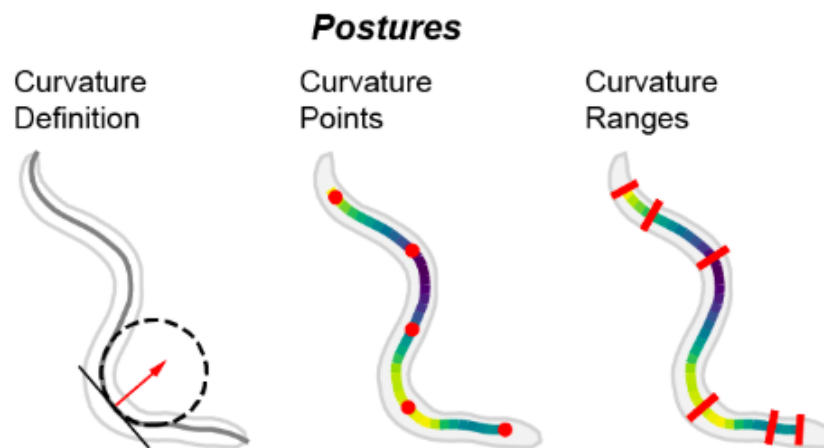


Figure 4.5: Kymograms show curvature down the body axis.

The colour in the kymograms indicates degree of dorsal/ ventral curvature, yellow/ blue high curvature, green no curvature, at different positions along the major body axis for each frame of the video recording. In this research red and blue were used to show dorsal and ventral curvature to increase the scale (Figure 8).

Kymograms were extracted for all individuals per strain; one representative figure for one individual at young and old adult, per strain, is presented here (Figure 4.10 and G.3).

4.3. Results

4.3.1. Ryanodine receptor variants affect young adult worm length

The amplitude and wavelength of the sinusoidal wave of *C. elegans* rely, in part, on the absolute size and length of the animal. To remove worm length as a factor impacting these measures, the mean length for each strain was first assessed.

Young adults were recorded moving freely for 1 minute. The absolute length of the animals was measured in TierpsyTracker 1.4.0 (Javer *et al.*, 2018) and verified by hand measuring several individuals using ImageJ (Schneider *et al.*, 2012) (Figure 4.6). This was to validate the worm tracking software and ensure that it was able to extract measurement data in a reliable and accurate manner.

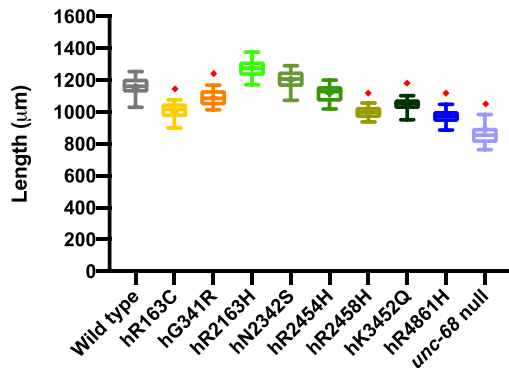
Young adult wild type *C. elegans* are referred to as 'approximately 1 mm long' (Corsi *et al.*, 2015). Here, wildtype average worm length was 1155 μm ($\pm 79 \mu\text{m}$) (Figure 4.6A). The *unc-68* null mutant strain had the shortest average worm length at young adult, 892 μm ($\pm 169 \mu\text{m}$), in agreement with this strain being described as smaller than wild type (Maryon *et al.*, 1998). The automatically extracted wild type and null mutant worm lengths were consistent with the hand measurements (Figure 4.6B).

Once again, the hR4861H variant strain appeared similar to the *unc-68* null mutant with a young adult mean length of 968 μm ($\pm 125 \mu\text{m}$), again alluding to this variant severely affecting UNC-68 function. That both of these strains are shorter than wild type as young adults is, perhaps, not surprising given the developmental delay observed for these strains. Interestingly, the other RyR variant strains had a range of median lengths, suggesting that the presence of these variants may also affect development.

Strains other than the null mutant and hR4861H variant strain were anecdotally noted as developing a little slower, sometimes not having as many eggs present as other strains when they were all synchronised at the same time

Strains for variants hR163C, hG341R and hR2458H were found to be shorter than wild type, measured as 1001 μm ($\pm 90 \mu\text{m}$), 1089 μm ($\pm 59 \mu\text{m}$), and 998 μm ($\pm 47 \mu\text{m}$) long respectively (Figure 4.6A). It was these three variant strains that were initially found to have reduced thrashing rates in S medium as young adults (Chapter 3), the results that led to this in-depth analysis of crawling. That these three variant strains were shorter than wild type and showed differences from wild type when swimming in liquid seems likely to be causally related.

A



B

Mean and standard deviation of young adult worm length for wild type, the CB540 (*unc-68(e540)*) null mutant and RyR variant *C. elegans* strains.

	Worm length (µm)	
	Mean	SD
Wild type	1155	79
hR163C	1001	90
hG341R	1089	59
hR2163H	1278	88
hN2342S	1202	121
hR2454H	1119	75
hR2458H	998	47
hK3452Q	1042	61
hR4861H	986	125
<i>unc-68</i> null	892	169

Box shading is consistent with the colour coding used throughout this thesis. RyR variant strains are listed according to the human variant they correspond to.

C

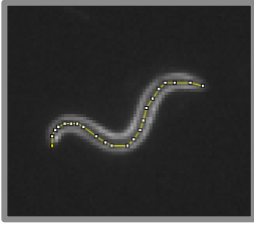
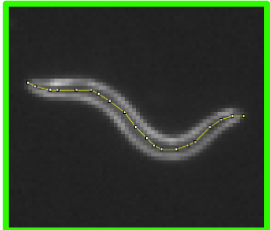
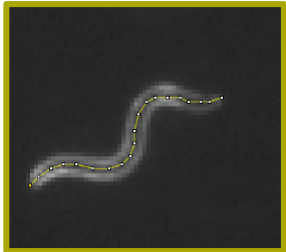
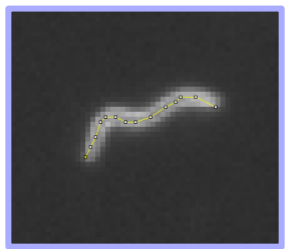
Strain (variant)	Image used for hand measuring	Hand measured length	Tracker average length
Wild type		1.15 mm	1.16 mm
hR2163H		1.21 mm	1.28 mm
hR2458H		1.00 mm	1.00 mm
<i>unc-68</i> null		0.85 mm	0.87 mm

Figure 4.6: The presence of RyR variants affect the length of young adults.

(A) Worm length, extracted from 1 minute long, 25 frames per second, video recordings of 20-30 individual young adults, for RyR variant strains, labelled by the human variant they correspond to, along with the wild type and the CB540 (*unc-68(e540)*) null mutant, were compared. Boxes indicate the median and interquartile range, with whiskers to the 10-90 percentile and + to indicate the mean. Strains shorter than wild type are indicated with a red diamond. (B) Mean and standard deviation (SD) of young adult worm lengths, in micrometres, extracted from video recordings. (C) Hand measurements of length for one individual of wild type, the *unc-68* null mutant and the largest and smallest RyR variant strains, hR2163H and hR2458H, were found to be in agreement with the average length measurements from the extracted compiled data set produced by TierpsyTracker 1.4.0. Both the hand measurement and mean measurement from the data analysis are shown to two decimal places in mm. Picture box outline and strain name colour corresponds to the strain's colour in the box plot above.

The hK3452Q variant strain was also found to be slightly shorter than wild type, with a mean length of 1042 μm ($\pm 61 \mu\text{m}$) (Figure 4.6A). The strain for variant hR2454H had a very similar length to wild type, measured at 1119 μm ($\pm 75 \mu\text{m}$). Only two variant strains were found to be longer than wild type, strains for variants hR2163H and hN2342S were found to be 1278 μm ($\pm 88 \mu\text{m}$) and 1202 μm ($\pm 121 \mu\text{m}$) long, respectively

UNC-68 is present in the pharynx and contributes to pharyngeal pumping; the *unc-68* null mutant has a reduced pumping rate (Maryon *et al.*, 1998). Bacteria is the food source of *C. elegans* in laboratory conditions and is consumed by *C. elegans* by pharyngeal pumping. Either neural and/ or muscle function required for pharyngeal pumping may be affected by the presence of these variants in *unc-68*, resulting in reduced feeding rate and consequently slower growth rate and shorter size at the onset of egg laying.

4.3.2. The sinusoidal wave of crawling in young adult *C. elegans* is affected by the presence of ryanodine receptor variants

The different average lengths of different worm strains has a consequence for any crawling parameters that are a measure of distance. As amplitude is a measure of the distance between the equilibrium and peak or trough of the wave, and wavelength a measure of the distance the wave travels in one oscillation, these measurements were assessed with respect to worm length (Figure 4.2A).

The crawling amplitudes of RyR variants, including the hR4861H variant strain, when expressed as a ratio of amplitude to length, were statistically significantly smaller than wild type (Table 4.1, Figure 4.7A). The average amplitude:length ratio for wild type was indistinct from the *unc-68* null mutant ($P=0.99$, One-way ANOVA with Tukey's multiple comparisons).

Table 4.1: Mean and standard deviation (SD) of crawling parameters amplitude, wavelength and frequency for the RyR variant strains, wild type and the CB540 (*unc-68(e540)*) null mutant.

Strain (variant)	Amplitude:Length		Wavelength:Length		Frequency (Hz)	
	Mean	SD	Mean	SD	Mean	SD
Wild type	0.184	0.061	0.63	0.16	0.35	0.10
hR163C	0.183	0.060	0.58	0.09	0.48	0.13
hG341R	0.170	0.051	0.58	0.08	0.46	0.08
hR2163H	0.177	0.056	0.61	0.09	0.40	0.11
hN2342S	0.163	0.051	0.61	0.13	0.49	0.13
hR2454H	0.177	0.061	0.59	0.12	0.44	0.15
hR2458H	0.165	0.043	0.55	0.08	0.43	0.10
hK3452Q	0.174	0.051	0.59	0.09	0.43	0.11
hR4861H	0.164	0.064	0.69	0.26	0.29	0.27
<i>unc-68</i> null	0.185	0.082	0.70	0.25	0.22	0.22

Box shading is consistent with the colour coding used throughout this thesis. RyR variant strains are listed according to the human variant they correspond to. Amplitude and wavelength are corrected for length. Amplitude is shown to three decimal places, and wavelength and frequency to two.

All RyR variant strains, except the hR4861H variant strain, had a statistically significantly smaller wavelength:length ratio than wild type ($P<0.005$, One-way ANOVA with Tukey's multiple comparisons) (Table 4.1, Figure 4.7A). The *unc-68* null mutant and the hR4861H variant strain had statistically significantly larger wavelength:length ratios than wild type ($P<0.005$, One-way ANOVA with Tukey's multiple comparisons).

When the values obtained after amplitude and wavelength are expressed as a ratio to length were plotted together the RyR variant strains sat apart from wild type (Figure 4.7A). For the most part the RyR variant strains grouped together, and separately from wild type and the null mutant. All RyR variant strains had a shorter amplitude:length ratio than wild type and all but the hR4861H variant strain had a shorter wavelength:length ratio. There is a slight positive correlation between amplitude:length and wavelength:length ratios; a larger amplitude:length ratio goes with a larger wavelength:length ratio, and vice versa, but this relationship was not statistically significant ($r=0.18$, $P=0.63$).

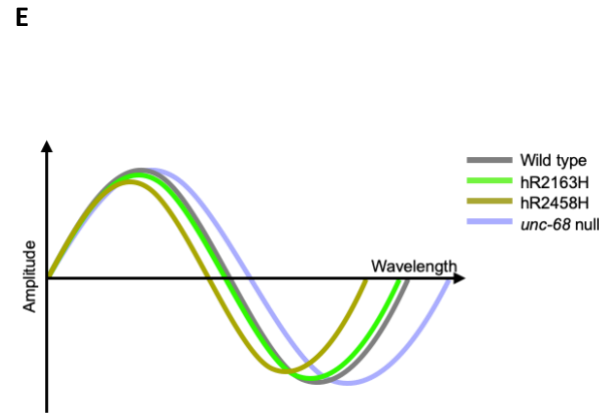
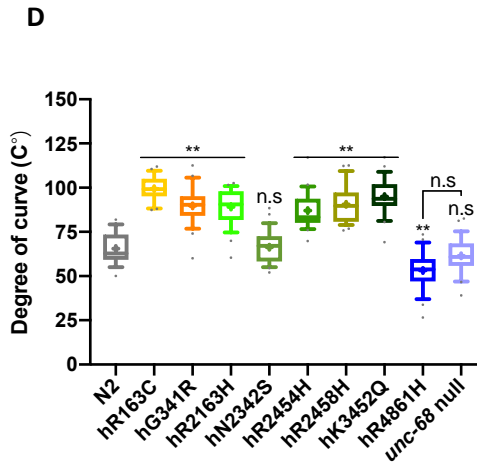
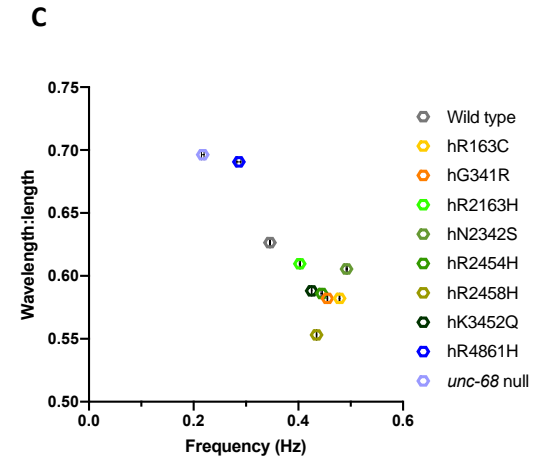
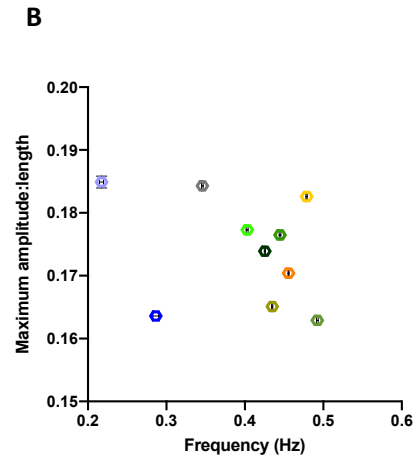
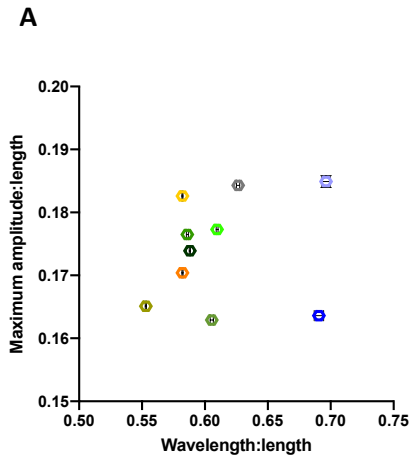
For the first time the hR4861H variant strain was distinct from the *unc-68* null mutant, for amplitude:length ratio. Previously this variant strain had been indistinguishable from the null mutant in thrashing and halothane assays (Chapter 3). This demonstrates that this variant is in fact non-null.

Changes to amplitude or wavelength effect the degree of curvature of the sinusoidal waveform (Figure 4.7D and E). If absolute wavelength remained the same and absolute amplitude decreased the wave would be flatter and the degree of curvature would be smaller. If absolute amplitude remained the same while absolute wavelength decreased the wave would be sharper and the degree of curvature would be larger. Here both absolute wavelength and absolute amplitude decreased in the RyR variant strains, compared to wild type. If they did so by the same amount, then the degree of curvature would remain constant. Comparison of mean percentage change of each crawling parameter between wild type and each of the RyR variant strains, and the *unc-68* null mutant, revealed that only the hN2342S variant strain had an equal change in wavelength and amplitude (Table 4.2), resulting in no statistically significant difference between wild type and the hN2342S variant strain for degree of curvature (Figure 4.7D).

The *unc-68* null mutant had a larger wavelength than wild type, by 11%, but the same amplitude, resulting in a smaller degree of curvature, although this was not statistically significant ($P=0.90$, One-way ANOVA with Tukey's test) (Figure 4.7A, D and E, Table

4.2). The smaller amplitude of the hR4861H variant strain than both wild type and the *unc-68* null mutant, but similar wavelength to the latter, resulted in the smallest degree of curvature of all strains assessed, which was statistically significantly smaller than wild type ($P < 0.005$, One-way ANOVA with Tukey's test) (Figure 4.7A and D, Table 4.2). For the other RyR variant strains, except that for hN2342S, both wavelength and amplitude were smaller than wild type, but the decrease was larger for wavelength, resulting in a larger degree of curvature and sharper wave than wild type ($P < 0.005$, One-way ANOVA with Tukey's test for multiple comparisons) (Figure 4.7D, Table 4.2).

When maximum amplitude was plotted against frequency (Figure 4.7B) the resulting graph was almost a mirror image of maximum amplitude versus wavelength (Figure 4.7A). Again, the RyR variant strains grouped closely together, this time with a slight negative correlation between amplitude:length and frequency; a larger amplitude:length ratio goes with a lower frequency, and vice versa, but again this relationship was not statistically significant ($r = -0.31$, $P = 0.38$). All RyR variant strains, except that for hR4861H, had a higher frequency than wild type (Table 4.1, Figure 4.7B). The *unc-68* null mutant had the lowest frequency and the hR4861H RyR variant has the second lowest frequency. These two strains had the largest wavelength:length ratios. The strain for variant hN2342S, which had no change in the degree of curvature compared to wild type, had the highest frequency of all strains (Table 4.1).



F Mean and standard deviation of degree of curvature for wild type, the CB540 (*unc-68(e540)*) null mutant and RyR variant *C. elegans* strains.

	Degree of curvature (C°)	
	Mean	SD
Wild type	65.54	8.60
hR163C	99.44	7.11
hG341R	89.73	10.85
hR2163H	89.05	10.82
hN2342S	66.33	9.36
hR2454H	87.12	10.20
hR2458H	90.57	10.96
hK3452Q	94.95	10.15
hR4861H	53.14	11.03
<i>unc-68</i> null	61.46	10.11

Box shading is consistent with the colour coding used throughout this thesis. RyR variant strains are listed according to the human variant they correspond to.

Figure 4.7: The RyR variant strains have decreased amplitude and wavelength of the crawling waveform compared to wild type, but increased frequency.

The mean maximum amplitude versus wavelength (A), maximum amplitude versus frequency (B), wavelength versus frequency (C), and degrees of curvature (D) for RyR variant strains, labelled by the human variant they correspond to, along with the wild type and the CB540 (*unc-68(e540)*) null mutant. Maximum amplitude and wavelength were normalized for worm length. Mean and SEM are indicated, although SEM is very small for frequency and for normalized maximum amplitude and wavelength (A, B and C). Correlation coefficients, where r is the strength of relationship and P the significance level and negative correlation is shown with a minus sign (-): A = $r=0.18$, $P=0.63$, B = $r=-0.31$, $P=0.38$, C = $r=-0.89$, $P<0.005$. Boxes indicate the median and interquartile range, with whiskers to the 10-90 percentile, and + to indicate the mean (D). Degree of curvature was measured for 26 individuals per strain. Significance is between variant strains and the wild type, apart from where indicated to the *unc-68* null mutant, ** $P<0.005$, n.s = not significant (one-way ANOVA, with Tukey's multiple comparison test). (E) The larger wavelength:length of the *unc-68* null mutant compared to wild type results in a smaller degree of curvature; the hR2163H and hR2458H variant strains both have larger degrees of curvature as a result of shorter wavelengths. (F) Mean and standard deviation (SD) of degree of curvature, mean and standard deviation for the other crawling parameters shown in this figure are shown in Table 4.1. Individual box plots of amplitude, wavelength and frequency are available in Appendix G.

Table 4.2: Mean percentage change from the wild type to RyR variant strains or the CB540 (*unc-68(e540)*) null mutant in wavelength, amplitude, frequency and degree of curvature (curve).

Strain (variant)	Wavelength	Amplitude	Frequency	Degree of curvature
hR163C	-7%	-1%	+38%	-52%
hG341R	-7%	-8%	+32%	-37%
hR2163H	-3%	-4%	+17%	-36%
hN2342S	-3%	-12%	+42%	-1%
hR2454H	-6%	-4%	+29%	-33%
hR2458H	-12%	-10%	+26%	-38%
hK3452Q	-6%	-6%	+23%	-45%
hR4861H	+10%	-11%	-17%	+19%
<i>unc-68</i> null	+11%	0%	-37%	+6%

Box shading is consistent with the colour coding used throughout this thesis. RyR variant strains are listed according to the human variant they correspond to. Percent change is calculated as $((S1-S2)/S1)*100$ where S1 is the mean measurement for wild type and S2 is the mean measurement of the different RyR variant strains for each parameter. Where the strain in question showed increased compared to wild type the percentage change is indicated with a plus sign (+), and where it showed a decrease compared to wild type the percentage change is indicated with a minus sign (-). Wavelength and amplitude measures were corrected for worm length.

For light, frequency and wavelength are inversely related, as all light waves travel through a vacuum at the same speed. If a wave is moving at a constant speed, then it will move a certain distance in a certain time. Wavelength (λ) and frequency (f) can be used to calculate wave speed,

$$v = \lambda f$$

However, animals can move at different speeds, so the frequency wavelength relationship need not hold for *C. elegans* crawling. Despite the body of the worm resembling a travelling wave, the wave shape never moves through time and the sinusoidal wave of *C. elegans* body shape resembles a static wave (Figure 4.2B) (Seddon, 2016). Nevertheless, when crawling wavelength and frequency for different strains were plotted together (Figure 4.7C) a statistically significant negative correlation was apparent ($r=-0.89$, $P<0.005$). Higher wavelength:length ratios are associated with lower frequencies, and vice versa, but the speed at which animals are moving also had an effect on frequency. For example, the hN2342S variant had the highest average frequency, 0.49 Hz (± 0.13 Hz), but not the shortest average wavelength. The hR2458H variant strain had the shortest average wavelength:length, 0.55 (± 0.08) times the length of the worm, but four RyR variant strains had a higher frequency.

4.3.3. Crawling speed is increased in young adult ryanodine receptor variant strains

Due to the discrepancies between frequency and wavelength for *C. elegans* crawling the midbody crawling speed of these RyR variant strains was extracted from the video analysis (Table 4.3).

The hN2342S variant strain had the fastest crawling speed (Table 4.3), accounting for this strain having the highest frequency but not shortest wavelength. Despite the hR2458H variant strain having the shortest average wavelength:length ratio of all strains it had the slowest crawling speed of the RyR variants and this, therefore reduced the crawling frequency. As young adults, all RyR variant strains, except that for hR4861H, moved faster than wild type (Table 4.3). Both the hR4861H variant strain and the *unc-68* null mutant had much slower crawling speeds than wild type and the other RyR variant strains, as described for the *unc-68* null mutant (Maryon *et al.*, 1996).

Wild type *C. elegans* was reported to have a crawling frequency of approximately 0.3 Hz (Gjorgjieva *et al.*, 2014), matching what was found here, with wild type having an average frequency of 0.35 Hz (± 0.1) (Table 4.1, Figure 4.7B and C). All RyR variant strains, except that for hR4861H, had a higher average frequency shorter wavelength and amplitude and faster crawling speed than wild type (Figure 4.7, Table 4.1, 4.2 and 4.3). It is not surprising that the RyR variant strains had a higher crawling frequency, as each wave is smaller than for wild type, and the RyR variant strains move more quickly, therefore they completed more waves in the same amount of time. While the hR4861H variant strain did have a similar frequency, wavelength and crawling speed to the *unc-68* null mutant, as for thrashing rate in liquid, the amplitude of this strain was very different and more akin to that of the other RyR variant strains. However, the combination of these parameters resulted in the smallest degree of curvature of all strains (Figure 4.7D). This suggests that the hR4861H variant UNC-68 protein is not actually completely inactive as it is different to the null mutant here.

Table 4.3: Mean and standard deviation (SD) of midbody crawling speed for RyR variant strains, wild type, and the CB540 (*unc-68(e540)*) null mutant.

Strain (variant)	Midbody crawling speed ($\mu\text{m}/\text{s}$)	
	Mean	SD
Wild type	198.2	94.9
hR163C	270.9	92.4
hG341R	263.6	57.7
hR2163H	281.7	97.8
hN2342S	319	104.7
hR2454H	251.2	116.1
hR2458H	225.3	65.4
hK3452Q	237.1	81.9
hR4861H	98.4	59.7
<i>unc-68</i> null	81.4	59.3

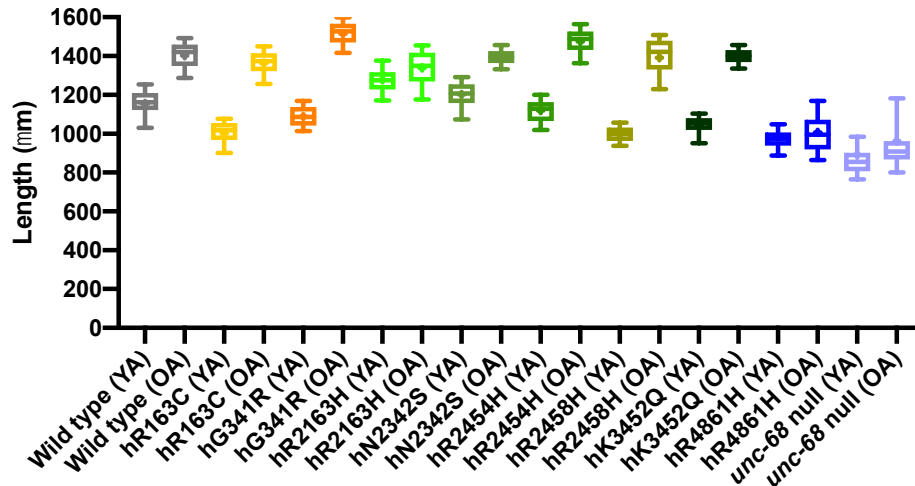
Box shading is consistent with the colour coding used throughout this thesis. RyR variant strains are listed according to the human variant they correspond to. Crawling speed is shown to one decimal place.

These data show that RyR variants do subtly affect amplitude and wavelength, and therefore degree of curvature, as well as frequency and speed of young adult *C. elegans* crawling. While the effects are small, with sufficient data, the consequences for the animal's locomotion are measurable.

4.3.4. Ryanodine receptor variant strains have altered adult growth rates

As the ryanodine receptor has been implicated in age-related diseases and disorders (Clodfelter *et al.*, 2002; Zhu *et al.*, 2005; Gaboardi *et al.*, 2018) crawling was also examined in aged *C. elegans*. The same procedure as used for ageing *C. elegans* for the thrashing assays was used here to produce old aged hermaphrodites, see section 2.3.2. Once aged, the same video and analysis pipeline was followed to generate crawling data for old adult animals.

A



B

Mean and standard deviation of old adult worm length for wild type, the CB540 (*unc-68(e540)*) null mutant and RyR variant *C. elegans* strains.

	Worm length (μm)	
	Mean	SD
Wild type	1401	79
hR163C	1363	90
hG341R	1516	59
hR2163H	1339	88
hN2342S	1394	121
hR2454H	1475	75
hR2458H	1392	47
hK3452Q	1397	61
hR4861H	1007	125
<i>unc-68</i> null	961	169

Box shading is consistent with the colour coding used throughout this thesis. RyR variant strains are listed according to the human variant they correspond to.

Figure 4.8: RyR variants affect growth rates of adult *C. elegans*.

- (4) Worm lengths were extracted from 1 minute long, 25 frames per second, video recordings of 20-30 individual young adults (YA) and 10-day old adults (OA), labelled by the human variant they correspond to, along with the wild type and the CB540 (*unc-68(e540)*) null mutant. Boxes indicate the median and interquartile range, with whiskers to the 10-90 percentile, and + to indicate the mean. Growth rate young to old adult varied for RyR variant strains. (B) Mean and standard deviation (SD) of old adult worm length, measure in micrometres, young adult worm lengths are shown in Figure 4.6. Worm lengths of the old adults are presented alone in Appendix G.

As before, worm length was considered important for analysis of any length data, i.e. amplitude and wavelength. Adult *C. elegans* do continue to grow. The volume of ageing wild type *C. elegans* shows a steep increase in from hatching to young adult, then a small increase in the first 3 days of adult life, and finally a steeper increase in volume up to 6 days of adulthood, where volume plateaus (Bolanowski *et al.*, 1981).

Here, adult animals were found to have grown between the young adult and old adult age, 10 days later, however growth rates varied between the strains (Figure 4.8, Table 4.4). The *unc-68* null mutant and hR4861H variant strain, which were the shortest as young adults, grew by 8% and 2%, respectively (Table 4.4). Wild type grew by 21%. The two variant strains that were larger than wild type as young adults, hR2163H and hN2342S, grew less than wild type, by 5% and 16% respectively. The other variant strains that were smaller than or similar to wild type grew by 32-39%.

4.3.5. Ryanodine receptor variants exacerbate age-related changes to crawling in

C. elegans

At the young adult stage, the RyR variant strains were more similar to each other than wild type or the *unc-68* null mutant across the crawling parameters. For old adults, this is no longer true. Ageing increased wavelength and amplitude for all strains, resulting in a decrease in frequency as animals have to move further to complete each wave. Degree of curvature decreased for all strains, except that for the hR4861H variant, and crawling speed decreased for all strains, with age. These changes did not happen to the same extent in all strains (Table 4.4), and the RyR variant strains no longer formed a distinct group (Figure 4.9). Variation between individuals of each strain increased in old age. This was also seen for thrashing with age (chapter 3).

Table 4.4: Mean percentage change from young adult to old adult in length, wavelength, amplitude, frequency, crawling speed and degree of curvature (curve).

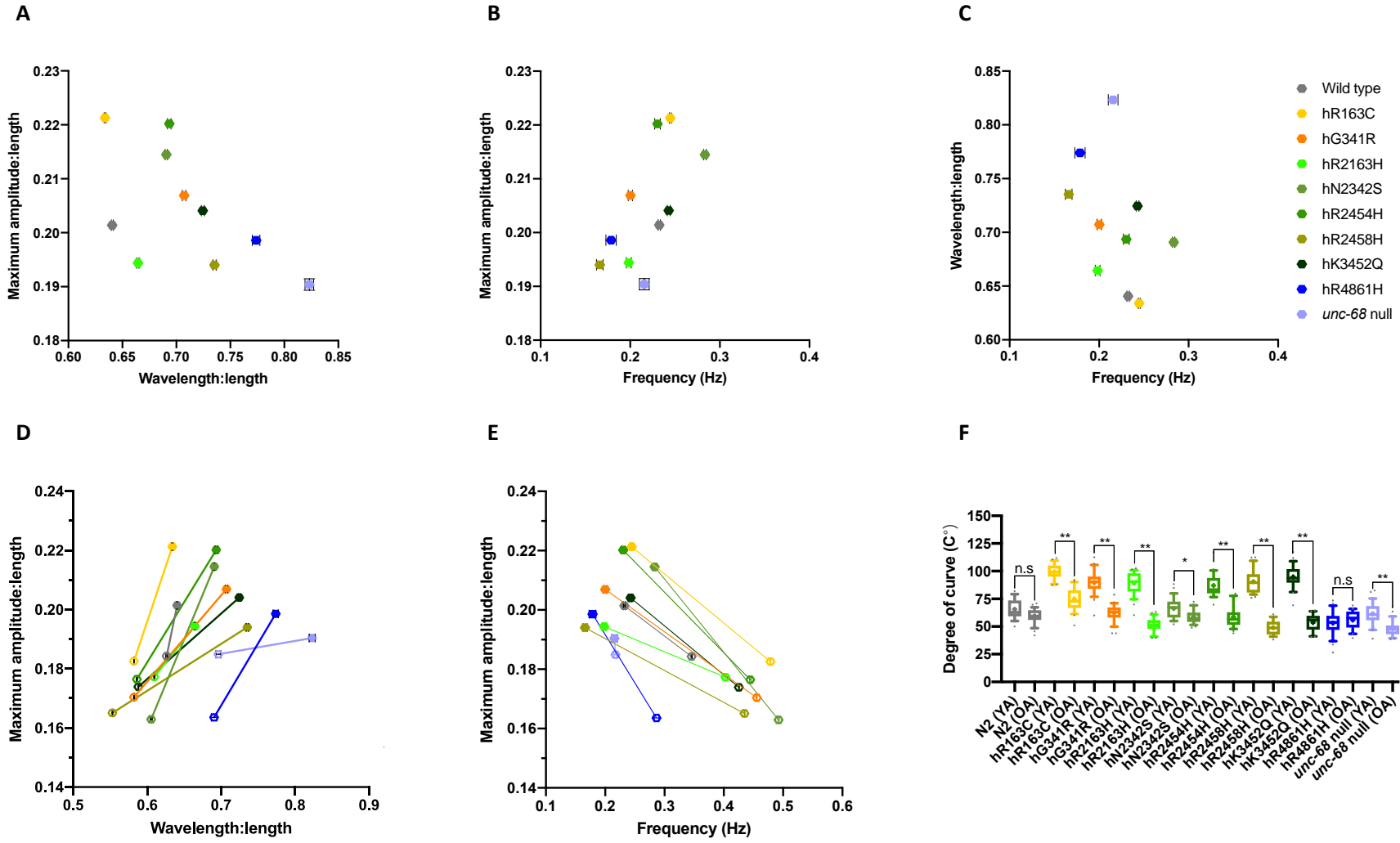
Strain (variant)	Length	Wavelength: length	Amplitude :length	Frequency	Crawling speed	Degree of curvature
Wild type	+21%	+2%	+9%	-33%	-26%	-9%
hR163C	+36%	+9%	+21%	-49%	-34%	-25%
hG341R	+39%	+22%	+21%	-56%	-65%	-31%
hR2163H	+5%	+9%	+10%	-51%	-64%	-42%
hN2342S	+16%	+14%	+32%	-42%	-40%	-11%
hR2454H	+32%	+18%	+25%	-48%	-49%	-33%
hR2458H	+39%	+33%	+18%	-62%	-76%	-46%
hK3452Q	+34%	+23%	+17%	-43%	-42%	-44%
hR4861H	+2%	+12%	+21%	-38%	-67%	+5%
<i>unc-68</i> null	+8%	+18%	+3%	-1%	-57%	-21%

Box shading is consistent with the colour coding used throughout this thesis. RyR variant strains are listed according to the human variant they correspond to. Percent change is calculated as $((T1-T2)/T1)*100$ where T1 is the mean measurement for young adults and T2 is the mean measurement for old adults of the different RyR variant strains for each parameter. Parameters that increased with age are indicated with a plus sign (+), and parameters that decreased from young to old adults are indicated with a minus sign (-). Wavelength and amplitude were corrected for worm length. RyR variants are listed according to the human variant they correspond to.

A negative correlation was seen between amplitude and wavelength in old adults; higher amplitude:length ratios go with lower wavelength:length ratios, however, this was not statistically significant ($r=-0.57$, $P=0.87$) (Figure 4.9A). However, a statistically significant positive correlation was seen for amplitude and frequency, with higher amplitude:length ratios being seen with higher frequencies, and vice versa ($r=0.64$, $P<0.05$) (Figure 4.9B). Previously wavelength:length and frequency had a strong inversely proportional relationship, with larger wavelength:length ratios being seen in strains with lower frequencies, and vice versa; these crawling parameters only have a weak negative correlation as old adults, which was not statistically significant ($r=-0.4$, $P=0.26$) (Figure 4.9C).

The mean percentage change in each parameter between the young and old adult stages (Table 4.4), and the length of the line showing how amplitude and wavelength with respect to length and frequency change from young to old adult (Figure 4.9D and E), showed how the age-related changes in crawling were different for each strain.

The wild type had the smallest age-related change for wavelength:length and crawling speed, and no statistically significant change in degree of curvature, with age (Table 4.4, Figure 4.9D and F); the *unc-68* null mutant had the smallest change in amplitude:length and frequency (Table 4.4, Figure 4.9E). Effects of ageing appeared more exaggerated in the RyR variant strains; this is demonstrated most clearly by the change in crawling speed and degree of curvature, with age (Table 4.4, Figure 4.9F). Where all RyR variant strains, except those for hR4861H and hN2342S, had a statistically significantly larger degree of curvature as young adults (Figure 4.7D), only the hR163C variant strain still had a statistically significantly larger degree of curvature in the old adults (Figure G.2E). The other old adult RyR variant strains either had similar degrees of curvature as old adult wild type or statistically significantly smaller degree of curvature. The hR2163H and hR4861H variant strains experienced the smallest degrees of change of the RyR variant strains with age, but both still showed more exaggerated age-related changes than wild type for most parameters. The hR2458H variant showed the most dramatic age-related changes of all strains.



G

Mean and standard deviation of old adult amplitude, wavelength, frequency and degree of curvature for wild type, the CB540 (*unc-68(e540)*) null mutant and RyR variant *C. elegans* strains.

	Amplitude: length		Wavelength: length		Frequency (Hz)		Degree of curvature (C°)	
	Mean	SD	Mean	SD	Mean	SD	Mean	SD
Wild type	0.20	0.07	0.64	0.12	0.23	0.12	59.43	6.81
hR163C	0.22	0.07	0.63	0.10	0.24	0.11	74.95	10.78
hG341R	0.21	0.08	0.71	0.18	0.20	0.15	62.16	7.89
hR2163H	0.19	0.07	0.66	0.13	0.20	0.20	51.32	6.67
hN2342S	0.21	0.07	0.69	0.14	0.28	0.14	58.83	6.40
hR2454H	0.22	0.08	0.69	0.15	0.23	0.20	58.56	10.01
hR2458H	0.19	0.08	0.74	0.18	0.17	0.18	49.02	6.39
hK3452Q	0.20	0.06	0.72	0.17	0.24	0.13	53.59	7.86
hR4861H	0.20	0.08	0.77	0.26	0.18	0.32	55.85	8.27
<i>unc-68</i> null	0.19	0.09	0.82	0.26	0.22	0.30	48.30	6.98

Box shading is consistent with the colour coding used throughout this thesis. RyR variant strains are listed according to the human variant they correspond to. Wavelength and amplitude were corrected for worm length.

Figure 4.9: Effect of RyR variants on crawling changes with age.

Crawling amplitudes, wavelengths and frequencies were extracted from 1 minute long, 25 frames per second, video recordings of 20-30 individual young and 10-day old adults, degree of curvature was hand measured for random 26 individuals from individual frames from the video recordings. Maximum amplitude versus wavelength (A – old adult and D – young and old adult), maximum amplitude versus frequency (B – old adult and E – young and old adult), wavelength versus frequency for old adults (C), and degree of curvature for young (YA) and old adults (OA) (F) for RyR variant strains labelled by the human variant they correspond to, along with the wild type and the CB540 (*unc-68(e540)*) null mutant. Maximum amplitude and wavelength were normalized for worm length. Mean and SEM are indicated, although SEM is very small for frequency and for normalized maximum amplitude and wavelength (A-E). Correlation coefficients for A-C, where r is the strength of relationship and P the significance level and negative correlation is shown with a minus sign (-): A = $r=-0.57$, $P=0.87$, B = $r=0.64$, $P<0.05$, C = $r=-0.4$, $P=0.26$. The change in maximum amplitude and wavelength (D) and maximum amplitude and frequency (E) from young adult (hollow symbols) to old adult (solid symbols), is indicated by a straight line. Boxes indicate the median and interquartile range, with whiskers to the 10-90 percentile, outliers as dots, and + to indicate the mean. Significance is between young and old adult for

each genotype, * $P < 0.05$, ** $P < 0.005$, n.s = not significant (one-way ANOVA, with Sidak's test for pre-selected pairs) (F). (G) Mean and standard deviation (SD) are shown for each parameter for old adults. Mean and standard deviation of crawling parameters for young adult animals are shown in Table 4.1 and Figure 4.7. Individual box plots of amplitude, wavelength, frequency and degree of curvature for aged animals alone are available in Appendix G.

A visual representation of crawling is provided by a kymogram. Kymograms show the bend angle along the body axis across time. Representative kymograms for strains as young and old adults demonstrate clearly the more dramatic ageing effects seen in the RyR variant strains than in wild type (Figure 4.10). In the kymograms red and blue stripes show extreme dorsal and ventral bending passing down the body. The inclination of the stripes and horizontal distance between the stripes shows the speed with which the wave is propagated down the body and the vertical distance between stripes indicates the wavelength.

At the young adult stage, the wild type kymogram shows the representative individual completing 11-12 waves in 40 seconds, i.e. ~ 0.35 Hz as reported earlier (Table 4.1, Figure 4.10A). The low inclination, and consequent large overlap between stripes, reflects the lower frequency and the long wavelength that was recorded for this strain. The two representative RyR variant strains, when young adults, complete more waves with less overlap between them than wild type, fitting with their higher frequencies and shorter wavelength. The wild type kymogram has wider dorsal and ventral stripes, with little green colour. The wider stripes demonstrate that this animal has a longer period between each undulation, with wide bend angles, and small degree of curvature, suggesting a more rapid transition between dorsal and ventral body bends (Figure 4.10C).

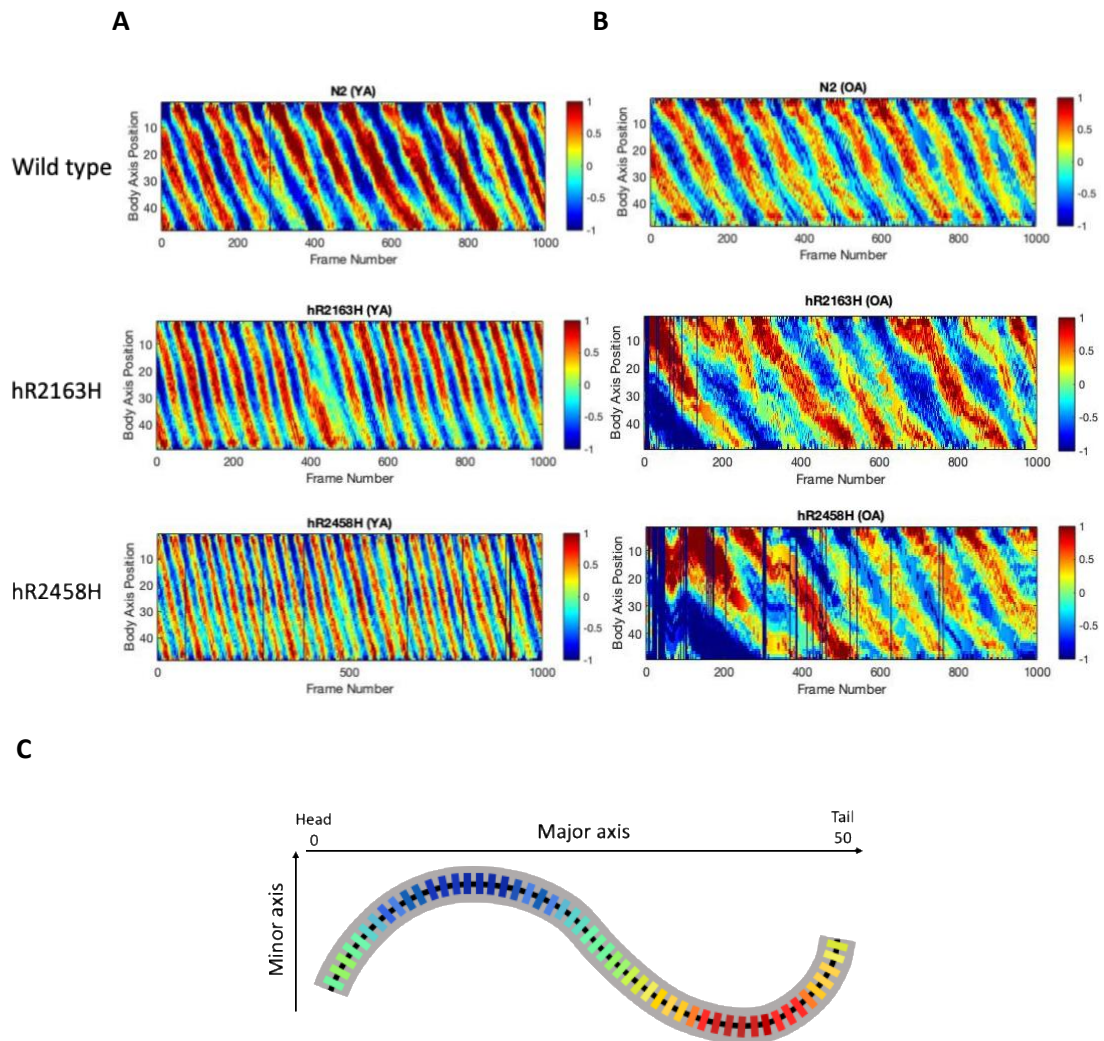


Figure 4.10: RyR variants intensify age-related reduction in crawling coordination.

Representative kymograms are presented for the wild type and for the hR2163H and hR2458H RyR variant strains for young adults (YA) (A) and old adults (OA) (B). Colour in the kymograms indicates degree of dorsal/ventral curvature (C) (red/blue high curvature, green no curvature) at different positions along the major body axis (0 anterior to 50 posterior) for each frame of the video recording. It should be noted that red and blue, respectively, do not indicate dorsal and ventral curvature but is arbitrarily assigned for each recording; the dorsal and ventral body could not be distinguished by the software. Individual frames where parameters could not be extracted are black. One young and one old adult representative kymogram for each strain is presented in Appendix G (Figure G.3).

The representative kymograms for the old adults show how crawling frequency decreased with age for all three strains (Figure 4.10B). Also evident is that the highly uniform, regular and organised crawling seen at young adult is no longer present in

aged animals. The decreased degree of curvature seen with age in all strains (Figure 4.9F), can be seen in the reduction of dark red and blue colours and more yellow and cyan in the old adult kymograms (Figure 4.10B). Wild type, although less coordinated at old adult than young adult, appears more coordinated than the two RyR variant strains at old age. Despite the hR2163H variant strain having relatively little change in amplitude and wavelength from young to old adult (Figure 4.9D), the kymogram reveals that its locomotion is still greatly affected by ageing, as demonstrated by its severe reduction in frequency and degree of curvature (Table 4.4, Figure 4.9E). The hR2458H variant strain has the most severe change from young to old adult in the kymograms. As an old adult, the hR2458H variant strain had a small degree of curvature, as shown by the amount of yellow and cyan in the kymogram, in line with this variant having a lower amplitude but higher wavelength, with respect to length than wild type. The hR2458H variant strain showed the greatest change in almost all crawling parameters between the two ages (Table 4.4, Figure 4.9D and E, and Figure 4.10).

4.4. Discussion

The aim of the research presented in this chapter was to quantify crawling parameters for strains carrying RyR variants and compare them to wild type to determine how locomotion changes in the presence of variant RyRs. Furthermore, the consequences of these RyR variants with age on locomotion were also examined to better understand the effects of variant RyRs in age-related disorders.

Prior to the analysis of crawling, these variant strains were found to have, previously undocumented, effects for development and growth that affected lengths of animals at the young and old adult stage.

For the most part, the young adult RyR variant strains had smaller crawling amplitudes and wavelengths than wild type, resulting in a larger degree of curvature. The frequency was higher and crawling speed faster for the majority of young adult RyR variant strains. Despite these differences being small, the presence of variant RyRs significantly altered crawling locomotion in *C. elegans*.

While ageing affected crawling coordination of all strains, it appeared more dramatic in the RyR variant strains. As old adults more than half of the RyR variant strains had a lower frequency than wild type. Only one strain had a larger degree of curvature than wild type in the old adults and most had a similar or smaller degree of curvature, showing large age-related changes in these strains. The kymograms revealed that crawling in the old adults is less regular than in the young adults, and that this was markedly more severe in the majority of RyR variant strains than in the wild type.

The hR4861H variant strain now showed differences to the *unc-68* null for the first time, as a young adult with a much smaller amplitude. This variant strain had a much larger reduction in frequency and increase in amplitude than the *unc-68* null mutant with age. This hR4861H variant strain is clearly not a null mutant and has consequences on locomotion not seen for the null mutant.

4.4.1. Growth rate is reduced in ryanodine receptor variant strains

The initial observation of different lengths of animals at the young adult stage suggested an effect of RyR variants on development. Such an effect of RyR variants in *C. elegans* is novel as growth rates and worm length were not measured previously for the extrachromosomal array strains (Nicoll Baines *et al.*, 2017).

The *unc-68* null mutant had the most severe consequences on young adult size. This effect of this mutation was reported previously and attributed to loss of UNC-68 function in the isthmus and terminal bulb of the pharynx resulting in reduced feeding (Maryon *et al.*, 1998). The pharynx is often likened to the mammalian heart, due to developmental, morphological and functional features (Mango, 2007; Fischer *et al.*, 2017). As UNC-68 is the only ryanodine receptor in *C. elegans*, it is involved in calcium release in the pharyngeal muscle required for the regular pumping motion (Maryon *et al.*, 1998), as well as being present in the pharyngeal neurons that initiate muscle contraction (Liu *et al.*, 2005). In mammals, RyR2 is responsible for calcium release from the sarcoplasmic reticulum in the heart (Ledbetter *et al.*, 1994; Lanner *et al.*, 2010).

The regular contraction of the pharyngeal muscle crushes bacteria and pumps the crushed bacteria into the gut of the worm, this is how the animal feeds (Avery and

Thomas, 1997). Mutants with abnormal pharyngeal anatomies or with inefficient pumping rate were found previously to have a shorter body size (Mörck and Pilon, 2006). The loss of an important neuromuscular calcium channel, in the *unc-68* null mutant, affects feeding rate (Maryon *et al.*, 1998); a reduced feeding rate is expected to have knock-on consequence for development and growth.

Here, the presence of variant RyRs also affected development and growth, the majority of RyR variant strains were smaller than wild type as young adults. It is possible that the presence of variant RyRs in the pharynx reduced food uptake, either by slowed pumping rate or reduced pumping force, affecting the growth rate of these RyR variant strains. Pharyngeal pumping rates in strains expressing RyRs carrying point mutations equivalent to known RyR2 disease causing variants have been studied (Fischer *et al.*, 2017). One of two *C. elegans* strains with optogenetically paced pharyngeal pumping, modelling RyR2 Catecholaminergic Polymorphic Ventricular Tachycardia (CPVT) disease variants, had a reduced pumping rate compared to wild type. The size and growth of animals in this study was not assessed so no link can be made between the reduced pumping rate of this RyR variant strain and worm length.

In contrast to five RyR variant strains that were smaller than wild type, the strains for variants hR2163H and hN2342S were larger than wild type as young adults. This suggests faster development and more growth in the same amount of time. Pumping rate or pumping force may be increased in these strains, allowing the animals to take up more food over time. However, there appears to be no published examples of such an effect.

There are, however, a number of different mechanisms known to increase the length of *C. elegans*. For example, the *daf-2* mutant shows increased body length with reduced activity of the insulin/IGF-I-like signalling (IIS) pathway (McCulloch and Gems, 2003). Dietary restriction is one way to reduce activity of the IIS pathway, but dietary restriction has been found to reduce body size, not increase it (Iser and Wolkow, 2007). As UNC-68 is not part of the IIS pathway it seems unlikely that two RyR variants would affect activity of the pathway; however, it is possible that the presence of RyR variants may trigger a stress response that feeds into the IIS pathway in a way the

UNC-68 does not. Nevertheless, increased food uptake seems the most likely explanation for the increased size seen for two RyR variant strains.

As old adults, there were still differences in the average size of the strains. These differences, however, did not correspond to those in young adults. Variants that were previously larger than wild type were found to be smaller and vice versa. Not only is development and growth up to the young adult stage effected by the presence of RyR variants but adult growth rate also. Differences in adult growth rate have also been attributed to feeding rate (Avery and You, 2012).

It is curious that the two strains that were longest as young adults had little growth between young and old adult stages. The limitation to adult growth is not that these strains have reached the maximum size possible for adult *C. elegans*, as a number of other variant strains were longer than them as old adults. High pumping rates in young adult animals can result in bacterial infection of the pharynx, likely through damage to the pharynx cuticle, which allows invasion through cuticle perforations (Zhao *et al.*, 2017). Wild type pumping rate has been demonstrated to be sufficient to result in pharyngeal infection. If the pumping rate is in fact higher in the two variant strains that were found to be largest as young adults, then this would likely result in more severe pharyngeal damage. Increased damage may be a result of either mechanical damage to the pharynx or increased bacterial infection. The adult growth of these animals may, therefore, be limited due to the inability to pump enough food after damage has accumulated due to faster pumping rate or force in early life.

Strains that were very small as young adults but grew by the largest amount, such as for the hG341R variant strain, may reflect the opposite scenario. Slower or reduced force of pumping early on may limit the amount of damage and allow for a longer period of food consumption and more growth as an adult. However, the *unc-68* null mutant and hR4861H variant strain were shortest at young adult and grew the least, so this is not the case for these strains. It may be that these strains have such limited pumping efficiency, that in spite of limited damage accumulation, they are still unable to ingest adequate food.

An interesting correlation was found for young adult worm length and thrashing rate in S medium. The three variant strains, those for hR163C, hG341R and hR2458H, were the shortest as young adults also found to have defective swimming locomotion in S medium (chapter 3). The shorter length of these strains at young adult may explain the reduced thrashing previously in young adults. However, this is not the case for old adults. The longest and the shortest variants of the old adults, those for hG341R and hR2163H respectively, both had a similar thrashing rate as old adults in S medium.

No effect of these RyR variants was specifically looked for in the pharynx. However, RyR2 variants in *unc-68*, expressed as extrachromosomal arrays, has been shown to reduce pumping rate, although this was not assessed with respect to worm length (Fischer *et al.*, 2017). A pharyngeal pumping assay would be required to identify if food ingestion is altered in the RyR variant strains, throughout the lifespan, and correlate it to the reduced growth rate seen for these strains.

4.4.2. Ryanodine receptor variants have subtle consequences for crawling in the young adults

The subtle differences in amplitude, wavelength, frequency, speed and degree of curvature demonstrate that crawling in these strains can be quantified and differences between the RyR variant strains and wild type revealed.

For most of the RyR variant strains, the shorter wavelength, in spite of the shorter amplitude, resulted in a larger degree of curvature. Only for the hN2342S variant strain was this not the case, with the reduction in both wavelength and amplitude, resulting in a similar degree of curvature to wild type. However, the presence of the hN2342S amino acid change did affect RyR function even in the absence of an MH triggering agent and this variant strain had the highest crawling frequency and fastest crawling speed of all strains.

The larger degree of curvature compared to wild type, and therefore increased sharpness of the wave, observed for most RyR variant strains would result from muscle hypercontraction. Despite a similar degree of curvature to wild type, the reduced

amplitude and wavelength of the hN2342S variant strain is also suggested to be due to an increase in muscle contraction. Increased muscle contraction could be due to more or longer release of calcium into the myoplasm, presumably due to these variants directly affecting the amount of calcium the ryanodine receptor is releasing. This may be through the channel opening more readily, closing more slowly or an increased passive calcium leak, as has been associated with CCD-causing mutations in RyR1 (Tong *et al.*, 1999). Witherspoon and Meiller (2016) outlines different aspects of RyR1 regulation, including complex protein-protein and protein-ligand interactions, as well as post-translational modifications, and the disease causing mutations that affect them. The mutations explored in this thesis may interfere with one or more of these aspects of RyR regulation thus affecting channel function and calcium release, and in this case resulting in an increase in calcium release and larger degree of curvature for crawling.

In support of this notion, the R163C mutation elevated cytosolic calcium concentration compared to wild type in muscle fibres isolated from knock-in mice (Giulivi *et al.*, 2011). This specific variant affects how RyR and the dihydropyridine receptor (DHPR) interact; the presence of the R163C mutation alters the conformation of the channel, which in turn alters retrograde signalling from the RyR to the DHPR, ultimately delaying inactivation of the DHPR signal and enhancing sarcolemma calcium entry (Esteve *et al.*, 2010). In the worm, the hR163C variant strain had a larger degree of curvature than wild type, suggesting an increased myoplasmic calcium concentration compared to wild type.

While the effects of the R163C mutation in mice was demonstrated in the muscle, the consequences of these RyR variants in *C. elegans* could be in either, or both, the body wall muscle cells and motor neurons. UNC-68 is found in both body wall muscle and neurons in *C. elegans* (Maryon *et al.*, 1996; Chen *et al.*, 2017a). Therefore, variant RyRs could increase calcium release from the endoplasmic reticulum (ER) in the excitatory B-type motor neurons, which stimulate muscle contraction, resulting in increased neurotransmitter release and therefore increased muscle contraction (Figure 4.1, Figure 4.11). In *C. elegans* neurotransmitter release at NMJs is graded (Liu *et al.*, 2009). In graded transmission, the size and duration of depolarisation is proportional to the

size and duration of the excitatory/ inhibitory input. The postsynaptic muscle response is scaled with the strength of stimulus to the motor neurons. Therefore, increased neurotransmitter release at NMJs would result in increased muscle contraction.

Alternatively, variant RyRs in the sarcoplasmic reticulum (SR) release more calcium in the myoplasm upon activation by the DHPR. The calcium ions released via the RyR on the SR facilitate muscle contraction (Figure 4.11) (Ríos *et al.*, 1991; Calderón *et al.*, 2014). Increased muscle contraction could even be due to the compounding effects of variant RyRs in the ER of motor neurons and SR of body wall muscles, whereby activation of the body wall muscles is increased due to neuronal variant RyRs, and the resulting calcium release into the myoplasm is further increased due to muscular RyRs.

The effects of variant RyRs in neural and muscle cells in *C. elegans* is explored further in chapter 5. Regardless of whether these variant RyRs are effecting calcium release in the motor neurons or body wall muscles, the overall effect of excessive calcium release via variant RyRs would be to increase the concentration of calcium ions in the myoplasm, which facilitate muscle contraction.

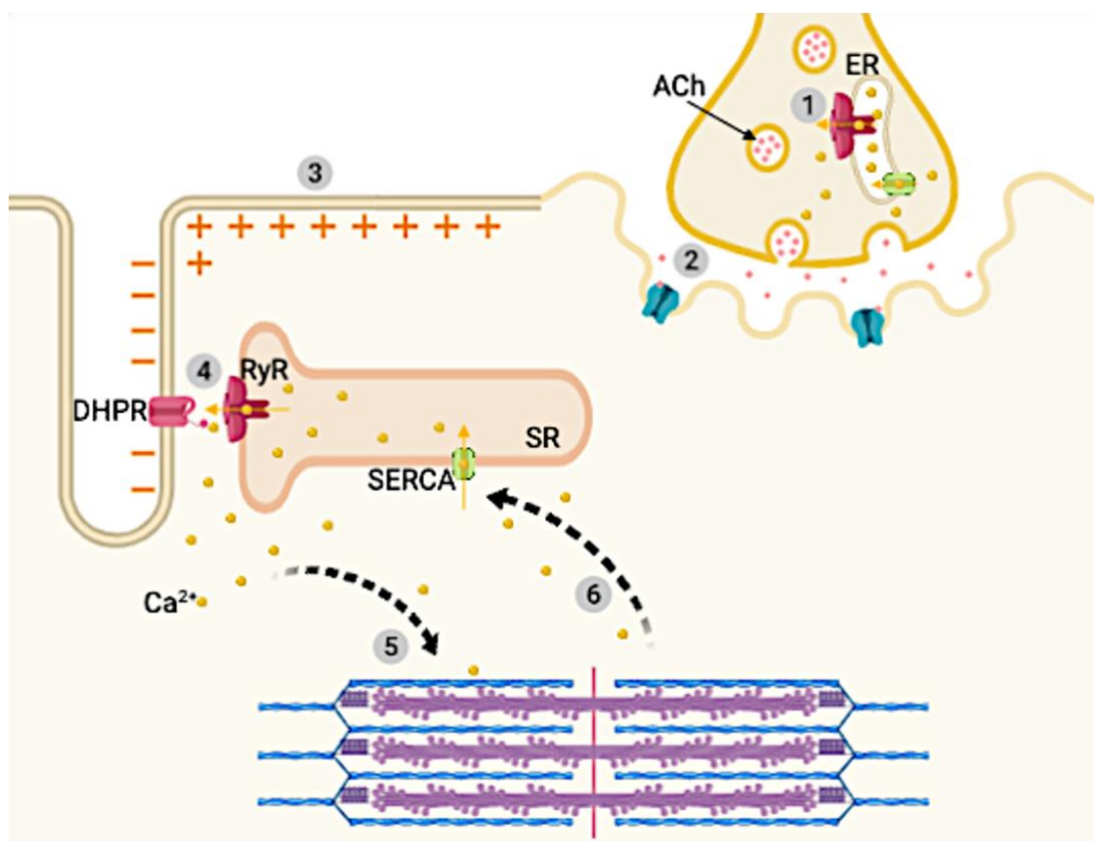


Figure 4.11: Increased muscle contraction due to increased calcium release via variant RyRs.

Increased calcium ion (yellow spheres) concentration in the cytoplasm of motor neurons results in neurotransmitter release, such as acetylcholine (ACh) (pink spheres), from motor neurons at NMJs, leading to muscle contraction as a result of E-C coupling. RyRs (pink channel) on the endoplasmic reticulum (ER) are thought to increase calcium concentration in neurons by calcium induced calcium release (CICR). Neurotransmitters bind to receptors on the sarcolemma (2), which leads to depolarisation of the muscle cell membrane (3). The voltage gated dihydropyridine receptor (DHPR) in the t-tubule sarcolemma senses the depolarisation and activates the ryanodine receptor (RyR) in the membrane of the sarcoplasmic reticulum (SR) (4). The RyR opens and calcium ions released, which bind to troponin C, inducing a conformational change in the troponin-tropomyosin complex allowing myosin to bind to actin and the myofilaments to slide past each other (5). The sarcoplasmic reticulum Ca^{2+} ATPase (SERCA) pumps cytoplasmic calcium back into the SR allowing muscle relaxation (6). In *C. elegans* the structure of NMJs is slightly different due to muscle arms extending toward the motor neurons, however the principles remain the same. Created with BioRender (<https://biorender.com/>), based on information from Jurkat-Rott and Lehmann-Horn (2005).

A subtly smaller degree of curvature was found for the *unc-68* null mutant compared to wild type, with a longer wavelength but same amplitude. The small reduction in degree of curvature is attributed to less available calcium in the myoplasm for muscle contraction due to the deletion of the RyR.

Interestingly the hR4861H variant, which had appeared to inactivate the RyR (Chapter 3) does not show the same effect for amplitude and degree of curvature as the *unc-68* null mutant. While the wavelength of the hR4861H variant strain is longer than wild type, the amplitude is smaller. The additive effect of these changes resulted in an even smaller degree of curvature than seen for the *unc-68* null mutant. It is speculated that the presence of the hR4861H amino acid change is having a negative effect on calcium release, possibly by impacting other proteins which control calcium release, to reduce calcium levels further than seen in the null mutant. As the degree of curvature is

further reduced in the hR4861H variant strain than in the null mutant it suggests that there is even less calcium in the cytoplasm than in the null. An alternative explanation could be reduced RyR protein levels in the hR4861H variant strain, however as the degree of curvature is reduced compared to the null mutant, this does not seem a likely explanation as protein levels could not be reduced more than in the null mutant. Reduced calcium release was seen in muscle fibres isolated from RyR1 Y522S variant knock-in mice (Andronache *et al.*, 2009). This variant also effects RyR retrograde signalling to DHPR, as the R163C variant is thought to (Giulivi *et al.*, 2011). However, in this case, the DHPR inactivation window is smaller, not larger, thus limiting calcium release. This mechanism was suggested to be compensatory to counteract the augmented calcium leak caused by this variant. The hR4861H variant in *C. elegans* may have a similar impact on RyR function. However, this variant may also be limiting calcium release from the SR via other channels.

4.4.3. Ryanodine receptor variants exacerbate age-related changes in crawling parameters

With the exception of the hR4861H strain, the crawling profiles of the variant strains suggest an excess of calcium in the cytosol. Calcium leakage through RyRs, across the life span, has been linked to defective calcium signalling and cellular damage (Bellinger *et al.*, 2008; Andersson *et al.*, 2011; Liu *et al.*, 2012; Momma *et al.*, 2017). Although subtle, the increased cytosolic calcium thought to arise from the RyR variants examined here could have more severe consequences with age. This has been suggested in. All RyR variant strains age more dramatically than the wild type and the *unc-68* null mutant, with larger percentage changes seen for crawling parameters with age. The kymograms demonstrate this effect, with the RyR variant strains changing from fast and organised, to very slow and disorganised, locomotion. Meanwhile, wild type shows some age-related reduction in speed and organisation of crawling, but not to the same extent.

Excessive calcium ions are thought to lead to an increase in production of reactive oxygen species (ROS). At normal levels, ROS are important signalling molecules that oxidise proteins, lipids and polynucleotides, and are produced by a number of sources,

many of which are modulated by calcium (Sauer *et al.*, 2001). Of particular note is the generation of ROS as a by-product of mitochondrial respiratory chain activity (Ermak and Davies, 2002). The free radical theory of ageing was first described in the 1950s (Harman, 1956). The theory proposes that ROS leads to oxidative damage resulting in the functional decline of organs, and death (Schriner *et al.*, 2005). Despite controversy over whether this is the ultimate cause of ageing (Wickens, 2001; Gladyshev, 2014), there is evidence that oxidative stress and damage, by free radicals, underlies many age-related diseases (Liguori *et al.*, 2018).

In the R163C knock-in mice, discussed above, the calcium concentration of the cytoplasm as well as the mitochondrial matrix are elevated, as is production of ROS in skeletal muscle (Giulivi *et al.*, 2011). Furthermore, impaired mitochondrial function has been found in muscle biopsies from MHS patients, as diagnosed by an IVCT (Chang *et al.*, 2019). Impaired mitochondrial function was thought to be a result of chronically elevated cytoplasmic calcium ion concentration, increasing mitochondrial activity and ROS production and subsequently causing organelle damage.

Of direct importance is that ROS is thought to oxidise RyRs and further exacerbate calcium leaks from internal stores (Andersson *et al.*, 2011; Umanskaya *et al.*, 2014). With increased leakage from internal stores, less calcium is released upon activation of RyRs and therefore muscle function is reduced. As demonstrated in RyR1 S2844D mutant mice, blocking of leaky RyRs reduces ROS production and increases skeletal muscle function of aged animals (Andersson *et al.*, 2011). Aged RyR variant strains had largely reduced frequency and scale of muscle contraction, suggesting reduced calcium release upon activation of RyR. Mitochondrial ROS production has been suggested to have a causative role in oxidation of RyR1 and the age-related decline in skeletal muscle function in mice (Umanskaya *et al.*, 2014). Transgenic mice with targeted overexpression of the human catalase gene to mitochondria had increased skeletal muscle force, reduced RyR1 oxidation and reduced calcium leakage from the SR.

ROS and calcium signalling interact in a bidirectional manner. ROS regulates calcium signalling and ROS is produced by calcium signalling (Gordeeva *et al.*, 2003). Oxidative damage by ROS aggravates RyR calcium leak resulting in a self-reinforcing cycle;

calcium leakage from the SR results in increased calcium uptake by mitochondria, increasing production of ROS, which oxidises RyRs and results in increased calcium leakage (Andersson *et al.*, 2011; Umanskaya *et al.*, 2014). Treatment of RyR1 Y522S knock-in mice with antioxidant supplements prevented the age-related reduction in maximal tension (Durham *et al.*, 2008).

There is some calcium leakage through wild type RyR, as seen with the oxidation of RyR1 in aged wild type mice (Andersson *et al.*, 2011). It is speculated that there is increased calcium leakage in the RyR variant strains in *C. elegans*, as indicated by the crawling profiles. This suggests that RyR variants lead to more damage with age for human carriers, likely through cellular damage due to chronically increased cytoplasmic calcium levels. This could be in the case in all RyR1 variants, not just those associated with MH.

Chapter 5

Exploring effects of ryanodine receptor variants on cholinergic pharmacology: Pre- and postsynaptic ryanodine receptor effects

5.1. Introduction

5.1.1. Aim of this chapter

So far in this research, exact specification of whether the effects of these RyR variants on locomotion have been due to perturbation of ryanodine receptors in muscle or nerve cells has been avoided, although briefly discussed in chapter 4. It is commonly thought that the effects of RyR1 variants in mice and humans are due to RyRs located on the sarcoplasmic reticulum of skeletal muscle cells. However, RyR1 is not only found in skeletal muscle and RyRs are important calcium channels in all excitable cells. Therefore, it is possible that the effects of these variants are, at least in part, due to the perturbation of RyRs in cells that are presynaptic to neuromuscular junctions. While muscle cells are relatively robust, small changes to calcium homeostasis in the smaller nerve cells may have larger consequences.

In this chapter, the response of the RyR variant strains to two cholinergic pharmaceutical agents was investigated. By impairing different aspects of neurotransmitter signalling at neuromuscular junctions, through application of aldicarb and levamisole, the contributions of pre- (neural) and postsynaptic (muscle) RyRs can be examined. The aim of the research reported in this chapter was to determine whether nerve and/ or muscle cell function is perturbed by the presence of variant RyRs.

5.1.2. The role of ryanodine receptors in neurons

RyRs are present in all excitable cells, as well as non-excitable cells (Zissimopoulos *et al.*, 2006). Despite being described most often as being found in specific, discrete, locations, this is not exclusively the case, as shown by expression of RyR1 in Purkinje cells (Furuichi *et al.*, 1994).

As well as the many skeletal and cardiac myopathies that variant RyRs have been associated with (Boncompagni *et al.*, 2006; Robinson *et al.*, 2006; Andersson *et al.*, 2011; Salvage *et al.*, 2019), RyRs have also been implicated with neuropathologies, such as Alzheimer's disease (LaFerla, 2002; Del Prete *et al.*, 2014; Liang *et al.*, 2015; Liang and Wei, 2015; Abu-Omar *et al.*, 2018). RyRs are not only present in nerve cells but are important for proper signal transmission in nerve cells. In mice, blocking RyRs altered the intracellular calcium concentration of the axoplasm and affected secretion of acetylcholine (ACh) neurotransmitters from the motor neurons (Khuzakhmetova *et al.*, 2014).

Specifically in *C. elegans*, strains carrying RyR variants, expressed as extrachromosomal arrays, demonstrated altered responses to caffeine, which were attributed to neural function (Nicoll Baines *et al.*, 2017). Furthermore, presynaptic RyRs have been suggested to be important for quantal size (Liu *et al.*, 2005). Mutations in, or blocking of, the RyR eliminated large-amplitude miniature postsynaptic currents (mPSCs). mPSCs occur at a high frequency in wild type *C. elegans* and result from the spontaneous or sporadic release of single vesicles from the presynaptic membrane (Wang, 2010). 'Quanta' is the name given to the amount of neurotransmitters within a single vesicle and determine the minimum size of an mPSC (Katz, 1971). It was hypothesized that calcium release via the RyR regulates quantal size in neurons (Liu *et al.*, 2005). In the absence of RyRs calcium levels in the presynaptic terminal are reduced, this may alter quantal size. Promoting vesicle loading with neurotransmitters, stimulating intervesicular fusion and increasing size/ duration of the fusion pore during kiss-and-run synaptic release are all discussed as possible mechanisms for how reduced calcium levels may alter quantal size (Liu *et al.*, 2005). When RyRs were blocked in *C. elegans* quantal size was reduced such that large-amplitude mPSCs were no longer generated.

RyRs function in neurons to increase the cytoplasmic calcium concentration upon nerve cell excitation, predominantly through calcium induced calcium release (CICR) (Mouton *et al.*, 2001) (Figure 1.5 and Figure 4.11). The arrival of an action potential opens voltage-gated calcium channels (VGCCs), calcium enters and binds directly to the RyRs, promoting channel opening. Increased intracellular calcium concentration

triggers synaptic vesicle exocytosis and the release of neurotransmitters (Südhof, 2012). As described previously (chapter 4), neurotransmitter release at NMJs in *C. elegans* is by graded synaptic transmission (Liu *et al.*, 2009). However, recent evidence has shown action potentials in chemosensory nerve cells (Liu *et al.*, 2018).

5.1.3. Acetylcholine signal transduction pathway

Acetylcholine (ACh) was the first neurotransmitter identified, through work in three parasitic nematode species in the 1950s (Mellanby, 1955). ACh is an important neurotransmitter, functioning in the central nervous system (CNS), at neuromuscular junctions (NMJs), and in the peripheral nervous system (PNS).

ACh is synthesised and then stored in vesicles until it needs to be released (Purves *et al.*, 2001) (Figure 5.1A). Upon release, ACh diffuses across the synaptic cleft and binds to ACh receptors (AChRs) on the post-synaptic membrane. The enzyme acetylcholinesterase (AChE) hydrolyses ACh into acetate and choline, and the latter is taken up by the presynaptic terminal for further ACh synthesis. AChE is found in the synaptic cleft in high concentrations, ensuring the rapid breakdown of ACh upon release from the presynaptic membrane, terminating signal transduction (Rand, 2007).

There are two types of AChRs. Receptors that bind nicotine are named the nicotinic acetylcholine receptors (nAChRs), and those that bind muscarine, the muscarinic acetylcholine receptors (mAChRs) (Purves, 1976).

In *C. elegans*, ACh is the main excitatory neurotransmitter at NMJs (Rand, 2007). *C. elegans* has the largest family of nAChR alpha subunit genes in a single species; alpha subunits are required for ACh receptor function (Jones and Sattelle, 2004). The body wall muscles of *C. elegans* express two types of nAChRs; those that respond to levamisole (L-type) and those that respond to nicotine (N-type) (Richmond and Jorgensen, 1999). *C. elegans* have two other types of ACh receptors; the muscarinic G-protein coupled receptors (Culotti and Klein, 1983), and ligand-gated chloride channels, which have no orthologs in vertebrates (Putrenko *et al.*, 2005). The main focus of this research was on nAChRs due to their presence at NMJs.

5.1.4. Cholinergic pharmacological agents

The pre- or post-synaptic contributions of the RyR variant effects can be discerned by disturbing the acetylcholine signal transduction pathway in *C. elegans*, which can be achieved using aldicarb and levamisole (Rand, 2007).

Aldicarb disturbs cholinergic signal transmission by binding to AChE and inhibiting the hydrolysis of ACh (Risher *et al.*, 1987) (Figure 5.1B). As a result of inhibiting the breakdown of ACh, the neurotransmitter accumulates in the synapse. In *C. elegans*, treatment with aldicarb results in hypercontraction and paralysis due to ACh build up at NMJs (Rand, 2007). Levamisole also disturbs cholinergic signal transmission. However, it does so by binding directly to and activating L-type nAChRs on nematode muscle cells (Robertson *et al.*, 2010) (Figure 5.1C). The binding of this agent to the nAChRs also results in hypercontracted paralysis, which is usually followed by relaxation and death, due to depolarisation of the muscle cell and subsequent increase in myoplasmic calcium (Rand, 2007; Martin *et al.*, 2012).

No effect of aldicarb suggests no presynaptic effect of the mutation. Mutations that do affect sensitivity to aldicarb are likely to fall into one of two classes: 1) mutations upstream of neurotransmitter release from the presynaptic membrane, affecting the amount of ACh secreted, 2) mutations downstream of neurotransmitter reception, affecting the muscle cell's response to ACh binding to the sarcolemma (Mahoney *et al.*, 2006; Rand, 2007). Mutations falling into the first class have presynaptic function and could affect ACh release by disrupting ACh synthesis, neurotransmitter loading into vesicles or vesicle release. Higher or lower amounts of ACh release would result in increased sensitivity or resistance to aldicarb, respectively (Rand, 2007). The former means that ACh levels build up faster than in wild type, upon aldicarb inhibition of AChE, resulting in faster paralysis and increased sensitivity (Figure 5.1B). The latter means that ACh levels build up more slowly than in wild type, upon aldicarb inhibition of AChE, resulting in paralysis taking longer and increased resistance. Mutations in the second class, affecting a post synaptic function, could affect binding of ACh to the receptors, or excitability of the muscle cell (Mahoney *et al.*, 2006). The muscle cell is more sensitive or less sensitive, to a common rate of build-up of ACh due to aldicarb inhibition of AChE, as compared to wild type. The former means that paralysis occurs

sooner, when the same level of ACh build up as wild type results in greater sensitivity. The latter means that paralysis occurs more slowly, not until a higher level of ACh has built up is the paralysis seen, demonstrating increased resistance.

To address the site of action of aldicarb-induced paralysis, levamisole is commonly used. Response to levamisole does not depend on ACh release as it is a cholinergic agonist, binding directly to L-type nAChRs (Figure 5.1C). Mutations effecting ACh (or levamisole) binding to the post synaptic membrane or any downstream signalling that affects the excitability of the muscle cell would result in a change in the paralysis response to levamisole (Rand, 2007). Mutations upstream of neurotransmitter release should not affect the response to levamisole and the time to levamisole induced paralysis.

Together, aldicarb and levamisole responses can indicate whether mutations affect functions pre- or postsynaptic to NMJs. A differential response to aldicarb but not levamisole suggests the mutation is presynaptic, while a changed response to both suggests that there is an effect of the mutation postsynaptically (Rand, 2007).

However, it should be noted that a changed response to both cholinergic pharmaceutical agents would not exclude the possibility of an effect of the variant RyRs in the neurons. As RyRs are located in both nerve and muscle tissues, the variants may affect calcium control in both tissues, resulting in an altered response to both aldicarb and levamisole.

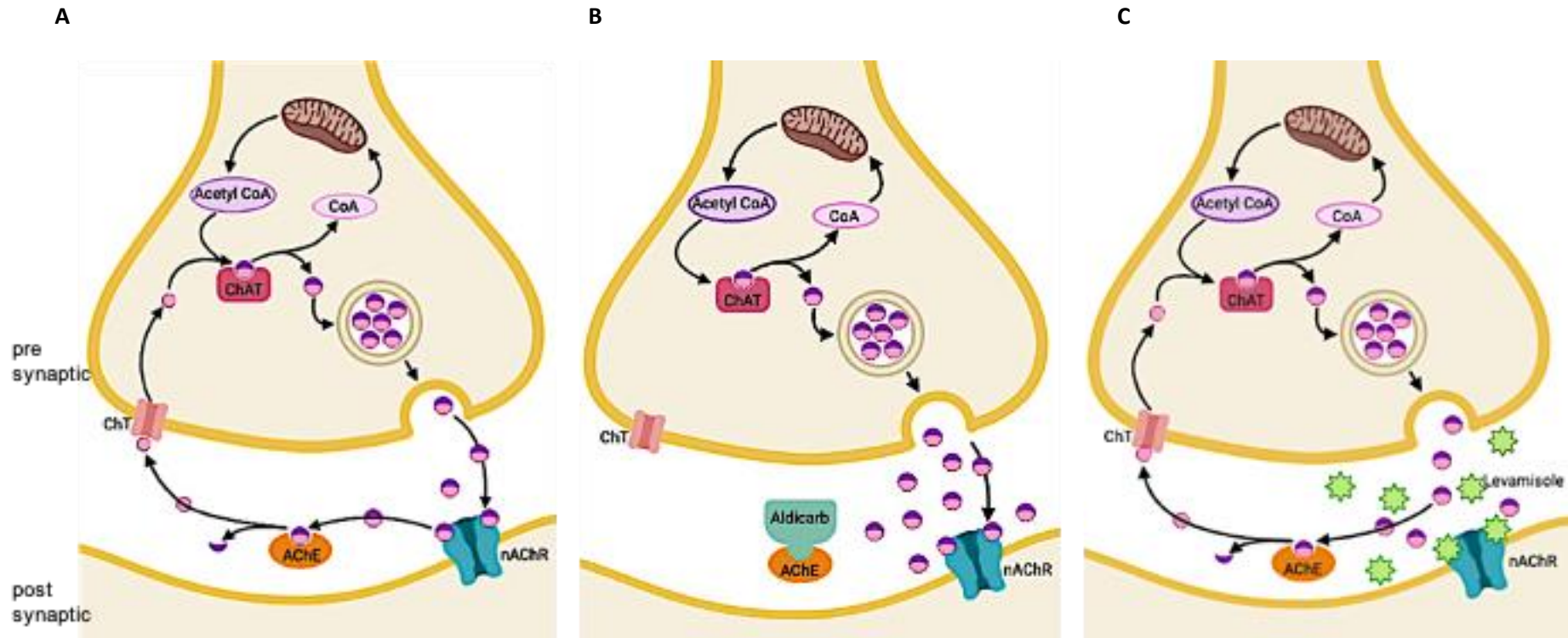


Figure 5.1: Aldicarb and levamisole disrupt cholinergic signal transmission.

(A) Acetylcholine (ACh) (Pink and purple spheres) is synthesised from choline (pink sphere) and Acetyl Coenzyme A (Acetyl CoA). ACh is packaged into vesicles until it is released. Upon release ACh binds to nicotinic acetylcholine receptors (nAChRs). The ACh signal is degraded by hydrolysis of ACh into choline and acetate (purple crescent) by acetyl cholinesterase (AChE). (B) Aldicarb (green inhibitor) binds to AChE and prevents hydrolysis of ACh resulting in a build-up of neurotransmitters in the synapse. This leads to constant activation of nAChRs. (C) Levamisole (Lime green stars) is an nAChR agonist and directly activates nAChRs. The figure is based on Mahoney *et al.* (2006); Rand (2007) and was created with BioRender (<https://biorender.com/>).

5.2. Methods

5.2.1. Aldicarb assays

Aldicarb sensitivity assays were conducted as previously described (Oh and Kim, 2017). 50 mm NGM plates containing 1 mM aldicarb, from a 100 mM aldicarb stock dissolved in 70% ethanol, were allowed to dry for at least one day. Plates were stored at 4 °C and used within 2 weeks of pouring. Plates were allowed to warm to room temperature overnight before use. Using forceps, a 16 mm diameter copper ring was dipped into 70% ethanol and passed through a flame for ~10 seconds. The ring was then placed immediately onto one side of an aldicarb-containing plate and held still with forceps until it had cooled, becoming slightly embedded into the agar plate. A second copper ring was added to the other side of the plate in the same way, allowing two assays to be conducted at once. Once the agar had cooled, 10 µL of an OP50 *E. coli* overnight culture was pipetted to the centre of each ring and allowed to dry for 30 minutes. The combination of food and the copper ring is to corral worms and limit individuals crawling off plates in response to the aldicarb during the assay. 20-30 individuals were picked to the centre of the ring and time to paralysis recorded. 80-100 individuals per strain were used, across a minimum of three repeats. Despite the use of the copper rings and food, some individuals crawled under the rings or burrowed into the crevice between the agar and the ring, these animals were excluded from the assay. Time to paralysis was measured by checking animals every 10 minutes for two hours and every 30 minutes thereafter up to four hours, when the assay was terminated. Any animals remaining unparalysed at the end of 240 minutes were recorded as such. Animals were determined as paralysed when they did not move of their own accord, or when prodded with a platinum wire. Once paralysed, individuals were removed. Hypersensitivity or increased resistance to aldicarb was determined with respect to wild type.

A preliminary assay tested the response times of wild type and the strain for the hR2163H variant at a range of aldicarb concentrations (Appendix H). This preliminary assay suggested that lower concentrations did not substantially increase the difference in time to paralysis between these two strains. 1 mM aldicarb was determined as a sufficiently low enough dose to see differences between different strains, while being

high enough that animals were paralysed within a reasonable time, this is supported by the findings of Oh and Kim (2017). Half the animals stopped moving within the first two hours, and so the animals were checked every 10 minutes up to 120 minutes but could be checked every 30 minutes thereafter.

5.2.2. Levamisole assays

For the levamisole assays, a 2 M stock of levamisole dissolved in M9 buffer was used to prepare seven solutions in M9 buffer; starting from 1 μ M, concentrations increased 10-fold successively to 1 M. 10-15 individuals were picked into 1 ml of M9, with or without levamisole, in each well of a 24 well plate. Individuals were observed either at the end of 1 hour, or every 10 minutes for two hours and scored for response to levamisole. Initially, only time to paralysis was recorded in a preliminary quantitative assay. Following observations of distinct altered behaviours in the presence of levamisole, a qualitative assay was conducted where all locomotion behaviours were documented and were later categorised and coded for ease of representation.

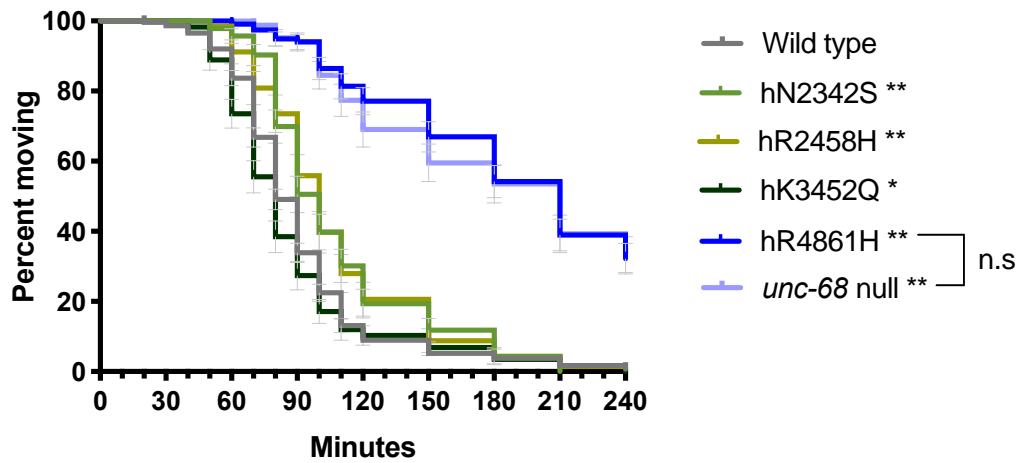
5.3. Results

5.3.1. Sensitivity to aldicarb is differential among the ryanodine receptor variants strains

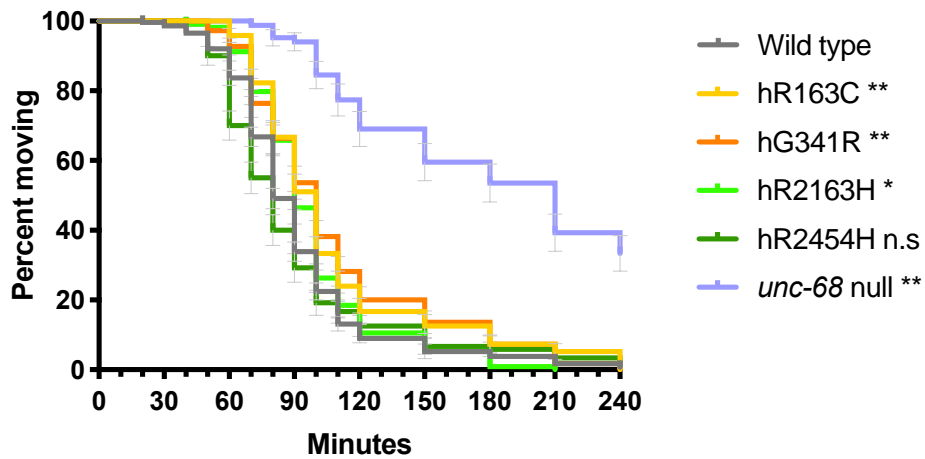
Aldicarb assays were conducted on young adult individuals. Sensitivity or resistance to aldicarb was determined with respect to wild type. In 1 mM aldicarb, the median time to paralysis of wild type was found to be 80 minutes (Figure 5.2). This corresponds with previous reports (Oh and Kim, 2017).

The *unc-68* null mutant was found to be resistant to aldicarb, taking 210 minutes for half of these individuals to become paralysed. Paralysis of all individuals was not achieved within the four-hour assay time. Once again, the hR4861H variant strain behaved like the null mutant, also taking 210 minutes for 50% of the individuals to become paralysed (Figure 5.2A).

A



B



C

Median time, in minutes, to paralysis in 1 mM aldicarb for wild type, the CB540 (*unc-68(e540)*) null mutant and RyR variant *C. elegans* strains.

	Median time to paralysis (Minutes)
Wild type	80
hR163C	100
hG341R	100
hR2163H	90
hN2342S	100
hR2454H	80
hR2458H	100
hK3452Q	80
hR4861H	210
<i>unc-68</i> null	210

Box shading is consistent with the colour coding used throughout this thesis. RyR variant strains are listed according to the human variant they correspond to.

Figure 5.2: RyR variants alter time to paralysis in 1 mM aldicarb.

Kaplan-Meier survival curves representing the percentage of individuals moving with time on plates containing 1 mM aldicarb. Data for the RyR variant strains, labelled by the human variant they correspond to, along with the wild type and the CB540 (*unc-68(e540)*) null mutant are distributed across two graphs for clarity (A and B). Comparison to the wild type, and of the hR4861H variant strain to the *unc-68* null mutant (square bracket), to assess if curves were significantly different, employed the Gehan-Breslow-Wilcoxon test; * = $P < 0.05$, ** = $P < 0.005$, n.s = not significant. Error bars are standard error calculated in GraphPad using the Greenwood method. (C) Median time to paralysis, in minutes, for wild type, the *unc-68* null mutant and RyR variant strains.

Five other RyR variants also showed increased resistance to aldicarb but not to the same extent as the *unc-68* null mutant and hR4861H variant strain. The strain for variant hR2163H had a median time to paralysis of 90 minutes and was significantly more resistant to aldicarb than wild type ($P < 0.05$, Gehan-Breslow-Wilcoxon test) (Figure 5.2B). The strains for variants hR163C, hG341R, hN2342S and hR2458H were also more resistant to aldicarb, compared to wild type, all having an even longer median time to paralysis of 100 minutes ($P < 0.005$, Gehan-Breslow-Wilcoxon test) (Figure 5.2A and B).

Two of the eight RyR variant strains assayed appeared more sensitive than wild type to 1 mM aldicarb, those for RyR variants hR2454H and hK3452Q. However, only for the hK3452Q variant was the increased sensitivity statistically significant ($P < 0.05$, Gehan-Breslow-Wilcoxon test) (Figure 5.2A). While the apparent increased sensitivity of the hR2454H variant strain was not statistically significant ($P = 0.058$, Gehan-Breslow-Wilcoxon test), the line for this strain does sit slightly below that for the wild type on the Kaplan-Meier curve and more repeats may have revealed significance (Figure 5.2B). All three of these strains, wild type and the variant strains hR2454H and hK3453Q, had a median time to paralysis of 80 minutes, possibly reflecting a lack of resolution in sampling intervals and suggesting more frequent sampling may have been beneficial.

5.3.2. Ryanodine receptor variant strains show novel responses to levamisole

As explained above, a response to aldicarb distinct from that in the wild type may indicate RyR variants affecting calcium release in the nerve cells, presynaptic to NMJs. However, it is possible that postsynaptic RyR variants are amplifying the effects of aldicarb, with no consequence of the variants presynaptically. Therefore, the response of these variant strains to levamisole was assessed. Should the variant strains show no differential effect in the presence of levamisole then it could be concluded that the effects seen with aldicarb were as a result of presynaptic RyR variants. A simple levamisole dose-response curve was set up, based on Qian *et al.* (2008) with the expectation that the RyR variant strains would not show any difference from the wild type, based on unpublished data for RyR variants expressed from extrachromosomal arrays in *C. elegans* (Ferreira and Kalogeropoulou, 2019).

Initial observations of the variant strains in 1 mM levamisole revealed a novel kinking phenotype where animals exhibited sharp bending in both directions at kinks between straight and rigid sections of the body. The kinking response was seen for the variant strains hR163C, hR2454H, hR2458H and hK3452Q. The wild type, *unc-68* null mutant and four other RyR variant strains did not exhibit this phenotype. The dose-response assay was inadequate for assessing the response of the RyR variant strains to levamisole due to this novel kinking response coupled with instances where strains showed recovery from paralysis.

To determine if kinking could be induced in the wild type or the four 'non-kinking' RyR variant strains, a qualitative assessment of response to levamisole was conducted. Careful observation of these strains, across four concentrations, every 10 minutes for two hours was conducted, and all responses recorded. These responses were categorised into ten summary responses (Table 5.1).

The phenotypes were categorised as follows: 0. No movement was total paralysis of all individuals across all repeats. 0/#. No movement with attenuated movement describes cases where approximately half of the individuals observed were not moving, while the other half were showing a movement response. 1. Swimming was only ever seen very early in the assays at low concentrations and describes a coordinated, smooth

thrashing motion. 2. Uncoordinated swimming refers to movement that was irregular or slower than normal. 3. Folding describes animals that were folding in half, and then unfolding repeatedly, near the vulva. 4. Curling describes animals that were 'C' shaped with either the head or tail leading movement, curling up into a coil and uncurling. 5. Body twitching describes large, jerky, sporadic movements along the length of the body. 6. Head/ tail twitching was the same jerky uncoordinated movements but restricted to the head and tail only. 7. Head waving was a fast, smooth, side to side motion from the neck. 8. Shivering was a subtle but full body trembling movement. 8. Kinking animals exhibited sharp bending in both directions at kinks between straight and rigid sections of the body, in varying positions down the length of the body.

An example video of the hR163C variant strain demonstrating the kinking phenotype in 1 mM levamisole after 1 hour is available online at <https://ianhope.leeds.ac.uk/c-elegans-kinking-behaviour/>. Frames from this example video are available in Appendix I showing the kinks along the body.

Almost all individuals, for each strain, in each concentration and at a particular time point predominantly showed the same response. However, in some cases different responses were seen by a substantial number of individuals and therefore two (or three) scores were given for a strain at a single time point. For example, wild type exposed to 1 μ M levamisole at 0 minutes (Table 5.1, wild type, first row). Green shading is used to indicate paralysis in approximately half of the animals that is scored as 0/#. For example wild type exposed to 1 μ M levamisole after 40 minutes (Table 5.1, wild type, first row).

Wild type showed at least partial paralysis in all four concentrations of levamisole. Partial paralysis in 100 μ M and full paralysis in 1 mM after one hour was seen here and reported previously (Qian *et al.*, 2008) (Table 5.1, wild type, first and second rows). Remarkably, recovery from paralysis was seen in the higher levamisole concentrations (Table 5.1, wild type, third and fourth rows). In 10 mM levamisole all animals were paralysed at 20 minutes but partially recovered by 60 minutes, showing a mixture of head/ tail and body twitching. In 100 mM levamisole the worms also recovered from

paralysis with twitching as well as head waving and shivering, before complete paralysis was seen again at 90 minutes.

The *unc-68* null mutant had a very similar response as wild type, showing paralysis in all concentrations of levamisole and recovery from paralysis in the highest two (Table 5.1, *unc-68* null mutant, third and fourth rows). However, the movement responses upon recovery from paralysis were different, with folding and curling for an extended period of time. Furthermore, onset of paralysis in 100 μ M levamisole was delayed in the null mutant compared to wild type, 80 minutes and 40 minutes respectively (Table 5.1, *unc-68* null mutant and wild type, first rows). Partial resistance to levamisole has been reported previously for the *unc-68* null mutant (Lewis *et al.*, 1980).

The RyR variant strains could be separated into two distinct groups; kinking (Table 5.1, in purple) and non-kinking. The non-kinking variant strains were those for hG341R, hR2163H, hN2342S and hR4861H. The hR4861H variant strain has frequently behaved like the *unc-68* null mutant, and here neither strains showed the kinking response. However, the hR4861H variant strain appeared more resistant to paralysis by levamisole than the null mutant. This variant strain did not show any paralysis in 100 μ M levamisole, recovered from 1 mM levamisole and recovered faster in the 10 mM levamisole than the null mutant (Table 5.1, hR4861H).

Table 5.1: Response of RyR variant strains, wild type and the CB540 (*unc-68(e540)*) null mutant, to levamisole in M9 buffer over 2 hours.

Key: No movement [0], No movement with attenuated movement [0/#], Swimming [1],

Uncoordinated swimming [2], Folding [3], Curling [4], Body Twitching [5], Head/ Tail twitching [6],

Head waving [7], Shivering [8], Kinking [9].

		Time (minutes)													
		0	10	20	30	40	50	60	70	80	90	100	110	120	
Wild type	100 μ M	1/2	1/2	1/2	2	0/2	0/2	0/2	0/2	0/2	0/2	0/2	0/2	0/2	
	1 mM	2	5	0	0	0	0	0	0	0	0	0	0	0	
	10 mM	3/4/5	0/5	0	0	0	0	6	6	5	5	6	6	5	
	100 mM	0	0/6	0/7	5	7/8	7/8	5	5	5	0	0	0	0	
hR163C	100 μ M	1/2	2/3	7	3/7	6/9	9	9	9	7/9	7/9	5/7	5/7	5/9	
	1 mM	2/4	3/9	9	9	9	9	9	8/9	8	7/8	5/7	5/7	5	
	10 mM	2/4/5	9	9	9	5/9	5/9	5/7/8	5/7/8	3/5/7	5	5/8	5/8	5/8	
	100 mM	3	9	8/9	7	7/8	5	0	0	0	0	0	0	0	
hG341R	100 μ M	1	1	1/2	1/2	1/2	1/2	0/2	0/2	0/2	0/2	0/2	0/2	0/2	
	1 mM	1/2	2/3	0	0	0	0	0	0	0	0	0	0	0	
	10 mM	1/3	0	0	0	0	0	0/6	0/5	0/5	0/7	0/7	0/7	0/7	
	100 mM	0	0	0	7	4/7	3/6	3	3	5	6	6	0	0	
hR2163H	100 μ M	1/2	2/3	0	0	0	0	0	0	0	0	0	0	0	
	1 mM	2/4	0	0	0	0	0	0	0	0	0	0	0	0	
	10 mM	3/4	0	0	0	0	0	0/3	0	0	3	3/7	5	5	
	100 mM	0	0	0	0	0/5	0/5	0	0	0	0	0	0	0	
hN2342S	100 μ M	1	1	1	1	1	0/1/2	0/2	0/2	0/2	0/2	0/2	0/2	0/2	
	1 mM	1/2	3	0/5	0/5	0/5	0/5	0/5	0/5	0/5	0/5	0/5	0	0	
	10 mM	4	0	0	0	0	0/5	5	5	0	0	0	0	3	
	100 mM	3/4	5	7/8	6/7	7/8	7	7/8	6	0	0	0	0	0	
hR2454H	100 μ M	1/2	0	0	0	6	6	6	3	5	5	6	6	5/9	
	1 mM	2	6	5	5/7	6/9	6/9	6/9	5	3/5	7	0/3	0/3	0/5	
	10 mM	2/3	9	9	7/9	5	5	6/8	6	8/9	3/8	3/8	3/8	3/8	
	100 mM	0	3/5	6	8	6	6	6	0	0	0	0	0	0	
hR2458H	100 μ M	1	1/2	1/2	1/2	1/2	1/2	0/2	0/2	0/2	0/2	0/2	0/2	0/2	
	1 mM	1/2	5	7	9	9	9	9	9	9	9	9	9	9	
	10 mM	3	9	9	9	9	8/9	3/8	8	3	3	3	3	3	
	100 mM	0/4	9	9	8	8	3/8	0/5	0	0	0	0	0	0	
hK3452Q	100 μ M	1	1	1/2	1/2	1/2	1/2	2	0/2	0/2	0/2	0/2	0/2	0/2	
	1 mM	1/2	3	6	9	9	9	9	9	9	9	8/9	8/9	8/9	
	10 mM	3/4	9	9	9	8/9	5/8	8	8	8	8	3/8	4/8	4/7	
	100 mM	0	9	9	7/8	7	6/7	0/8	0/8	0	0	0	0	0	
hR4861H	100 μ M	2/4	4	2/5	2	2	2	2	2	2	3/4	3/4	4	4	
	1 mM	2/4	5	6	6	0	0	0/5	0/5	0/5	0/5	3/5	3/5	0/4	
	10 mM	4	0	0	5	3	3	3/4	3/4	4	4/7	4/7	4	4	
	100 mM	4	3/5	3/6	4	4	6	6	0	0	0	0	0	0	
CB540 (<i>unc-68(e540)</i>)	100 μ M	2/4	2/4	2/4	4	4	4	4	4	0/4	0	0	0	0	
	1 mM	2/4	2/4	0	0	0	0	0	0	0	0	0	0	0	
	10 mM	3	0	0	0	0	0	3	3	3	3	5	5	5	6
	100 mM	2/3	0	0	0	0	4	4	4	3/4	0	0	0	0	

Box shading is consistent with the colour coding used throughout this thesis. RyR variants are identified by the human variant they correspond to, Double lines separate different strains.

The hN2342S RyR variant strain also showed some resistance to paralysis, with delayed full paralysis in 1 mM levamisole delayed compared to wild type (Table 5.1, hN2342S, second row). The hG341R variant strain behaved almost exactly the same as wild type in terms of its response to levamisole across all concentrations. Conversely, the hR2163H variant strain showed increased sensitivity to levamisole; earlier onset to paralysis was seen in all concentrations with very little recovery from paralysis. Full

paralysis was seen in 100 μ M levamisole by 20 minutes for the hR2163H variant strain (Table 5.1, hR2163H, first row). Full paralysis was not seen in the wild type strain at all in the 100 μ M levamisole concentration.

The four RyR variant strains that did show kinking were hR163C, hR2454H, hR2458H and hK3452Q. The hR163C variant strain had the earliest onset of kinking, showing the behaviour from 40 minutes in 100 μ M levamisole (Table 5.1, hR163C, first row). The two variant strains for hR2458H and hK3452Q both had similar kinking responses, but onset was not as rapid as was seen for the hR163C variant strain and not in the lowest levamisole concentration. The hR2454H variant strain exhibited the weakest kinking response with only a small temporal window, in the 1 mM and 10 mM levamisole concentrations (Table 5.1, hR2454H, second and third rows) and a slight kinking response in the lowest concentration at 120 minutes (Table 5.1, hR2454H, first row). The kinking response in these strains appears to correlate with when paralysis occurred in the wild type and non-kinking RyR variant strains (Table 5.1, yellow and purple). Full paralysis was only seen in the highest levamisole concentration for the four kinking strains.

5.4. Discussion

The aim of this research was to reveal the mechanisms perturbed by the missense amino acid changes using cholinergic pharmaceutical agents.

The RyR variants altered the response to the AChE inhibitor, aldicarb. Two RyR variant strains had subtly increased sensitivity, while the rest of the RyR variant strains were more resistant, taking longer to become paralysed, compared to the wild type. The *unc-68* null mutant and the hR4861H variant took the longest to become paralysed showing substantial resistance to aldicarb.

The response of these variant strains to the nAChR agonist levamisole was more complex. A simple dose-response assay was insufficient to illustrate the range of phenotypes. A thorough analysis of the RyR variant strains' responses to a range of levamisole concentrations allowed categorisation into two distinct groups, kinking and

non-kinking strains. Of the non-kinking strains, one variant strain was hypersensitive to levamisole, one indistinct from wild type and two showed some resistance to paralysis by levamisole, compared to wild type. The RyR variant strains that showed the novel kinking response also showed a range of sensitivities and appeared to show the kinking response in place of paralysis.

5.4.1. Ryanodine receptor variants may have presynaptic effects as indicated by an altered response to aldicarb

The increased aldicarb resistance of six of the RyR variant strains could be due to these single amino acid changes reducing the amount of neurotransmitter released, resulting in delayed paralysis (Figure 5.1B). Conversely, the increased sensitivity to aldicarb for two RyR variant strains, could be due to an increase in the amount of neurotransmitter released, accelerating paralysis.

The implication of a role for calcium release from the RyR in quantal loading of vesicles in *C. elegans* (Liu *et al.*, 2005), offers a plausible explanation for how these variants may affect time to paralysis in the presence of aldicarb. Furthermore, blocking calcium release from presynaptic RyRs has also been shown to decrease quantal secretion in mice neuromuscular junctions, as a direct consequence of reduced calcium concentration in the axoplasm (Khuzakhmetova *et al.*, 2014).

If the altered response to aldicarb is due to altered RyR functionality presynaptic to NMJs, then RyR variants hR163C, hG341R, hR2163H, hN2342S, hR2458H and hR4861H result in reduced calcium release from the ER via RyR, while the variants hR2454H and hK3452Q increase RyR mediated calcium release from the ER, in *C. elegans*. These changes to axoplasmic calcium concentration may be affecting quantal loading and/ or secretion, and therefore neurotransmitter build up in synapse in the presence of aldicarb. Reduced calcium release in to axoplasm would result in slower neurotransmitter build up in the synapse and increased resistance to aldicarb.

However, it is also possible that altered sensitivity to aldicarb is due to the RyR variants functionality postsynaptically to NMJs, which is thought to be the case in the *unc-68*

null mutant. The strong resistance of the null mutant to aldicarb is expected, regardless of any presynaptic effects of the RyR, as the UNC-68 receptor does function in muscle cells. The complete loss of RyR from the muscle cells would result in delayed paralysis due to loss of calcium release from the sarcoplasmic reticulum. Despite aldicarb resulting in a build-up of ACh at the NMJ, the down-stream target of E-C coupling, the RyR, cannot be activated to release calcium from the sarcoplasmic reticulum, and so the calcium signal in the muscle cell is not amplified. Therefore, muscle hypercontraction, and paralysis, is delayed as it takes longer for paralysis-inducing calcium concentrations to accumulate in the myoplasm.

Variant RyRs may also be affecting calcium release from the SR in muscle cells, resulting in altered aldicarb response. If this were the case, then calcium release from the SR via variant RyRs would be reduced in the hR163C, hG341R, hR2163H, hN2342S, hR2458H and hR4861H variant strains but increased in the hR2454H and hK3452Q strains, as described for calcium release from the ER in nerve cells. However, the direct consequence of these changes is calcium availability in the myoplasm for muscle contraction.

Regardless of whether these variant RyRs are affecting calcium release pre or post-synaptically, it is interesting that six RyR variant strains response to aldicarb in a way that suggests reduced calcium release via variant RyRs in the presence of aldicarb. Previously the degree of curvature of five of these strains suggested excessive calcium release via variant RyRs resulting in increased muscle contraction (chapter 4). Only for the hR4861H variant do these results seem consistent.

To assess if whether presynaptic variant RyRs altered the response to aldicarb, the response to levamisole of these strains was analysed. As explained previously, should there be no differential response of the RyR variant strains in response to levamisole, compared to wild type, then the altered response seen in aldicarb for these strains can be attributed to altered function of RyR variants presynaptic to NMJs (Rand, 2007). Unfortunately, this analysis was not conclusive.

5.4.2. The responses to levamisole suggest postsynaptic effects of ryanodine receptor variants

Several strains did show changes in sensitivity to levamisole, therefore suggesting that these mutations in RyRs have direct consequences within muscle cells (Rand, 2007). Increased sensitivity to levamisole, as seen for the hR2163H variant strain, suggests increased calcium release from the SR via variant RyRs, resulting in faster paralysis. This is in direct contrast to the result in aldicarb for this strain, where increased resistance was seen. Both the hN2342S and hR4861H variant strains appeared slightly more resistant to levamisole, possibly indicating slightly reduced calcium release from the SR. Resistance of these variant strains to aldicarb was also seen. One variant strain, that for hG341R, had a similar response to levamisole like the wild type did, suggesting no effect of this variant in the muscle cells.

Recovery from levamisole paralysis was observed for all RyR variant strains, as well as the wild type and the *unc-68* null mutant. Levamisole recovery was reported previously, but only when animals were removed from levamisole and placed on an agar plate (Lewis *et al.*, 1980). Interestingly, it was noted that animals that were removed from levamisole while undergoing contraction usually recovered while those that had fully relaxed did not. The initial phase of paralysis seen here for wild type may not have reached as far as the relaxation, allowing recovery. The later phase of paralysis may have as recovery was not seen, although this could be due to termination of the assay at 240 minutes.

Recovery responses *during* exposure to other drugs has been investigated and described in *C. elegans* (Spensley *et al.*, 2018). Nicotine and levamisole both activate nAChRs, but with one crucial difference; nicotine only binds to N-type nAChRs while levamisole only binds to L-type nAChRs (Richmond and Jorgensen, 1999). Both types of nAChRs are present at NMJs in *C. elegans* (Williamson *et al.*, 2009). Applying mAChR blockers, in conjunction with nicotine, revealed that mAChR signalling drives recovery from paralysis caused by sustained N-type nAChR signalling (Spensley *et al.*, 2018). Perhaps mAChR activity allows recovery from levamisole paralysis too. Such a mechanism would require confirmation with similar experiments but using levamisole

in place of nicotine, as well as further investigation into the mechanism by which the mAChRs are able to drive recovery. Questions would remain as to how the RyR missense amino acid changes could modify the recovery compared to wild type.

The most striking finding in the levamisole response assay was the kinking phenotype observed for four of the RyR variant strains, hR163C, hR2454H, hR2458H and hK3452Q. Such a response of *C. elegans* to levamisole has not been previously reported as far as could be found, which may suggest that this is a unique response of strains carrying variant RyRs. The kinking response shows neither sensitivity nor resistance to levamisole but is a novel response to the nAChR agonist. A kinking phenotype has been used to describe the crawling locomotion of various mutations in certain *C. elegans* genes of the uncoordinated class (*unc*). The *unc-68* gene is a member of this gene class. The *unc* genes can be involved in either nerve cell or muscle cell function (Herndon and Hall, 2013), but the *unc* genes that confer a kinking phenotype on agar are usually associated with neural function (Brenner, 1974). As previously described, *unc-68* is associated most strongly with muscle function (Maryon *et al.*, 1998), but there is evidence of *unc-68* in nerve cells (Liu *et al.*, 2005; Chen *et al.*, 2017a). The *unc-68* null mutant did not exhibit the kinking phenotype in levamisole described here. However, four of the strains carrying variants in *unc-68* did demonstrate this phenotype.

None of the strains assessed here demonstrated a crawling kinking phenotype, in the absence of levamisole, so it is presumed that the crawling kinking phenotype seen for mutations in genes in the *unc* class is different to the kinking phenotype described here in the presence of levamisole. Crawling in the presence of levamisole was not assessed, however, it has been shown that these RyR variants, when expressed as extrachromosomal arrays, do not confer a kinking phenotype when exposed to 100 μ M levamisole on an agar plate (Ferreira and Kalogeropoulou, 2019). This may be due to a number of reasons; 1) over expression of the transgene in the extrachromosomal array strains masking the response, 2) that swimming is required to reveal this response, or 3) that 100 μ M levamisole is too low a concentration. Only one genome-edited RyR variant strain demonstrated a clear kinking response when swimming in 100 μ M levamisole.

An altered response to the levamisole assay was thought to indicate effects of RyR variants in muscle cells, however, the kinking response seen here for four RyR variant strains could be due to the variant RyRs disturbing calcium control in the nervous system. Upon exposure to levamisole neural calcium mishandling by variant RyRs may result in random excitation of inhibitory motor neurons. As described, ACh is an important neurotransmitter in the *C. elegans* nervous system. The circuitry associated with the motor neurons of the ventral nerve cord (VNC) are mainly cholinergic, with the exception of the inhibitory, GABAergic, DD and VD motor neurons (Pereira *et al.*, 2015). The D-type motor neurons are postsynaptic to stimulatory cholinergic A and B-type motor neurons of the VNC (Zhen and Samuel, 2015)(Figure 4.1). Calcium mishandling by variant RyRs in the nervous system may result in random excitation of inhibitory motor neurons, which would lead to temporary relaxation of some body wall muscle cells, due to release of GABA, which would otherwise be hypercontracted, due to levamisole.

It is postulated that Kinking is paralysis in most muscle cells due to levamisole binding to nAChRs on the sarcolemma with relaxation in random muscle cells due to RyR variants in GABAergic neurons stimulating GABA release. That kinking was only seen in half of RyR variants may suggest those that show kinking have more extreme effects on RyR function presynaptically. Of the four RyR variant strains that conferred the kinking response, three had the largest increase in degree of curvature, thought to be as a result of excessive calcium release, and the largest decrease in body length compared to wild type as young adults, thought to be a consequence of impaired pharyngeal pumping (chapter 4). The last variant strain that exhibited the kinking response did have an increased degree of curvature and reduced length as a young adult, but not to the same extent as the other kinking variant strains. Interestingly, this variant strain had the weakest kinking response.

5.4.3. Effects of ryanodine receptor variants in neural and muscle cells

Previously, a presynaptic effect of these RyR variants, expressed from extrachromosomal arrays, was found for response to caffeine (Nicoll Baines *et al.*, 2017). These array strains have failed to show an altered response to lower

concentrations of levamisole when crawling on an agar surface, but have shown altered responses to aldicarb (Ferreira and Kalogeropoulou, 2019). This, again, suggests effects of the RyR variants, expressed as extrachromosomal arrays, in neural cells. However, the previous work also showed effects of these altered RyRs in muscle cells, with increased myofilament disorganisation at younger ages in the RyR variant strains compared to wild type controls (Nicoll Baines *et al.*, 2017).

As an altered response was seen for the RyR variants to both aldicarb and levamisole in this research, it can only be commented that RyR variants affect calcium release from the SR in muscle cells. This does not rule out an effect of presynaptic RyRs but does show that there is at least some consequence of postsynaptic RyR variants on locomotion.

Only one variant strain, hG341R, responded differently to aldicarb, with increased resistance, but had a wild type response to levamisole. This suggests that, at least for this strain, the variant RyR had an effect on presynaptic cells. Unfortunately, the same could not be definitively stated for the other variant strains. However, the hR2163H variant strain had conflicting responses to aldicarb and levamisole, with the resistance to aldicarb suggesting reduced calcium release via the RyR and increased sensitivity to levamisole suggesting increased calcium release via the RyR. It is possible that variant RyRs could have different effects in different tissues due to the macromolecular complex regulating its activation and this is what is being seen here, possibly suggesting a role of this variant in neural tissue. Furthermore, the complex kinking phenotype in levamisole is not easily explained simply by postsynaptic RyRs and could, instead, be due to inhibitory action on muscle cells, via GABA signalling, as discussed above.

The complexity of calcium signalling via RyR in many different cellular processes is shown here. While aldicarb and levamisole assays have been useful to discern pre and postsynaptic mutations previously (Rand, 2007), this was not possible with the RyR variant strains. RyR mediated calcium signalling in pre- and postsynaptic cells appears too complex for this type of assay.

A more robust method of demonstrating tissue-specific effects would be to drive expression of these variants using tissue-specific promoters. This is possible in *C. elegans*. Neural specific expression of *unc-68* can be driven by the *rab-3* promoter, while muscle specific expression can be driven by the *myo-3* promoter, as has been done previously (Liu *et al.*, 2005). This approach has been called SKI LODGE (Single-copy Knock-in Loci for Defined Gene Expression) and could be useful to demonstrate the function, and dysfunction, of RyR variants in different tissues (Silva-García *et al.*, 2019).

Results suggest variant RyRs may affect calcium release in presynaptic cells, effecting neurotransmission, however, it also seems likely that there are consequences of these RyR variants in muscle cells. Further work, possibly using the SKI LODGE approach, is required to demonstrate clearly that RyR variants, expressed at endogenous levels, effect calcium homeostasis in presynaptic cells.

Chapter 6

Confirming a malignant hyperthermia related phenotype in heterozygous ryanodine receptor variant *C. elegans*: genetic dominance in ryanodine receptor related pathologies

6.1. Introduction

6.1.1. Aim of this chapter

The aim of the research reported in this chapter was to determine whether variant RyRs show genetic dominance over wild type RyRs, in *C. elegans*. Many RyR-related myopathies, including MH, show genetic dominance. As shown in chapter 3, *C. elegans* designed to express RyRs equivalent to human RyR1 MH disease variants express an MH-related phenotype of hypersensitivity to halothane, however, this was only shown in homozygotes. Finding sensitivity to halothane in heterozygote RyR variant *C. elegans* would further demonstrate the value of these strains in modelling MH and other RyR-related diseases, due to their similarity to the human condition.

6.1.2. Genetic dominance in malignant hyperthermia

Many disease causing RyR1 variants, such as those that cause MH, are inherited in an autosomal dominant pattern (Halsall and Hopkins, 2003; Loy *et al.*, 2011; Miller *et al.*, 2018). Only one copy of the variant allele is required for the phenotype associated with that allele to be seen. Both MH and CCD are associated with genetic dominance (Robinson *et al.*, 2006); most of the RyR variants studied here have been associated with MH, plus several also being associated with CCD. LOAM, represented by the K3452Q variant in this research, has shown genetic dominance through *RYR1* sequencing of patients presenting with neuromuscular symptoms later in life (Jungbluth *et al.*, 2009).

The research presented so far focuses only on homozygous RyR variants expressed in genome-edited *C. elegans*. However, the previous work with RyR variant extrachromosomal array strains did find genetic dominance in strains that expressed both variant and wild type RyRs (Nicoll Baines *et al.*, 2017). It is important to verify whether the genome-edited RyR variant strains show genetic dominance to further

support the similarity between them and the situation in humans. This finding would not only validate these strains as good models of MH but add further weight to the novel findings for neuromuscular defects in the absence of a triggering agent (chapters 3 and 4), and the suggestion of these defects being due to variant RyRs in the neurons (chapter 5).

Generating heterozygote *C. elegans* through mating is relatively straight forward. By crossing *unc-68* variant hermaphrodites with males that are wild type for *unc-68*, all resulting cross-progeny hermaphrodites would be heterozygous at the *unc-68* locus. Presumably, RyRs encoded by heterozygote RyR variant/ wild type animals would be made up of a mixture of variant and wild type subunits (Figure 6.1).

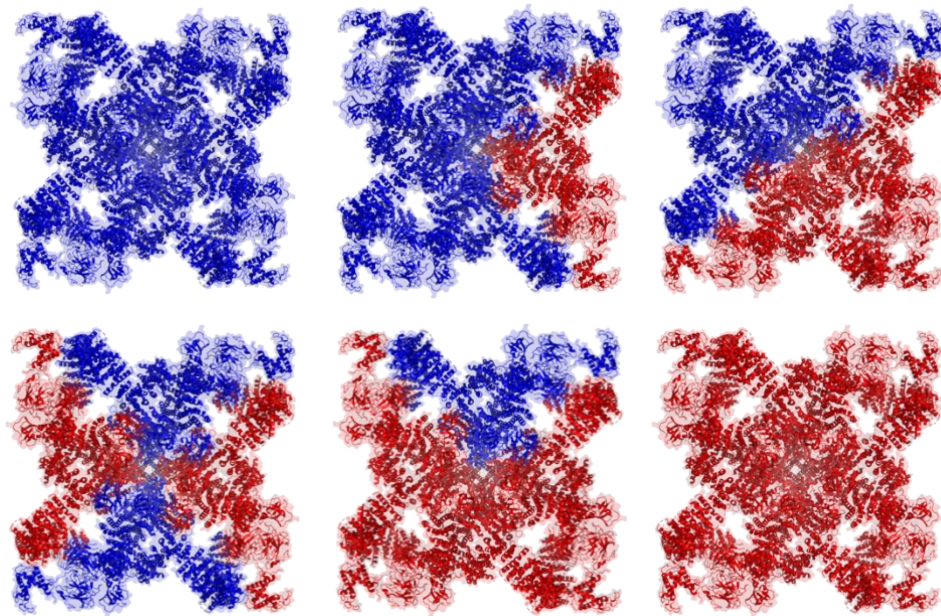


Figure 6.1: Quaternary structure of the RyR in wild type / variant *unc-68* animals.

Combination of RyR subunits is expected in the ratio of 1:4:6:4:1 in heterozygote animals. Of the channels made up of two wild type and two variant subunits they could assemble so that identical channels are opposite or next to each other as shown on top row far right and bottom row far left. The homotetramers are viewed from cytoplasm. Arbitrarily, blue indicates wild type subunits and red the variant subunits. Generated using PyMOL, based on the closed conformation of rabbit RYR1, as predicted from Yan *et al.* (2015) (PDB code 3J8H).

The quaternary structure of the RyR channel in heterozygotes with both wild type and variant *unc-68* has five possible conformations (Figure 6.1). As the RyR channel is a homotetramer, it is predicted that the subunits would combine in a ratio of 1:4:6:4:1; 1 – (wild type)₄, 4 – (wild type)₃, (variant)₁, 6 – (wild type)₂, (variant)₂, 4 – (wild type)₁, (variant)₃, 1 – (variant)₄. Although, this may not be the case if there was differential affinity between the different subunits. The channels made up of two wild type and two variant subunits could combine so that variant subunits are opposite or next to each other. Furthermore, RyR channels adjacent to each other communicate; an aberrant conformational change in a variant tetramer could have direct consequences upon adjacent, fully functioning, tetramers.

6.2. Methods

6.2.1. Generating heterozygous ryanodine receptor variant individuals in *C. elegans*

Generating *unc-68* variant / wild type heterozygous strains was achieved by mating. A GFP marker was used to distinguish cross- and self-progeny. N2 wild type males from stocks maintained in Leeds were crossed with OH441 hermaphrodites (from the Caenorhabditis Genetics Center) to generate heterozygous *otIs45[unc-119::gfp]* / wild type progeny, half of which were male (Figure 6.2). The male progeny from this cross were then crossed with hermaphrodites of the RyR variant strains. All cross-progeny from this mating were heterozygous at the *unc-68* locus and half of the cross-progeny carried the *unc-119::gfp* marker. Of the individuals carrying the GFP marker, only hermaphrodites were used in phenotyping assays. N2 wild type and CB540 (*unc-68(e540)*) null mutant heterozygote individuals were generated in parallel for direct comparison.

The first cross (N2 wild type males x OH441 hermaphrodites) was set up in a 3:2 male to hermaphrodite ratio. The second cross between the *otIs45[unc-119::gfp]* / wild type males and *unc-68* variant hermaphrodites was set up four days prior to assaying for halothane sensitivity. Two L4 *unc-68* variant homozygous hermaphrodites were picked to a fresh NGM plate along with four or five *otIs45[unc-119::gfp]* / wild type heterozygous males. This was done in triplicate. L4 hermaphrodites were used to

ensure they had not begun producing self-progeny. More males than hermaphrodites were used to increase the chances that hermaphrodites were mated.

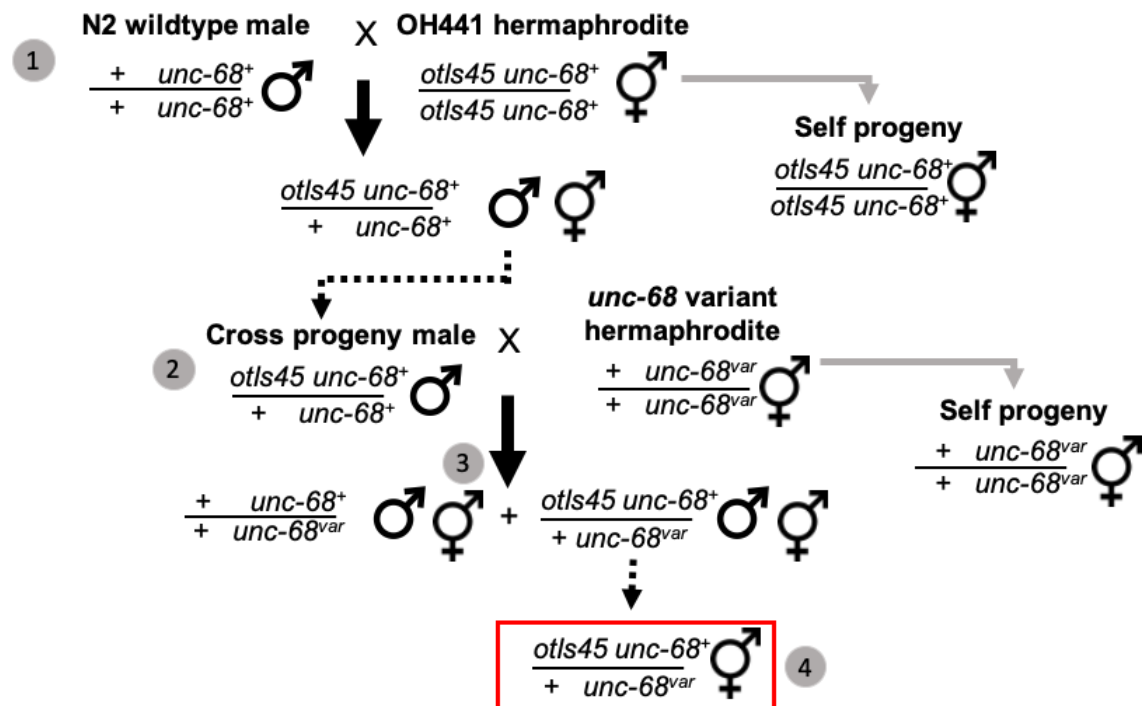


Figure 6.2: Heterozygous wild type / variant *unc-68* animals were generated by mating.

N2 wild type males (σ) were mated with OH441 hermaphrodites (♀) (1). Male progeny from this cross were all heterozygous and were mated with *unc-68* variant hermaphrodites (2). The dotted arrow shows males resulting from cross 1 being used in cross 2. As a result of cross 2, hermaphrodite and male progeny heterozygous at the *unc-68* locus would be generated, half of these would also be heterozygous for the *otIs45* allele and express GFP (3). The GFP expressing hermaphrodites were used in phenotyping assays, shown by the red box (4). Self-progeny of the RyR variant hermaphrodites (shown by a grey arrow) were excluded as they did not carry the GFP marker. This was also done in parallel for N2 wild type and the CB540 (*unc-68(e540)*) null mutant for direct comparison. The UNC-119 GFP marker was integrated by gamma radiation and is in chromosome V, the same chromosome as *unc-68*, therefore the *otIs45* allele and *unc-68* are shown on the same line.

6.2.2. Halothane and thrashing assays for the heterozygote variant animals

Halothane and swimming assays were conducted for young adult heterozygous animals as previously described (section 3.2.1). However, only the highest

concentration of halothane (5 mM) was used to confirm an MH-related phenotype of hypersensitivity to halothane. Thrashing rate in S medium was also determined for heterozygotes.

To obtain young adult heterozygous animals, three days after cross 2 was set up, which was one day prior to the assay, the cross progeny were screened for the GFP marker. L4 hermaphrodites expressing the marker were picked to a fresh NGM plate seeded with OP50 *E. coli*. The next day, four days after the cross was set up, the heterozygous hermaphrodites were screened for halothane sensitivity.

6.3. Results

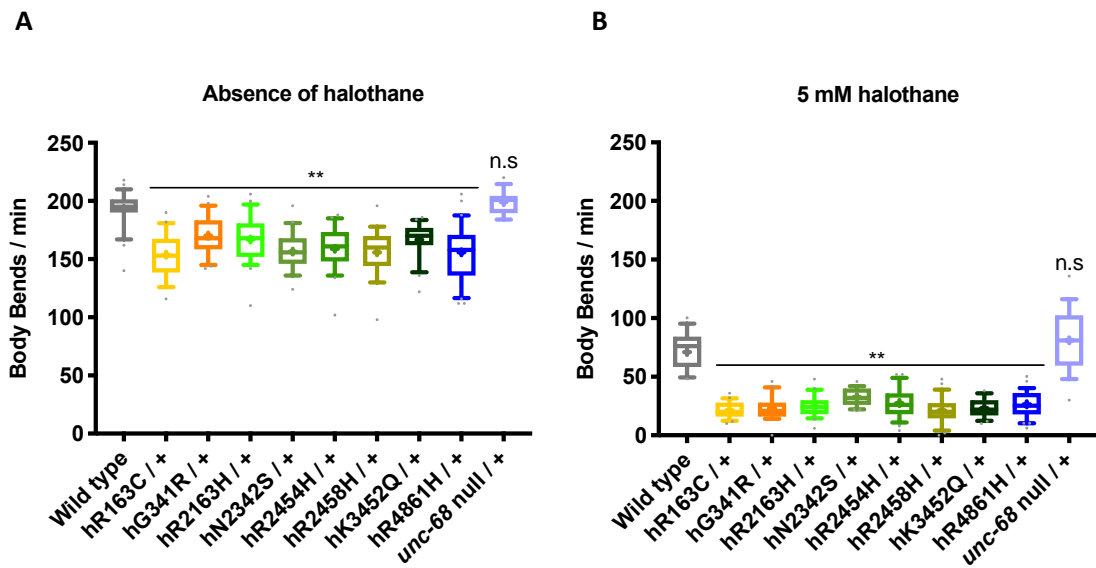
6.3.1. Halothane hypersensitivity and locomotion defects are present in all ryanodine receptor variant heterozygote animals

To confirm genetic dominance in the heterozygous RyR variant animals, sensitivity to halothane was tested. Individual young adult hermaphrodites were picked into S medium or S medium with 5 mM halothane and body bends counted.

To confirm that there was no effect of the different genetic background, except for the *unc-68* variant locus, the wild type control was subjected to the same cross and only the hermaphrodites carrying the GFP marker were assayed. The resulting progeny are fully wild type for *unc-68* and therefore referred to as “heterozygous” to emphasize the direct comparison to the RyR variant / wild type heterozygote animals. The “heterozygote” wild type animals completed 193 (± 16) body bends per minute in S medium alone, which was similar to the starting homozygous wildtype animals in S medium, 199 (± 14) body bends per minute ($P=0.66$, One-way ANOVA with Tukey’s multiple comparison test) (see below, Figure 6.4A).

The *unc-68* null phenotype is recessive to wildtype (Maryon *et al.*, 1996). Here, when a heterozygous *unc-68* null mutant was generated by mating, the thrashing rate, 199 (± 10) body bends per minute, was indistinguishable from the “heterozygote” wild type control, ($P=0.99$, One-way ANOVA with Tukey’s test) (Figure 6.3A). This shows that the *unc-68* null phenotype is recessive to wild type, in agreement with the

previously published data. Surprisingly, the same was not seen for the hR4861H variant, which had behaved similarly to the null mutant in most assays to this point.



C
Mean and standard deviation of thrashing rates in the absence of halothane and in 5 mM halothane for wild type and the CB540 (*unc-68(e540)*) null mutant and RyR variant *C. elegans* strains when heterozygous for wild type *unc-68*.

	Absence of halothane		5 mM halothane	
	Mean	SD	Mean	SD
Wild type	193	16	71	17
hR163C / +	154	19	22	7
hG341R / +	170	18	23	10
hR2163H / +	167	22	25	9
hN2342S / +	157	17	33	7
hR2454H / +	159	20	28	13
hR2458H / +	156	20	21	11
hK3452Q / +	167	16	23	8
hR4861H / +	156	25	26	11
<i>unc-68</i> null / +	199	10	81	26

Box shading is consistent with the colour coding used throughout this thesis. RyR variant strains are listed according to the human variant they correspond to.

Figure 6.3: Locomotion effects and halothane hypersensitivity in heterozygous RyR variant individuals.

Thrashing rate in S medium, in body bends per minute, for heterozygous RyR variant animals with the modified *unc-68* over a wild type *unc-68* introduced by mating, labelled by the human variant they correspond to, in the absence of (A) and presence of (B) 5 mM halothane. (C) Mean and standard deviation (SD) of thrashing rate, in body bends per minute, for wild type, the null mutant and RyR variants when

expressed over wild type *unc-68*. Corresponding wild type and CB540 (*unc-68(e540)*) null mutant individuals were generated and assayed in the same way for direct comparison. Wild type shows the data for the crossed “heterozygote” animals. 25 individuals were examined per strain. Boxes indicate the median and interquartile range, with whiskers to the 10-90 percentile, outliers as dots, and + to indicate the mean. Significance is between variant strains or the *unc-68* null mutant and the wild type. ** $P < 0.005$, n.s = not significant (one-way ANOVA, with Tukey’s multiple comparison test).

Heterozygous hR4861H individuals had a mean thrashing rate of 156 (± 25) body bends per minute in S medium alone (Figure 6.3A). This was significantly lower than for the “heterozygote” wild type control ($P < 0.005$, One-way ANOVA with Tukey’s test). This demonstrates that the hR4861H allele is not a null, despite showing some similarity to the null mutant when homozygous. The hR4861H UNC-68 is expressed and interferes with the wild type protein’s function in heterozygous *C. elegans*. This is also the case in the human condition, where this missense RyR1 variant causes MH and CCD when present in the heterozygote state (Monnier *et al.*, 2001).

As a heterozygote, the hR4861H variant individuals were found to have a similar thrashing rate to all other RyR variant heterozygotes. The heterozygotes for all RyR variants had reduced thrashing in the absence of halothane compared to the wild type control ($P < 0.005$, One-way ANOVA with Tukey’s test) (Figure 6.3A). A single copy of any RyR variant studied here is sufficient to confer an effect on neuromuscular function, even in normal conditions, in the absence of any external triggering agent.

When exposed to 5 mM halothane, the heterozygote *unc-68* null mutant was indistinguishable from the “heterozygote” wild type control, completing 81 (± 26) and 71 (± 17) body bends per minute respectively ($P = 0.39$, One-way ANOVA with Tukey’s test) (Figure 6.3B). Once again, this shows the null phenotype is recessive to wild type.

Conversely, all RyR variant heterozygotes had a reduced thrashing rate compared to the wild type “heterozygote” control when exposed to 5 mM halothane, indicating hypersensitivity to the MH triggering agent (Figure 6.3B, Table 6.1). The RyR variant

heterozygotes completed between 21 (± 11) and 33 (± 7) body bends per minute, which is less than half of the “heterozygote” wild type thrashing rate ($P < 0.005$, One-way ANOVA with Tukey’s test). The heterozygous RyR variant animals also had larger percentage decreases in thrashing rate from 5 medium to 5 mM halothane, greater than 80%, except for the hN2342S variant heterozygous animals, which showed a 79% decrease, compared to 63% for wild type and 59% for the heterozygous *unc-68* null mutant (Table 6.1). Therefore, the reduced thrashing rate seen in 5 mM halothane for the heterozygous RyR variant animals compared to wild type is not just a result of the reduced thrashing rate seen in the absence of halothane for these animals, but increased sensitivity to halothane. These results demonstrate genetic dominance of variant RyRs over wild type, in agreement with previous research in *C. elegans* (Nicoll Baines *et al.*, 2017), and the inheritance pattern of MH and other RyR-related myopathies (Halsall and Hopkins, 2003; Loy *et al.*, 2011; Miller *et al.*, 2018).

Table 6.1: Percentage change of mean thrashing rates from the absence of, to presence of 5 mM halothane for RyR variant heterozygote animals, and wild type and CB540 (*unc-68(e540)*) null mutant controls.

Strain (Variant)	Absence to 5 mM halothane
Wild type	-63%
hR163C / +	-86%
hG341R / +	-86%
hR2163H / +	-85%
hN2342S / +	-79%
hR2454H / +	-83%
hR2458H / +	-86%
hK3452Q / +	-86%
hR4861H / +	-83%
<i>unc-68</i> null / +	-59%

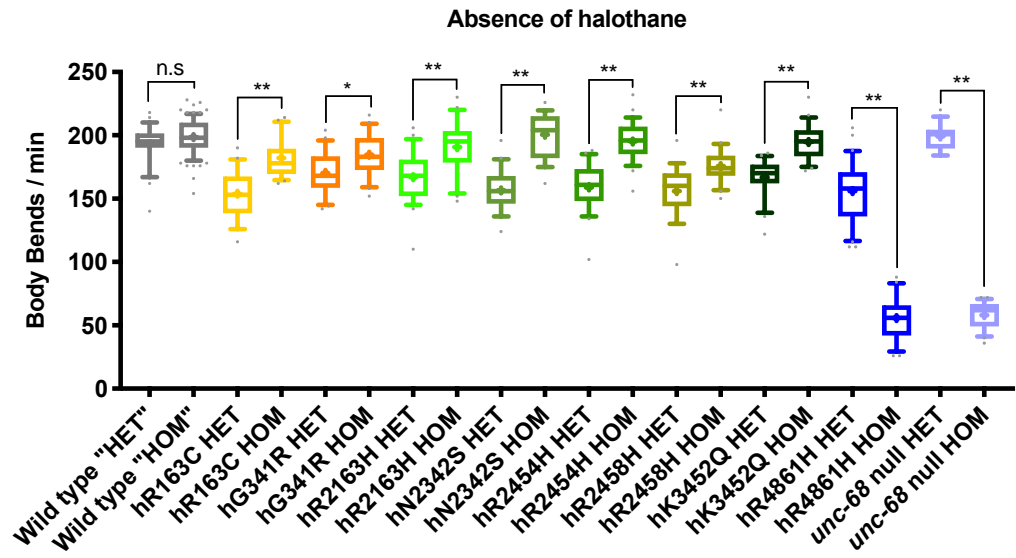
Box shading is consistent with the colour coding used throughout this thesis. RyR variant strains are listed according to the human variant they correspond to. Percent change is calculated as $((C1-C2)/C1)*100$ where C1 is the absence of halothane and C2 is 5 mM halothane. All strains showed a decrease from C1 to C2, indicated by a minus sign (-).

6.3.2. Ryanodine receptor variants in the heterozygote animals disrupt locomotion more than in the homozygotes

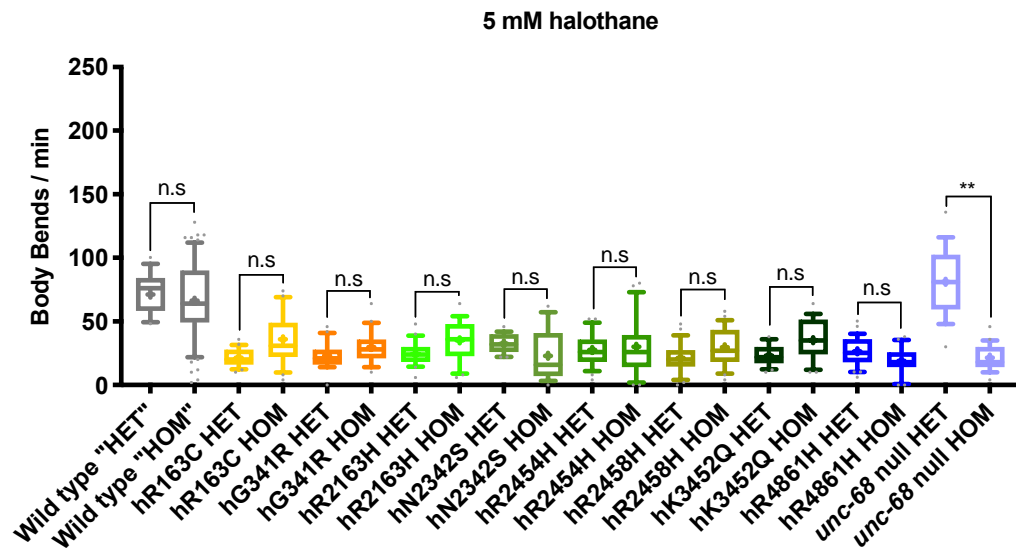
RyR variant heterozygotes and homozygotes were compared (Figure 6.4). In the absence of halothane, the presence of a wild type copy of *unc-68* significantly increases thrashing rate in S medium for hR4861H variant animals (from 56 (± 19) to 156 (± 25) body bends per minutes ($P < 0.005$, One-way ANOVA with Sidak's test for multiple comparisons) (Figure 6.4A). However, this is the only case of locomotion improving in the heterozygous RyR variant animals compared to the homozygous animals and reflects the lack of channel function for the hR4861H UNC-68 homotetramer.

With the exception of hR4861H, the RyR variant heterozygotes had a stronger locomotion defect than the corresponding homozygotes. The RyR variants that had conferred a locomotion defect when present in the homozygous young adults, hR163C, hG341R and hR2458H, all conferred a worse locomotion defect in the heterozygote young adults ($P < 0.005$, $P < 0.05$ and $P < 0.005$ respectively, One-way ANOVA with Sidak's test). The remaining four variants, hR2163H, hN2342S, hR2454H and hK3452Q, which had permitted apparently wild type-like locomotion in the homozygotes, conferred a locomotion defect when present in heterozygotes ($P < 0.005$, One-way ANOVA with Sidak's test). This shows that the presence of a variant UNC-68 is not only sufficient to confer an effect on neuromuscular function, but that the presence of a variant UNC-68 with wild type UNC-68 actually enhances the consequences of the variant RyR, in the absence of a triggering agent.

A



B



C

Mean and standard deviation of thrashing rates in the absence of halothane and in 5 mM halothane for heterozygous and homozygous RyR variant *C. elegans* strains and the corresponding wild type and CB540 (*unc-68(e540)*) controls.

	S medium		5 mM halothane	
	Mean	SD	Mean	SD
Wild type "HOM"	199	14	66	30
Wild type "HET"	193	16	71	17
hR163C HOM	182	16	36	20
hR163C HET	154	19	22	7
hG341R HOM	185	18	30	13
hG341R HET	170	18	23	10
hR2163H HOM	191	21	35	16
hR2163H HET	167	22	25	9
hN2342S HOM	201	18	23	20
hN2342S HET	157	17	33	7
hR2454H HOM	195	16	30	24
hR2454H HET	159	20	28	13
hR2458H HOM	176	15	30	15
hR2458H HET	156	20	21	11
hK3452Q HOM	195	14	35	16
hK3452Q HET	167	16	23	8
hR4861H HOM	56	19	19	11
hR4861H HET	156	25	26	11
<i>unc-68</i> null HOM	58	11	22	10
<i>unc-68</i> null	199	10	81	26

Box shading is consistent with the colour coding used throughout this thesis. RyR variant strains are listed according to the human variant they correspond to.

Figure 6.4: Comparison of heterozygous and homozygous RyR variants on locomotion and halothane sensitivity.

Thrashing rate in S medium, in body bends per minute, for 25 individuals, in the absence of (A) and presence of (B) 5 mM halothane. RyR variants are identified by the human variant they correspond to, and were either heterozygous (HET), with the modified *unc-68* over a wild type *unc-68* introduced by mating, or homozygous (HOM) for the modified *unc-68*. Corresponding wild type and CB540 (*unc-68(e540)*) null mutant individuals were generated and assayed in the same way, although the wild type "heterozygotes" ("HET") and "homozygotes" ("HOM") are fully wild type for *unc-68*. Boxes indicate the median and interquartile range, with whiskers to the 10-90 percentile, outliers as dots, and + to indicate the mean. Significance is between heterozygotes and homozygotes. * $P < 0.05$, ** $P < 0.005$, n.s = not significant (one-way ANOVA, with Sidak's multiple comparison test). (C) Mean and standard deviation (SD) of thrashing rate, in body bends per minute, in the absence and presence of 5 mM halothane for heterozygous and homozygous RyR variant strains and corresponding wildtype and CB540 (*unc-68(e540)*) controls.

When exposed to 5 mM halothane the rate of thrashing in the RyR variant heterozygotes was indistinguishable from the homozygotes (Figure 6.4B). The only *unc-68* allele to show a difference between the heterozygote and homozygote in 5 mM halothane was the null, consistent with the recessive nature of the *unc-68* null phenotype. Once again, this shows the genetic dominance of the RyR missense variants.

6.4. Discussion

The aim of the research described in this chapter was to confirm genetic dominance of RyR variants in *C. elegans*. This was achieved as it was shown that heterozygote RyR variant animals are hypersensitive to halothane.

Of further interest is the thrashing defects that were apparent in all RyR variant heterozygotes, even if not in the corresponding homozygote. Despite a wild type copy of RyR rescuing the null locomotion phenotype and partially recovering thrashing in the hR4861H variant heterozygotes, the heterozygote RyR variant animals had reduced thrashing rates in S medium, compared to the “heterozygous” wild type control and their homozygous counterparts.

6.4.1. Thrashing defects are intensified in ryanodine receptor variant heterozygote animals

The data presented suggest functional alterations in heterozygous individuals in the absence of an MH trigger. Previously, no effect of RyR variants on locomotion when expressed in *C. elegans* from extrachromosomal arrays, in representations of the homozygous or heterozygous conditions, was seen in the absence of a triggering agent (Nicoll Baines *et al.*, 2017). The previous explanation for the inconsistency between array strains and CRISPR-Cas9 genome-edited strains still stands - expression levels of UNC-68 are likely to be critical for this altered phenotype. Higher levels of expression from the extrachromosomal arrays may mask altered phenotypes.

Particularly striking, is that the thrashing defect in the genome-edited strains as heterozygotes is worse than in the corresponding homozygotes, with the exception of the hR4861H variant. A mixture of normal and variant subunits appears to disrupt channel function more than when all four subunits are distorted in the same way in variant homozygotes.

As described previously, Witherspoon and Meilleur (2016) divide the complex interactions and modifications that regulate RyR into six groups. These groups include interdomain interactions, post translational modifications, and retrograde and orthograde signalling. Mutations in RyR1 that interrupt these regulatory groups are associated with a number of pathologies and MH is linked to at least four of the six regulatory groups. A possible explanation for the further compromised functionality of variant / wild type RyRs could involve the amino acid changes impacting upon multiple aspects of RyR function.

It is possible that a single mutation in RyR is able to disrupt multiple components of the regulatory groups described by Witherspoon and Meilleur (2016). For example, several CCD causing mutations introduced into rabbit *RYR1* disrupt the interaction between RyR1 and triadin as well as influencing voltage-gated calcium release from the SR in mice myotubes (Goonasekera *et al.*, 2007). As described previously, binding of triadin to RyR modulates RyR activity dependent on the calcium concentration of the SR (Györke *et al.*, 2004). If the triadin-RyR interaction were affected by one of the mutations here, RyR activity could be reduced and calcium release from the SR decreased in the variant homozygote. Simultaneously, the mutation could also increase voltage-gated calcium release from the SR/ ER. The presence of wild type subunits in the variant heterozygote could rescue one of the effects of the variant RyR, such as the interaction with triadin. This would result in normal RyR triadin control, without affecting the change to voltage-gated calcium release. This could result in increased calcium release in the variant heterozygote compared to the variant homozygote and wild type.

As described previously, while MH is described as asymptomatic in the absence of a trigger, several RyR1-related diseases show inherent consequences for neuromuscular

function (MacLennan, 2000; Robinson *et al.*, 2006; Illingworth *et al.*, 2014; Laforgia *et al.*, 2018). With MH causing *RYR1* variants in the human population being present heterozygously (Gardner *et al.*, 2020), and functional alterations being found in all heterozygote animals here, subtle consequences for neuromuscular function may be present but undetected in the human population for carriers of *RYR1* variants.

In the presence of halothane, the RyR heterozygote animals show hypersensitivity, demonstrating genetic dominance of RyR variants. This finding is in agreement with previous work where these variants were expressed as extrachromosomal arrays in *C. elegans* (Nicoll Baines *et al.*, 2017), as well as work in mice and humans (Robinson *et al.*, 2006; Carpenter *et al.*, 2009a). However, the threshold of calcium response of myotubes from homozygous R163C knock-in mice to the IVCT agent caffeine has been shown to be further decreased than for heterozygous R163C knock-in mice (Yang *et al.*, 2006). This suggests that myotubes from homozygous RyR variant mice are more sensitive than corresponding heterozygous mice. Another study has found homozygous and heterozygous MH RyR1 mutations distinguishable based on responses to caffeine but could not differentiate between them for response to halothane (Lynch *et al.*, 1997). As only response to halothane was assessed here this may explain the similarity between homozygote and heterozygote RyR variants for the MH-related phenotype.

Nevertheless, both homozygous and heterozygous RyR variant strains demonstrated increased sensitivity to halothane compared to wild type here and the genetic dominance seen for these strains adds further support for the use of these strains as models for MH and other RyR-related pathologies.

Chapter 7

General Discussion

In this research I used *C. elegans* to explore effects of RyR variants *in vivo*. I have demonstrated that these RyR variant strains do confer an MH-related phenotype of increased halothane sensitivity, which is also present in RyR variant heterozygote animals, demonstrating genetic dominance, as in the human situation.

More strikingly, I have demonstrated that both RyR variant homozygotes and heterozygotes confer locomotion defects in the absence of an MH triggering agent, when in liquid. Investigation into these locomotion defects in RyR variant homozygote animals revealed different effects on crawling for different RyR variants, and suggested consequences of these variants in age-related locomotion degeneration.

I also focussed on the potential focus of these RyR variants being in neural and/ or muscle cells. Differential responses of these RyR variant strains to the cholinergic pharmaceutical agents suggested these variants may affect RyR functionality in both neural and muscle cells, although this was not shown conclusively.

7.1. Ryanodine receptor variants increase *C. elegans* sensitivity to halothane independently of age and zygosity

This research provides evidence for *C. elegans* as a valid model of MH, and other RyR-related diseases. A measurable MH-related phenotype, hypersensitivity to halothane, was found for both RyR variant homozygote and heterozygote animals, carrying mutations in the endogenous chromosomal location. This reflects the human situation where MH is inherited in an autosomal dominant fashion (Halsall and Hopkins, 2003; Loy *et al.*, 2011; Miller *et al.*, 2018). Such consequences of RyR variants in *C. elegans* had been recorded previously (Nicoll Baines *et al.*, 2017). However, the mutations were expressed then from an extrachromosomal array. The use of genome editing, as opposed to a transgene, means that the expression levels and distribution of the

modified RyR reflects that of the wild type, and is therefore more likely to reflect the natural situation in *C. elegans* and the natural human situation.

Halothane sensitivity was found to be similar between RyR variant homozygote and heterozygote animals, as well as between young and old adult homozygote animals. Two RyR variant strains did show a significant increase in sensitivity to halothane between young and old adult in the homozygotes. The variant strain that was frequently similar to the *unc-68* null mutant and the hK3452Q variant strain. The latter is the only RyR variant studied here to also be implicated in an age-related disorder, Late-onset axial myopathy (LOAM) (Løseth *et al.*, 2013), but that could be a coincidence. The onset of axial myopathy is thought to be a specific late manifestation of *RYR1* mutations associated with MHS, but with much lower prevalence than MHS, suggesting the presence of additional modifiers. The cause of LOAM is suggested to be a particular vulnerability of the axial musculature to a combination of RyR1 dysfunction and normal ageing. Leaky RyR1 channels have been shown to have a detrimental effect on muscle structure and function with age (Andersson *et al.*, 2011), however environmental and other genetic modifiers may play a role in the development of LOAM (Løseth *et al.*, 2013). The specific involvement of some RyR1 variants rather than others in LOAM is not understood. An N-terminal domain (NTD) mutation G40V, thought to interrupt the interaction with the DHPR, was identified in a 77-year-old patient presenting with late-onset neuromuscular symptoms (Jungbluth *et al.*, 2009). It was thought that the locations of this mutation, in the NTD of *RYR1*, resulted in a different phenotype to CCD-causing mutations typically thought to be located in the CTD 'hot spot' (Sei *et al.*, 2004; Jungbluth *et al.*, 2009). However, the idea of *RYR1* 'hot spots' is not as popular anymore with many mutations existing outside of these regions; next generation sequencing (NGS) has made sequencing of full cDNA of *RYR1* feasible (Laforgia *et al.*, 2018). Furthermore the LOAM *RYR1* variant studied here is not in the NTD, but the helical domain (Løseth *et al.*, 2013). The increase in hypersensitivity seen for the LOAM-associated RyR variant strain, with age, may suggest that this variant channel was not fully compromised by halothane in the young adults, but with age the channel became more sensitive to perturbation. This is in line with the notion that LOAM is associated with particular vulnerability to a combination of RyR1 dysfunction and ageing.

The increased sensitivity in the hR4861H variant strain with age in the homozygous RyR variant animals was attributed to this variant severely affecting protein function when present homozygously, and therefore being comparable to the null mutant.

Hypersensitivity to halothane was unaffected by zygosity in all of the RyR variant strains. However, more severe responses to caffeine have been found for homozygous R163C knock-in mice compared to heterozygous mice, as described in chapter 6 (Yang *et al.*, 2006). Homozygous and heterozygous MH RyR1 mutations are indistinguishable in response to halothane, despite the former being more sensitive to caffeine (Lynch *et al.*, 1997). Perhaps assessment of response to caffeine of the homozygous and heterozygous RyR variant animals would also reveal differences in sensitivity based on zygosity. Nonetheless, genetic dominance was seen in these animals with only one copy of an RyR variant being required for hypersensitivity to the MH-trigger halothane, as is reported in humans.

Hypersensitivity to halothane was unaffected by age and zygosity in the majority of the RyR variant strains studied, suggesting that in young adult RyR variant homozygotes, and indeed heterozygotes, the variant RyR is already fully compromised for halothane exposure in *C. elegans*.

7.2. Ryanodine receptor variants have inherent consequences for locomotion in *C. elegans*

The expression of modified RyRs at the endogenous level, and distribution, revealed significant consequences for locomotion, in the absence of a triggering agent, which had not been reported for expression of the same variants from an extrachromosomal array (Nicoll Baines *et al.*, 2017). These subtle consequences for locomotion had different strengths for different RyR variant strains; this is similar to the human condition, where muscle biopsies for different RyR1 variants presented different MH phenotype severities (Carpenter *et al.*, 2009b). While RyR1 variants are sometimes associated with muscle weakness (MacLennan, 2000; Robinson *et al.*, 2006; Illingworth *et al.*, 2014; Laforgia *et al.*, 2018), there is no real evidence for locomotion phenotypes

in patients with RyR1 variants. However due to the relatively low prevalence of MHS/ RyR1 mutations, such a phenotype would need to be particularly marked in an individual for it to be detected. There is a lack of data and statistical power for large-scale analyses on human populations and such subtle phenotypes would be missed.

At the first larval stage, all of the RyR variant strains exhibited strong locomotion defects with reduced thrashing rate in liquid, compared to wild type. In young adult RyR variant heterozygote and homozygote animals, and old adult RyR variant homozygote animals the reductions in thrashing rates were more subtle than in L1s.

The further development of the nervous and muscular systems from L1 to young adult (Sulston and Horvitz, 1977) may offer an explanation for the more marked thrashing defects in the early larval stage *C. elegans*, compared to later life stages. The mutations in *unc-68* may have more of an impact at the L1 stage. Alternatively, the simpler neuromuscular system in L1s may mean the neuromuscular system is less robust to perturbation, due to less overlap or redundancy in functionality. A further consideration is that there could be gradual adaptation through the worm's lifespan to specifically reduce the consequences of the subtle defects in RyR function due to the mutations in *unc-68*; locomotion would progressively improve with age. If calcium ion levels are subtly perturbed, perhaps there is a homeostatic response to correct the problem, however this has to be gradual to avoid catastrophic consequence, and therefore subtle locomotion defects are still seen in the young adults. Changes in expression of calcium homeostasis machinery has been observed in response to heart disease and neurodegeneration (Chakroborty *et al.*, 2009; Dally *et al.*, 2009; Naranjo and Mellström, 2012). Therefore, it is possible that components in the macromolecular complex that regulate RyR function, *unc-68* itself, and/ or other channels which regulate calcium ion release/ uptake from the SR/ ER, may experience changes in gene expression upon calcium ion mishandling. There is evidence of a compensatory mechanism in Y522S *RYR1* variant knock-in mice, described previously (Andronache *et al.*, 2009). The voltage-dependence of the DHPR inactivation was shifted to more negative potentials due to retrograde signalling from RyR1, resulting in less calcium ion release, which was thought to counteract the calcium leakage seen by this variant RyR channel. Between the L1 and young adult stage a compensatory mechanism may be

employed to mitigate the effects of the RyR variants on calcium homeostasis. Nevertheless, while all RyR variant strains show reduced thrashing compared to wild type at the L1 stage, only some of these variant strains show statistically significant reduced thrashing at later life stages, suggesting some RyR variants perturb the function of the RyR more than others, or that compensatory mechanisms are only employed/ successful in some instances.

7.2.1. Worm length may affect thrashing rate in young adults

Shorter worm lengths in young adults for six of the eight RyR variant strains was attributed to decreased pharyngeal pumping and feeding rate. As the only RyR in *C. elegans*, *unc-68* functions in pharyngeal muscle as well as in the body wall muscles and neurons, which were discussed extensively here (Maryon *et al.*, 1996; Chen *et al.*, 2017a). The effect of reduced food uptake was thought to delay development in these strains, resulting in shorter lengths at the young adult stage. The four shortest RyR variant strains at young adult were also the only RyR variant strains to have statistically significantly reduced thrashing rates in liquid compared to wild type as young adults. Thrashing rate may be effected by worm length.

Crawling analysis was not carried out for L1s, and therefore L1 worm lengths were not quantified for the different RyR variant strains. However, considering the correlation between reduced thrashing rate and shorter worm lengths in the young adults, the reduced thrashing rate of all RyR variant strains as L1s may be a reflection of shorter worm lengths at hatching. Such a result would indicate an embryonic developmental delay as a result of RyR variants in *unc-68*; problems with neuromuscular function could affect elongation of the embryo, resulting in shorter, but fatter, animals at hatching. Shorter length at hatching could not be attributed to reduced food intake as there is no feeding prior to hatching. However, reduced feeding of the mother may result in smaller eggs or less yolk provision, affecting worm length of the L1s. In order to understand the contributions of worm length on thrashing rate in the L1s, the length of the L1 animals would need to be quantified.

In the old adults, four of the eight RyR variant strains had a reduced thrashing rate compared to wild type; three of these are the same as those with reduced thrashing

rate in young adults. Of the four RyR variant strains with reduced thrashing rate in the old adults, three were also the shortest of the RyR variant strains at old adult, and shorter than wild type, again suggesting an effect of worm length on thrashing rate. However, the fourth RyR variant strain to have reduced thrashing rate in the old adults was the largest of all the strains, including the wild type. Therefore, while reduced worm length may play a role in reduced thrashing rate in liquid for old adults, other factors also contribute to this locomotion defect.

7.2.2. Muscle contraction is increased in young adult ryanodine receptor variant strains

While measurement of thrashing rate in liquid did reveal differences between some RyR variant strains and wild type in the absence of a triggering agent, in-depth analysis of worm crawling revealed that all RyR variant strains are phenotypically distinct from both wild type and the *unc-68* null mutant. Furthermore, the RyR variant strains were distinct from each other with varied consequences for crawling parameters. As mentioned above, RyR1 variants do cause different phenotypes in humans, with some variants being associated with more severe IVCT phenotypes and others weaker phenotypes (Carpenter *et al.*, 2009b). Some variants show different strengths of response to different agents within the IVCT, such as showing a strong response to caffeine but weaker response to halothane. Having different severities of response to different triggering agents suggests that variants affect different mechanisms of RyR function. Furthermore, while some RyR1 variants are only associated with MH, others are associated with other myopathies such as CCD with more severe overt phenotypes (MacLennan, 2000; Robinson *et al.*, 2006).

Differences were found for the RyR variant strains for crawling amplitude and wavelength, for both young and old adults, compared to wild type. These subtle differences affected the degree of curvature of the crawling waveform, which presumably reflects differences in RyR channel properties. A larger degree of curvature would result from a sharper wave, suggesting an increase in strength and/ or duration of muscle contraction. Such an effect was seen for six of the eight RyR variant strains as young adults suggesting an increase in calcium release into the myoplasm due to the single amino acid change in UNC-68. RyR1 variants are frequently referred to as 'leaky', releasing excessive calcium into the cytoplasm (Andronache *et al.*, 2009;

Andersson *et al.*, 2011; Liu *et al.*, 2012; Lamboley *et al.*, 2016; Chen *et al.*, 2017b). It has been demonstrated that the presence of the R163C *RYR1* variant in mice does increase calcium concentration of the cytoplasm, likely through increase calcium release via variant RyRs. Here this variant, and others, are suggested to increase calcium release via variant RyRs as degree of curvature was increased suggesting muscle hypercontraction.

The two RyR variants that did not have a greater degree of curvature in the crawling analysis did have changes in amplitude and wavelength. While the hN2342S variant did reduce the amplitude and wavelength, the degree of curvature remained similar to wild type. This strain had the greatest increase in crawling frequency due to the smaller wave as a result of the reduced amplitude and wavelength. While degree of curvature can be used to compare the extent of muscle contraction, it does not necessarily reflect the extent of muscle contraction in this case. The smaller wave seen for this strain compared to wild type does suggest increased muscle contraction as would be required to manipulate the body into a shorter and narrower wave shape. Presumably even subtly increased muscle contraction is due to increased calcium ion release via the variant RyRs. While this variant strain did show altered phenotypes in all assays, it was never identified as having a dramatic or severe response. The hN2342S variant may produce a more subtle effect on RyR function. It is important to use a variety of parameters to assess worm crawling to get an accurate representation of how it changes between strains.

The other variant that did not have a larger degree of curvature than wild type, that for hR4861H, actually had a smaller degree of curvature. This may suggest that muscle contraction is reduced compared to wild type. The hR4861H variant strain frequently behaved like the null mutant suggesting dramatically reduced calcium release via the RYR. This variant may change the structure of the RyR in a way that calcium ion flow is impeded, and muscles cannot contract normally. Such an effect of *RYR1* variants has been linked to muscle weakness in CCD (Lyfenko *et al.*, 2007). In this case a deletion mutation in *RYR1* reduced calcium ion release by disrupting RyR1 gating and eliminating calcium ion permeation through the open channel. Point mutations in RyR1, associated with CCD, have also been shown to reduce the maximal levels of

calcium being released (Lynch *et al.*, 1999). However, in this case, despite calcium release being reduced, the cytoplasmic calcium concentration was increased. This suggests increased calcium leakage but decreased calcium flow upon activation, possibly due to depletion of calcium in the SR. This was predicted to manifest as muscle weakness. Such a scenario is possible here, where calcium leakage is increased, reducing the calcium concentration of the lumen of the SR, and therefore limiting calcium ion release upon activation of the RyR. This would result in reduced muscle contraction.

While the effects of the variant RyRs are discussed here in terms of the muscle cells, these variant RyRs could be altering calcium homeostasis in the nerve cells as discussed previously in section 4.4.2. Altering calcium release in the nerve cells in the ways described above would affect muscle contraction in the same manner, but by altering excitation of the muscle cells. Again, the effects seen here could be the cumulative effects of variant RyRs in nerve and muscle cells.

7.2.3. Ryanodine receptor variants increase crawling speed of young adult *C. elegans*

As well as the increased frequency described for all RyR variant strains, except that for hR4861H, crawling speed was elevated. It is notable that thrashing rate in liquid was decreased in four of eight RyR variant strains as young adults, but crawling speed was increased in all but one of the RyR variant strains. In fact, of the four RyR variant strains that showed a decrease in thrashing rate in liquid as young adults, two had some of the largest increases in crawling speed compared to wild type at the same age. This may reflect the different energy demands for different locomotor patterns; swimming in M9 has been determined to be more energetically demanding than crawling on an agar surface by measuring the difference between active and standard metabolic rates in each environment (Laranjeiro *et al.*, 2017). It could also reflect the different mechanical demands for different locomotor patterns, with swimming requiring the muscle to contract and relax more quickly than crawling as demonstrated by studying patterns of muscle activation in swimming and crawling locomotion in *C. elegans* (Pierce-Shimomura *et al.*, 2008). Swimming and crawling locomotion are produced by distinct patterns of contractions of the body wall muscles. If calcium ion concentration in the myoplasm is elevated due to calcium leakage through variant

RyRs then relaxation of the muscles may be slower than needed for swimming. As crawling is a slower movement, such an effect of variant RyRs may increase speed of muscle contraction, due to increased myoplasmic calcium.

The crawling speed of the RyR variants is at the limit for which *C. elegans* are reported to move (80-300 $\mu\text{m/s}$) (Rabets *et al.*, 2014). *C. elegans* move forward for longer and rest less in the absence of food (Shingai, 2000). Therefore, it would be expected that the speeds recorded here would be faster than average, as speeds were recorded in the absence of food. However, the RyR variant strains conferred a marked increase in speed compared to wild type, in the same conditions. An increase in crawling speed is a reflection on activity of the animal, suggesting activity may be increased in most of the RyR variant strains.

The B-type motor neurons modulate speed and amplitude of local segment waves (Bryden and Cohen, 2008). Elevated excitability of neurons has been attributed to enhanced spontaneous activity of mutant *C. elegans* previously (Lüersen *et al.*, 2016). The *twk-7* null mutant had increased crawling speed, with lower amplitude but similar wavelength to wild type. The two-pore domain K2P potassium channels, encoded by *twk-7* in *C. elegans*, has essential roles in neural function whereby a background potassium leak via K2P channels lowers excitability of neural cells (Thomas and Goldstein, 2009). Through a similar mechanism, RyR variants may increase excitability of neural cells via increased calcium concentration in neurons, due to increased calcium release from the ER through the RyR. This suggests the primary effects of these variant RyRs, on crawling speed, could be in the neural cells.

An increase in crawling speed, as seen for all but one of the RyR variant strains, may also be due to different locomotion efficiencies compared to wild type. Increased crawling speed has been associated with decreased locomotion efficiency (Lüersen *et al.*, 2016), suggesting that the presence of RyR variants decreased the crawling efficiency of *C. elegans*.

As discussed above, the increased energy demand of thrashing in liquid may be responsible for the lower thrashing rate of several RyR variant strains, while the

increased crawling speed may be at the expense of crawling efficiency. With the larger degree of curvature and increased crawling speed seen for most RyR variant strains, it could be concluded that crawling is less efficient in these strains. Animals are exhibiting more muscle contraction and moving faster than wild type in the same environment. If these strains also conferred less efficient thrashing in liquid, this may explain their reduced thrashing rate compared to wild type. As thrashing is more energy demanding (Laranjeiro *et al.*, 2017), the less efficient locomotion may have reduced energy stores more quickly in several of these RyR variant strains resulting in repeated pausing, and therefore reducing the thrashing rate. Determining crawling efficiency by quantifying percentage slip, which is how much the wave propagates backwards down the worm (Gray and Lissmann, 1964), would reveal if crawling is less efficient in the RyR variant strains. Percentage slip has been used previously to specifically determine the efficiency of different strains crawling on an agar surface (Lüersen *et al.*, 2016; Keaveny and Brown, 2017).

7.3. Ryanodine receptor variants exacerbate the effects of ageing in

C. elegans

The ryanodine receptor has been implicated in neural and muscular age-related diseases and disorders (Clodfelter *et al.*, 2002; Zhu *et al.*, 2005; Del Prete *et al.*, 2014; Gaboardi *et al.*, 2018; Santulli *et al.*, 2018). Here RyR variants exacerbated effects of ageing on locomotion.

7.3.1. Thrashing rate in liquid decreased more in ryanodine receptor variant strains, with age

In the absence of halothane, thrashing rate reduced for all strains between young and old adult. However, most of the RyR variants strains had a subtly larger decrease than wild type. Only two RyR variant strains had a smaller decrease in thrashing rate from young to old adult than wild type. Interestingly, the hR2458H variant strain had the least dramatic decrease in thrashing rate in the absence of a trigger from young to old adult, but had the most marked degeneration in crawling, between the same ages, of all strains. The effect of this variant on the RyR was thought to exacerbate the age-

related degeneration of locomotion, when crawling, however this is not seen for thrashing rate in liquid. These contrasting results may, once again, highlight the different energy, or mechanical, demands of the two locomotor patterns and the efficiency with which these strains are moving. As only thrashing rate is determined for locomotion in liquid, the results may reflect energy efficiency only. The hR2458H variant strain may have very inefficient locomotion as a young adult, reflected in its slower thrashing rate, but be comparatively as efficient as wild type as an old adult. As a number of parameters were determined for crawling, this may be a better reflection of the effects these RyR variants have on ageing, where the hR2458H variant strain shows more dramatic changes. These complex, and different, responses of the RyR variant strains in different assays demonstrate the need to assess multiple phenotypes to understand effects of these RyR variants.

7.3.2. Crawling parameters show exaggerated changes with age in ryanodine receptor variant strains

By assessing numerous parameters for crawling locomotion in both young and old adults, it was determined that the RyR variants exacerbate the effects of ageing seen in wild type. For the majority of parameters, wild type saw the smallest change with age, and had the most regular and organised kymogram as an old adult. The marked increase in age-related effects for locomotion in the RyR variant strains was attributed to excessive calcium leakage in the RyR variant strains, as suggested by increased muscle contraction in the young adults, which could contribute to oxidative damage in a self-reinforcing cycle (Gordeeva *et al.*, 2003; Durham *et al.*, 2008).

Calcium leakage, via RyRs, has been suggested to lead to defective calcium signalling in later-life, along with cellular damage (Bellinger *et al.*, 2008; Andersson *et al.*, 2011; Liu *et al.*, 2012; Momma *et al.*, 2017). As discussed previously, increased ROS production leads to oxidative damage, which underlies many age-related disorders (Schriner *et al.*, 2005; Liguori *et al.*, 2018). Increased ROS production in *RYR1* variant knock-in mice has been demonstrated (Giulivi *et al.*, 2011), as well as impaired mitochondrial function in MHS patients, thought to result from the chronic elevation of cytoplasmic calcium concentration (Chang *et al.*, 2019). Oxidative damage, as a consequence of increased

ROS production, is thought to exacerbate calcium leakage via RyRs (Andersson *et al.*, 2011; Umanskaya *et al.*, 2014).

For crawling, as for thrashing in liquid, the LOAM-associated RyR variant strain did not show the most marked age-related changes, which was not expected. The hK3452Q variant strain had the second largest decrease in degree of curvature, with age, but for other crawling parameters other RyR variant strains had more exaggerated age-related changes. The hR2458H variant strain demonstrated the most marked age-related changes in the crawling analysis, however there is no specific mention of this variant in age-related disorders. This may suggest that this RyR variant should be assessed, with respect to age, in mammalian models to discern whether the RyR1 R2458H variant does confer exaggerated age-related changes, as suggested here.

Nevertheless, all of the RyR variants demonstrated effects on age-related degeneration of locomotion in *C. elegans*, which is thought to be through excessive calcium release leading to cell damage. This supports the implication of the RyR in age-related diseases (Clodfelter *et al.*, 2002; Zhu *et al.*, 2005; Del Prete *et al.*, 2014; Gaboardi *et al.*, 2018; Santulli *et al.*, 2018). RyR variants not yet associated with human pathology, which are more frequent in the human population than myopathic variants, may have similar consequences and exacerbate ageing. This identifies the RyR as a potential therapeutic target for age-related neuromuscular diseases.

7.4. Patterns throughout this thesis

Different *RYR1* variants appear to have different strengths of MH IVCT phenotypes and variations in phenotype strengths was repeatedly shown here (Carpenter *et al.*, 2009b). RyR variant strains showed different phenotypes, to each other and to wild type, throughout this research. An attempt was made to find common patterns or trends with respect to protein domains, associated diseases and/ or phenotypes across the variants, both in this research and two previous studies assessing genotype-phenotype correlations of some RyR1 variants in MHS patient muscle biopsies and HEK293 cell lines (Carpenter *et al.*, 2009b; Murayama *et al.*, 2016).

The hR4861H variant strain behaved similarly to the *unc-68* null mutant in many assays. This was attributed to this variant eliminating RyR calcium channel function when present in the homozygous state. Behaviour was most similar to the *unc-68* null mutant for thrashing rate in S medium, halothane response in young and old adults, and for crawling speed, and neither the *unc-68* null mutant nor the hR4861H variant strain conferred the kinking phenotype in levamisole. The hR4861H variant homozygotes showed aldicarb resistance and an even smaller crawling amplitude than the *unc-68* null mutant. However, in the heterozygote assays, the hR4861H variant behaved like the other RyR variant strains revealing that this variant protein must be expressed and stable, at least in the presence of wild type RyR. The R4861H variant is located in the transmembrane domain of RYR1 and so could fundamentally and directly disrupt or reduce the size of the pore through which calcium ions pass such that the homotetrameric hR4861H form cannot function as a calcium channel. The small proportion of the tetramers composed purely of wild type subunits, although less than would be present for a wild type / null heterozygote, is sufficient in the hR4861H variant heterozygote for the level of calcium channel needed for good locomotion. Alternatively, the pore opening of RyRs formed with inclusion of wild type subunits within a mixed tetramer with the hR4861H variant may still allow calcium ions through. The latter seems the more likely scenario, such that the functional pore in the mixed tetramer could then be opened by halothane because of the presence of the variant subunit in the protein.

The hG341R and hR2163H variant strains showed some similarity to each other in their responses in the assays. While the hG341R variant strain did have statistically significantly reduced thrashing as a young adult compared to wild type in the absence of a trigger and the hR2163H variant strain did not, these RyR variant strains had similar thrashing rates to each other. Furthermore, as old adults, in the absence of halothane, both of these variant strains conferred a reduced thrashing rate compared to wild type. The degree of curvature, as a result of smaller amplitudes and wavelengths, was also similarly increased for these two strains compared to wild type. The age-related reductions in degree of curvature and crawling speed were also comparable between these two strains. These results for locomotion suggest that calcium release is increased via variant RyRs encoded by *unc-68* carrying mutations

equivalent to the hG341R and hR2163H *RyR1* variants. However, both of these variant strains exhibited resistance to aldicarb and neither conferred the kinking response in levamisole, which may suggest reduced calcium flow/ leakage via these variant channels. As discussed previously, variant RyR channels may have different effects in different tissues, which could explain these conflicting results. The hG341R variant strain had a very similar response to wild type to levamisole, suggesting this variant may function in nerve cells, while the hR2163H variant strain may have shown some sensitivity to levamisole compared to wild type, suggesting some function of this variant in muscle cells. Both the G341R and the R2163H variants are associated with MH, although the R2163H variant has also been associated with CCD (Carpenter *et al.*, 2009b; Yan *et al.*, 2015). The R2163 residue is located in the helical domain of the RyR, while the G341 residue is located in the N-terminal domain. Previously, the R2163H variant was associated with more severe forms of four of five IVCT phenotypes with strong contractures and short response times (Carpenter *et al.*, 2009b). The G341R variant only showed statistically more severe responses for two phenotypes. HEK293 cells expressing R2163H RyR1 channels were found to have increased resting calcium levels of the cytoplasm and decreased resting calcium concentration of the ER, consistent with increased calcium release via the RyR (Murayama *et al.*, 2016). Unfortunately, the consequence of the G341R mutation on resting calcium levels in ER and cytoplasm were not assessed.

The hR2454H and hK3452Q variant strains also showed some similarity to each other in their responses throughout this research. Neither showed thrashing defects in the absence of halothane at either age, although the hK3452Q variant strain did have subtly increased sensitivity to halothane in the old adults. Both variant strains had similar crawling speeds as young adults and similar age-related changes in crawling speed and degree of curvature, although the hK3452Q variant strain had a larger degree of bending as young adults. These were the only two strains to show some sensitivity to aldicarb. Both of these RyR variant strains also conferred kinking in levamisole. Altogether, the consequences of these two variants for the phenotypes assessed here suggest increase calcium release via the variant RyRs. Both residues are located in the helical domain and so could be perturbing the RyR function similarly. However, the R2454H *RyR1* variant is associated with MH and CCD (Yan *et al.*, 2015),

while the K3452Q variant is associated with LOAM (Løseth *et al.*, 2013). The R2454H variant has been found to have a severe response for two of five IVCT phenotypes (Carpenter *et al.*, 2009b) and the resting calcium concentration of the ER was reduced compared to wild type in HEK239 cells, but not to the same extent as other RyR1 variants (Murayama *et al.*, 2016). The K3452Q mutation was not assessed in either the muscle biopsy or HEK329 cell genotype-phenotype study. However, due to the similarity between the hR2454H and hK3452Q variant strains in this research, it could be concluded that both of these variants increase calcium leakage/ release via the RyRs but to less of an extent than other RyR1 variants.

The increased sensitivity to aldicarb compared to wild type and kinking phenotype in levamisole of the hR2454H and hK3452Q variant strains may suggest increased RyR calcium flow/ leakage. In contrast, the resistance to aldicarb compared to wild type and failure to show the levamisole induced kinking response of the hG341R and hR2163H variant strains would suggest reduced RyR calcium flow/ leakage. Increased sensitivity to aldicarb compared to wild type suggests more neurotransmitter release into the synaptic cleft and/ or increase calcium release from the SR to facilitate more rapid paralysis. The kinking response in levamisole was attributed to misfiring of inhibitory GABAergic neurons, and for this to happen excessive calcium would be released into the axoplasm of such neurons.

The hR163C, hN2342S and hR2458H variant strains did not match to either of these patterns and are distinct from each other.

The hR163C variant strain did confer a thrashing defect in the young adults in the absence of halothane, similar to the hG341R and hR2163H variant strains. However, the hR163C variant strain had a more exaggerated increase in degree of curvature and showed little change in crawling speed with age, unlike the hG341R and hR2163H variant strains. While this variant strain did confer resistance to aldicarb, compared to wild type, as the hG341R and hR2163H variant strains did, it also showed the kinking phenotype in levamisole. The R163C *RYR1* variant has been associated with both MH and CCD, like the R2163H *RYR1* variant and the R163 residue is located in the N-terminal domain, like the G341 residue (Robinson *et al.*, 2006; Yan *et al.*, 2015). The

R163C variant has been studied extensively, compared to other RyR1 variants, and has been found to increase calcium release from the SR resulting in an increase in cytoplasmic calcium ion concentration, as well as alter retrograde signalling to the DHPR (Yang *et al.*, 2006; Esteve *et al.*, 2010; Giulivi *et al.*, 2011; Murayama *et al.*, 2016). This variant is associated with more severe IVCT reactions similar to the R2163H variant (Carpenter *et al.*, 2009b).

The hR2458H variant strain exhibited aldicarb resistance, compared to wild type, and the kinking response in levamisole, as well as a thrashing defect in the absence of halothane as young adults. These responses are similar to the hR163C variant strain. However, this variant strain differed to the hR163C variant strain for change in thrashing rate, as well as crawling parameters, with age. Ageing in the hR2458H variant strain, for the crawling parameters, was more dramatic than in the hR163C variant strain. The R2458H variant has been associated with MH and the R2458 residue is located in the helical domain of the RyR, like the R2454 and K3452 residues (Yan *et al.*, 2015). Similarly to the R2454H variant in HEK239 cells, the R2458H variant reduced resting calcium concentration of the ER compared to wild type but not to the same extent as other RyR1 variants, including R163C and R2163H (Murayama *et al.*, 2016). The R2458H variant did not elicit any severe IVCT phenotypes when MHS patient muscle biopsies were assessed (Carpenter *et al.*, 2009b). It is interesting that this variant has the most dramatic consequences for ageing response here, and yet appears to have relatively mild phenotypes in humans. Again, this strengthens the need for this variant to be assessed with age in mammalian models.

As discussed previously, the hN2342S variant appears to have weaker phenotypes than the other assessed in this research. The hN2342S variant was identified through genetic analysis of a patient who had an MH response to general anaesthetic and subsequent positive IVCT result (Marchant *et al.*, 2004), but has not been functionally characterised and is not considered a diagnostic MH variant. In liquid, this variant appeared to have no obvious locomotion defects at either age. Although amplitude and wavelength of the crawling waveform did change in this variant strain, compared to wild type, the bend angle remained similar, possibly suggesting only a subtle increase in calcium release via this variant channel. The age-related changes in

crawling parameters were subtle, and this variant strain did not confer the kinking response to levamisole. However, the hN2342S variant strain did show greater aldicarb resistance than wild type and had the most marked increase in speed compared to wild type in the young adults. The N2342 residue is located in the RyR helical domain. This variant has not been extensively studied, but results here suggest that although subtle, the N2342S variant does change calcium handling via the RyR, possibly subtly increasing calcium release/ leakage, which may have subtle consequences for human carriers.

The different consequences for the various RyR variants may arise from the distinct ways in which they affect calcium release from the ER/ SR. Nevertheless, the variation in responses here echoes the variation in responses in the human conditions associated with *RYR1* missense variants (Carpenter *et al.*, 2009b; Murayama *et al.*, 2016). Attempting to determine the way in which these RyR variants each alter the function of RyR is difficult in light of the inconsistency of responses between different types of assays. That two strains, those for hR163C and hR2458H, conferred both aldicarb resistance, compared to wild type, and the kinking response in levamisole is difficult to reconcile. Perhaps the aldicarb resistance is due to reduced calcium release in muscle cells due to these RyR variants, while the kinking response is due to increased calcium release in neural cells. It is possible these variants could affect calcium release in different tissues in different ways, as the RyR forms a macromolecular complex with other proteins in order to control calcium release from the ER and SR, and the mechanisms of calcium release differ in different cell types (Lanner *et al.*, 2010; Santulli *et al.*, 2018). Therefore, the same variant could affect RyR function differently dependant on tissue type. This was also thought to be the case for the hG341R and hR2163H variants that seemingly increased calcium release in the crawling analysis but impeded calcium release in the pharmacological assays.

Despite the differing severities of phenotypes, all RyR variants modelled in *C. elegans* conferred a hypersensitive response to halothane and showed genetic dominance, consistent with an MH-related phenotype. Furthermore, all of the RyR variants conferred locomotion defects in the absence of triggering agents, and exacerbated ageing compared to wild type, as demonstrated by the in-depth crawling analysis.

Most of the known pathogenic missense variants in the three *RYR* genes in the human genome are at low frequency in the human population. For instance, of 48 MH *RYR1* variants considered to be diagnostic (The European Malignant Hyperthermia Group, n.d.), only 20 were identified in 141,456 individuals, and of these, the highest allele count was 32 (Lek *et al.*, 2016). However, over 3000 *RYR1* variants and around 2000 *RYR2* and *RYR3* variants were identified respectively. Many of these missense mutations are in residues that are conserved between the three RyR genes. The conservation of these residues suggests they are likely to be of functional value, and missense variants would interfere with this function. While RyRs can clearly tolerate some missense mutations without serious consequences for normal channel function, these amino acid changes may have more subtle effects. The human population has a large amount of individual variation, making these comparatively small differences in RyR function more difficult to detect. Therefore, assessment of such RyR variants *in vivo* is important in order to understand the effects of subtle consequences.

7.5. Future work

There are a number of directions for future work arising from this research. Firstly, the contributions of these RyR variants to neural and muscle cell function should be assessed. Using the SKI LODGE approach, discussed in chapter 5, these variants could be expressed using tissue specific promoters *rab-3* for neural tissue and *myo-3* for muscle tissue, as has been done previously (Liu *et al.*, 2005; Sun *et al.*, 2014; Silva-García *et al.*, 2019). It has been shown that the uncoordinated locomotion associated with the *unc-68* null mutant is greatly improved with, *rab-3* driven, expression of wild type *unc-68* in neural tissue, while mutants expressing wild type *unc-68* only in muscle tissues were less rescued, as shown by locomotion velocity (Liu *et al.*, 2005). Further to this, *rab-3* driven expression of wild type *unc-68* in nerve cells alone also rescues the regenerative outgrowth defect seen in *unc-68* null mutants after axotomy (Sun *et al.*, 2014). Using the same approach and determining the effects of these RyR variants on *C. elegans* locomotion would allow for direct assessment of effects of RyR variants in neural and muscle cells.

If the effects of these RyR variants in muscle and neural cells is discerned, direct imaging of ER and/ or SR calcium ion levels could be conducted to understand how RyR variants affect calcium ion release from these internal stores. There are a number of strategies that can measure the flow of free calcium over the ER membrane, including genetically encoded calcium indicators (Tian *et al.*, 2009; Samtleben *et al.*, 2013). GCaMP is a genetically encoded calcium indicator, created from a fusion of GFP, calmodulin and M13. GCaMP3 is a low affinity variant of GCaMP, which can be targeted to the ER lumen by fusing of calreticulin to the amino terminus, and retained in the ER by fusing an ER retention signal, from the binding immunoglobulin protein (BiP), to the carboxy terminus; this subcellular targeted version of the calcium indicator has been termed GCaMPer (Henderson *et al.*, 2015). Calreticulin and BiP are ER calcium-binding chaperones and changes in GCaMPer fluorescence report ER calcium levels. Activating the RyR with 4-chloro-m-cresol reduced GCaMPer fluorescence in neuroblastoma cells, which are often use as *in vitro* models of neuronal function, thus demonstrating that calcium release from the ER, via RyR, does reduce fluorescence. GCaMPer fluorescence was also measured in rat primary cortical neurons and shown to decrease when calcium was released from the ER due to IP₃R activation (Henderson *et al.*, 2015). GCaMP has been used to visualise calcium dynamics in *C. elegans* neurons (Tian *et al.*, 2009) and could be targeted to the *C. elegans* ER to measure the effects of RyR variants on ER calcium levels. If RyR variants were to increase calcium release/ leakage from the ER, a decrease in the GCaMPer fluorescence may be seen. However, nerve cells in *C. elegans* may be too small to provide the resolution needed and so a similar approach could be applied for measuring the effects of RyR variants on the calcium ion concentration of the sarcoplasmic reticulum, as muscle cells may be an easier target.

The novel kinking phenotype seen in response to treatment with levamisole is also of interest for future research. While it was postulated that the phenotype was due to RyR variants in GABAergic neurons affecting GABA signal transmission, this was not demonstrated. By generating double GABA null and RyR variant mutants, for the four RyR variant strains that did confer the kinking phenotype, it could be demonstrated whether kinking was seen as a consequence of misfiring of GABAergic neurons. *unc-25* encodes glutamic acid decarboxylase, which catalyses the formation of GABA from

glutamic acid (Jin *et al.*, 1999). The *unc-25* null mutant, in *C. elegans*, shows complete loss of anti-GABA staining (Gendrel *et al.*, 2016). If the kinking phenotype in response to levamisole was lost in *unc-25;unc-68^{variant}* mutants then this response could be attributed to GABA and muscle cell relaxation in response to spontaneous inhibitory neuron excitation. This would also demonstrate that the RyR variants in *C. elegans* are affecting calcium release in neurons.

RyRs have been implicated in neurodegenerative diseases, such as Alzheimer's disease (AD), although, this is controversial (LaFerla, 2002; Del Prete *et al.*, 2014; Liang *et al.*, 2015; Liang and Wei, 2015; Abu-Omar *et al.*, 2018). Worm models of amyloid-beta peptide-induced neurodegeneration are available (McColl *et al.*, 2012; Alexander *et al.*, 2014; Griffin *et al.*, 2017). Therefore, it is possible to study the effects of these RyR variants on amyloid-beta aggregation. Assessing how amyloid-beta aggregation is affected in the presence of RyR variants may further support a role of RyR in neurodegeneration. If these variants do increase calcium leakage and result in oxidative damage to cells, as suggested in chapter 5, it would be expected that amyloid-beta aggregation would be increased in amyloid-beta / RyR variant double mutant strains.

Dantrolene, an RyR antagonist used to treat patients during an MH episode, has been shown to be an effective therapeutic for various types of AD animal models (Chakroborty *et al.*, 2012; Oulès *et al.*, 2012; Peng *et al.*, 2012; Liang and Wei, 2015). Memory deficits and amyloid plaque load were reduced in AD animal models treated with dantrolene; this was attributed to inhibition of aberrant calcium release from the ER. Treatment of the *C. elegans* RyR variant strains with dantrolene across their lifespan may reduce the exacerbation of age-related effects on locomotion seen here. Such a result would demonstrate that the exacerbation of age-related effects is indeed due to excessive calcium release/ leakage via variant RyRs. Should amyloid-beta aggregation be increased in the AD model/ RyR variant strains, discussed above, treatment of these strains with dantrolene and measuring the effects on amyloid load would support the use of dantrolene as a probe compound for treatments of AD.

Having identified subtle effects on locomotion in the absence of an MH trigger for all of the RyR variants in *C. elegans*, effects of *RYR1* variants on neuromuscular function in humans in the absence of a trigger may be more widespread than currently thought. Assessment of muscle performance in mammalian models and human carriers of *RYR1* variants, which are not currently associated with such phenotypes in the absence of an MH trigger, is required. If consequences are noted, it may suggest that human carriers of *RYR1* variants may experience more dramatic age-related degeneration in muscle performance.

Appendix A

UNC-68 alignment to human RYR1, RYR2 and RYR3

ryanodine receptor 1 isoform X1 [Homo sapiens]

Sequence ID: [XP_006723380.1](#) Length: 5032 Number of Matches: 8

Range 1: 2494 to 4254 [GenPept](#) [Graphics](#)

[▼ Next Match](#) [▲ Previous Match](#)

Score	Expect	Method	Identities	Positives	Gaps
1330 bits(3441)	0.0	Compositional matrix adjust.	746/1834(41%)	1119/1834(61%)	115/1834(6%)
Query 2715	LLPNHKGSVLLFLDRVYGIDQQDMLFHVLEQSFLPDLRAATMMDSPRALESDTALALNRY				2774
	+P+HK S++LFLDRVYGI+ QD L HVL+ FLPD+RAA +D+ ++ ALALNRY				
Sbjct 2494	FVPDHKASVLLFLDRVYGIENQDFLLHVLVDVGFLLPDMRAAASLDTATFSTTEMALALNRY				2553
Query 2775	LCNSVPLLLTNHSHFFADAHEHHSALLDATLHTVYRMNRLKSLTKNQDAVSDFLVAITRE				2834
	LC +VLPL+T + FA EH + ++D+ LHTVYR++R +SLTK QRD + D L+++ R				
Sbjct 2554	LCLAVLPLITKCAPLFAFAGTEHRAIMVDSMLHTVYRLSRGRSLTKAQRDVEDCLMSLCRY				2613
Query 2835	LPPAMMIKLLKKVITDILTMNDMNVLPRLITLHYERCGKYY---GSGNHYGVASEQE				2890
	+ P+M+ LL++++ D+ +N+ + PL+L+T HYERC KYE G N +GV SE+E				

ryanodine receptor 2 isoform X7 [Homo sapiens]

Sequence ID: [XP_006711870.1](#) Length: 4965 Number of Matches: 9

Range 1: 2469 to 4208 [GenPept](#) [Graphics](#)

[▼ Next Match](#) [▲ Previous Match](#)

Score	Expect	Method	Identities	Positives	Gaps
1424 bits(3686)	0.0	Compositional matrix adjust.	780/1812(43%)	1140/1812(62%)	97/1812(5%)
Query 2714	GLLPNHKGSVLLFLDRVYGIDQQDMLFHVLEQSFLPDLRAATMMDSPRALESDTALALNR				2773
	G P+HK +++LFLDRVYGI+ QD L H+LE FLPDLRAA +D+ +D ALALNR				
Sbjct 2469	GFCPDHKAAMVLLFLDRVYGIQDFLLHLLLEVGFLLPDLRAAASLDTAALSATDMALALNR				2528
Query 2774	YLCNSVPLLLTNHSHFFADAHEHHSALLDATLHTVYRMNRLKSLTKNQDAVSDFLVAITR				2833
	YLC +VLPLLT + FA EHH++L+D+ LHTVYR+++ SLTK QRD++ L+I				
Sbjct 2529	YLCTAVLPLLLTRCAPLFAFAGTEHHSALDLSLLHTVYRLSKGCSLTKAQRDSIEVCLLSICG				2588
Query 2834	ELPPAMMIKLLKKVITDILTMNDMNVLPRLITLHYERCGKYY---GSGNHYGVASEQE				2890

ryanodine receptor 3 [Homo sapiens]

Sequence ID: [CAA04798.1](#) Length: 4870 Number of Matches: 7

Range 1: 2359 to 4107 [GenPept](#) [Graphics](#)

[▼ Next Match](#) [▲ Previous Match](#)

Score	Expect	Method	Identities	Positives	Gaps
1310 bits(3390)	0.0	Compositional matrix adjust.	742/1820(41%)	1137/1820(62%)	106/1820(5%)
Query 2717	PNHKGSVLLFLDRVYGIDQQDMLFHVLEQSFLPDLRAATMMDSPRALESDTALALNRYLC				2776
	P+HK ++LFLDRVYGI Q L H+LE FLPDLRA+ +D+ ++ ALALNRY+C				
Sbjct 2359	PDHKAPMVLLFLDRVYGIKDQTFLLHLLLEVGFLLPDLRASASLDTVSLSTTEAALALNRYIC				2418
Query 2777	NSVPLLLTNHSHFFADAHEHHSALLDATLHTVYRMNRLKSLTKNQDAVSDFLVAITRELP				2836
	++VLPLLT + FA EH ++L+D+TL T+YR+++ +SLTK QRD + + L+AI L				
Sbjct 2419	SAVPLLLTRCAPLFAFAGTEHCTSLIDSTLQTIYRLSKGRSLTKAQRDTIEECLAICNHLR				2478
Query 2837	PAMMIKLLKKVITDILTMNDMNVLPRLITLHYERCGKYY---GSGNHYGVASEQEKR				2892
	P+M+ +LL++++ D+ +N+ +PL+L+T HYE+C KYE G G+ YG+A E+E				

Figure A.1: BLASTP results for *C. elegans* UNC-68 when searched for in humans.

BLASTP results of the *C. elegans* UNC-68 protein in humans. Alignments to RYR1, RYR2 and RYR3 were found. Identities and positives are highlighted with a red circle (41-43% identity, 61-62% positives, positives are considered as a conservative substitution). Alignment was completed using <https://blast.ncbi.nlm.nih.gov/>

Appendix B

Table B.1. Sequences used to guide cutting and repair of the genome in the CRISPR-Cas9 genome-edited strain generated at NemaMetrix

Design information for the CRISPR-Cas9 genome-edited strains

Strain (Variant)	sgRNA 1 Sequence + PAM	sgRNA 2 sequence + PAM	Left homology arm	Right homology arm
COP1879 (hG341R)	GCAGATGCTGGATGAGAAAGAGG	GGAAATGCTACAATCAGATA TGG	GAATAAGATCCAAAGAAAGCAGATGCTGGATGAGA	ATATGGAGAGACAAAATGCTTTTATTTCACACCGTGA
COP1883 (hR2163H)	CC TCAATACAAATCCCGGAGCTTC	CCG CGAGCTTCTTACCCTGACAAT	GAAAAAGATGTGACAGACTTCTGGGTACTCCTCAT	GCTTCTTACCCTGACAATTTGAGCAFACTGAAGAGG
COP1947 (hR2454H)	TAAGTGTGCTCCTCGATCCAA TGG	CCC CAATCTCCAGCTCCCGTCAA	TCTGTAGACTTTGCTCGCTAAGTGTGCTCCTGATC	TCTCGCAGCTCCGTCAAATCGAAGgtttgaaattca
COP1944 (hR2458H)	TAAGTGTGCTCCTCGATCCAA TGG	CCC CAATCTCCAGCTCCCGTCAA	TCTGTAGACTTTGCTCGCTAAGTGTGCTCCTGATC	TCTCGCAGCTCCGTCAAATCGAAGgtttgaaattca
COP1932 (hK3452Q)	ACACCAACGTGGGAGACGGAC GG	CTATGTGGCTCAATTTGAAGAG G	CGTGTCAATGGCTCAAAAACCAACCGTGGGAGAC	AAGAGGATGCTGCAGCCACGGGGCTGGAGACATG
COP1950 (hR4861H)	CCA TCAATGATGACACTTTGTAGTC	CTATGTTCAAAGAGGGTGAAGAG G	TACACAAACTTGCACAACAACACTCATTTCTCACCATCA	AAGAGGGGAGAGAGCCAGATCGAAAAGTGTCACAAT

20 nt sgRNA sequences, with the PAM sequence, used to guide cutting of the genome and the 35 nt left and right homology arm sequences for each mutant strain generated at NemaMetrix. Sequences are shown in the forward sequence of unc-68 isoform a. Red bases correspond to the PAM sequence and were not included in the sgRNA sequence. Cas9 can cut either strand of the DNA; where the PAM sequence is at the 5' end of the forward genomic sequence the PAM sequence is CCN, when at the 3' end it is NGG. The reverse complement of the genomic sequence was used for the sgRNA sequence when the PAM site was at the 5' end. The sgRNAs and left and right homology sequences are the same for the COP1947 (hR2454H) and COP1944 (hR2458H) mutant strains due to their close proximity, however, the sequence between the homology arms differed so only the desired edit was made in each case (Table 2.2).

Appendix C

Example sequencing alignment

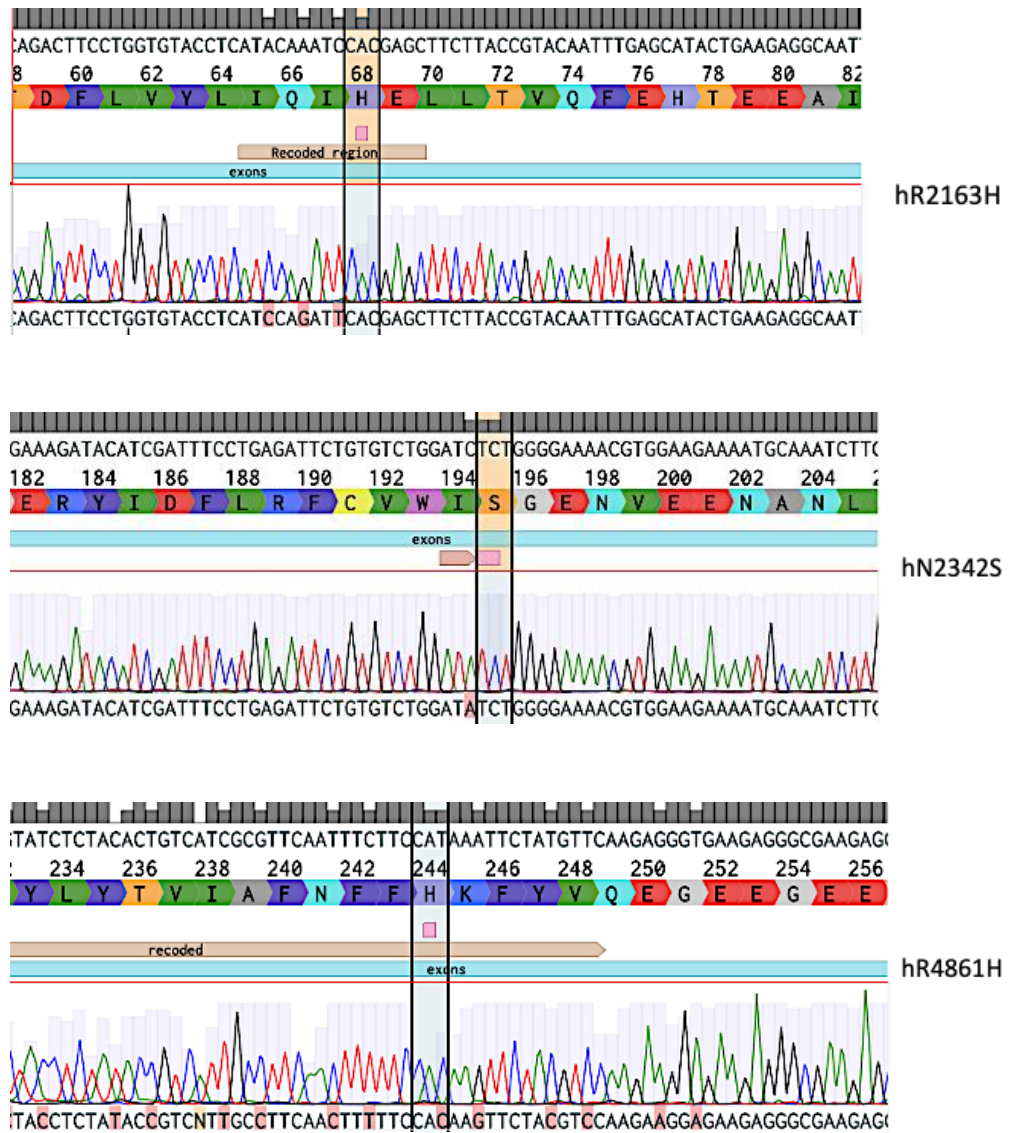


Figure C.1: Example sequencing alignments for RyR variant strains to confirm correct genomic sequence.

Single worm PCR, gel extraction and sequencing was performed to confirm the genotype of each of the RyR variant strains. Representative sequencing results for variant strains hR2163H, hN2342S and hR4861H is shown. Recoded regions are shown in brown and the red mis-matched nucleotides represent the silent mutations. The changed residue is highlighted, the mutated nucleotides are shown in pink. Alignment of the sequencing data to the template was performed in Benchling, <https://benchling.com/>.

Appendix D

Comparison of Leeds and NemaMetrix N2 background strains

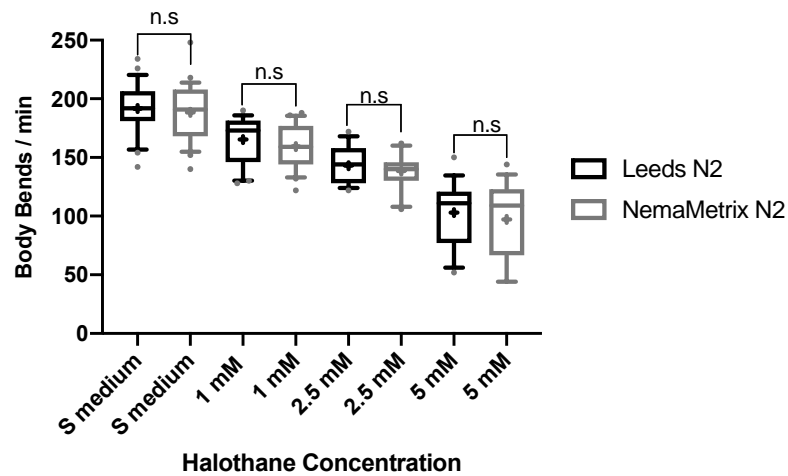


Figure D.1: Leeds N2 and NemaMetrix N2 strains show no differences in response to halothane.

Thrashing rate in S medium, in body bends per minute, for Leeds and NemaMetrix N2 strains, used for injection to generate CRISPR-Cas9 genome-edited RyR variant strains, in the absence of and presence of 1 mM, 2.5 mM and 5 mM halothane. 25 individuals were examined per strain. Boxes indicate the median and interquartile range, with whiskers to the 10-90 percentile, outliers as dots, and + to indicate the mean. Significance is between the two N2 strains in each concentration, n.s = not significant (one-way ANOVA, with Tukey's multiple comparison test). Black represents Leeds N2 and grey represents NemaMetrix N2.

Appendix E

Statistical comparison of thrashing rate of the ryanodine receptor variant strains, the wild type and CB540 null mutant when exposed to 4% DMSO

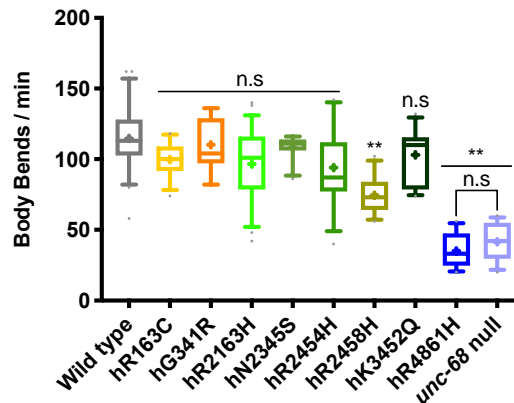
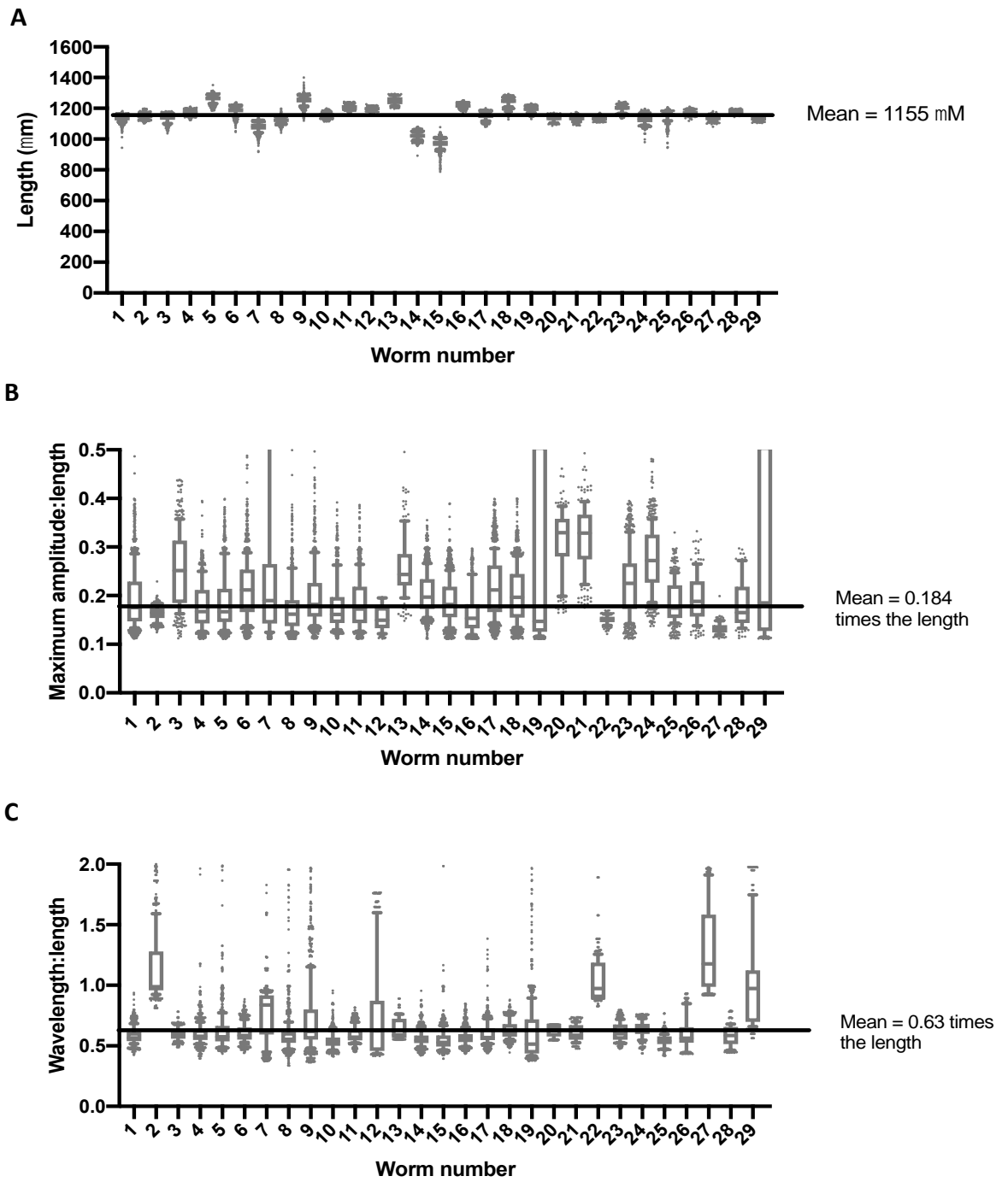


Figure E.1: RyR variant strains are not more sensitive to DMSO than wild type.

Thrashing rate in 4% DMSO dissolved in S medium, in body bends per minute, for RyR variants, labelled by the human variant they correspond to, along with the wild type and the CB540 (*unc-68(e540)*) null mutant. 25 individuals were examined per strain. Boxes indicate the median and interquartile range, with whiskers to the 10-90 percentile, outliers as dots, and + to indicate the mean. Significance is between variant strains and the wild type, apart from where indicated to the *unc-68* null mutant. ** $P < 0.005$, n.s = not significant (one-way ANOVA, with Tukey's multiple comparison test).

Appendix F

Crawling parameters for individual wild type animals



D

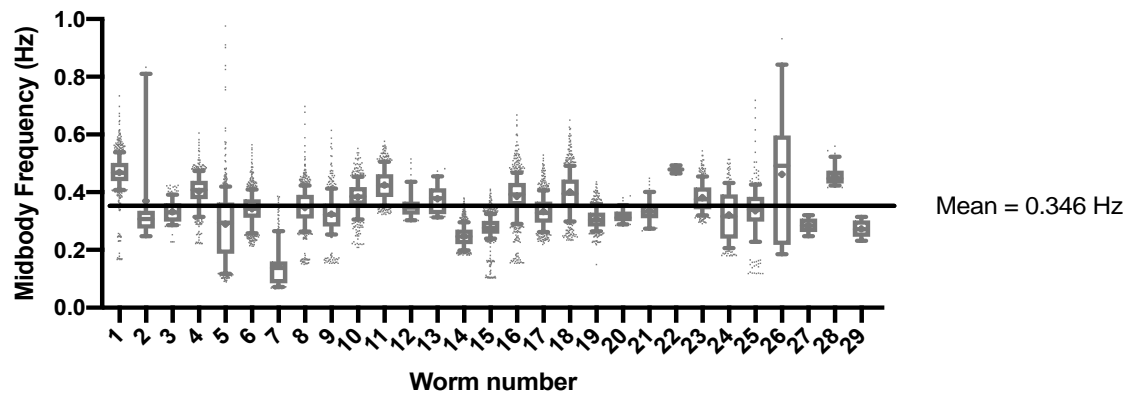


Figure F.1: Crawling parameters for individual wild type animals.

Worm length (A), amplitude:length ratio (B), wavelength:length ratio (C) and frequency (D) for 29 wild type young adult individuals extracted from 1 minute long, 25 frames per second, video recordings of. Boxes indicate the median and interquartile range, with whiskers to the 10-90 percentile, outliers as dots, and + to indicate the mean. Black line shows the mean for the strain. The mean represents the data for the strain accurately.

Appendix G

Young and old adult crawling parameters

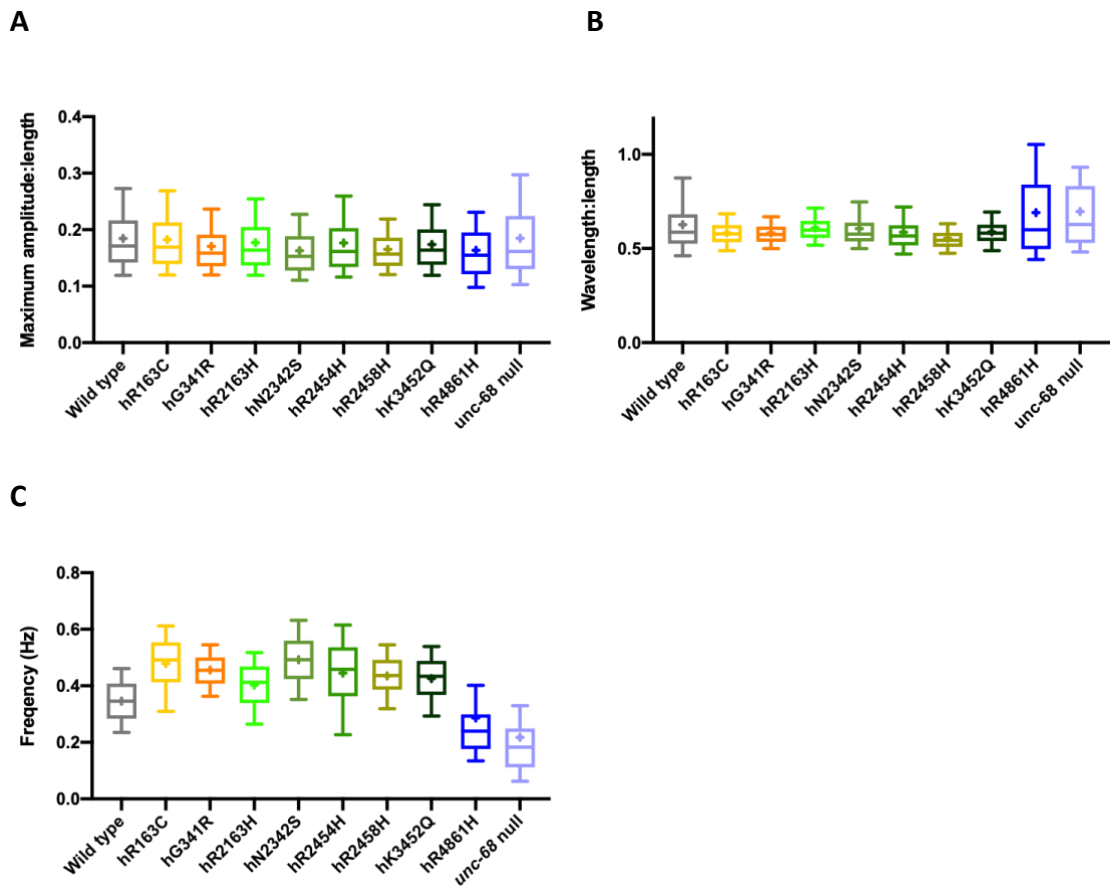


Figure G.1: Amplitude, wavelength and frequency of young adults.

The mean maximum amplitude:length ratio (A), wavelength:length ratio (B) and frequency (C) for RyR variant strains, labelled by the human variant they correspond to, along with the wild type and the CB540 (*unc-68(e540)*) null mutant. Boxes indicate the median and interquartile range, with whiskers to the 10-90 percentile, and + to indicate the mean.

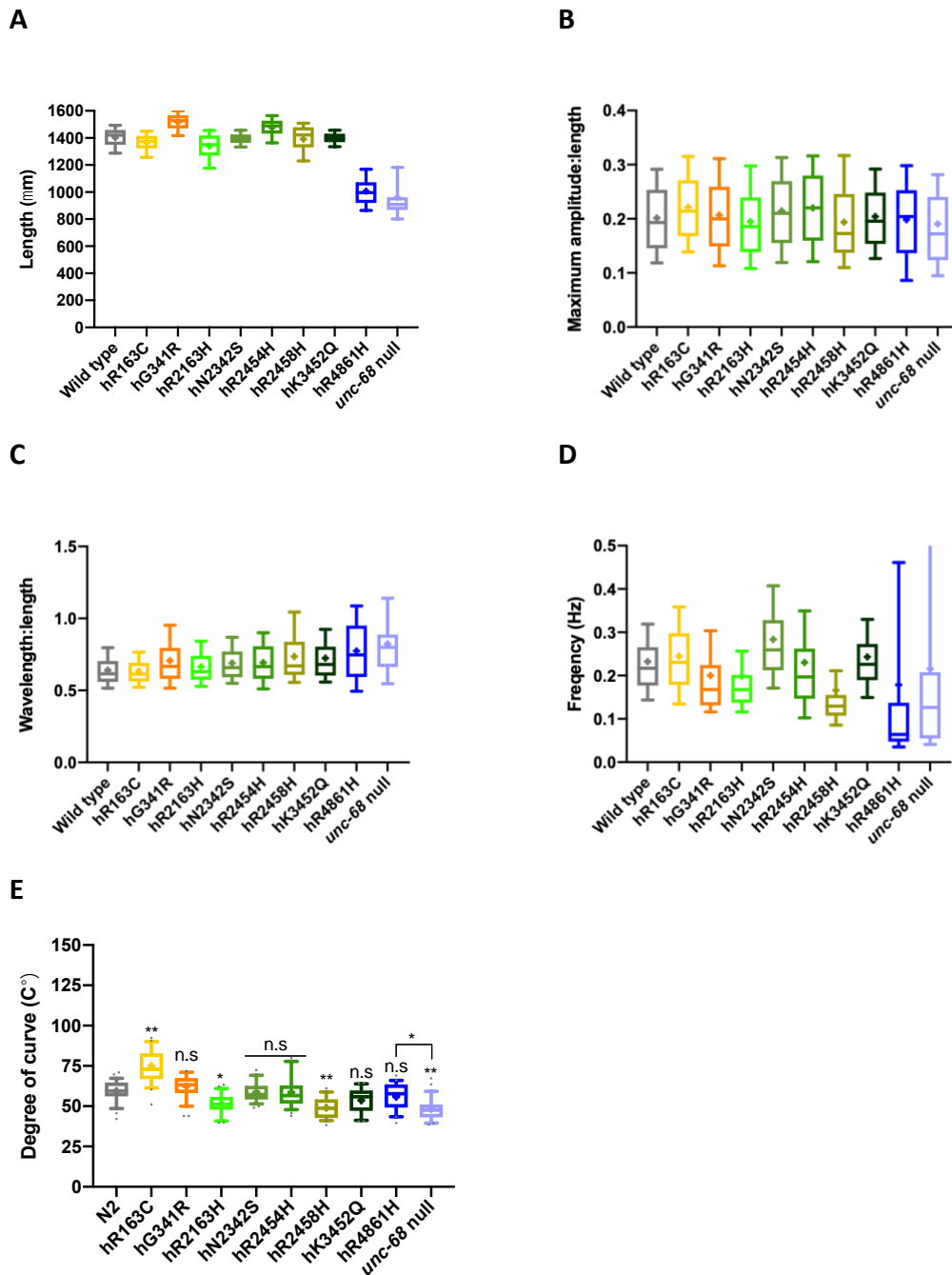


Figure G.2: Length, amplitude, wavelength, frequency and degree curvature of old adults.

Worm length (A) and crawling amplitude:length ratio (B), wavelength:length ratio (C) and frequency (D) extracted from 1 minute long, 25 frames per second, video recordings of 20-30 individual old adults, and degree of curvature (E), hand measured for random 26 individuals from individual frames from the video recordings, for RyR variant strains, labelled by the human variant they correspond to, along with the wild type and the CB540 (*unc-68(e540)*) null mutant, were compared. Boxes indicate the median and interquartile range, with whiskers to the 10-90 percentile, outliers as dots, and + to indicate the mean.

Table G.1: Mean and standard deviation (SD) of old adult midbody crawling speed for wild type, RyR variant strains and the CB540 (*unc-68(e540)*) null mutant.

Strain (variant)	Midbody crawling speed ($\mu\text{m}/\text{S}$)	
	Mean	SD
Wild type	147.2	87.9
hR163C	178.1	93.6
hG341R	91.72	58.8
hR2163H	101	65.3
hN2342S	190.7	105.1
hR2454H	127.1	87.6
hR2458H	53.3	46.2
hK3452Q	138	90.5
hR4861H	32.82	28.5
<i>unc-68</i> null	34.93	44.7

Box shading is consistent with the colour coding used throughout this thesis. Crawling speed is shown to one decimal place. RyR variant strains are listed according to the human variant they correspond to.

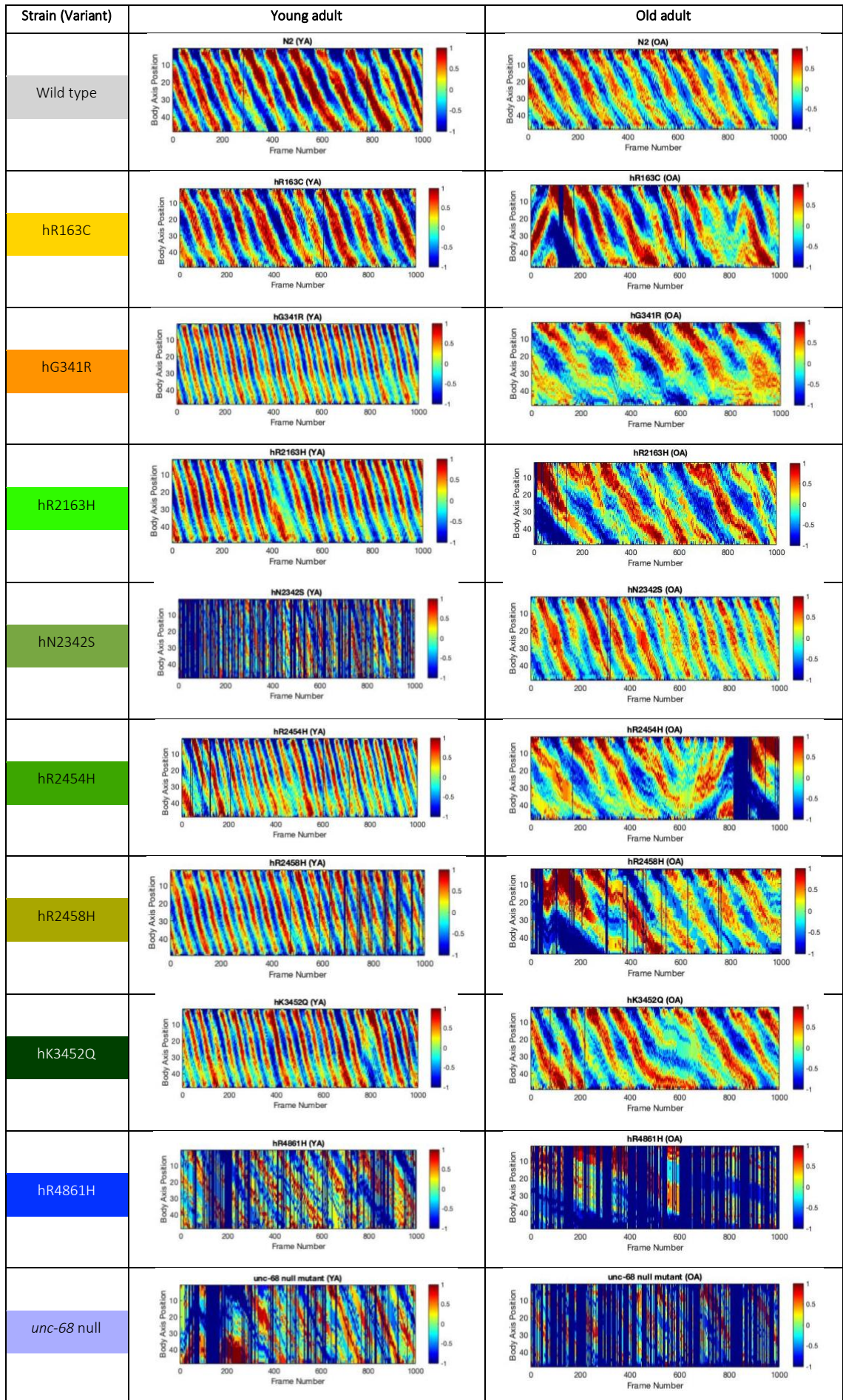


Figure G.3: Representative kymogram for one young and one old adult individual of each strain.

Representative kymograms are presented for one young and one old adult individual of each strain. Colour in the kymograms indicates degree of dorsal/ ventral curvature (red/ blue high curvature, green no curvature) at different positions along the major body axis (0 anterior to 50 posterior) for each frame of the video recording. Box shading is consistent with the colour coding used throughout this thesis. It should be noted that red and blue, respectively, do not indicate dorsal and ventral curvature but is arbitrarily assigned for each recording; the dorsal and ventral body could not be distinguished by the software. Individual frames where the worm skeleton could not be calculated are dark blue. Recording of the *unc-68* null mutant and the hR4861H variant was difficult due to their limited movement and smaller size and in many frames the skeleton was not calculated, especially in the old adults. In the recordings of the hN2342S young adult variant strain the skeleton could not be calculated continuously for each individual, although these animals were moving well and were not too small. The analysis was re-run for this variant strain but still the skeleton was not calculated in all frames. The effects of ageing appear more dramatic in the RyR variant strains than in wild type as shown by the disorganisation of the kymogram.

Appendix H

Aldicarb concentration comparison

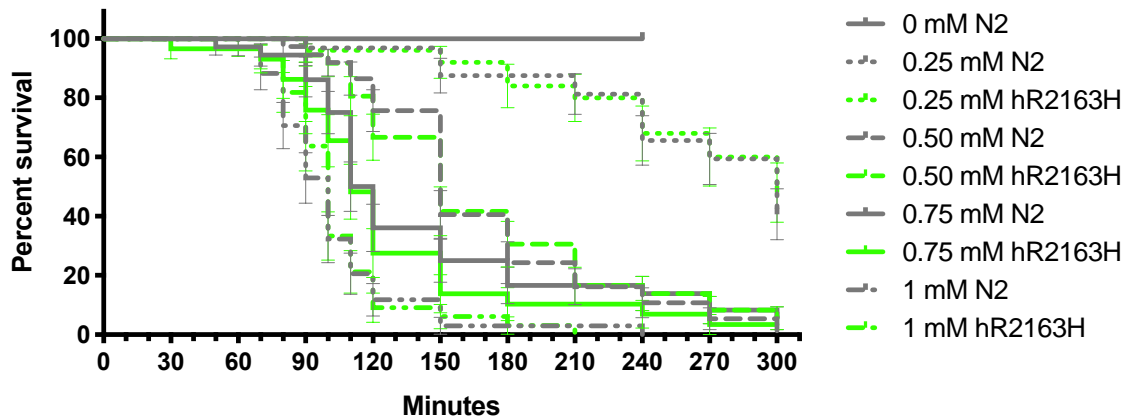


Figure H.1: Aldicarb concentration comparison for wild type and the hR2163H variant strain.

Kaplan-Meier survival curves representing the percentage of individuals moving with time on plates containing different concentrations of aldicarb. Data for the hR2163H RyR variant strain and wild type. 0.25 mM aldicarb is shown by a dotted line, 0.5 mM aldicarb is shown by a dashed line, 0.75 mM aldicarb is shown by a straight line and the 1 mM aldicarb concentration is shown by a dashed and dotted line. The difference between wild type and the RyR variant strain is not increased in lower concentrations of aldicarb.

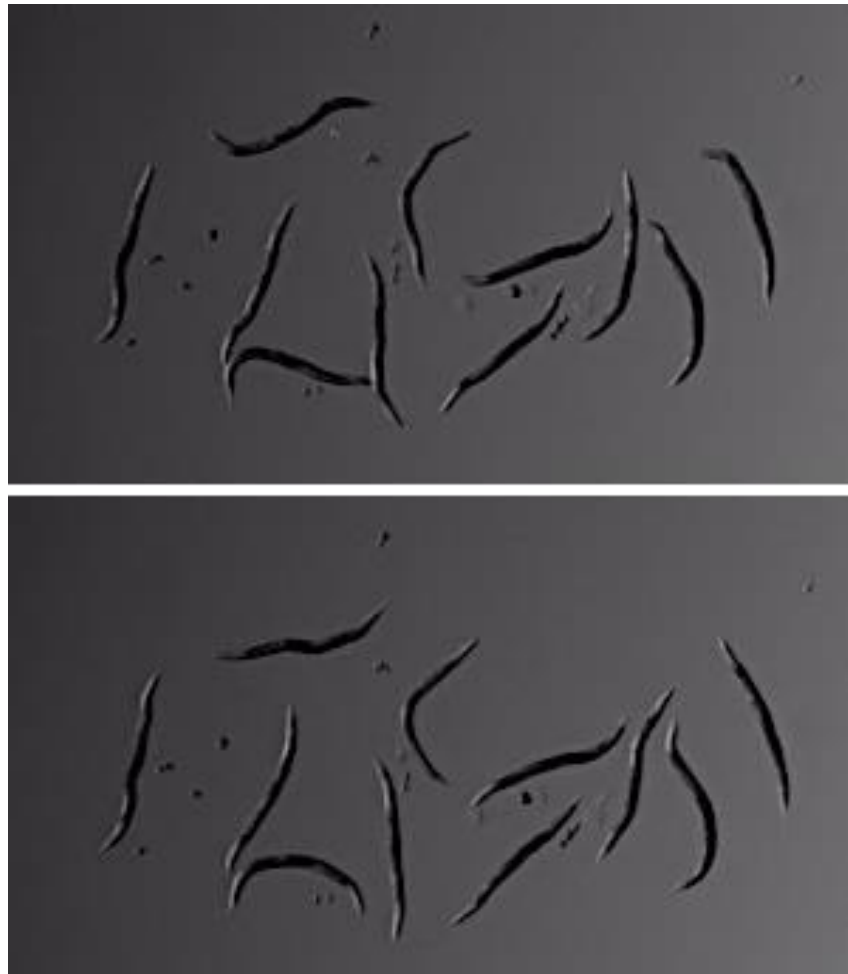
Appendix I**Images showing kinking upon exposure to 1 mM levamisole**

Figure I.1: Kinking response in 1 mM levamisole after 1 hour exposure.

Frames from an example video showing the hR163C variant strain kinking in 1 mM levamisole dissolved in M9 after 1 hour exposure. Kinks can be seen along the body between straight rigid sections. Full video available at <https://ianhope.leeds.ac.uk/c-elegans-kinking-behaviour/>

References

Abu-Omar, N., Das, J., Szeto, V. and Feng, Z.-P. 2018. Neuronal Ryanodine Receptors in Development and Aging. *Molecular Neurobiology*. **55**(2), pp.1183-1192.

Ackerman, M.J., Priori, S.G., Willems, S., Berul, C., Brugada, R., Calkins, H., Camm, A.J., Ellinor, P.T., Gollob, M., Hamilton, R. *et al.* 2011. HRS/EHRA Expert Consensus Statement on the State of Genetic Testing for the Channelopathies and Cardiomyopathies. *Heart Rhythm*. **8**(8), pp.1308-1339.

Adeokun, A.M., West, S.P., Ellis, F.R., Halsall, P.J., Hopkins, P.M., Foroughmand, A.M., Iles, D.E., Robinson, R.L., Stewart, A.D. and Curran, J.L. 1997. The G1021A substitution in the *RYR1* gene does not cosegregate with malignant hyperthermia susceptibility in a British pedigree. *American journal of human genetics*. **60**(4), pp.833-841.

Alexander, A.G., Marfil, V. and Li, C. 2014. Use of *Caenorhabditis elegans* as a model to study Alzheimer's disease and other neurodegenerative diseases. *Frontiers in genetics*. **5**, pp.279-279.

Altun, Z.F. and Hall, D.H. 2009a. *Introduction*. In *WormAtlas*. [Online]. Available from: <https://www.wormatlas.org>

Altun, Z.F. and Hall, D.H. 2009b. *Muscle system, somatic muscle*. In *WormAtlas*. [Online]. Available from: <https://www.wormatlas.org>

Alzayady, K.J., Sebé-Pedrós, A., Chandrasekhar, R., Wang, L., Ruiz-Trillo, I. and Yule, D.I. 2015. Tracing the Evolutionary History of Inositol, 1, 4, 5-Trisphosphate Receptor: Insights from Analyses of *Capsaspora owczarzaki* Ca²⁺ Release Channel Orthologs. *Molecular Biology and Evolution*. **32**(9), pp.2236-2253.

Amburgey, K., McNamara, N., Bennett, L.R., McCormick, M.E., Acsadi, G. and Dowling, J.J. 2011. Prevalence of congenital myopathies in a representative pediatric united states population. *Annals of neurology*. **70**(4), pp.662-665.

- Anderson, E.N., Corkins, M.E., Li, J.-C., Singh, K., Parsons, S., Tucey, T.M., Sorkaç, A., Huang, H., Dimitriadi, M., Sinclair, D.A. and Hart, A.C. 2016. *C. elegans* lifespan extension by osmotic stress requires FUDR, base excision repair, FOXO, and sirtuins. *Mechanisms of Ageing and Development*. **154**, pp.30-42.
- Andersson, D.C., Betzenhauser, M.J., Reiken, S., Meli, A.C., Umanskaya, A., Xie, W., Shiomi, T., Zalk, R., Lacampagne, A. and Marks, A.R. 2011. Ryanodine Receptor Oxidation Causes Intracellular Calcium Leak and Muscle Weakness in Aging. *Cell Metabolism*. **14**(2), pp.196-207.
- Andronache, Z., Hamilton, S.L., Dirksen, R.T. and Melzer, W. 2009. A retrograde signal from RyR1 alters DHP receptor inactivation and limits window Ca²⁺ release in muscle fibers of Y522S RyR1 knock-in mice. *Proc Natl Acad Sci U S A*. **106**(11), pp.4531-4536.
- Anzalone, A.V., Randolph, P.B., Davis, J.R., Sousa, A.A., Koblan, L.W., Levy, J.M., Chen, P.J., Wilson, C., Newby, G.A., Raguram, A. and Liu, D.R. 2019. Search-and-replace genome editing without double-strand breaks or donor DNA. *Nature*. **576**(7785), pp.149-157.
- Arribere, J.A., Bell, R.T., Fu, B.X.H., Artiles, K.L., Hartman, P.S. and Fire, A.Z. 2014. Efficient marker-free recovery of custom genetic modifications with CRISPR/Cas9 in *Caenorhabditis elegans*. *Genetics*. **198**(3), pp.837-846.
- Avery, L. and Thomas, J.H. 1997. Chapter 24 Feeding and Defecation In: Riddle, D.Blumenthal, T. and Meyer, B. eds. *C. elegans II*. 2nd Edition ed. Cold Spring Harbor (NY): Cold Spring Harbor Laboratory Press.
- Avery, L. and You, Y. 2012. *C. elegans feeding*. *WormBook: The Online Review of C. elegans Biology*. [Online]. Available from: <http://www.wormbook.org>
- Avila, G., O'Brien, J.J. and Dirksen, R.T. 2001. Excitation-contraction uncoupling by a human central core disease mutation in the ryanodine receptor. *Proceedings of the National Academy of Sciences of the United States of America*. **98**(7), pp.4215-4220.

- Bannister, R.A. 2016. Bridging the myoplasmic gap II: more recent advances in skeletal muscle excitation–contraction coupling. *The Journal of Experimental Biology*. **219**(2), p175.
- Barrangou, R. 2015. The roles of CRISPR–Cas systems in adaptive immunity and beyond. *Current Opinion in Immunology*. **32**, pp.36-41.
- Beard, N.A., Casarotto, M.G., Wei, L., Varsányi, M., Laver, D.R. and Dulhunty, A.F. 2005. Regulation of ryanodine receptors by calsequestrin: effect of high luminal Ca²⁺ and phosphorylation. *Biophysical journal*. **88**(5), pp.3444-3454.
- Bellinger, A.M., Reiken, S., Dura, M., Murphy, P.W., Deng, S.-X., Landry, D.W., Nieman, D., Lehnart, S.E., Samaru, M., LaCampagne, A. and Marks, A.R. 2008. Remodeling of ryanodine receptor complex causes “leaky” channels: A molecular mechanism for decreased exercise capacity. *Proceedings of the National Academy of Sciences*. **105**(6), pp.2198-2202.
- Berri, S., Boyle, J.H., Tassieri, M., Hope, I.A. and Cohen, N. 2009. Forward locomotion of the nematode *C. elegans* is achieved through modulation of a single gait. *HFSP Journal*. **3**(3), pp.186-193.
- Bers, D.M. 2002. Cardiac excitation–contraction coupling. *Nature*. **415**(6868), pp.198-205.
- Bolanowski, M.A., Russell, R.L. and Jacobson, L.A. 1981. Quantitative measures of aging in the nematode *Caenorhabditis elegans*. I. Population and longitudinal studies of two behavioral parameters. *Mech Ageing Dev*. **15**(3), pp.279-295.
- Bolotin, A., Quinquis, B.F., Sorokin, A.F. and Ehrlich, S.D. 2005. Clustered regularly interspaced short palindrome repeats (CRISPRs) have spacers of extrachromosomal origin. *Microbiology*. **151**, pp.2551–2561.
- Boncompagni, S., d'Amelio, L., Fulle, S., Fanò, G. and Protasi, F. 2006. Progressive disorganization of the excitation–contraction coupling apparatus in aging human

skeletal muscle as revealed by electron microscopy: a possible role in the decline of muscle performance. *The Journals of Gerontology Series A: Biological Sciences and Medical Sciences*. **61**(10), pp.995-1008.

Bosanac, I., Yamazaki, H., Matsu-ura, T., Michikawa, T., Mikoshiba, K. and Ikura, M. 2005. Crystal Structure of the Ligand Binding Suppressor Domain of Type 1 Inositol 1,4,5-Trisphosphate Receptor. *Molecular Cell*. **17**(2), pp.193-203.

Bouchard, R., Pattarini, R. and Geiger, J.D. 2003. Presence and functional significance of presynaptic ryanodine receptors. *Progress in Neurobiology*. **69**(6), pp.391-418.

Boyle, J., Berri, S. and Cohen, N. 2012. Gait Modulation in *C. elegans*: An Integrated Neuromechanical Model. *Frontiers in Computational Neuroscience*. **6**(10).

Brady, J.E., Sun, L.S., Rosenberg, H. and Li, G. 2009. Prevalence of Malignant Hyperthermia Due to Anesthesia in New York State, 2001–2005. *Anesthesia & Analgesia*. **109**(4), pp.1162-1166.

Brenner, S. 1973. The Genetics of Behaviour. *British Medical Bulletin*. **29**(3), pp.269-271.

Brenner, S. 1974. The Genetics of *Caenorhabditis elegans*. *Genetics*. **77**(1), pp.71-94.

Brenner, S. 2003. Nobel lecture: nature's gift to science. *Bioscience reports*. **23**(5), pp.225-237.

Brini, M. 2004. Ryanodine receptor defects in muscle genetic diseases. *Biochemical and Biophysical Research Communications*. **322**(4), pp.1245-1255.

Brohus, M., Søndergaard, M.T., Wayne Chen, S.R., van Petegem, F. and Overgaard, M.T. 2019. Ca(2+)-dependent calmodulin binding to cardiac ryanodine receptor (RyR2) calmodulin-binding domains. *The Biochemical journal*. **476**(2), pp.193-209.

Bryden, J. and Cohen, N. 2008. Neural control of *Caenorhabditis elegans* forward locomotion: the role of sensory feedback. *Biological Cybernetics*. **98**(4), pp.339-351.

Calderón, J.C., Bolaños, P. and Caputo, C. 2014. The excitation-contraction coupling mechanism in skeletal muscle. *Biophysical reviews*. **6**(1), pp.133-160.

Callaway, C., Seryshev, A., Wang, J.P., Slavik, K.J., Needleman, D.H., Cantu, C., Wu, Y., Jayaraman, T., Marks, A.R. and Hamilton, S.L. 1994. Localization of the high and low affinity [3H]ryanodine binding sites on the skeletal muscle Ca²⁺ release channel. *Journal of Biological Chemistry*. **269**(22), pp.15876-15884.

Cannell, M.B., Kong, C.H.T., Imtiaz, M.S. and Laver, D.R. 2013. Control of sarcoplasmic reticulum Ca²⁺ release by stochastic RyR gating within a 3D model of the cardiac dyad and importance of induction decay for CICR termination. *Biophysical journal*. **104**(10), pp.2149-2159.

Carpenter, D., Ismail, A., Robinson, R.L., Ringrose, C., Booms, P., Iles, D.E., Halsall, P.J., Steele, D., Shaw, M.-A. and Hopkins, P.M. 2009a. A RYR1 mutation associated with recessive congenital myopathy and dominant malignant hyperthermia in Asian families. *Muscle & nerve*. **40**(4), pp.633-639.

Carpenter, D., Robinson, R.L., Quinnell, R.J., Ringrose, C., Hogg, M., Casson, F., Booms, P., Iles, D.E., Halsall, P.J., Steele, D.S., Shaw, M.A. and Hopkins, P.M. 2009b. Genetic variation in RYR1 and malignant hyperthermia phenotypes. *British Journal of Anaesthesia*. **103**(4), pp.538-548.

Chakroborty, S., Briggs, C., Miller, M.B., Goussakov, I., Schneider, C., Kim, J., Wicks, J., Richardson, J.C., Conklin, V., Cameransi, B.G. and Stutzmann, G.E. 2012. Stabilizing ER Ca²⁺ channel function as an early preventative strategy for Alzheimer's disease. *PLoS One*. **7**(12), pe52056.

Chakroborty, S., Goussakov, I., Miller, M.B. and Stutzmann, G.E. 2009. Deviant Ryanodine Receptor-Mediated Calcium Release Resets Synaptic Homeostasis in Presymptomatic 3xTg-AD Mice. *The Journal of Neuroscience*. **29**(30), p9458.

Chang, L., Daly, C., Miller, D.M., Allen, P.D., Boyle, J.P., Hopkins, P.M. and Shaw, M.-A. 2019. Permeabilised skeletal muscle reveals mitochondrial deficiency in malignant

hyperthermia-susceptible individuals. *British Journal of Anaesthesia*. **122**(5), pp.613-621.

Chen, B., Liu, P., Hujber, E.J., Li, Y., Jorgensen, E.M. and Wang, Z.-W. 2017a. AIP limits neurotransmitter release by inhibiting calcium bursts from the ryanodine receptor. *Nature communications*. **8**(1), pp.1380-1380.

Chen, S.R. and MacLennan, D.H. 1994. Identification of calmodulin-, Ca(2+)-, and ruthenium red-binding domains in the Ca²⁺ release channel (ryanodine receptor) of rabbit skeletal muscle sarcoplasmic reticulum. *Journal of Biological Chemistry*. **269**(36), pp.22698-22704.

Chen, W., Koop, A., Liu, Y., Guo, W., Wei, J., Wang, R., MacLennan, D.H., Dirksen, R.T. and Chen, S.R.W. 2017b. Reduced threshold for store overload-induced Ca(2+) release is a common defect of RyR1 mutations associated with malignant hyperthermia and central core disease. *The Biochemical journal*. **474**(16), pp.2749-2761.

Chen, W., Wang, R., Chen, B., Zhong, X., Kong, H., Bai, Y., Zhou, Q., Xie, C., Zhang, J., Guo, A. *et al.* 2014. The ryanodine receptor store-sensing gate controls Ca²⁺ waves and Ca²⁺-triggered arrhythmias. *Nature medicine*. **20**(2), pp.184-192.

Cheng, W., Altafaj, X., Ronjat, M. and Coronado, R. 2005. Interaction between the dihydropyridine receptor calcium channel β -subunit and ryanodine receptor type 1 strengthens excitation-contraction coupling. *Proceedings of the National Academy of Sciences of the United States of America*. **102**(52), p19225.

Clodfelter, G.V., Porter, N.M., Landfield, P.W. and Thibault, O. 2002. Sustained Ca²⁺-induced Ca²⁺-release underlies the post-glutamate lethal Ca²⁺ plateau in older cultured hippocampal neurons. *European Journal of Pharmacology*. **447**(2), pp.189-200.

Corsi, A.K., Wightman, B. and Chalfie, M. 2015. A Transparent window into biology: A primer on *Caenorhabditis elegans*. *Genetics*. **200**(2), pp.387-407.

- Culotti, J.G. and Klein, W.L. 1983. Occurrence of muscarinic acetylcholine receptors in wild type and cholinergic mutants of *Caenorhabditis elegans*. *The Journal of Neuroscience*. **3**(2), p359.
- Dally, S., Monceau, V., Corvazier, E., Bredoux, R., Raies, A., Bobe, R., del Monte, F. and Enouf, J. 2009. Compartmentalized expression of three novel sarco/endoplasmic reticulum Ca²⁺-ATPase 3 isoforms including the switch to ER stress, SERCA3f, in non-failing and failing human heart. *Cell calcium*. **45**(2), pp.144-154.
- Darbandi, S. 2010. *A Comparative Study of Ryanodine Receptors (RyRs) Gene Expression Levels in the Basal Ray-Finned Fish, Bichir (Polypterus ornatipinnis) and the Derived Euteleost Zebrafish (Danio rerio)* Masters of Science in Bioscience, Technology and Public Policy Program thesis, The University of Winnipeg.
- Del Prete, D., Checler, F. and Chami, M. 2014. Ryanodine receptors: physiological function and deregulation in Alzheimer disease. *Molecular neurodegeneration*. **9**, pp.21-21.
- Delbono, O., O'Rourke, K.S. and Ettinger, W.H. 1995. Excitation-calcium release uncoupling in aged single human skeletal muscle fibers. *J Membr Biol*. **148**(3), pp.211-222.
- Demuro, A., Parker, I. and Stutzmann, G.E. 2010. Calcium signaling and amyloid toxicity in Alzheimer disease. *The Journal of biological chemistry*. **285**(17), pp.12463-12468.
- Denham, J.E., Ranner, T. and Cohen, N. 2018. Signatures of proprioceptive control in *Caenorhabditis elegans* locomotion. *Philosophical Transactions of the Royal Society B: Biological Sciences*. **373**(1758), p20180208.
- Derelle, R. and Lang, B.F. 2011. Rooting the Eukaryotic Tree with Mitochondrial and Bacterial Proteins. *Molecular Biology and Evolution*. **29**(4), pp.1277-1289.

des Georges, A., Clarke, O.B., Zalk, R., Yuan, Q., Condon, K.J., Grassucci, R.A., Hendrickson, W.A., Marks, A.R. and Frank, J. 2016. Structural Basis for Gating and Activation of RyR1. *Cell*. **167**(1), pp.145-157.e117.

Deshpande, L.S., Sun, D.A., Sombati, S., Baranova, A., Wilson, M.S., Attkisson, E., Hamm, R.J. and DeLorenzo, R.J. 2008. Alterations in neuronal calcium levels are associated with cognitive deficits after traumatic brain injury. *Neuroscience Letters*. **441**(1), pp.115-119.

Deufel, T., Sudbrak, R., Feist, Y., Rübsam, B., Du Chesne, I., Schäfer, K.L., Roewer, N., Grimm, T., Lehmann-Horn, F. and Hartung, E.J. 1995. Discordance, in a malignant hyperthermia pedigree, between in vitro contracture-test phenotypes and haplotypes for the MHS1 region on chromosome 19q12-13.2, comprising the C1840T transition in the *RYR1* gene. *American journal of human genetics*. **56**(6), pp.1334-1342.

Dickinson, D.J. and Goldstein, B. 2016. CRISPR-Based Methods for *Caenorhabditis elegans* Genome Engineering. *Genetics*. **202**(3), pp.885-901.

Dickinson, D.J., Ward, J.D., Reiner, D.J. and Goldstein, B. 2013. Engineering the *Caenorhabditis elegans* genome using Cas9-triggered homologous recombination. *Nature methods*. **10**(10), pp.1028-1034.

Dixon, S.J. and Roy, P.J. 2005. Muscle arm development in *Caenorhabditis elegans*. *Development*. **132**(13), p3079.

Dobrev, D. and Wehrens, X.H.T. 2014. Role of RyR2 phosphorylation in heart failure and arrhythmias: Controversies around ryanodine receptor phosphorylation in cardiac disease. *Circulation research*. **114**(8), pp.1311-1319.

Duerr, J.S., Han, H.-P., Fields, S.D. and Rand, J.B. 2008. Identification of major classes of cholinergic neurons in the nematode *Caenorhabditis elegans*. *Journal of Comparative Neurology*. **506**(3), pp.398-408.

- Durham, W.J., Aracena-Parks, P., Long, C., Rossi, A.E., Goonasekera, S.A., Boncompagni, S., Galvan, D.L., Gilman, C.P., Baker, M.R., Shirokova, N., Protasi, F., Dirksen, R. and Hamilton, S.L. 2008. RyR1 S-Nitrosylation Underlies Environmental Heat Stroke and Sudden Death in Y522S RyR1 Knockin Mice. *Cell*. **133**(1), pp.53-65.
- Efremov, R.G., Leitner, A., Aebersold, R. and Raunser, S. 2015. Architecture and conformational switch mechanism of the ryanodine receptor. *Nature*. **517**, p39.
- El-Gebali, S., Mistry, J., Bateman, A., Eddy, S.R., Luciani, A., Potter, S.C., Qureshi, M., Richardson, L.J., Salazar, G.A., Smart, A. *et al.* 2018. The Pfam protein families database in 2019. *Nucleic Acids Research*. **47**(D1), pp.D427-D432.
- Ellis, F.R., Halsall, P.J., Ording, H., Fletcher, R., Rankley, E., Heffron, J.J., Lehane, M., Mortier, W., Stetnbereitner, Sporn, P., Theunynck, D. and Verburg, R. 1984. A protocol for the investigation of malignant hyperpyrexia (MH) susceptibility. The European Malignant Hyperpyrexia Group. *British journal of anaesthesia*. **56**(11), pp.1267-1269.
- Eltit, J.M., Bannister, R.A., Moua, O., Altamirano, F., Hopkins, P.M., Pessah, I.N., Molinski, T.F., López, J.R., Beam, K.G. and Allen, P.D. 2012. Malignant hyperthermia susceptibility arising from altered resting coupling between the skeletal muscle L-type Ca²⁺ channel and the type 1 ryanodine receptor. *Proceedings of the National Academy of Sciences of the United States of America*. **109**(20), pp.7923-7928.
- Ermak, G. and Davies, K.J.A. 2002. Calcium and oxidative stress: from cell signaling to cell death. *Molecular Immunology*. **38**(10), pp.713-721.
- Esteve, E., Eltit, J.M., Bannister, R.A., Liu, K., Pessah, I.N., Beam, K.G., Allen, P.D. and Lopez, J.R. 2010. A malignant hyperthermia-inducing mutation in *RYR1* (R163C): alterations in Ca²⁺ entry, release, and retrograde signaling to the DHPR. *J Gen Physiol*. **135**(6), pp.619-628.
- Evans, T.C. 2006. *Transformation and microinjection*. [Online]. Available from: <http://www.wormbook.org>

- Fabiato, A. 1983. Calcium-induced release of calcium from the cardiac sarcoplasmic reticulum. *American Journal of Physiology-Cell Physiology*. **245**(1), pp.C1-C14.
- Ferreira, C. and Kalogeropoulou, E. 2019. *Personal communication*, September 2019.
- Fire, A., Xu, S., Montgomery, M.K., Kostas, S.A., Driver, S.E. and Mello, C.C. 1998. Potent and specific genetic interference by double-stranded RNA in *Caenorhabditis elegans*. *Nature*. **391**(6669), pp.806-811.
- Firestone, L.L., Alifimoff, J.K. and Miller, K.W. 1994. Does general anesthetic-induced desensitization of the Torpedo acetylcholine receptor correlate with lipid disordering? *Molecular Pharmacology*. **46**(3), p508.
- Fischer, E., Gottschalk, A. and Schuler, C. 2017. An optogenetic arrhythmia model to study catecholaminergic polymorphic ventricular tachycardia mutations. *Sci Rep*. **7**(1), p17514.
- Frankowski, H., Alavez, S., Spilman, P., Mark, K.A., Nelson, J.D., Mollahan, P., Rao, R.V., Chen, S.F., Lithgow, G.J. and Ellerby, H.M. 2013. Dimethyl sulfoxide and dimethyl formamide increase lifespan of *C. elegans* in liquid. *Mechanisms of Ageing and Development*. **134**(3), pp.69-78.
- Fruen, B.R., Bardy, J.M., Byrem, T.M., Strasburg, G.M. and Louis, C.F. 2000. Differential Ca²⁺ sensitivity of skeletal and cardiac muscle ryanodine receptors in the presence of calmodulin. *American Journal of Physiology-Cell Physiology*. **279**(3), pp.C724-C733.
- Furuichi, T., Furutama, D., Hakamata, Y., Nakai, J., Takeshima, H. and Mikoshiba, K. 1994. Multiple types of ryanodine receptor/Ca²⁺ release channels are differentially expressed in rabbit brain. *J Neurosci*. **14**(8), pp.4794-4805.
- Gaboardi, A.J., Kressler, J., Snow, T.K. and Balog, E.M. 2018. Aging impairs regulation of ryanodine receptors from extensor digitorum longus but not soleus muscles. *Muscle & nerve*. **57**(6), pp.1022-1025.

- Galeotti, N., Quattrone, A., Vivoli, E., Norcini, M., Bartolini, A. and Ghelardini, C. 2008. Different involvement of type 1, 2, and 3 ryanodine receptors in memory processes. *Learning & memory* **15**(5), pp.315-323.
- Gardner, L., Miller, D., Daly, C., Gupta, P., House, C., Sa, D., Shaw, M.-A. and Hopkins, P. 2020. Investigating the genetic susceptibility to exertional heat illness. *Journal of Medical Genetics*. **(In press)**.
- Gasiunas, G., Barrangou, R., Horvath, P. and Siksnys, V. 2012. Cas9-crRNA ribonucleoprotein complex mediates specific DNA cleavage for adaptive immunity in bacteria. *Proceedings of the National Academy of Sciences of the United States of America*. **109**(39), pp.E2579-E2586.
- Gems, D. and Riddle, D.L. 2000. Defining Wild-Type Life Span in *Caenorhabditis elegans*. *The Journals of Gerontology: Series A*. **55**(5), pp.B215-B219.
- Gendrel, M., Atlas, E.G. and Hobert, O. 2016. A cellular and regulatory map of the GABAergic nervous system of *C. elegans*. *eLife*. **5**, pe17686.
- Giannini, G., Conti, A., Mammarella, S., Scrobogna, M. and Sorrentino, V. 1995. The ryanodine receptor/calcium channel genes are widely and differentially expressed in murine brain and peripheral tissues. *The Journal of cell biology*. **128**(5), pp.893-904.
- Gieseler, K., Qadota, H. and Benian, G. 2005. *Development, structure, and maintenance of C. elegans body wall muscle*. [Online]. Available from: <http://www.wormbook.org>
- Giulivi, C., Ross-Inta, C., Omanska-Klusek, A., Napoli, E., Sakaguchi, D., Barrientos, G., Allen, P.D. and Pessah, I.N. 2011. Basal bioenergetic abnormalities in skeletal muscle from ryanodine receptor malignant hyperthermia-susceptible R163C knock-in mice. *The Journal of biological chemistry*. **286**(1), pp.99-113.
- Gjorgjieva, J., Biron, D. and Haspel, G. 2014. Neurobiology of *Caenorhabditis elegans* Locomotion: Where Do We Stand? *Bioscience*. **64**(6), pp.476-486.

Gladyshev, V.N. 2014. The free radical theory of aging is dead. Long live the damage theory! *Antioxidants & redox signaling*. **20**(4), pp.727-731.

Goonasekera, S.A., Beard, N.A., Groom, L., Kimura, T., Lyfenko, A.D., Rosenfeld, A., Marty, I., Dulhunty, A.F. and Dirksen, R.T. 2007. Triadin binding to the C-terminal luminal loop of the ryanodine receptor is important for skeletal muscle excitation contraction coupling. *The Journal of general physiology*. **130**(4), pp.365-378.

Gordeeva, A.V., Zvyagilskaya, R.A. and Labas, Y.A. 2003. Cross-talk between reactive oxygen species and calcium in living cells. *Biochemistry (Mosc)*. **68**(10), pp.1077-1080.

Gray, J. and Lissmann, H.W. 1964. The Locomotion of Nematodes. *Journal of Experimental Biology*. **41**(1), p135.

Griffin, E.F., Caldwell, K.A. and Caldwell, G.A. 2017. Genetic and Pharmacological Discovery for Alzheimer's Disease Using *Caenorhabditis elegans*. *ACS Chem Neurosci*. **8**(12), pp.2596-2606.

Guerrini, R., Menegazzi, P., Anacardio, R., Marastoni, M., Tomatis, R., Zorzato, F. and Treves, S. 1995. Calmodulin binding sites of the skeletal, cardiac, and brain ryanodine receptor Ca²⁺ channels: modulation by the catalytic subunit of cAMP-dependent protein kinase? *Biochemistry*. **34**(15), pp.5120-5129.

Guis, S., Figarella-Branger, D., Monnier, N., Bendahan, D., Kozak-Ribbens, G., Mattei, J.-P., Lunardi, J., Cozzone, P.J. and Pellissier, J.-F. 2004. Multimicore Disease in a Family Susceptible to Malignant Hyperthermia: Histology, In Vitro Contracture Tests, and Genetic Characterization. *Archives of Neurology*. **61**(1), pp.106-113.

Gupta, P.K. and Hopkins, P.M. 2017. Diagnosis and management of malignant hyperthermia. *BJA Education*. **17**(7), pp.249-254.

Györke, I., Hester, N., Jones, L.R. and Györke, S. 2004. The role of calsequestrin, triadin, and junctin in conferring cardiac ryanodine receptor responsiveness to luminal calcium. *Biophysical journal*. **86**(4), pp.2121-2128.

- Hakamata, Y., Nakai, J., Takeshima, H. and Imoto, K. 1992. Primary structure and distribution of a novel ryanodine receptor/calcium release channel from rabbit brain. *FEBS Letters*. **312**(2-3), pp.229-235.
- Halsall, P.J. and Hopkins, P.M. 2003. Malignant hyperthermia. *BJA Education*. **3**(1), pp.5-9.
- Hamilton, S. and Terentyev, D. 2018. Proarrhythmic Remodeling of Calcium Homeostasis in Cardiac Disease; Implications for Diabetes and Obesity. *Front Physiol*. **9**, p1517.
- Harman, D. 1956. Aging: a theory based on free radical and radiation chemistry. *J Gerontol*. **11**(3), pp.298-300.
- Hasan, G. and Rosbash, M. 1992. Drosophila homologs of two mammalian intracellular Ca(2+)-release channels: identification and expression patterns of the inositol 1,4,5-triphosphate and the ryanodine receptor genes. *Development*. **116**(4), p967.
- Hashmi, S., Wang, Y., Parhar, R.S., Collison, K.S., Conca, W., Al-Mohanna, F. and Gaugler, R. 2013. A *C. elegans* model to study human metabolic regulation. *Nutrition & Metabolism*. **10**(1), p31.
- He, D., Fiz-Palacios, O., Fu, C.-J., Fehling, J., Tsai, C.-C. and Baldauf, Sandra L. 2014. An Alternative Root for the Eukaryote Tree of Life. *Current Biology*. **24**(4), pp.465-470.
- Henderson, M.J., Baldwin, H.A., Werley, C.A., Boccardo, S., Whitaker, L.R., Yan, X., Holt, G.T., Schreiter, E.R., Looger, L.L., Cohen, A.E., Kim, D.S. and Harvey, B.K. 2015. A Low Affinity GCaMP3 Variant (GCaMPer) for Imaging the Endoplasmic Reticulum Calcium Store. *PloS one*. **10**(10), pp.e0139273-e0139273.
- Herndon, L.A. and Hall, D.H. 2013. *Glossary U*. [Online]. Available from: <http://www.wormatlas.org/>

- Herndon, L.A., Schmeissner, P.J., Dudaronek, J.M., Brown, P.A., Listner, K.M., Sakano, Y., Paupard, M.C., Hall, D.H. and Driscoll, M. 2002. Stochastic and genetic factors influence tissue-specific decline in ageing *C. elegans*. *Nature*. **419**(6909), pp.808-814.
- Hertle, D.N. and Yeckel, M.F. 2007. Distribution of inositol-1,4,5-trisphosphate receptor isotypes and ryanodine receptor isotypes during maturation of the rat hippocampus. *Neuroscience*. **150**(3), pp.625-638.
- Hirani, N., Westenberg, M., Gami, M.S., Davis, P., Hope, I.A. and Dolphin, C.T. 2013. A simplified counter-selection recombineering protocol for creating fluorescent protein reporter constructs directly from *C. elegans* fosmid genomic clones. *BMC Biotechnology*. **13**(1), p1.
- Hohenwarter, M. 2002. *GeoGebra: Ein Softwaresystem für dynamische Geometrie und Algebra der Ebene*. Masters thesis, Paris Lodron University, Salzburg, Austria.
- Holbrook, R. 2016. *Personal communication*, March 2016.
- Hopkins, P.M. 2000. Malignant hyperthermia: advances in clinical management and diagnosis. *British Journal of Anaesthesia*. **85**(1), pp.118-128.
- Hopkins, P.M. 2011. Malignant hyperthermia: pharmacology of triggering. *British Journal of Anaesthesia*. **107**(1), pp.48-56.
- Hopkins, P.M., Fiszer, D., Shaw, M.-A. and Roiz de Sa, D. 2016. In Reply. *Anesthesiology*. **124**(2), p511.
- Hopkins, P.M., Rüffert, H., Snoeck, M.M., Girard, T., Glahn, K.P.E., Ellis, F.R., Müller, C.R., Urwyler, A., Bandschapp, O., Gillies, R. *et al.* 2015. European Malignant Hyperthermia Group guidelines for investigation of malignant hyperthermia susceptibility. *BJA: British Journal of Anaesthesia*. **115**(4), pp.531-539.
- Horstick, E.J., Linsley, J.W., Dowling, J.J., Hauser, M.A., McDonald, K.K., Ashley-Koch, A., Saint-Amant, L., Satish, A., Cui, W.W., Zhou, W. *et al.* 2013. Stac3 is a component of the

excitation–contraction coupling machinery and mutated in Native American myopathy. *Nature Communications*. **4**(1), p1952.

Horvitz, H.R. 2003. Worms, life, and death (Nobel lecture). *Chembiochem*. **4**(8), pp.697-711.

Illingworth, M.A., Main, M., Pitt, M., Feng, L., Sewry, C.A., Gunny, R., Vorstman, E., Beeson, D., Manzur, A., Muntoni, F. and Robb, S.A. 2014. *RYR1*-related congenital myopathy with fatigable weakness, responding to pyridostigimine. *Neuromuscular disorders : NMD*. **24**(8), pp.707-712.

Iser, W.B. and Wolkow, C.A. 2007. DAF-2/insulin-like signaling in *C. elegans* modifies effects of dietary restriction and nutrient stress on aging, stress and growth. *PLoS one*. **2**(11), pp.e1240-e1240.

Islander, G., Rydenfelt, K., Ranklev, E. and Bodelsson, M. 2007. Male preponderance of patients testing positive for malignant hyperthermia susceptibility. *Acta anaesthesiologica Scandinavica*. **51**(5), pp.614-620.

Itkin, A., Dupres, V., Dufrêne, Y.F., Bechinger, B., Ruyschaert, J.-M. and Raussens, V. 2011. Calcium Ions Promote Formation of Amyloid β -Peptide (1–40) Oligomers Causally Implicated in Neuronal Toxicity of Alzheimer's Disease. *PLOS ONE*. **6**(3), pe18250.

Javer, A., Currie, M., Lee, C.W., Hokanson, J., Li, K., Martineau, C.N., Yemini, E., Grundy, L.J., Li, C., Ch'ng, Q., Schafer, W.R., Nollen, E.A.A., Kerr, R. and Brown, A.E.X. 2018. An open-source platform for analyzing and sharing worm-behavior data. *Nature Methods*. **15**(9), pp.645-646.

Jiang, D., Chen, W., Xiao, J., Wang, R., Kong, H., Jones, P.P., Zhang, L., Fruen, B. and Chen, S.R.W. 2008. Reduced threshold for luminal Ca^{2+} activation of RyR1 underlies a causal mechanism of porcine malignant hyperthermia. *The Journal of biological chemistry*. **283**(30), pp.20813-20820.

- Jin, Y., Jorgensen, E., Hartweg, E. and Horvitz, H.R. 1999. The *Caenorhabditis elegans* Gene *unc-25* Encodes Glutamic Acid Decarboxylase and Is Required for Synaptic Transmission But Not Synaptic Development. *The Journal of Neuroscience*. **19**(2), p539.
- Jinek, M., Chylinski, K., Fonfara, I., Hauer, M., Doudna, J.A. and Charpentier, E. 2012. A programmable dual-RNA-guided DNA endonuclease in adaptive bacterial immunity. *Science*. **337**(6096), pp.816-821.
- Jones, A.K. and Sattelle, D.B. 2004. Functional genomics of the nicotinic acetylcholine receptor gene family of the nematode, *Caenorhabditis elegans*. *BioEssays*. **26**(1), pp.39-49.
- Jones, P.P., Guo, W. and Chen, S.R.W. 2017. Control of cardiac ryanodine receptor by sarcoplasmic reticulum luminal Ca(2). *The Journal of general physiology*. **149**(9), pp.867-875.
- Jungbluth, H., Lillis, S., Zhou, H., Abbs, S., Sewry, C., Swash, M. and Muntoni, F. 2009. Late-onset axial myopathy with cores due to a novel heterozygous dominant mutation in the skeletal muscle ryanodine receptor (*RYR1*) gene. *Neuromuscul Disord*. **19**(5), pp.344-347.
- Jurkat-Rott, K. and Lehmann-Horn, F. 2005. Muscle channelopathies and critical points in functional and genetic studies. *The Journal of Clinical Investigation*. **115**(8), pp.2000-2009.
- Kalogeropoulou, E. 2018. *Role of the SAA and SMB neurons in locomotion in the nematode Caenorhabditis elegans, with a focus on steering*. Doctor of Philosophy thesis, The University of Leeds.
- Karczewski, K.J., Francioli, L.C., Tiao, G., Cummings, B.B., Alföldi, J., Wang, Q., Collins, R.L., Laricchia, K.M., Ganna, A., Birnbaum, D.P. *et al.* 2019. Variation across 141,456 human exomes and genomes reveals the spectrum of loss-of-function intolerance across human protein-coding genes. *bioRxiv*. p531210.

- Katz, B. 1971. Quantal mechanism of neural transmitter release. *Science*. **173**(3992), pp.123-126.
- Keaveny, E.E. and Brown, A.E.X. 2017. Predicting path from undulations for *C. elegans* using linear and nonlinear resistive force theory. *Physical biology*. **14**(2), pp.025001-025001.
- Khuzakhmetova, V.F., Samigullin, D.V. and Bukharaeva, E.A. 2014. The role of presynaptic ryanodine receptors in regulation of the kinetics of the acetylcholine quantal release in the mouse neuromuscular junction. *Biochemistry (Moscow) Supplement Series A: Membrane and Cell Biology*. **8**(1), pp.144-152.
- Kim, H., Ishidate, T., Ghanta, K.S., Seth, M., Conte, D., Jr., Shirayama, M. and Mello, C.C. 2014. A co-CRISPR strategy for efficient genome editing in *Caenorhabditis elegans*. *Genetics*. **197**(4), pp.1069-1080.
- Kirienko, N.V., Mani, K. and Fay, D.S. 2010. Cancer models in *Caenorhabditis elegans*. *Developmental dynamics : an official publication of the American Association of Anatomists*. **239**(5), pp.1413-1448.
- Komor, A.C., Kim, Y.B., Packer, M.S., Zuris, J.A. and Liu, D.R. 2016. Programmable editing of a target base in genomic DNA without double-stranded DNA cleavage. *Nature*. **533**(7603), pp.420-424.
- Kunst, G., Graf, B.M., Schreiner, E., Martin, E. and Fink, R.H. 1999. Differential effects of sevoflurane, isoflurane, and halothane on Ca²⁺ release from the sarcoplasmic reticulum of skeletal muscle. *Anesthesiology*. **91**(1), pp.179-186.
- Kushnir, A., Wajsberg, B. and Marks, A.R. 2018. Ryanodine receptor dysfunction in human disorders. *Biochimica et Biophysica Acta (BBA) - Molecular Cell Research*. **1865**(11, Part B), pp.1687-1697.
- LaFerla, F.M. 2002. Calcium dyshomeostasis and intracellular signalling in alzheimer's disease. *Nature Reviews Neuroscience*. **3**(11), pp.862-872.

- Laforgia, N., Capozza, M., De Cosmo, L., Di Mauro, A., Baldassarre, M.E., Mercadante, F., Torella, A.L., Nigro, V. and Resta, N. 2018. A Rare Case of Severe Congenital RYR1-Associated Myopathy. *Case reports in genetics*. **2018**, pp.6184185-6184185.
- Lai, C.H., Chou, C.Y., Ch'ang, L.Y., Liu, C.S. and Lin, W. 2000. Identification of novel human genes evolutionarily conserved in *Caenorhabditis elegans* by comparative proteomics. *Genome research*. **10**(5), pp.703-713.
- Lamboley, C.R., Wyckelsma, V.L., McKenna, M.J., Murphy, R.M. and Lamb, G.D. 2016. Ca(2+) leakage out of the sarcoplasmic reticulum is increased in type I skeletal muscle fibres in aged humans. *The Journal of physiology*. **594**(2), pp.469-481.
- Lanner, J.T., Georgiou, D.K., Joshi, A.D. and Hamilton, S.L. 2010. Ryanodine receptors: structure, expression, molecular details, and function in calcium release. *Cold Spring Harb Perspect Biol*. **2**(11), pa003996.
- Laranjeiro, R., Harinath, G., Burke, D., Braeckman, B.P. and Driscoll, M. 2017. Single swim sessions in *C. elegans* induce key features of mammalian exercise. *BMC biology*. **15**(1), pp.30-30.
- Laver, D.R. 2018. Regulation of the RyR channel gating by Ca(2+) and Mg(2). *Biophysical reviews*. **10**(4), pp.1087-1095.
- Ledbetter, M.W., Preiner, J.K., Louis, C.F. and Mickelson, J.R. 1994. Tissue distribution of ryanodine receptor isoforms and alleles determined by reverse transcription polymerase chain reaction. *J Biol Chem*. **269**(50), pp.31544-31551.
- Lee, E.H. 2010. Ca²⁺ channels and skeletal muscle diseases. *Progress in Biophysics and Molecular Biology*. **103**(1), pp.35-43.
- Lek, M., Karczewski, K.J., Minikel, E.V., Samocha, K.E., Banks, E., Fennell, T., O'Donnell-Luria, A.H., Ware, J.S., Hill, A.J., Cummings, B.B. *et al.* 2016. Analysis of protein-coding genetic variation in 60,706 humans. *Nature*. **536**, p285.

Leong, P. and MacLennan, D.H. 1998. A 37-amino acid sequence in the skeletal muscle ryanodine receptor interacts with the cytoplasmic loop between domains II and III in the skeletal muscle dihydropyridine receptor. *J Biol Chem.* **273**(14), pp.7791-7794.

Lewis, J.A., Wu, C.H., Berg, H. and Levine, J.H. 1980. The genetics of levamisole resistance in the nematode *Caenorhabditis elegans*. *Genetics.* **95**(4), pp.905-928.

Liang, J., Kulasiri, D. and Samarasinghe, S. 2015. Ca²⁺ dysregulation in the endoplasmic reticulum related to Alzheimer's disease: A review on experimental progress and computational modeling. *Biosystems.* **134**, pp.1-15.

Liang, L. and Wei, H. 2015. Dantrolene, a treatment for Alzheimer disease? *Alzheimer disease and associated disorders.* **29**(1), pp.1-5.

Liguori, I., Russo, G., Curcio, F., Bulli, G., Aran, L., Della-Morte, D., Gargiulo, G., Testa, G., Cacciatore, F., Bonaduce, D. and Abete, P. 2018. Oxidative stress, aging, and diseases. *Clinical interventions in aging.* **13**, pp.757-772.

Lin, L., Koblin, D.D. and Wang, H.H. 1995. Effects of halothane on the nicotinic acetylcholine receptor from *Torpedo californica*. *Biochemical Pharmacology.* **49**(8), pp.1085-1089.

Litman, R.S., Griggs, S.M., Dowling, J.J. and Riazi, S. 2018. Malignant Hyperthermia Susceptibility and Related Diseases. *Anesthesiology: The Journal of the American Society of Anesthesiologists.* **128**(1), pp.159-167.

Liu, Q., Chen, B., Yankova, M., Morest, D.K., Maryon, E.B., Hand, A.R., Nonet, M.L. and Wang, Z.W. 2005. Presynaptic Ryanodine Receptors Are Required for Normal Quantal Size at the *Caenorhabditis elegans* Neuromuscular Junction. *The Journal of Neuroscience.* **25**(29), p6745.

Liu, Q., Hollopeter, G. and Jorgensen, E.M. 2009. Graded synaptic transmission at the *Caenorhabditis elegans* neuromuscular junction. *Proceedings of the National Academy of Sciences.* **106**(26), p10823.

Liu, Q., Kidd, P.B., Dobosiewicz, M. and Bargmann, C.I. 2018. *C. elegans* AWA Olfactory Neurons Fire Calcium-Mediated All-or-None Action Potentials. *Cell*. **175**(1), pp.57-70.e17.

Liu, X., Betzenhauser, Matthew J., Reiken, S., Meli, Albano C., Xie, W., Chen, B.-X., Arancio, O. and Marks, Andrew R. 2012. Role of Leaky Neuronal Ryanodine Receptors in Stress- Induced Cognitive Dysfunction. *Cell*. **150**(5), pp.1055-1067.

Løseth, S., Voermans, N.C., Torbergsen, T., Lillis, S., Jonsrud, C., Lindal, S., Kamsteeg, E.-J., Lammens, M., Broman, M., Dekomien, G. *et al.* 2013. A novel late-onset axial myopathy associated with mutations in the skeletal muscle ryanodine receptor (*RYR1*) gene. *Journal of Neurology*. **260**(6), pp.1504-1510.

Loy, R.E., Orynbayev, M., Xu, L., Andronache, Z., Apostol, S., Zvaritch, E., MacLennan, D.H., Meissner, G., Melzer, W. and Dirksen, R.T. 2011. Muscle weakness in Ryr1 I4895T/WT knock-in mice as a result of reduced ryanodine receptor Ca²⁺ ion permeation and release from the sarcoplasmic reticulum. *The Journal of General Physiology*. **137**(1), p43.

Lüersen, K., Gottschling, D.-C. and Döring, F. 2016. Complex Locomotion Behavior Changes Are Induced in *Caenorhabditis elegans* by the Lack of the Regulatory Leak K⁺ Channel TWK-7. *Genetics*. **204**(2), pp.683-701.

Lyfenko, A.D., Ducreux, S., Wang, Y., Xu, L., Zorzato, F., Ferreira, A., Meissner, G., Treves, S. and Dirksen, R.T. 2007. Two central core disease (CCD) deletions in the C-terminal region of *RYR1* alter muscle excitation-contraction (EC) coupling by distinct mechanisms. *Human mutation*. **28**(1), pp.61-68.

Lynch, P.J., Tong, J., Lehane, M., Mallet, A., Giblin, L., Heffron, J.J., Vaughan, P., Zafra, G., MacLennan, D.H. and McCarthy, T.V. 1999. A mutation in the transmembrane/luminal domain of the ryanodine receptor is associated with abnormal Ca²⁺ release channel function and severe central core disease. *Proc Natl Acad Sci U S A*. **96**(7), pp.4164-4169.

Lynch, P.J.B., Krivosic-Horber, R.M., Reyford, H.M., Monnier, N.P., Quane, K.M., Adnet, P.M., Haudecoeur, G.P., Krivosic, I.M., McCarthy, T.P. and Lunardi, J.P. 1997.

Identification of Heterozygous and Homozygous Individuals with the Novel *RYR1* Mutation Cys35Arg in a Large Kindred. *Anesthesiology: The Journal of the American Society of Anesthesiologists*. **86**(3), pp.620-626.

MacLennan, D.H. 2000. Ca²⁺ signalling and muscle disease. *European Journal of Biochemistry*. **267**(17), pp.5291-5297.

MacLennan, D.H. and Zvaritch, E. 2011. Mechanistic models for muscle diseases and disorders originating in the sarcoplasmic reticulum. *Biochimica et Biophysica Acta (BBA) - Molecular Cell Research*. **1813**(5), pp.948-964.

Mahoney, T.R., Luo, S. and Nonet, M.L. 2006. Analysis of synaptic transmission in *Caenorhabditis elegans* using an aldicarb-sensitivity assay. *Nature Protocols*. **1**, p1772.

Mango, S.E. 2007. *The C. elegans pharynx: a model for organogenesis*. [Online]. Available from: <http://www.wormbook.org>

Marchant, C.L., Ellis, F.R., Halsall, P.J., Hopkins, P.M. and Robinson, R.L. 2004. Mutation analysis of two patients with hypokalemic periodic paralysis and suspected malignant hyperthermia. *Muscle & Nerve*. **30**(1), pp.114-117.

Markaki, M. and Tavernarakis, N. 2010. Modeling human diseases in *Caenorhabditis elegans*. *Biotechnol J*. **5**(12), pp.1261-1276.

Marks, A.R., Tempst, P., Hwang, K.S., Taubman, M.B., Inui, M., Chadwick, C., Fleischer, S. and Nadal-Ginard, B. 1989. Molecular cloning and characterization of the ryanodine receptor/junctional channel complex cDNA from skeletal muscle sarcoplasmic reticulum. *Proceedings of the National Academy of Sciences*. **86**(22), p8683.

Martin, R.J., Robertson, A.P., Buxton, S.K., Beech, R.N., Charvet, C.L. and Neveu, C. 2012. Levamisole receptors: a second awakening. *Trends in parasitology*. **28**(7), pp.289-296.

- Maryon, E.B., Coronado, R. and Anderson, P. 1996. *unc-68* encodes a ryanodine receptor involved in regulating *C. elegans* body-wall muscle contraction. *The Journal of cell biology*. **134**(4), pp.885-893.
- Maryon, E.B., Saari, B. and Anderson, P. 1998. Muscle-specific functions of ryanodine receptor channels in *Caenorhabditis elegans*. *J Cell Sci*. **111 (Pt 19)**, pp.2885-2895.
- McColl, G., Roberts, B.R., Pukala, T.L., Kenche, V.B., Roberts, C.M., Link, C.D., Ryan, T.M., Masters, C.L., Barnham, K.J., Bush, A.I. and Cherny, R.A. 2012. Utility of an improved model of amyloid-beta (A β (1-42)) toxicity in *Caenorhabditis elegans* for drug screening for Alzheimer's disease. *Mol Neurodegener*. **7**, p57.
- McCulloch, D. and Gems, D. 2003. Body size, insulin/IGF signaling and aging in the nematode *Caenorhabditis elegans*. *Experimental Gerontology*. **38**(1), pp.129-136.
- McIntire, S.L., Jorgensen, E., Kaplan, J. and Horvitz, H.R. 1993. The GABAergic nervous system of *Caenorhabditis elegans*. *Nature*. **364**(6435), pp.337-341.
- McPherson, P.S., Kim, Y.-K., Valdivia, H., Knudson, C.M., Takekura, H., Franzini-Armstrong, C., Coronado, R. and Campbell, K.P. 1991. The brain ryanodine receptor: A caffeine-sensitive calcium release channel. *Neuron*. **7**(1), pp.17-25.
- Meissner, G., Darling, E. and Eveleth, J. 1986. Kinetics of rapid calcium release by sarcoplasmic reticulum. Effects of calcium, magnesium, and adenine nucleotides. *Biochemistry*. **25**(1), pp.236-244.
- Meissner, G. and Henderson, J.S. 1987. Rapid calcium release from cardiac sarcoplasmic reticulum vesicles is dependent on Ca²⁺ and is modulated by Mg²⁺, adenine nucleotide, and calmodulin. *Journal of Biological Chemistry*. **262**(7), pp.3065-3073.
- Mellanby, H. 1955. The identification and estimation of acetylcholine in three parasitic nematodes (*Ascaris lumbricoides*, *Litomosoides carinii*, and the microfilariae of *Dirofilaria repens*). *Parasitology*. **45**(3-4), pp.287-294.

Mickelson, J.R. and Louis, C.F. 1996. Malignant hyperthermia: excitation-contraction coupling, Ca²⁺ release channel, and cell Ca²⁺ regulation defects. *Physiol Rev.* **76**(2), pp.537-592.

Miller, D.M., Daly, C., Aboelsaod, E.M., Gardner, L., Hobson, S.J., Riasat, K., Shepherd, S., Robinson, R.L., Bilmen, J.G., Gupta, P.K., Shaw, M.A. and Hopkins, P.M. 2018. Genetic epidemiology of malignant hyperthermia in the UK. *British journal of anaesthesia.* **121**(4), pp.944-952.

Mojica, F.J., Diez-Villasenor C Fau - Garcia-Martinez, J., Garcia-Martinez J Fau - Soria, E. and Soria, E. 2005 Intervening sequences of regularly spaced prokaryotic repeats derive from foreign genetic elements. *J Mol Evol.* **60**(174-82).

Momma, K., Homma, T., Isaka, R., Sudevan, S. and Higashitani, A. 2017. Heat-Induced Calcium Leakage Causes Mitochondrial Damage in *Caenorhabditis elegans* Body-Wall Muscles. *Genetics.* **206**(4), p1985.

Monnier, N., Krivosic-Horber, R., Payen, J.-F., Kozak-Ribbens, G., Nivoche, Y., Adnet, P., Reyford, H. and Lunardi, J. 2002. Presence of Two Different Genetic Traits in Malignant Hyperthermia Families: Implication for Genetic Analysis, Diagnosis, and Incidence of Malignant Hyperthermia Susceptibility. *Anesthesiology: The Journal of the American Society of Anesthesiologists.* **97**(5), pp.1067-1074.

Monnier, N., Procaccio, V., Stieglitz, P. and Lunardi, J. 1997. Malignant-Hyperthermia Susceptibility Is Associated with a Mutation of the α 1-Subunit of the Human Dihydropyridine-Sensitive L-Type Voltage-Dependent Calcium-Channel Receptor in Skeletal Muscle. *The American Journal of Human Genetics.* **60**(6), pp.1316-1325.

Monnier, N., Romero, N.B., Lerule, J., Landrieu, P., Nivoche, Y., Fardeau, M. and Lunardi, J. 2001. Familial and sporadic forms of central core disease are associated with mutations in the C-terminal domain of the skeletal muscle ryanodine receptor. *Human Molecular Genetics.* **10**(22), pp.2581-2592.

- Mörck, C. and Pilon, M. 2006. *C. elegans* feeding defective mutants have shorter body lengths and increased autophagy. *BMC developmental biology*. **6**, pp.39-39.
- Morrisette, J., Xu, L., Nelson, A., Meissner, G. and Block, B.A. 2000. Characterization of RyR1-slow, a ryanodine receptor specific to slow-twitch skeletal muscle. *American Journal of Physiology-Regulatory, Integrative and Comparative Physiology*. **279**(5), pp.R1889-R1898.
- Mouton, J., Marty, I., Villaz, M., Feltz, A. and Maulet, Y. 2001. Molecular interaction of dihydropyridine receptors with type-1 ryanodine receptors in rat brain. *Biochem J*. **354**(Pt 3), pp.597-603.
- Murayama, T., Kurebayashi, N., Ogawa, H., Yamazawa, T., Oyamada, H., Suzuki, J., Kanemaru, K., Oguchi, K., Iino, M. and Sakurai, T. 2016. Genotype-Phenotype Correlations of Malignant Hyperthermia and Central Core Disease Mutations in the Central Region of the RYR1 Channel. *Human mutation*. **37**(11), pp.1231-1241.
- Nakai, J., Imagawa, T., Hakamata, Y., Shigekawa, M., Takeshima, H. and Numa, S. 1990. Primary structure and functional expression from cDNA of the cardiac ryanodine receptor/calcium release channel. *FEBS Letters*. **271**(1-2), pp.169-177.
- Nance, J. and Frøkjær-Jensen, C. 2019. The *Caenorhabditis elegans* Transgenic Toolbox. *Genetics*. **212**(4), pp.959-990.
- Naranjo, J.R. and Mellström, B. 2012. Ca²⁺-dependent Transcriptional Control of Ca²⁺ Homeostasis. *Journal of Biological Chemistry*. **287**(38), pp.31674-31680.
- Narita, K., Akita, T., Hachisuka, J., Huang, S.M., Ochi, K. and Kuba, K. 2000. Functional coupling of Ca²⁺ channels to ryanodine receptors at presynaptic terminals. Amplification of exocytosis and plasticity. *The Journal of General Physiology*. **115**(4), p519.

- Nelson, T.E., Lin, M. and Volpe, P. 1991. Evidence for intraluminal Ca⁺⁺ regulatory site defect in sarcoplasmic reticulum from malignant hyperthermia pig muscle. *The Journal of pharmacology and experimental therapeutics*. **256**(2), pp.645-649.
- Neylon, C.B., Richards, S.M., Larsen, M.A., Agrotis, A. and Bobik, A. 1995. Multiple types of ryanodine receptor/Ca²⁺ release channels are expressed in vascular smooth muscle. *Biochem Biophys Res Commun*. **215**(3), pp.814-821.
- Nicoll Baines, K., Ferreira, C., Hopkins, P.M., Shaw, M.A. and Hope, I.A. 2017. Aging Effects of *Caenorhabditis elegans* Ryanodine Receptor Variants Corresponding to Human Myopathic Mutations. *G3*. **7**(5), pp.1451-1461.
- Ogawa, Y., Murayama, T. and Kurebayashi, N. 2002. Ryanodine receptor isoforms of non-Mammalian skeletal muscle. *Front Biosci*. **7**, pp.d1184-1194.
- Oh, K.H. and Kim, H. 2017. Aldicarb-induced Paralysis Assay to Determine Defects in Synaptic Transmission in *Caenorhabditis elegans*. *Bio-protocol*. **7**(14), pe2400.
- Ohno, S. 2016. The genetic background of arrhythmogenic right ventricular cardiomyopathy. *Journal of arrhythmia*. **32**(5), pp.398-403.
- Ottini, L., Marziali, G., Conti, A., Charlesworth, A. and Sorrentino, V. 1996. Alpha and beta isoforms of ryanodine receptor from chicken skeletal muscle are the homologues of mammalian *RyR1* and *RyR3*. *The Biochemical journal*. **315 (Pt 1)**(Pt 1), pp.207-216.
- Oulès, B., Del Prete, D., Greco, B., Zhang, X., Lauritzen, I., Sevalle, J., Moreno, S., Paterlini-Bréchet, P., Trebak, M., Checler, F., Benfenati, F. and Chami, M. 2012. Ryanodine receptor blockade reduces amyloid- β load and memory impairments in Tg2576 mouse model of Alzheimer disease. *The Journal of neuroscience : the official journal of the Society for Neuroscience*. **32**(34), pp.11820-11834.
- Oyamada, H., Murayama, T., Takagi, T., Iino, M., Iwabe, N., Miyata, T., Ogawa, Y. and Endo, M. 1994. Primary structure and distribution of ryanodine-binding protein

isoforms of the bullfrog skeletal muscle. *The Journal of biological chemistry*. **269**(25), pp.17206-17214.

Paul-Pletzer, K., Yamamoto, T., Bhat, M.B., Ma, J., Ikemoto, N., S., J.L., Morimoto, H., Williams, P.G. and Parness, J. 2002 Identification of a dantrolene-binding sequence on the skeletal muscle ryanodine receptor. *J Biol Chem*. **227**(34918-23).

Peng, J., Liang, G., Inan, S., Wu, Z., Joseph, D.J., Meng, Q., Peng, Y., Eckenhoff, M.F. and Wei, H. 2012. Dantrolene ameliorates cognitive decline and neuropathology in Alzheimer triple transgenic mice. *Neurosci Lett*. **516**(2), pp.274-279.

Peng, W., Shen, H., Wu, J., Guo, W., Pan, X., Wang, R., Chen, S.R.W. and Yan, N. 2016. Structural basis for the gating mechanism of the type 2 ryanodine receptor RyR2. *Science*. **354**(6310), paah5324.

Pereira, L., Kratsios, P., Serrano-Saiz, E., Sheftel, H., Mayo, A.E., Hall, D.H., White, J.G., LeBoeuf, B., Garcia, L.R., Alon, U. and Hobert, O. 2015. A cellular and regulatory map of the cholinergic nervous system of *C. elegans*. *eLife*. **4**, pe12432.

Periasamy, M. and Kalyanasundaram, A. 2007. SERCA pump isoforms: their role in calcium transport and disease. *Muscle Nerve*. **35**(4), pp.430-442.

Perkins, J., Wong, K., Warren, R., Schein, J., Stott, J., Holt, R., Jones, S., Marra, M. and Moerman, D. 2005. A *C. elegans* Fosmid Library. In: *15th International C. elegans Conference, UCLA, Los Angeles, CA*.

Pierce-Shimomura, J.T., Chen, B.L., Mun, J.J., Ho, R., Sarkis, R. and McIntire, S.L. 2008. Genetic analysis of crawling and swimming locomotory patterns in *C. elegans*. *Proceedings of the National Academy of Sciences*. **105**(52), p20982.

Polster, A., Perni, S., Bichraoui, H. and Beam, K.G. 2015. Stac adaptor proteins regulate trafficking and function of muscle and neuronal L-type Ca²⁺ channels. *Proceedings of the National Academy of Sciences of the United States of America*. **112**(2), pp.602-606.

- Ponting, C.P. 2000. Novel repeats in ryanodine and IP3 receptors and protein O-mannosyltransferases. *Trends in Biochemical Sciences*. **25**(2), pp.47-50.
- Pourcel, C., Salvignol, G. and Vergnaud, G. 2005. CRISPR elements in *Yersinia pestis* acquire new repeats by preferential uptake of bacteriophage DNA, and provide additional tools for evolutionary studies. *Microbiology*. **15**(653-663).
- Praitis, V., Casey, E., Collar, D. and Austin, J. 2001. Creation of low-copy integrated transgenic lines in *Caenorhabditis elegans*. *Genetics*. **157**(3), pp.1217-1226.
- Prior, H., Jawad, A.K., MacConnachie, L. and Beg, A.A. 2017. Highly Efficient, Rapid and Co-CRISPR-Independent Genome Editing in *Caenorhabditis elegans*. *G3 (Bethesda, Md.)*. **7**(11), pp.3693-3698.
- Priori, S.G., Napolitano, C., Tiso, N., Memmi, M., Vignati, G., Bloise, R., Sorrentino, V. and Danieli, G.A. 2001. Mutations in the cardiac ryanodine receptor gene (hRyR2) underlie catecholaminergic polymorphic ventricular tachycardia. *Circulation*. **103**(2), pp.196-200.
- Purves, D., Augustine, G.J., Fitzpatrick, D., Katz, L.C., LaMantia, A.S., McNamara, J.O. and Williams, S.M. 2001. Acetylcholine. *Neuroscience. 2nd edition*. Sunderland (MA): Sinauer Associates.
- Purves, R.D. 1976. Function of muscarinic and nicotinic acetylcholine receptors. *Nature*. **261**(5556), pp.149-151.
- Putrenko, I., Zakikhani, M. and Dent, J.A. 2005. A Family of Acetylcholine-gated Chloride Channel Subunits in *Caenorhabditis elegans*. *Journal of Biological Chemistry*. **280**(8), pp.6392-6398.
- Qian, H., Robertson, A.P., Powell-Coffman, J.A. and Martin, R.J. 2008. Levamisole resistance resolved at the single-channel level in *Caenorhabditis elegans*. *FASEB journal : official publication of the Federation of American Societies for Experimental Biology*. **22**(9), pp.3247-3254.

- Rabets, Y., Backholm, M., Dalnoki-Veress, K. and Ryu, W.S. 2014. Direct measurements of drag forces in *C. elegans* crawling locomotion. *Biophysical journal*. **107**(8), pp.1980-1987.
- Rand, J.B. 2007. *Acetylcholine*. [Online]. Available from: <http://www.wormbook.org>.
- Rees, H.A. and Liu, D.R. 2018. Base editing: precision chemistry on the genome and transcriptome of living cells. *Nature reviews. Genetics*. **19**(12), pp.770-788.
- Renganathan, M., Messi, M.L. and Delbono, O. 1997. Dihydropyridine Receptor-Ryanodine Receptor Uncoupling in Aged Skeletal Muscle. *The Journal of Membrane Biology*. **157**(3), pp.247-253.
- Riazi, S., Kraeva, N. and Hopkins, P.M. 2018. Malignant Hyperthermia in the Post-Genomics Era: New Perspectives on an Old Concept. *Anesthesiology*. **128**(1), pp.168-180.
- Riazi, S., Kraeva, N., Muldoon, S.M., Dowling, J., Ho, C., Petre, M.-A., Parness, J., Dirksen, R.T. and Rosenberg, H. 2014. Malignant hyperthermia and the clinical significance of type-1 ryanodine receptor gene (*RYR1*) variants: proceedings of the 2013 MHAUS Scientific Conference. *Canadian journal of anaesthesia = Journal canadien d'anesthesie*. **61**(11), pp.1040-1049.
- Richmond, J.E. and Jorgensen, E.M. 1999. One GABA and two acetylcholine receptors function at the *C. elegans* neuromuscular junction. *Nature Neuroscience*. **2**(9), pp.791-797.
- Riddle, D., Blumenthal, T., Meyer, B. and Priess, J. 1997. Section I Introduction: the Neural Circuit for Locomotion. In: Riddle, D., *et al.* eds. *C. elegans II*. 2nd edition ed. Cold Spring Harbor (NY): Cold Spring Harbour Laboratory Press.
- Rieckher, M., Kourtis, N., Pasparaki, A. and Tavernarakis, N. 2009. Transgenesis in *Caenorhabditis elegans*. *Methods Mol Biol*. **561**, pp.21-39.

- Ríos, E., Gillespie, D. and Franzini-Armstrong, C. 2019. The binding interactions that maintain excitation–contraction coupling junctions in skeletal muscle. *The Journal of General Physiology*. **151**(4), pp.593-605.
- Ríos, E., Ma, J. and González, A. 1991. The mechanical hypothesis of excitation–contraction (EC) coupling in skeletal muscle. *Journal of Muscle Research & Cell Motility*. **12**(2), pp.127-135.
- Risher, J.F., Mink, F.L. and Stara, J.F. 1987. The toxicologic effects of the carbamate insecticide aldicarb in mammals: a review. *Environmental health perspectives*. **72**, pp.267-281.
- Robertson, A.P., Clark, C.L. and Martin, R.J. 2010. Levamisole and ryanodine receptors. I: A contraction study in *Ascaris suum*. *Molecular and biochemical parasitology*. **171**(1), pp.1-7.
- Robinson, R., Carpenter, D., Shaw, M.-A., Halsall, J. and Hopkins, P. 2006. Mutations in *RYR1* in malignant hyperthermia and central core disease. *Human Mutation*. **27**(10), pp.977-989.
- Robinson, R.L., Anetseder, M.J., Brancadoro, V., van Broekhoven, C., Carsana, A., Censier, K., Fortunato, G., Girard, T., Heytens, L., Hopkins, P.M. *et al.* 2003. Recent advances in the diagnosis of malignant hyperthermia susceptibility: How confident can we be of genetic testing? *European Journal of Human Genetics*. **11**(4), pp.342-348.
- Rosenberg, H., Davis, M., James, D., Pollock, N. and Stowell, K. 2007. Malignant hyperthermia. *Orphanet journal of rare diseases*. **2**, pp.21-21.
- Rosenberg, H., Pollock, N., Schiemann, A., Bulger, T. and Stowell, K. 2015. Malignant hyperthermia: a review. *Orphanet journal of rare diseases*. **10**, pp.93-93.
- Rossi, D., Murayama, T., Manini, I., Franci, D., Ogawa, Y. and Sorrentino, V. 2007. Expression and functional activity of ryanodine receptors (RyRs) during skeletal muscle development. *Cell Calcium*. **41**(6), pp.573-580.

- Salvage, S.C., Gallant, E.M., Beard, N.A., Ahmad, S., Valli, H., Fraser, J.A., Huang, C.L.H. and Dulhunty, A.F. 2019. Ion channel gating in cardiac ryanodine receptors from the arrhythmic RyR2-P2328S mouse. *Journal of Cell Science*. **132**(10), pjcs229039.
- Samsó, M. 2017. A guide to the 3D structure of the ryanodine receptor type 1 by cryoEM. *Protein science : a publication of the Protein Society*. **26**(1), pp.52-68.
- Samtleben, S., Jaepel, J., Fecher, C., Andreska, T., Rehberg, M. and Blum, R. 2013. Direct imaging of ER calcium with targeted-esterase induced dye loading (TED). *Journal of visualized experiments : JoVE*. (75), pp.e50317-e50317.
- Santulli, G., Lewis, D., des Georges, A., Marks, A.R. and Frank, J. 2018. Ryanodine Receptor Structure and Function in Health and Disease. *Sub-cellular biochemistry*. **87**, pp.329-352.
- Sauer, H., Wartenberg, M. and Hescheler, J. 2001. Reactive oxygen species as intracellular messengers during cell growth and differentiation. *Cell Physiol Biochem*. **11**(4), pp.173-186.
- Schneider, C.A., Rasband, W.S. and Eliceiri, K.W. 2012. NIH Image to ImageJ: 25 years of image analysis. *Nature Methods*. **9**, p671.
- Scholfield, C.N. 1980. Potentiation of inhibition by general anaesthetics in neurones of the olfactory cortex in vitro. *Pflügers Archiv*. **383**(3), pp.249-255.
- Schriner, S.E., Linford, N.J., Martin, G.M., Treuting, P., Ogburn, C.E., Emond, M., Coskun, P.E., Ladiges, W., Wolf, N., Van Remmen, H., Wallace, D.C. and Rabinovitch, P.S. 2005. Extension of Murine Life Span by Overexpression of Catalase Targeted to Mitochondria. *Science*. **308**(5730), p1909.
- Schüler, C., Fischer, E., Shaltiel, L., Steuer Costa, W. and Gottschalk, A. 2015. Arrhythmogenic effects of mutated L-type Ca²⁺-channels on an optogenetically paced muscular pump in *Caenorhabditis elegans*. *Scientific Reports*. **5**(1), p14427.

- Seddon, I. 2016. *Quantifying the locomotion of C. elegans and their response to photo stimulation* Honors Program thesis.
- Sei, Y., Sambuughin, N.N., Davis, E.J., Sachs, D., Cuenca, P.B., Brandom, B.W., Tautz, T., Rosenberg, H., Nelson, T.E. and Muldoon, S.M. 2004. Malignant hyperthermia in North America: genetic screening of the three hot spots in the type I ryanodine receptor gene. *Anesthesiology*. **101**(4), pp.824-830.
- Shan, J., Xie, W., Betzenhauser, M., Reiken, S., Chen, B.X., Wronska, A. and Marks, A.R. 2012. Calcium leak through ryanodine receptors leads to atrial fibrillation in 3 mouse models of catecholaminergic polymorphic ventricular tachycardia. *Circ Res*. **111**(6), pp.708-717.
- Shaw, M., Zhan, H., Elmi, M., Pawar, V., Essmann, C. and Srinivasan, M.A. 2018. Three-dimensional behavioural phenotyping of freely moving *C. elegans* using quantitative light field microscopy. *PLoS One*. **13**(7), pe0200108.
- Shingai, R. 2000. Durations and frequencies of free locomotion in wild type and GABAergic mutants of *Caenorhabditis elegans*. *Neuroscience Research*. **38**(1), pp.71-84.
- Silva-García, C.G., Lanjuin, A., Heintz, C., Dutta, S., Clark, N.M. and Mair, W.B. 2019. Single-Copy Knock-In Loci for Defined Gene Expression in *Caenorhabditis elegans*. *G3*. **9**(7), pp.2195-2198.
- Sitsapesan, R. and Williams, A.J. 1997. Regulation of current flow through ryanodine receptors by luminal Ca²⁺. *The Journal of membrane biology*. **159**(3), pp.179-185.
- Sorek, R., Lawrence, C.M. and Wiedenheft, B. 2013. CRISPR-Mediated Adaptive Immune Systems in Bacteria and Archaea. *Annual Review of Biochemistry*. **82**(1), pp.237-266.
- Sorrentino, V., Barone, V. and Rossi, D. 2000. Intracellular Ca²⁺ release channels in evolution. *Current opinion in genetics & development*. **10**(6), pp.662-667.

Spensley, M., Del Borrello, S., Pajkic, D. and Fraser, A.G. 2018. Acute Effects of Drugs on *Caenorhabditis elegans* Movement Reveal Complex Responses and Plasticity. *G3*. **8**(9), p2941.

Stiernagle, T. 2006. *Maintenance of C. elegans*. [Online]. Available from: <http://www.wormbook.org>.

Stinchcomb, D.T., Shaw, J.E., Carr, S.H. and Hirsh, D. 1985. Extrachromosomal DNA transformation of *Caenorhabditis elegans*. *Mol Cell Biol*. **5**(12), pp.3484-3496.

Strazis, K.P. and Fox, A.W. 1993. Malignant hyperthermia: a review of published cases. *Anesthesia and analgesia*. **77**(2), pp.297-304.

Stutzmann, G.E., Smith, I., Caccamo, A., Oddo, S., LaFerla, F.M. and Parker, I. 2006. Enhanced Ryanodine Receptor Recruitment Contributes to Ca²⁺ Disruptions in Young, Adult, and Aged Alzheimer's Disease Mice. *The Journal of Neuroscience*. **26**(19), p5180.

Südhof, T.C. 2012. Calcium control of neurotransmitter release. *Cold Spring Harbor perspectives in biology*. **4**(1), pp.a011353-a011353.

Sulston, J.E. 2003. *Caenorhabditis elegans*: The Cell Lineage and Beyond (Nobel Lecture). *ChemBioChem*. **4**(8), pp.688-696.

Sulston, J.E. and Horvitz, H.R. 1977. Post-embryonic cell lineages of the nematode, *Caenorhabditis elegans*. *Dev Biol*. **56**(1), pp.110-156.

Sulston, J.E., Schierenberg, E., White, J.G. and Thomson, J.N. 1983. The embryonic cell lineage of the nematode *Caenorhabditis elegans*. *Developmental Biology*. **100**(1), pp.64-119.

Sun, L., Shay, J., McLoed, M., Roodhouse, K., Chung, S.H., Clark, C.M., Pirri, J.K., Alkema, M.J. and Gabel, C.V. 2014. Neuronal regeneration in *C. elegans* requires subcellular calcium release by ryanodine receptor channels and can be enhanced by optogenetic stimulation. *The Journal of neuroscience : the official journal of the Society for Neuroscience*. **34**(48), pp.15947-15956.

- Szent-Györgyi, A.G. 1975. Calcium regulation of muscle contraction. *Biophysical journal*. **15**(7), pp.707-723.
- Tabara, H., Grishok, A. and Mello, C.C. 1998. RNAi in *C. elegans*: soaking in the genome sequence. *Science*. **282**(5388), pp.430-431.
- Takeshima, H., Nishimura, S., Matsumoto, T., Ishida, H., Kangawa, K., Minamino, N., Matsuo, H., Ueda, M., Hanaoka, M., Hirose, T. and Numa, S. 1989. Primary structure and expression from complementary DNA of skeletal muscle ryanodine receptor. *Nature*. **339**(6224), pp.439-445.
- Tammaro, A., Di Martino, A., Bracco, A., Cozzolino, S., Savoia, G., Andria, B., Cannavo, A., Spagnuolo, M., Piluso, G., Aurino, S. and Nigro, V. 2011. Novel missense mutations and unexpected multiple changes of *RYR1* gene in 75 malignant hyperthermia families. *Clinical Genetics*. **79**(5), pp.438-447.
- Taylor, C.W. and Tovey, S.C. 2010. IP(3) receptors: toward understanding their activation. *Cold Spring Harbor perspectives in biology*. **2**(12), pp.a004010-a004010.
- The *C. elegans* Sequencing Consortium. 1998. Genome Sequence of the Nematode *C. elegans*: A Platform for Investigating Biology. *Science*. **282**(5396), p2012.
- The European Malignant Hyperthermia Group. n.d. *Genetics in Malignant Hyperthermia*. [Online]. [Accessed November 2019]. Available from: <https://www.emhg.org/diagnostic-mutations>
- Thomas, D. and Goldstein, S.A.N. 2009. Two-P-Domain (K2P) Potassium Channels: Leak Conductance Regulators of Excitability. In: Squire, L.R. ed. *Encyclopedia of Neuroscience*. Oxford: Academic Press, pp.1207-1220.
- Thompson, O., Edgley, M., Strasbourger, P., Flibotte, S., Ewing, B., Adair, R., Au, V., Chaudry, I., Fernando, L., Hutter, H. *et al.* 2013. The Million Mutation Project: A new approach to genetics in *Caenorhabditis elegans*. *Genome Research*.

- Tian, L., Hires, S.A., Mao, T., Huber, D., Chiappe, M.E., Chalasani, S.H., Petreanu, L., Akerboom, J., McKinney, S.A., Schreiter, E.R., Bargmann, C.I., Jayaraman, V., Svoboda, K. and Looger, L.L. 2009. Imaging neural activity in worms, flies and mice with improved GCaMP calcium indicators. *Nature methods*. **6**(12), pp.875-881.
- Timmons, L. and Fire, A. 1998. Specific interference by ingested dsRNA. *Nature*. **395**(6705), p854.
- Tobin, J.R., Jason, D.R., Challa, V.R., Nelson, T.E. and Sambuughin, N. 2001. Malignant Hyperthermia and Apparent Heat Stroke. *JAMA*. **286**(2), pp.168-169.
- Todd, J.J., Sagar, V., Lawal, T.A., Allen, C., Razaqyar, M.S., Shelton, M.S., Chrismer, I.C., Zhang, X., Cosgrove, M.M., Kuo, A. *et al.* 2018. Correlation of phenotype with genotype and protein structure in *RYR1*-related disorders. *Journal of neurology*. **265**(11), pp.2506-2524.
- Tong, J., McCarthy, T.V. and MacLennan, D.H. 1999. Measurement of Resting Cytosolic Ca²⁺ Concentrations and Ca²⁺ Store Size in HEK-293 Cells Transfected with Malignant Hyperthermia or Central Core Disease Mutant Ca²⁺ Release Channels. *Journal of Biological Chemistry*. **274**(2), pp.693-702.
- Tripathy, A., Xu, L., Mann, G. and Meissner, G. 1995. Calmodulin activation and inhibition of skeletal muscle Ca²⁺ release channel (ryanodine receptor). *Biophysical journal*. **69**(1), pp.106-119.
- Umanskaya, A., Santulli, G., Xie, W., Andersson, D.C., Reiken, S.R. and Marks, A.R. 2014. Genetically enhancing mitochondrial antioxidant activity improves muscle function in aging. *Proceedings of the National Academy of Sciences of the United States of America*. **111**(42), pp.15250-15255.
- Urwyler, A., Deufel, T., McCarthy, T. and West, S. 2001. Guidelines for molecular genetic detection of susceptibility to malignant hyperthermia. *British Journal of Anaesthesia*. **86**(2), pp.283-287.

Van Petegem, F. 2012. Ryanodine receptors: structure and function. *The Journal of biological chemistry*. **287**(38), pp.31624-31632.

Vidal-Gadea, A., Topper, S., Young, L., Crisp, A., Kressin, L., Elbel, E., Maples, T., Brauner, M., Erbguth, K., Axelrod, A., Gottschalk, A., Siegel, D. and Pierce-Shimomura, J.T. 2011. *Caenorhabditis elegans* selects distinct crawling and swimming gaits via dopamine and serotonin. *Proceedings of the National Academy of Sciences of the United States of America*. **108**(42), pp.17504-17509.

Volkov, A.G., Paula, S. and Deamer, D.W. 1997. Two mechanisms of permeation of small neutral molecules and hydrated ions across phospholipid bilayers. *Bioelectrochemistry and Bioenergetics*. **42**(2), pp.153-160.

Wang, X., Wang, X., Li, L. and Wang, D. 2010. Lifespan extension in *Caenorhabditis elegans* by DMSO is dependent on *sir-2.1* and *daf-16*. *Biochemical and Biophysical Research Communications*. **400**(4), pp.613-618.

Wang, Z.-W. 2010. Origin of quantal size variation and high-frequency miniature postsynaptic currents at the *Caenorhabditis elegans* neuromuscular junction. *Journal of neuroscience research*. **88**(16), pp.3425-3432.

Wei, R., Wang, X., Zhang, Y., Mukherjee, S., Zhang, L., Chen, Q., Huang, X., Jing, S., Liu, C., Li, S. *et al.* 2016. Structural insights into Ca²⁺-activated long-range allosteric channel gating of RyR1. *Cell Research*. **26**, p977.

Weiss, R.G., O'Connell, K.M.S., Flucher, B.E., Allen, P.D., Grabner, M. and Dirksen, R.T. 2004. Functional analysis of the R1086H malignant hyperthermia mutation in the DHPR reveals an unexpected influence of the III-IV loop on skeletal muscle EC coupling. *American Journal of Physiology-Cell Physiology*. **287**(4), pp.C1094-C1102.

White, J.G., Southgate, E., Thomson, J.N. and Brenner, S. 1986. The structure of the nervous system of the nematode *Caenorhabditis elegans*. *Philos Trans R Soc Lond B Biol Sci*. **314**(1165), pp.1-340.

- Wickens, A.P. 2001. Ageing and the free radical theory. *Respir Physiol.* **128**(3), pp.379-391.
- Williamson, S.M., Robertson, A.P., Brown, L., Williams, T., Woods, D.J., Martin, R.J., Sattelle, D.B. and Wolstenholme, A.J. 2009. The nicotinic acetylcholine receptors of the parasitic nematode *Ascaris suum*: formation of two distinct drug targets by varying the relative expression levels of two subunits. *PLoS pathogens.* **5**(7), pp.e1000517-e1000517.
- Witherspoon, J.W. and Meilleur, K.G. 2016. Review of RyR1 pathway and associated pathomechanisms. *Acta neuropathologica communications.* **4**(1), pp.121-121.
- World Health Organization. 2019. *Model List of Essential Medicines, 21st List.* [Online]. [Accessed October 2019]. Available from: <https://www.who.int>
- Wormbase.org. 2016. *Unc-68 (gene).* [Online]. [Accessed 11 Jan 2016]. Available from: <http://www.wormbase.org>
- Xiong, H., Feng, X., Gao, L., Xu, L., Pasek, D.A., Seok, J.H. and Meissner, G. 1998. Identification of a two EF-hand Ca²⁺ binding domain in lobster skeletal muscle ryanodine receptor/Ca²⁺ release channel. *Biochemistry.* **37**(14), pp.4804-4814.
- Xiong, H., Pears, C. and Woollard, A. 2017. An enhanced *C. elegans* based platform for toxicity assessment. *Scientific Reports.* **7**(1), p9839.
- Yan, Z., Bai, X., Yan, C., Wu, J., Li, Z., Xie, T., Peng, W., Yin, C., Li, X., Scheres, S.H.W., Shi, Y. and Yan, N. 2015. Structure of the rabbit ryanodine receptor RyR1 at near-atomic resolution. *Nature.* **517**(7532), pp.50-55.
- Yang, T., Riehl, J., Esteve, E., Matthaei, Klaus I., Goth, S., Allen, Paul D., Pessah, Isaac N. and Lopez, José R. 2006. Pharmacologic and Functional Characterization of Malignant Hyperthermia in the R163C RyR1 Knock-in Mouse. *Anesthesiology: The Journal of the American Society of Anesthesiologists.* **105**(6), pp.1164-1175.

- Yaras, N., Ugur, M., Ozdemir, S., Gurdal, H., Purali, N., Lacampagne, A., Vassort, G. and Turan, B. 2005. Effects of diabetes on ryanodine receptor Ca release channel (RyR2) and Ca²⁺ homeostasis in rat heart. *Diabetes*. **54**(11), pp.3082-3088.
- Yin, C.-C., D’Cruz, L.G. and Lai, F.A. 2008. Ryanodine receptor arrays: not just a pretty pattern? *Trends in Cell Biology*. **18**(4), pp.149-156.
- Yu, Z., Tibbits, G.F. and McNeill, J.H. 1994. Cellular functions of diabetic cardiomyocytes: contractility, rapid-cooling contracture, and ryanodine binding. *Am J Physiol*. **266**(5 Pt 2), pp.H2082-2089.
- Zalk, R., Clarke, O.B., des Georges, A., Grassucci, R.A., Reiken, S., Mancina, F., Hendrickson, W.A., Frank, J. and Marks, A.R. 2015. Structure of a mammalian ryanodine receptor. *Nature*. **517**(7532), pp.44-49.
- Zhang, F., Wen, Y. and Guo, X. 2014. CRISPR/Cas9 for genome editing: progress, implications and challenges. *Human Molecular Genetics*. **23**(R1), pp.R40-R46.
- Zhao, Y., Gilliat, A.F., Ziehm, M., Turmaine, M., Wang, H., Ezcurra, M., Yang, C., Phillips, G., McBay, D., Zhang, W.B., Partridge, L., Pincus, Z. and Gems, D. 2017. Two forms of death in ageing *Caenorhabditis elegans*. *Nature Communications*. **8**(1), p15458.
- Zhen, M. and Samuel, A.D.T. 2015. *C. elegans* locomotion: small circuits, complex functions. *Current opinion in neurobiology*. **33**, pp.117-126.
- Zhu, X., Altschaf, B.A., Hajjar, R.J., Valdivia, H.H. and Schmidt, U. 2005. Altered Ca²⁺ sparks and gating properties of ryanodine receptors in aging cardiomyocytes. *Cell calcium*. **37**(6), pp.583-591.
- Zissimopoulos, S., West, D.J., Williams, A.J. and Lai, F.A. 2006. Ryanodine receptor interaction with the SNARE-associated protein snapin. *Journal of Cell Science*. **119**(11), p2386.